

THE UNIVERSITY OF HULL

Thermal Chemical Conversion of Plastics Waste for
Production of Carbon Nanotubes

being a Thesis submitted for the Degree of Doctor of
Philosophy (PhD) in the University of Hull

by

Xiaotong Liu

November 2018

Abstract

With continuous growth for more than 50 years, global plastics production increased to 336 million tonnes in 2016, and over 27 million tonnes of post-consumer plastic wastes were produced. Waste management is necessary to minimise the plastic waste in order to reduce their negative impacts. Catalytic-pyrolysis of plastic waste provides an environmental friendly and economic method to produce valuable products such as H₂ rich syngas and carbon nanotubes (CNTs). Recently, CNTs attract a great interest and have been widely explored due to the excellent and unique chemical, mechanical, thermal and physical properties. However, the quality and quantity of CNTs produced from waste plastics need to be improved. The quality of CNTs can significantly affect and limit their applications. The aim of this research is to improve the quantity and quality of CNTs by developing efficient catalysts. Four groups of different catalysts (Ni/Fe- based; Ni/AAO, Ni/ceramic, and Ni/sphere) have been investigated in relation to their performance on the production of CNTs from catalytic gasification of waste polypropylene, using a two-stage fixed-bed reaction system. The influences of reaction parameters for each group of catalysts on product yields and the production of CNTs in terms of morphology have been studied using a range of techniques; gas chromatography (GC); X-ray diffraction (XRD); temperature programme oxidation (TPO); scanning electron microscopy (SEM); transmission electron microscopy (TEM). It was found reaction temperature, catalytic particle size, steam addition, and catalytic metal content have significant effect on CNTs production. The particular optimum of each parameter for different catalysts could contribute to the enhancement of the quality and quantity of CNTs. For example, the

optimum reaction temperature for Ni/AAO was suggested at 700 °C, because the catalyst might not be activated at 600 °C, which produced a low yield of CNTs. However, a reaction temperature of 800 °C resulted in a low yield of CNTs. In addition, the results indicated that a higher loading of Ni on AAO resulted in the formation of metal particles with various sizes, thus leading to the production of non-uniform CNTs. Carbon deposition was also found decreasing with an increase of steam injection, but the quality of CNTs formation in relation to the uniform of CNTs seemed to be improved in the presence of steam. For Fe/Ni-based catalysts study, the results show that the Fe-based catalysts, in particular with large particle size (about 80 nm), produced the highest yield of hydrogen (25.60 mmol H₂ g⁻¹ plastic) and the highest yield of carbons (29 wt.%), as well as the largest fraction of graphite carbons (as obtained from TPO analysis of the reacted catalyst). Both Fe- and Ni-based catalysts with larger metal particles produced higher yield of hydrogen compared with the catalysts with smaller metal particles, respectively.

Nomenclature

AAO	Anodic aluminium oxide
CNTs	Carbon nanotubes
CVD	Chemical vapour deposition
DCS	Differential scanning calorimetry
GC	Gas chromatographs
HRTEM	High resolution transmission electron microscopy
HDPE	High density polyethylene
ICP	Inductively coupled plasma
LDPE	Low density polyethylene
MWNTs	Multiwall nanotubes
PANI	Polyaniline
PAM	Porous alumina membrane
PC	Polycarbonate
PCS	Polycarbosilane
PE	Polyethylene
PET	Polyethylene terephthalate
PI	Polyimide
PP	Polypropylene
PS	Polystyrene
PU	Polyurethane
PUR	Polyurethane

PVC	Polyvinyl chloride
SD	Standard deviation
SEM	Scanning electron microscopy
SWNTs	Single-walled nanotubes
TEM	Transmission electron microscopy
TEOS	Tetraethoxysilane
TGA	Thermogravimetric analysis
TPO	Temperature program oxidation
XRD	X-ray diffraction
Al	Aluminium
Al ₂ O ₃	Aluminium oxide
C	Carbon
C ₃	Propane
Ca	Calcium
C ₂ H ₂	Acetylene
C ₅ H ₁₂	Isopentane
C ₆ H ₁₂	Cyclohexane
Co	Cobalt
CO	Carbon monoxide
CO ₂	Carbon dioxide

Cu	Copper
Co ₃ O ₄	Cobalt(II,III) oxide
Fe	Iron
Fe ₂ O ₃	Iron(III) oxide
Fe ₃ O ₄	Iron(II,III) oxide
H ₂	Hydrogen
HZSM-5	Zeolite socony mobil-5
Mg	Magnesium
MgO	Magnesium oxide
MnO ₂	Manganese dioxide
Mo	Molybdenum
Mo ₂ C	Molybdenum carbide
Ni	Nickel
NiO	Nickel oxide
NH ₃	Ammonia
O ₂	Oxygen
Ru	Ruthenium
SnO ₂	Tin dioxide
SiO ₂	Silicon dioxide
TiO ₂	Titanium dioxide
V ₂ O ₅	Vanadium(V) oxide
ZrO ₂	Zirconium dioxide

Acknowledgement

I'd like to give my thanks to all the people who ever helped, supported and encouraged me during my PhD study.

Specially thank to my supervisor, Dr. Chunfei Wu. My PhD has been an amazing experience and I thank Dr. Chunfei Wu, not only for his tremendous academic support, but also for giving me so many valuable opportunities. He provided me such many opportunities to attend conferences and training, broadening my vision and enriching my experience.

Also thank to Dr. Xuebin Ke, my second supervisor and Dr. Dipesh Patel who gives me lots of suggestions and improved my presentation and writing skills. Special mention goes to Garry who taught me SEM equipment operation with much patience. And also Ann, she gave me lots of help on TEM analysis.

Finally, many thanks go to parents for almost unbelievable support. They are the most important people in my world and I dedicate this thesis to them.

Table of Contents

Abstract.....	ii
Nomenclature	iv
Acknowledgement.....	vii
List of Figures.....	xiv
List of Tables	xxiii
Thesis structure.....	xxvi
Chapter 1. Introduction.....	1
1.1 Plastic waste	2
1.1.1 Plastics history	2
1.1.2 Composition and classification of plastics.....	3
1.1.3 Plastics demand and consumption	4
1.2 Plastics waste management.....	5
1.2.1 Landfill.....	6
1.2.2 Energy recovery	7
1.2.3 Recycling	8
1.2.3.1 Mechanical recycling	8
1.2.3.2 Chemical recycling.....	9
1.3 Carbon nanotubes	10
1.3.1 Structure and properties	10

1.3.2	Applications of CNTs	12
1.3.2.1	Lithium battery	13
1.3.2.2	Supercapacitor	14
1.3.2.3	CNTs-based composites	15
1.3.2.4	Catalysts support	17
1.3.3	Synthesis of carbon nanotubes	18
1.3.3.1	Arc discharge	18
1.3.3.2	Laser ablation	20
1.3.3.3	Chemical vapour deposition	21
1.3.4	CNTs commercial value	24
1.4	Research aim and objectives	25
1.4.1	Research aim	25
1.4.2	Research objectives	26
Chapter 2.	Literature review	27
2.1	Catalyst for CNTs growth	28
2.1.1	Active sites for CNTs growth	28
2.1.1.1	Fe-based catalysts	30
2.1.1.2	Ni-based catalysts	31
2.1.1.3	Bi-metal and tri-metal based catalyst	31
2.1.1.4	Other metal based catalysts	32
2.1.2	Catalytic support for CNT growth	32
2.1.2.1	Silicon oxide support	33

2.1.2.2	Aluminium oxide support.....	34
2.1.2.3	Magnesium oxide	35
2.1.2.4	Zeolite.....	36
2.1.2.5	Template support.....	36
2.1.3	Catalytic promoter.....	38
2.1.4	Catalytic particle sizes	39
2.1.5	Catalytic metal content loaded.....	42
2.2	Growth mechanism of CNTs	46
2.3	Effect of parameters on synthesis of CNTs	49
2.3.1	Carbon precursor.....	49
2.3.2	Temperature	57
2.3.2.1	Pyrolysis temperature.....	57
2.3.2.2	Catalytic temperature	60
2.3.3	Additional steam to system	69
2.4	CNTs quality and quantity evaluation	74
2.4.1	Electron microscope analysis.....	76
2.4.2	Raman spectroscopy analysis.....	77
2.4.3	Thermogravimetric analysis.....	77
Chapter 3.	Experimental	79
3.1	Materials preparation	80
3.1.1	Raw materials.....	80
3.1.2	Catalysts preparation.....	80

3.1.2.1	Ni/Fe-based catalysts.....	80
3.1.2.2	AAO membrane support catalysts.....	81
3.1.2.3	Ceramic membrane support catalysts.....	81
3.1.2.4	Al ₂ O ₃ sphere catalyst.....	82
3.2	CNTs synthesis from waste plastics	82
3.2.1	Ni/Fe-based catalytic-chemical conversion of waste plastics.....	82
3.2.2	Ni/AAO catalytic-chemical conversion of waste plastic	84
3.2.3	Ceramic and sphere support catalytic-chemical conversion of waste plastics.....	85
3.3	Sample Characterisations	86
3.3.1	SEM analysis.....	86
3.3.2	TEM analysis	87
3.3.3	XRD analysis	88
3.3.4	TGA analysis.....	88
Chapter 4.	Carbon nanotubes growth with Ni/Fe- based catalysts	90
4.1	Characterisations of the fresh catalysts.....	91
4.2	Gas yield and composition	95
4.3	The production of CNTs	97
4.3.1	The Influence of metal species on CNTs production.....	97
4.3.2	The influence of metal particle size on CNTs production	99
Chapter 5.	Carbon nanotubes growth with AAO membrane.....	102
5.1	Role of AAO Membrane Substrate.....	103
5.2	Production of CNTs over AAO membrane supported catalysts.....	106

5.2.1	Effect of the conditioning catalyst on CNTs formation	108
5.2.2	Effect of Ni content on the production of CNTs.....	113
5.2.3	Effect of reaction temperature on the production of CNTs	117
5.2.4	Effect of Steam Addition on the Production of CNTs	121
Chapter 6. Carbon nanotubes growth with ceramic supported catalysts.....		126
6.1	Characterisation of fresh Ni/ceramic catalyst	127
6.2	Carbon nanotubes production	131
6.2.1	Effect of Reaction Temperature on CNTs Growth	133
6.2.2	Effect of Ni Content on the Production of CNTs.....	137
Chapter 7. Carbon nanotubes growth with aluminium sphere supported catalysts.....		143
7.1	Growth mechanism of CNTs on sphere supported catalysts	144
7.2	Optimum reaction parameters investigation	147
7.2.1	Influence of nickel loading	148
7.2.2	Influence of reaction temperature	151
Chapter 8. Conclusion and future work		154
8.1	Summary of catalysts studied.....	155
8.2	Challenges and future work	156
References.....		159
Appendices.....		186
Appendices A - Materials and equipment in the research.....		186
A1.	Raw materials	186

A2.	Ni/Fe-based catalysts.....	186
A3.	AAO membrane supported catalysts.....	187
A4.	Ceramic supported catalysts calculation	187
A5.	Sphere supported catalysts calculation.....	188
A6.	Equipment	188
Appendices B - Support materials for Ni/AAO catalysts study		192
Appendices C - Support materials for Ni/ceramics catalysts study		196
Appendices D - Publications		198
Appendices E - Conferences and training attendance		200
E1.	Conference.....	200
E2.	Training	205
E2.1	Fundamentals of bioenergy	205
E2.2	EU 'RISE' project.....	206
E2.3	Electron microscope training	208
E2.4	BRISK.....	209

List of Figures

Chapter 1

Figure 1.1 Plastics demand by polymer types in UK (Watch, 2003)	5
Figure 1.2 Percentages of different treatment methods for plastics waste from 2006 to 2016 (Plastics Europe, 2017)	6
Figure 1.3 Carbon nanotubes structure and classification (Zuo, 2018)	10
Figure 1.4 Molecular models of exhibited by SWNTs based on the chirality (Zuo, 2018)	11
Figure 1.5 CNTs applications for present, near term, and long term (Mittal et al., 2015)	13
Figure 1.6 Electrode/electrolyte interface for charging the electrical double layer (Izadi et al., 2010)	15
Figure 1.7 General schematic reactor for CNTs synthesis by arc discharge (Bethune et al., 1993)	19
Figure 1.8 General schematic reactor for CNTs synthesis by laser ablation (Zhang et al., 1999)	20
Figure 1.9 Schematic reactor of a horizontal CVD setup system (Mubarak et al., 2014)	22
Figure 1.10 Schematic reactor of a CVD vertical setup system. (1) reactor, (2) furnace, (3) distributor, (4) thermocouple, (5) rotameter, (6) carbon source, (7) carrier gas, (8) outlet, (9) pressure sensor (Danafar et al., 2009)	22

Chapter 2

Figure 2.1 Methane conversion and carbon deposition for different metals based catalysts (Ago et al., 2006)	29
Figure 2.2 Methane conversion and carbon yield with different amount of Mo addition (Wei et al., 2008)	39
Figure 2.3 TEM results of CNTs growth in presence (a)10–20 μm , and (b) 200–300 μm (Danafar et al., 2011)	40
Figure 2.4 Production of PP pyrolysis over different Ru loaded catalysts (Park et al., 2010)	43
Figure 2.5 SEM results for CNTs produced over $\text{Fe}_2\text{O}_3/\text{Al}_2\text{O}_3$ and $\text{Fe}_2\text{O}_3/\text{SiO}_2$ (7-77 wt.% as Fe_2O_3) from methane decomposition (Takenaka et al., 2004)	45
Figure 2.6 Carbon deposition yield with increasing Fe content of catalysts from $\text{H}_2\text{-C}_2\text{H}_4$ pyrolysis (Venegoni et al., 2002)	45
Figure 2.7 CNTs formation mechanism for AAO membrane support with different sizes metal particles (Jeong et al., 2004)	46
Figure 2.8 CNTs growth mechanisms via catalytic pyrolysis approaches (Yellampalli, 2011)	47
Figure 2.9 SEM (a) and TEM (b) result Ni/ceramic 740 $^\circ\text{C}$ from HDPE pyrolysis (Wei et al., 2008)	48
Figure 2.10 Growth mechanism of CNT agglomerate formation (Wei et al., 2008).....	48
Figure 2.11 SEM images of Au-CNT-AAO prepared at 700 $^\circ\text{C}$ (Lee et al., 2012).....	49
Figure 2.12 CNTs production from different plastic pyrolysis (Borsodi et al., 2016) ...	56

Figure 2.13 Gas production from pyrolysis of different catalysts:plastics ratio (Wu et al., 2010b)	57
Figure 2.14 Effect of pyrolysis temperature on carbon distributions (Park et al., 2010).	58
Figure 2.15 Gas composition at different pyrolysis temperatures (Liu et al., 2011)	59
Figure 2.16 Product yield at different pyrolysis temperature (Liu et al., 2011)	60
Figure 2.17 Effect of catalytic temperature on carbon deposition (Park et al., 2010)....	61
Figure 2.18 Yield of CNTs grown at (a) 0.6 Torr and (b) at 760 Torr (Li et al., 2002)..	63
Figure 2.19 TEM results for CNTs formed (a) at 700 °C and (b) at 900 °C (Yao et al., 2018)	64
Figure 2.20 Mass of CNTs and gas produced at different catalytic temperatures (Liu et al., 2011)	65
Figure 2.21 CNTs formed at (a) 500 °C, (b) 600 °C, (c) 700 °C, (d) 800 °C (Liu et al., 2011)	66
Figure 2.22 CNTs growth rate and diameter change with growth temperatures (Lee et al., 2001)	68
Figure 2.23 TGA results for CNTs growth at different temperatures (Lee et al., 2001)..	68
Figure 2.24 TEM results of grown CNTs for temperatures at (a) 675 °C, (b) 700 °C, (c) 750 °C, and (d) 800 °C (Golshadi et al., 2014)	69
Figure 2.25 Mechanism of CNTs formation by CVD with water addition (Hu et al., 2008)	70

Figure 2.26 Methane conversion of the Fe ₉₄ -Mo ₆ /MgO catalysts in the presence of different water concentrations (Ago et al., 2006)	71
Figure 2.27 CNTs cap formation mechanism with water vapour (Lee et al., 2012)	72
Figure 2.28 TEM images CNT using different amount of water vapor (a) 0, (b) 150 and (c) 700 sccm (Liu et al., 2010).....	73
Figure 2.29 Electron microscope analysis of CNTs (a) SEM, (b) TEM, (c) HRTEM (Latorre et al., 2015)	76
Figure 2.30 Raman spectroscopy analysis of CNTs (Pillai et al., 2008)	77
Figure 2.31 Thermogravimetric analysis of CNTs (Esteves et al., 2018).....	78
 <i>Chapter 3</i>	
Figure 3.1 Reactor for Ni/Fe-based catalysts study (Acomb et al., 2015).....	83
Figure 3.2 Reactor for AAO membrane supported catalysts study	85
Figure 3.3 Reactor for ceramic and sphere supported catalysts study	86
Figure 3.4 SEM schematic diagram (Stokes, 2008)	87
Figure 3.5 X-rays to diffract into specific direction (Ewald, 1962).....	88
 <i>Chapter 4</i>	
Figure 4.1 XRD results for Ni-based catalysts before and after reaction	92
Figure 4.2 XRD results for Fe-based catalysts before and after reactions.....	92
Figure 4.3 TPR results for fresh catalysts	93
Figure 4.4 TEM results for fresh catalysts (A) Ni/SiO ₂ -L-fresh (B) Ni/SiO ₂ -S-fresh (C) Fe/SiO ₂ -L-fresh (D) Fe/SiO ₂ -S-fresh, and analysis for metal particles sizes (a) Ni/SiO ₂ -L-fresh (b) Ni/SiO ₂ -S-fresh (c) Fe/SiO ₂ -L-fresh (d) Fe/SiO ₂ -S-fresh	94

Figure 4.5 TPO results for Fe- and Ni-based catalysts after reaction.....	98
Figure 4.6 SEM results for catalysts after reaction.....	98
Figure 4.7 TEM results for reacted catalysts (a) Fe-L-Reacted (98 nm) (b) Fe-S-Reacted (50 nm) (c) Ni-L-Reacted (23 nm) (d) Ni-S-Reacted (18 nm)	100
 <i>Chapter 5</i>	
Figure 5.1 XRD results for original AAO membrane without Ni loading and surface SEM image.....	103
Figure 5.2 SEM (A-D) and TEM (i-v) results for fresh 0.1/AAO, 0.5/AAO, 1.0/AAO, and 2.0/AAO.....	105
Figure 5.3 SEM results for CNTs formation on 0.1/AAO membrane with (a) 0 g; (b) 0.2 g; (c) 0.5 g; and (d) 1 g Ni/Al ₂ O ₃ conditioning catalysts on the top.....	109
Figure 5.4 TEM results for CNTs formation on 0.1/AAO membrane with (a) 0.2 g; (b) 0.5 g; and (c) 1 g Ni/Al ₂ O ₃ conditioning catalysts on the top.....	110
Figure 5.5 (a) TGA-TPO and (b) DTG-TPO results for the reacted catalysts obtained using different amounts of conditioning catalysts	110
Figure 5.6 Diameter distribution for CNTs production with (a) 0 g; (b) 0.2 g; (c) 0.5 g; and (d) 1 g Ni/Al ₂ O ₃ conditioning catalysts on the top	111
Figure 5.7 SEM results of the reacted Ni/AAO catalyst (A) 0.1/AAO; (B) 0.5/AAO; (C) 1.0/AAO and (D) 2.0/AAO.....	114
Figure 5.8 TEM results of CNTs for the reacted 0.1/AAO catalyst at different magnification	115
Figure 5.9 Mechanisms of CNTs growth using membrane-based catalyst	115

Figure 5.10 CNTs diameter distribution for different content of AAO membrane	117
Figure 5.11 SEM results of 0.1/AAO catalyst for CNTs growth at different temperatures. (A) 600 °C; (B) 700 °C; (C) 800 °C; and (D) cross-section for cracking boundary at 800 °C	118
Figure 5.12 DTG-TPO results of the reacted 0.1/AAO catalyst tested at 600 °C, 700 °C and 800 °C.....	119
Figure 5.13 SEM results of the reacted 0.1/AAO catalyst at 700°C with different rate of steam injected. (A) 2 ml h ⁻¹ and (B) 5 ml h ⁻¹	121
Figure 5.14 DTG-TPO results of the reacted 0.1/AAO catalyst tested with 0, 2 and 5 ml h ⁻¹ steam injection.....	122
 <i>Chapter 6</i>	
Figure 6.1 SEM results for original ceramic membrane (A) surface, (B) cross-section	127
Figure 6.2 XRD analysis for original ceramic membrane and fresh Ni/ceramic catalysts	129
Figure 6.3 TEM results and diameter distribution of NiO for (A) 0.1, (B) 0.5, (C) 1.0 and (D) 2.0 fresh Ni/ceramic catalysts	130
Figure 6.4 TPR analysis of the Ni/ceramic catalysts with different Ni content loadings (0.1, 0.5, 1.0, and 2.0 Ni mol/L)	130
Figure 6.5 SEM (left) results for CNTs synthesis at (A) 600 °C, (B) 700 °C and (C) 800 °C; TEM (right) results (i) 600 °C, (ii) 700 °C, (iii) 800 °C.....	134

Figure 6.6 DTG-TPO and DSC results of the spent 0.5/ceramic at 600 °C, 700 °C, and 800 °C	135
Figure 6.7 Trends of standard deviation (SD) of CNTs diameter and filamentous/amorphous carbon ratio at 600 °C, 700 °C, and 800 °C.....	139
Figure 6.8 SEM results of CNTs formation for 0.1/ceramic (A), 0.5/ceramic (B), 1.0/ceramic (C), and 2.0/ceramic (D) and corresponding TEM (i-v)	139
Figure 6.9 Diameter distribution comparison for fresh and spent 1.0/ceramic catalysts at 800 °C	140
Figure 6.10 DTG-TPO and DSC results of the spent 0.1/ceramic, 0.5/ceramic, 1.0/ceramic and 2.0/ceramic catalysts at 700 °C.....	142
 <i>Chapter 7</i>	
Figure 7.1 XRD and EDX-TEM analysis for original fresh Ni/sphere catalysts without Ni loading.....	144
Figure 7.2 Original sphere structure (A) sphere support schematic shape; (B) surface SEM image; (C) cross-section SEM image; (D) cross-section TEM image.....	145
Figure 7.3 Growth mechanism of CNTs on 1.0/sphere catalyst (A) fresh catalyst schematic image; (B) spent catalysts schematic image; SEM results for cross-section of spent catalysts at (C) 600 °C, (D) 700 °C, (E) 800 °C; SEM results for surface of spent catalysts at (c) 600 °C, (d) 700 °C, (e) 800 °C	146
Figure 7.4 TEM results for (A) 0.1 and (B) 1.0 fresh Ni/sphere catalysts.....	147
Figure 7.5 SEM, TEM results and diameter distribution CNTs for (A)(a) 0.1 and (B)(b) 1.0 spent Ni/sphere catalysts.....	150

Figure 7.6 DTG-TPO and DSC results of the spent 0.1 and 1.0/sphere at 800 °C	150
Figure 7.7 DTG-TPO and DSC results of the spent 1.0/sphere catalysts at 600 °C, 700 °C, and 800 °C.....	153
<i>Appendices</i>	
Figure A-A1 Waste plastics pellets (a) PP pellets (b)HDPE pellets.....	186
Figure A-A2 AAO membrane (a) blank membrane, (b) 1.0/AAO.....	187
Figure A-A3 Two-stage catalytic-pyrolysis reaction system.....	188
Figure A-A4 Scanning electron microscope (SEM) stereoscan 360	189
Figure A-A5 Transition electron microscope (TEM) JEOL 2010.....	189
Figure A-A6 X-ray diffraction.....	190
Figure A-A7 Thermogravimetric analyser (TGA) STA-780 Series	190
Figure A-A8 TA instruments, SDT-Q600	191
Figure A-A9 Broken AAO membrane during calcine process.....	191
Figure A-B1 Cross-section SEM result for original AAO membrane without Ni loading	192
Figure A-B2 XRD results for Ni/AAO catalysts with different Ni content	193
Figure A-B3 (A) TGA-TPO and (B) DTG-TPO results of the reacted Ni/AAO catalysts with different Ni content.....	193
Figure A-B4 TGA-TPO results of the reacted 0.1/AAO catalyst tested at 600 °C, 700 °C and 800 °C.....	193
Figure A-B5 TGA-TPO results of the reacted 0.1/AAO catalyst tested with 0, 2 and 5 mL h ⁻¹ steam injection.....	194

Figure A-B6 CNTs diameter distribution results of the reacted Ni/AAO catalysts with different Ni content (A) 0.1/AAO, (B) 0.5/AAO, (C) 1.0/AAO (D) 2.0/AAO	194
Figure A-B7 CNTs diameter distribution results of the reacted 0.1/AAO catalysts at different temperature (A) 600 °C, (B) 700 °C, (C) 800 °C	194
Figure A-B8 CNTs diameter distribution results of the reacted 0.1/AAO catalysts with different steam injection (A) 2mlh ⁻¹ (B) 5mlh ⁻¹	195
Figure A-B9 cross sectional SEM results of the reacted AAO catalyst with different Ni content. (A) 0.1/AAO; (B) 0.5/AAO; (C) 1.0/AAO and (D) 2.0/AAO catalyst...	195
Figure A-C1 TGA-TPO results of the spent 0.5/ceramic at 600 °C, 700 °C, and 800 °C	196
Figure A-C2 TGA-TPO results of the spent 0.1/ceramic, 0.5/ceramic, 1.0/ceramic and 2.0/ceramic catalysts at 700 °C	196
Figure A-C3 CNTs average diameter distribution for the spent 0.1/ceramic, 0.5/ceramic, 1.0/ceramic and 2.0/ceramic catalysts at 700 °C.....	197
Figure A-E1 Poster for H2FC supergen and Pyro 2016 conferences	201
Figure A-E2 Oral presentation prize for the 24 th annual SC-CSCST conference	202
Figure A-E3 Poster for Pyro 2018 conference.....	203
Figure A-E4 Poster prize for Pyro 2018 conference.....	204
Figure A-E5 online GC-MS.....	208
Figure A-E6 Certification for electron microscopy training.....	209
Figure A-E7 Catalytic pyrolysis of plastics with online GC	210

List of Tables

Chapter 1

Table 1.1 Carbon content in major commercial plastics (Zhuo et al., 2014).....	10
Table 1.2 Properties for different types of CNTs (Mittal et al., 2015)	12
Table 1.3 Examples of metal support carbon nanotubes/fibres catalysts used in different reactions (Pham et al., 2002)	18
Table 1.4 The increase of CNTs demand with in different application and regions (Dasgupta et al., 2011).....	25

Chapter 2

Table 2.1 Carbon structure formed over Fe catalysts with different substrate (Li et al., 1996; Sohn et al., 2001; Deng et al., 2002; Kichambare et al., 2002)	30
Table 2.2 Studies on Al ₂ O ₃ supported catalysts for CNTs synthesis (Danafar et al., 2009)	35
Table 2.3 Average diameter for CNTs and catalytic particles for different Fe content (Sinnott et al., 1999).....	43
Table 2.4 Production for different types of plastics pyrolysis (Anuar et al., 2016).....	51
Table 2.5 Gas composition and carbon production of pyrolysis-gasification of LDPE, PP and PS (Yao et al., 2018)	54
Table 2.6 The composition of production obtained by plastics pyrolysis (Borsodi et al., 2016)	55
Table 2.7 Mass balance for different catalyst : plastics ratio (Wu et al., 2010b)	56

Table 2.8 Studies on optimum temperature operated with different conditions for CNTs growth (Danafar et al., 2009).....	62
Table 2.9 The composition of the product gas at different decomposition temperatures (Liu et al., 2011).....	65
Table 2.10 CNTs length and growth change with different catalytic temperatures (Kim et al., 2005)	69
Table 2.11 Common techniques for CNTs analysis (Wepasnick et al., 2010)	75
 <i>Chapter 4</i>	
Table 4.1 Production of plastics waste by CVD over Ni/Fe-based catalysts.....	96
 <i>Chapter 5</i>	
Table 5.1 X-ray diffraction crystallite size measurements of NiO.....	106
Table 5.2 Overall view of experiments parameters and carbon deposition.....	107
 <i>Chapter 6</i>	
Table 6.1 ICP results of Ni/ceramic catalysts with different Ni contents.....	128
Table 6.2 Overall view of experiments parameters and carbon deposition.....	131
 <i>Appendices</i>	
Table A-A1 Ni/Fe-based catalysts calculations.....	186
Table A-A2 Molar mass reference.....	186
Table A-A3 AAO membrane catalysts calculations.....	187
Table A-A4 Ni/ceramic catalysts calculations.....	187
Table A-A5 Ni/sphere catalysts calculations.....	188
Table A-B1 EDX results of Ni/AAO catalysts with different Ni contents.....	192
Table A-E1 Conferences attended during PhD.....	200

Table A-E2 Training attended during PhD	205
Table A-E3 Compounds produced with the time from GC-MS analysis (mass:4.04 mg)	207

Thesis structure

This work is presented in eight chapters. Chapter 1 and 2 provide basic information on plastic waste background, CNTs materials introduction, synthesis methods, catalysts previous study, and current challenges relative to this research, in addition the main aim and objectives are stated. Chapter 3 is detailed experimental procedure including each group catalysts preparation, thermal chemical conversion process and catalyst characterization techniques. Chapter 4, 5, 6 and 7 are discussion and results for Ni/Fe-based; Ni/AAO, Ni/ceramic, and Ni/sphere catalysts, respectively. Among them, Chapter 4, 5, and 6 are the content which has been published by me as the first author. Then followed by conclusion and further study, (Chapter 8) and reference.

Appendices involved all the supply information in relation to experimental work and the whole PhD experience, contains 5 parts (A-E). Part A presents the reactor, analysis equipment, catalysts and some calculation involved in this study. Part B and C are the supply information which is corresponding to Chapter 5 and 6, respectively. Part D indicates papers published by me as first author (4 papers) and as co-author (3 papers); Finally, Part E lists all the conferences and training attended during the PhD study, including awards earned, posters presented and training content.

Chapter 1. Introduction

1.1 Plastic waste

1.1.1 Plastics history

Plastics materials are key enablers for innovation and contribute to the development of economy and society. First man-made plastic was designed by Alexander Parkes in Birmingham, UK in 1862 (Astrup et al., 2009). His studying developed successfully and widely among the manufacture area. After decades, a Belgian-American chemist, Leo Hendrik Baekeland, developed the first completely synthetic plastics (Astrup et al., 2009). In 1920, German chemist, Hermann Staudinger, hypothesised that plastics were composed of very large molecules held together by strong chemical bonds (Mwanza et al., 2017). This led an increasing research on plastics field. A vary of plastics research and new products were developed during the 1920s and 1930s, such as nylon, methyl and methacrylate (Mwanza et al., 2017).

Nowadays, plastic has become one of the most common materials. It is widely used in almost every aspect of our lives due to its relatively low cost, versatility and imperviousness to water. Packing (39.9%), construction (19.7%), automotive (10%) and electrical and electronic equipment (6.2%) contribute the most plastics demand; polyethylene (PE) is the highest share of plastics production by polymer types (Plastics Europe, 2017).

1.1.2 Composition and classification of plastics

Plastics is made up of a binder together with plasticisers, fillers, pigments and other additives (Al-Salem et al., 2009). The binder gives plastics the main characteristic. Binders are normally natural materials. Plasticisers are added to a binder to improve the toughness and flexibility of plastics. Fillers aim to improve properties such as hardness. Pigments work on imparting plastics' colour (Ragaert, et al., 2017).

Plastics can be classified into 'thermoplastic' and 'thermosets'. Thermoplastic is a plastic family that can be melted when heated and hardened when cooled. This type of plastics normally contains a linear or branched macromolecular structure. Thermoplastic group has fusible property, which can be re-heated and re-cooled (Singh et al., 2017). The plastic family is also treated as recycled plastics, including polyethylene terephthalate (PET), polypropylene (PP), polyethylene (PE) etc.. Thermosets is a family of plastics that undergo a chemical change when heated, and cannot be re-melted or reformed after heated or cooled. This family of plastics include polyurethane (PUR), vinyl ester, epoxy resins and etc.

This research only focuses on thermoplastic materials which mainly have 7 main families of plastics are: polypropylene (PP), low density polyethylene (LDPE), high density polyethylene (HDPE), polyvinyl chloride (PVC), polystyrene (PS), and polyethylene terephthalate (PET) (Singh et al., 2017).

1.1.3 Plastics demand and consumption

With continuous growth for more than 50 years, global plastics production increased to 336 million tonnes in 2016, about 2.8% increase compared to 2015, and nearly 48% compared to 2002 (Plastics Europe, 2017). Europe is the second largest producer of plastic materials, about 19% (Plastics Europe, 2017). In EU, there were more than 60,000 companies, produced about 60 M tonnes plastics in 2016 (Plastics Europe, 2017). The total European plastics demand was about 50 M tonnes in 2016, Figure 1.1 shows plastics demand by polymer types in the UK (Watch, 2003). The largest type of plastic used in the UK is LDPE. The main outlet for LDPE is plastics film which is used both in packing and non-packing applications. PP is the second largest usage in market, which is normally used for food packing, sweet and snack wrappers, containers, automotive parts, bank notes, etc. PVC is a group of polymer which can be processed into varieties of short-life or long-life products (Sadat et al., 2011). PVC is commonly used in window frames, profiles, pipes, cable insulation, garden house, etc., thereby it is discarded at a high rate (Janajreh et al., 2015). HDPE is basically made up of carbon and hydrogen atoms together to form a high molecular weight product. Plastic bottles are usually made by PET. It has excellent tensile and impact strength, chemical resistance, colour ability and good thermal stability.

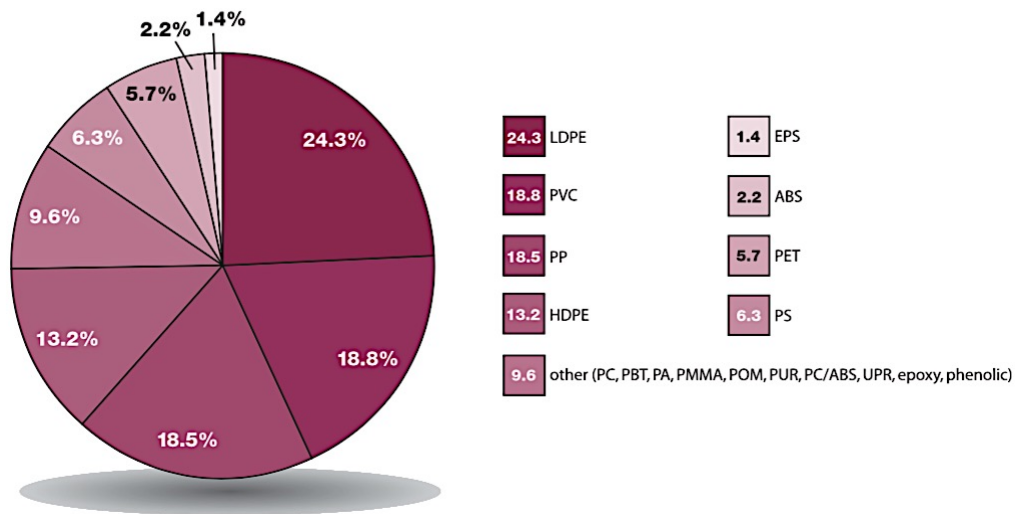


Figure 1.1 Plastics demand by polymer types in UK (Watch, 2003)

1.2 Plastics waste management

Waste management is necessary to minimise the plastic waste in order to reduce their negative impacts. In 2016, over 27 million tonnes of post-consumer plastic wastes were produced in the official waste streams (Plastics Europe, 2017). There are 3 methods to treat such large number of plastic waste: (1) landfill; (2) energy recovery; and (3) recycling. From 2006 to 2016, the volume percentage of plastic waste collected for landfill had decreased by 53%, recycling was increased by 74%, and energy recovery increased 71% (Figure 1.2) (Plastics Europe, 2017).

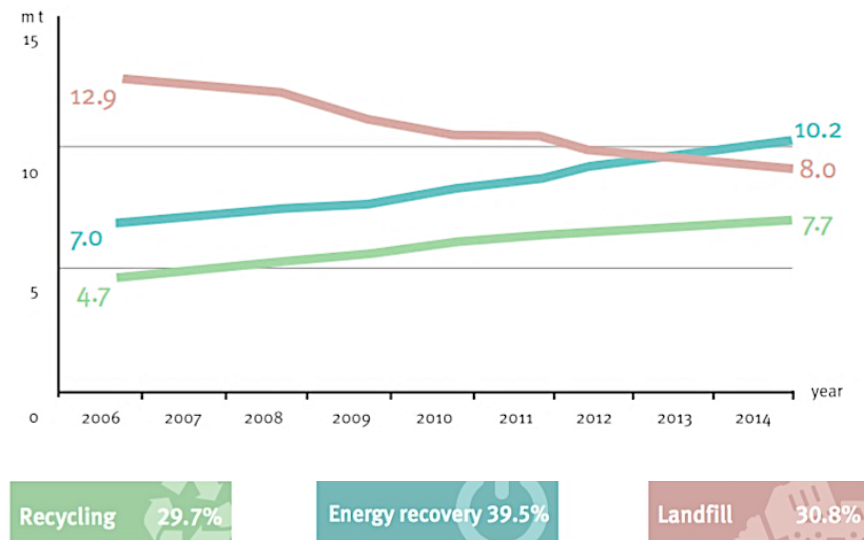


Figure 1.2 Percentages of different treatment methods for plastics waste from 2006 to 2016 (Plastics Europe, 2017)

1.2.1 Landfill

The increasing use of plastics brings benefits to society in terms of economic activity, jobs and quality of life. However, the impacts of plastic waste on our health and the environment are becoming apparent. Plastic wastes in landfill could have lots of negative impacts, mainly from the chemicals contained in plastic. Plastic is a non-biodegradable material; it can be remained as waste in the environments for decades even centuries. For example, in the marine environment, plastic waste has effects for the alteration of habitats and the transport of alien species (Science for environment policy, 2011). There are several chemicals within plastic material such as Bisphenol A, phthalates and flame retardants, which are all acknowledged to damage the endocrine system (Science for environment policy, 2011). Harmful chemicals from chlorinated plastic released into the surrounding soil, then may further seep into ground or other surrounding water ecosystem.

It can cause serious harm to aquatic species. There are also toxic monomers, which have been reported harmful for human health, linked to cancer and reproductive problems. Therefore, landfill is not a recommended treatment method for plastic waste management.

1.2.2 Energy recovery

Since 2006, energy recovery of plastics has attracted an increasing attention. In 2015, 59.6% of plastics were recovered, while in 2016 this number is increased to 61.9%, this growth shows a continuously strong trend (Plastics Europe, 2017). Energy recovery is a necessary, responsible and beneficial treatment method for plastic waste management, when plastics waste can't be sustainably recycled. Since, not all plastics can be recycled after consumption as their recyclability is affected by a variety of factors, for example the material composition of products. For some plastics waste after sorting and recycling operations, they can't always be recycled, energy recovery is the most resource efficient treatment method compared to landfill. Currently combined heat and power recovery plants (CHP Plants) use plastics waste together with other high calorific materials as a source of heat and power which is estimated to account for 10% of a country's energy needs (Barnes et al., 2009). The energy content of plastic is comparable with heating oil (42.6 MJ/l) (Kumar et al., 2011). Energy recovery of plastic waste provides an economic source of energy. However, in 2012 the EU Hazardous Waste Incineration Directive highly regulated the pollution control measures. Energy recovery of plastics waste yields toxic and noxious dioxins was noticed and carefully monitored (Kumar et al., 2011). Then,

many researchers start to recommend 'recycling' treatment method for waste plastics instead of 'energy recovery'.

1.2.3 Recycling

1.2.3.1 Mechanical recycling

Mechanical recycling was reported as the most common method for the recycling of plastic waste (Salem et al., 2009). Mechanical recycling is the recycle of materials from plastics waste while maintaining the polymers' molecular structure. This process is typically composed by collection, sorting, washing and grinding of the material (Ragaert et al., 2017). All types of thermo-plastics can be mechanically recycled without quality impairment. The composition of products, method and efficiency of plastics waste collected scheme; sorting and recycling technologies and the demand for plastics recyclers play important roles in determining types and amount of plastics waste which need to be mechanically recycled while ensuring environmental benefits and reasonable costs (Gu et al., 2016). At the moment, the most common sorting methods for mechanical recycling in UK is to sort the plastics into polymer type and colour (Gu et al., 2016). The techniques such as X-ray fluorescence, infrared and near infrared spectroscopy, electrostatics and flotation are normally used to sort plastics waste automatically (Ozbakkaloglu et al., 2016). Then, the sorted plastic is either melted down directly and produced into a new shape, or melted down after being shredded into flakes and then processed into granules called retranslate (Ragaert et al., 2017).

1.2.3.2 Chemical recycling

Chemical recycling of plastics waste is a recycling method which breaks down polymers into their constituent monomers that can be re-used for refineries, chemical production or petrochemical (Kumar et al., 2011). A widely variety of feedstock chemical recycling technologies are recently being explored such as pyrolysis, hydrogenation, gasification and thermal cracking. The production of plastics chemical recycling are majorly hydrocarbons, which can be further used either as fuels sources for heat and power generation; or as feedstocks for producing new materials.

Due to the high carbon contents existing in plastics (Table 1.1), waste plastics can therefore provide carbon sources for carbon-based value-added products by chemical recycling (Zhuo et al., 2014). The products include hydrocarbons, carbon black/activated carbon, carbon fibres, fullerenes, carbon nanotubes, and graphene. In particular, thermal-chemical recycling of waste plastics is a promising advanced technology. It has been reported that through high temperature pyrolysis (>800 °C) or gasification of waste plastics, hydrogen-enriched syngas was produced (Al-Salem et al., 2009). Syngas can be directly combusted for the production of heat and power. In addition, syngas can be converted to liquid fuel through Fischer-Tropsch process (Gershman, 2013). For example, Erkiaga et al. (2015) generated a syngas stream rich in H_2 from pyrolysis of plastic waste (HDPE) over Ni catalysts. Furthermore, co-production of carbon nanotubes (CNTs) from pyrolysis or gasification of waste plastics has also attracted interest.

Table 1.1 Carbon content in major commercial plastics (Zhuo et al., 2014)

<i>Polymer</i>	<i>Molecular formula</i>	<i>Carbon content (wt.%)</i>
polyethylene (PE)	$(C_2H_4)_n$	85.6
polypropylene (PP)	$(C_3H_6)_n$	85.6
polystyrene (PS)	$(C_8H_8)_n$	92.2
polyethylene terephthalate (PET)	$(C_{10}H_8O_4)_n$	62.6
Polyacrylonitrile (PAN)	$(C_3H_3N)_n$	67.9

1.3 Carbon nanotubes

1.3.1 Structure and properties

Carbon nanotubes (CNTs) were first reported in details by Lijima in 1991. CNTs have hollow cylinders of graphite sheet in the order of micrometres (1×10^{-6} m) and diameters in the order of nanometres (1×10^{-9} m) (Zhuo et al., 2014). A single-walled nanotubes (SWNTs) is a tube made of a rolled up cylindrical tube formed by the wrapping of single layer graphene; a multiwall nanotube (MWNTs) comprises several, concentrically arranged cylinders (Figure 1.3) (Zuo, 2018). On the basis of atomic arrangement there are three types of structures including zigzag, armchair and chiral structures (Figure 1.4).

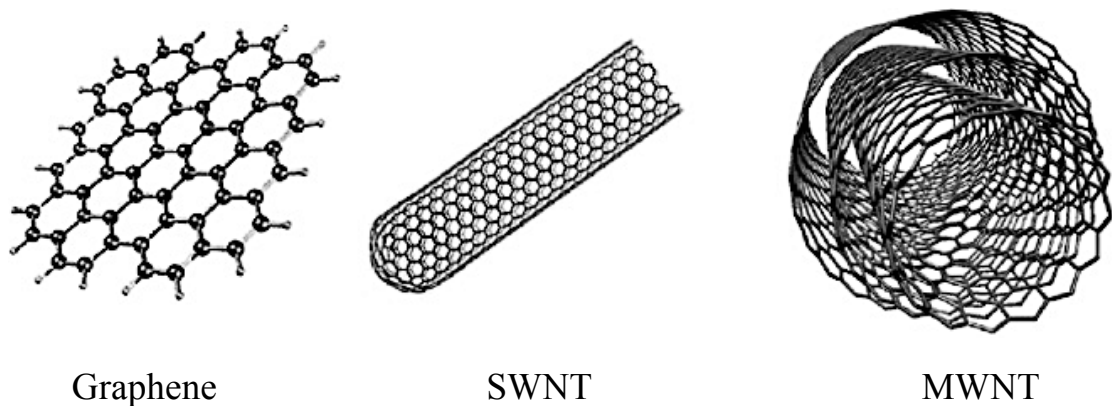


Figure 1.3 Carbon nanotubes structure and classification (Zuo, 2018)

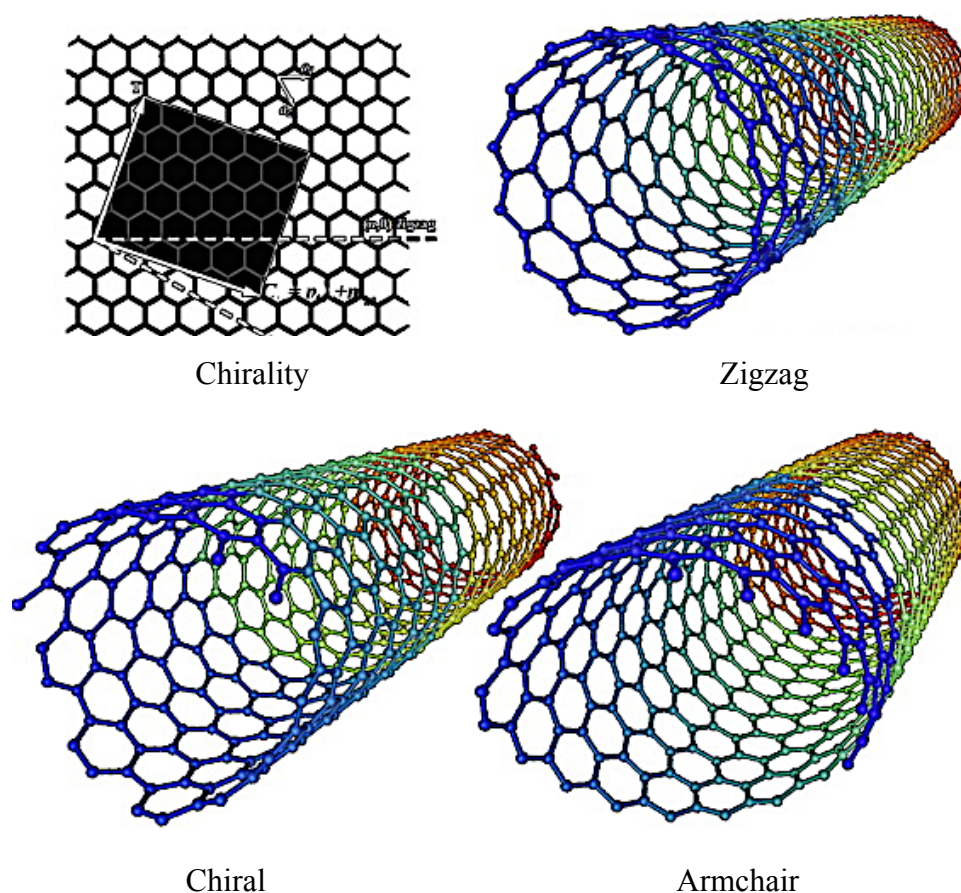


Figure 1.4 Molecular models of exhibited by SWNTs based on the chirality (Zuo, 2018)

Properties of carbon nanotubes highly depend on morphology, size and diameter. Table 1.2 summarises some properties of SWNT and MWNT (Mittal et al., 2015). The electrical property of CNTs depends on both chirality (armchair, zigzag or chiral) and tube diameter. CNTs could be either metallic (about 100 times more conductive than copper) or semi-conductive (Menon et al., 2000). SWNTs with zigzag structure are normally semi-conductor, but armchair SWNTs are metallic. The electrical properties of MWNTs are more difficult to predict because of their complexity structure. CNTs have excellent and unique mechanical properties namely high Young's modulus, high tensile strength, high aspect ratio, low density, etc. SWNTs have high tensile strength, more than 100 times that of the stainless steel. They were reported having the most resistant fibres with a

Young modulus of 2.8–3.6 TPa and 1.7–2.4 TPa for SWNTs and MWNTs (Serp et al., 2003), respectively and a resistance to traction of 250 GPa (Mittal et al., 2015). CNTs are also flexible, which can be bent several times at 90° without structural changes and the structure of CNTs materials is not easily changed even at high pressure (over 1.5 GPa) (Esteves et al., 2018). Furthermore, CNTs have high thermal stability and thermal conductivity. The thermal stability of CNTs is an important aspect to enable their applications under different thermal conditions.

Table 1.2 Properties for different types of CNTs (Mittal et al., 2015)

<i>Property</i>	<i>SWCNT</i>	<i>MWCNT</i>
Type of CNTs		
Specific gravity (g/cm ³)	0.8	1.8
Electrical conductivity (S/cm)	10 ² -10 ⁶	10 ³ -10 ⁵
Electron mobility (cm ² /(Vs))	10 ⁵	10 ⁴ -10 ⁵
Thermal conductivity (W/(mK))	6000	2000
Coefficient of thermal expansion (K ⁻¹)	Negligible	Negligible
Thermal stability in air (°C)	> 600	> 600

1.3.2 Applications of CNTs

Due to CNTs have excellent and unique chemical, mechanical, thermal and physical properties, they have been widely explored for applications in various areas. Figure 1.5 shows different applications of CNTs for present, short-term and long-term (Mittal et al., 2015). Some common applications of CNTs will be introduced in this section.

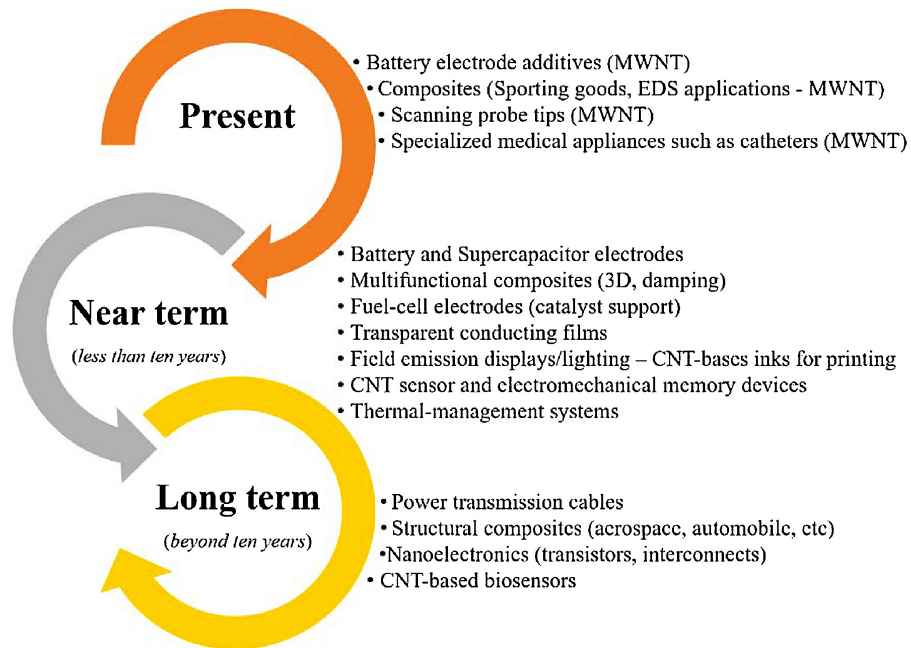


Figure 1.5 CNTs applications for present, near term, and long term (Mittal et al., 2015)

1.3.2.1 Lithium battery

Batteries development with small sizes but high capacity for energy storage and multi-functions for various applications such as electric vehicles, and electronic devices are very important. The lithium battery which contains lithium as lithium ions or metal lithium shows great advantages in high energy battery applications and is widely used. CNTs is acknowledged having ability to improve the battery performance to in lithium battery systems, due to their outstanding electric and mechanical properties.

CNTs have been developed and used in different types of batteries, including Li-ion, Li-S, and Li-air batteries. These batteries can store and release energy by ions transformation between the cathode and anode electrodes. Carbon materials (e.g. meso-carbon microbeads and vapor grown carbon fiber) play an important role in the commercialization of Li-ion batteries (Endo et al., 2001). CNTs were reported to enhance

the performance of Li-ion batteries with its outstanding electronic, thermal, and mechanical properties (Ji et al., 2011). They can be used directly as anode side materials of Li-ion batteries with high capacities, as well as cathode side materials, commonly contributing as conductive additives. CTNs materials have high aspect ratios which can effectively develop blocks in constructing conductive networks incorporation with active electrode materials. During cycling process, these blocks provide the electrodes with a stable structure which can be against the volume fluctuation (Kaskhedikar et al., 2009). For example, the performance of silicon electrode can be greatly enhanced with CNTs addition by simple mechanical synthesised method. Compare to original silicon electrode with 300 mAh g⁻¹ capacity and failed after 10 cycles, silicon/CNT electrodes which were made by ball milling method showed a capacity of 1200 mAh g⁻¹ and an initial coulombic efficiency of 80%, which were much higher than the original ones (Kaskhedikar et al., 2009). CNTs can also be added to other metal oxides such as SnO₂, TiO₂, Co₃O₄, MnO₂, Fe₃O₄ to form high efficient anodes by different methods like ball milling, hydrothermal process and electrodeposition (Xiao et al. 2013). For instance, Fe₃O₄/CNTs composites can be obtained by the co-dispersion of Fe₃O₄ nanoparticles and CNTs in liquid following by the filtration, the composites show better performance compared with Fe₃O₄/carbon black composites on both the specific capacity and stability (Ban et al., 2010).

1.3.2.2 Supercapacitor

CNTs can also be used in supercapacitor which is a device with high power density and long cycling stability (Schnorr et al., 2011). CNTs are constructed with sp² hybridized carbons which have high chemical stability, high voltage and high current; they are also

hexahedral which can allow ions to access easily. It was proposed that the presence of mesoporous due to the central canal of CNTs allowed an easy accessibility of the ions to the electrode/electrolyte interface for charging the electrical double layer (Frackowiak et al., 2000) (Figure 1.6). In addition, CNTs are highly electrical conductive which could decrease the resistance. Therefore, CNTs are considered as ideal materials for producing capacitor to next generation electrode. There are two ways to increase the capacity of CNTs electrode: (1) modify the CNTs surface by acid or base treatment; (2) construct composites or hybrid electrodes with other active materials, such as the metal oxides (e.g. RuO_2 , MnO_2 , Fe_2O_3 , NiO , Co_3O_4 , V_2O_5), the conductive polymers (e.g. polyaniline and polypyrrole), or conventional activated carbon (Izadi et al., 2010; Zhang et al., 2013).



Figure 1.6 Electrode/electrolyte interface for charging the electrical double layer (Izadi et al., 2010)

1.3.2.3 CNTs-based composites

CNTs are excellent nanofillers for composites because of their superior thermal, electrical and mechanical properties. For example, the low mass of CNTs loading leads to light weight of nanocomposites, and higher strength. In addition, CNTs exhibit high electrical

and thermal conductivity which can enhance the charge and heat transportation of composites. The development of composites with CNTs addition could increase the commercial value and extend materials' applications. CNTs are widely used as reinforcements in high strength, light mass and high performance composites, including applications in sport gears, spacecraft and aircrafts. Current studies of CNTs-based composites mainly focus on CNTs/polymer, CNTs/metal and CNTs/ceramic. The most popular studied CNTs/polymer include polyurethane (PU), Nylon, polyaniline (PANI), polycarbonate (PC), PS, PET, PP and so on (Zhang et al., 2013). Jia et al. (2012) reported the tensile strength and elongation of nanocomposites reached 156.4 MPa and 140%, respectively with 0.27 wt.% CNTs into a PI matrix, which were increased by 90% and 250%, respectively, compared with the values of pristine PI (polyimide), and the toughness of the nanocomposites was improved by 470%. CNT/ceramic composites are widely used as tough materials, it's expected the composites have excellent toughness, high creep resistance and good thermal stability by combining CNTs with ceramics. The electrical conductivity of CNT/ceramic composites is also reported to have significant enhancement, as the interconnected CNT network provides conducting path (Rul et al., 2004). CNTs have also been investigated to reinforce metal matrices such as Al, Ni, Cu or Mg for further aerospace and automobile applications (Zhang et al., 2013). He et al. found the strength of compressive yield had a 350% increase with 1.6 vol.% CNT addition to Al material, a 184% increase in tensile strength and a 33% increase in hardness with 6.5 vol.% CNTs addition (He et al., 2007). The electrical resistivity of CNT/metals composite increased as CNTs clusters contributed to the interfacial area and strain in matrix (Zhang et al., 2013).

1.3.2.4 Catalysts support

The development of carbon-based catalysts has been reported to improve catalytic performance (Zhang et al., 2017). Carbon materials can be used as catalytic supports due to the following properties: inertness for some reactions, good mechanical properties, porosity structure, and the possibility of being adjusted in different forms with a required size and shape for different applications (Esteves et al., 2018). For example, CNTs can be tailored in different structure such as sphere, powder and extrudates; CNTs materials show good resistance within acid or basic environments; the porosity and hydrophobic can be controlled by changing their surface chemistry; CNTs also show high thermal and mechanistically stabilities; and the possibility of turning the specific metal-support interaction which has effect on activity of catalysts (Pérez et al., 2016). However, CNTs also suffer from some disadvantages, including (1) carbon materials are difficult to use within high temperature environment, (2) it's difficult to achieve high preparation reproducibility as uncontrolled amounts of carbon obtained in different batches for same materials (Esteves et al., 2018).

CNTs have been studied as catalysts support in different reactions and classified in groups as followed: hydrogenation-dehydrogenation, oxidation-reduction, combination and decomposition, dehydration, isomerization, polymerization, and Fischer-Tropsch reaction (Serp et al., 2003). Table 1.3 summarises some studies on CTNs and nanofibers supported catalysts, the researchers mainly focused on effect of CNTs addition on catalysts activity. For example, the synthesis of carbon nanofibers with a controlled diameter of about 50 nm had been achieved at 550–650 °C by the decomposition of ethane on a CNTs

supported nickel catalyst. Higher purity and yield had been produced with CNTs added to the catalysts (Pham et al., 2002). Savva et al. (2010) presented work on H₂ and secondary CNTs production from catalytic decomposition of ethylene over different metals/CNTs catalysts. The activity was found to decrease in the order Co > Fe > Cu.

Table 1.3 Examples of metal support carbon nanotubes/fibres catalysts used in different reactions (Pham et al., 2002)

<i>Reaction</i>	<i>Catalysts</i>
Hydrogenation of crotonaldehyde	Ni/GNF-P, Ni/GNF-R
Hydrogenation of cinnamaldehyde	Ru/GNF, Pd/GNF
Partial hydrogenation of 3-methy-2-butenal	Pt/SWNT
Benzene hydrogenation	Ni/CNT
Dehydrogenation of cyclohexanol	Co/CNT
Hydrogenation of cinnamaldehyde	Pd/MWNT
Fischer-Tropsch reaction	Nb-Co-Fe/CNT, Co/CNT, Co/GNF, Fe/K/Cu/CNT, Co-Fe/CNT, CNT-Al ₂ O ₃

1.3.3 Synthesis of carbon nanotubes

1.3.3.1 Arc discharge

Lijima (1993) reported CNTs production through an electric arc discharge technique, a general schematic reactor was shown in Figure 1.7. The arc discharge technique has anode and cathode which are made of high purity graphite rods, these two rods are brought together within a helium atmosphere condition and a voltage is applied until a stable arc is achieved (Thostenson et al., 2001). The size of the graphite rods controls process variables. As the anode is consumed, adjusting the position of the anode can keep

a constant gap between the anode and cathode. Then, the material deposits on the cathode could contain CNTs and other carbon particles. A small amount of metallic catalyst particles is normally doped on the electrodes to produce single walled nanotubes. For example, Bethune et al. (1993) produced CNTs which had very small diameters (about 1.2 nm) and walls only one single atomic layer thick by vaporizing carbon and cobalt in an arc discharge reactor. Shi et al. (2000) produced SWCNTs with high yield in quantity of tens of grams per day by operating a graphite rod with a hole filled with a mixture of Y–Ni alloy powder and graphite or calcium carbide and nickel as anode, under the arc conditions of 40~60 A d.c. and helium pressure of 500 or 700 torr. A group of platinum metals (such as Ru, Rh, Ir, Pt, Pd, Os) within carbon nano-capsules were studied to synthesise of SWCNTs by arc discharge technique; only Rh, Pd, and Pt showed catalytic activity for SWCNTs growth (Saito et al., 1996).

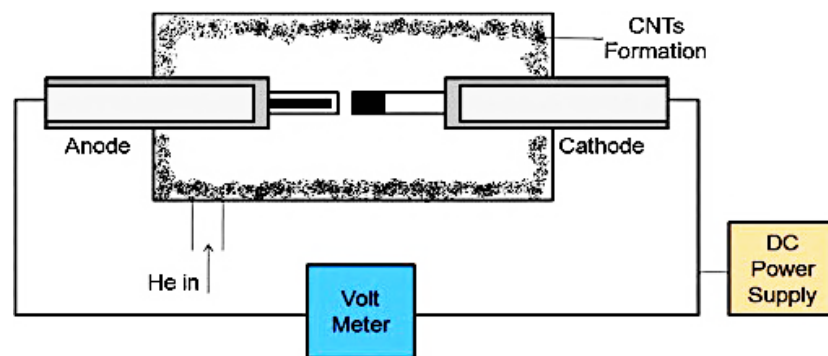


Figure 1.7 General schematic reactor for CNTs synthesis by arc discharge (Bethune et al., 1993)

1.3.3.2 Laser ablation

Laser ablation technique was initially used for fullerenes synthesis, and then improved to allow CNTs productions. In this technique, a laser is operated to vaporize a graphite target rod within a controlled atmosphere oven at high temperatures (about 1200 °C). The general laser ablation reactor is shown in Figure 1.8 (Mubarak et al., 2014). The graphite target rod is normally doped with cobalt or nickel catalysts to produce SWNTs, and the condensed material is then collected on a water-cooled target. For example, Thess et al. (1996) synthesised over 70% in yields of SWNTs by condensation of a laser-vaporised carbon-nickel-cobalt mixture at 1200 °C. Zhang et al. (1999) investigated nickel and cobalt catalysts on SWCNTs production from fullerene materials at 400 °C by laser ablation method. It was suggested that SWCNTs formation was controlled by both the availability of proper precursors and the activity of the metal catalyst (Zhang et al., 1999).

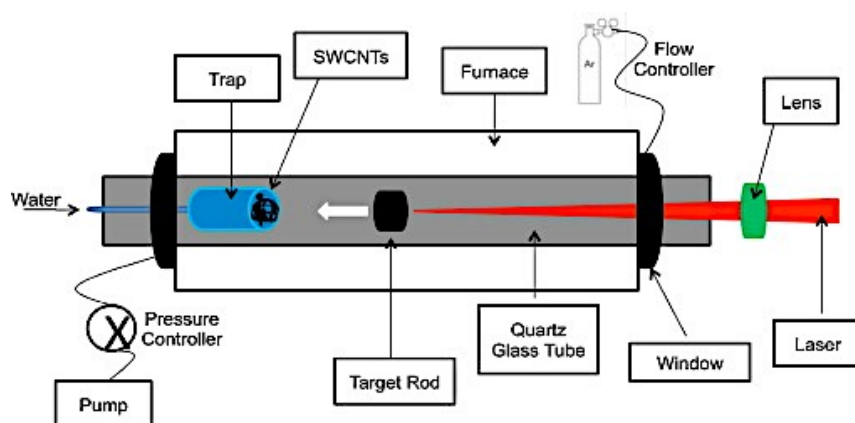


Figure 1.8 General schematic reactor for CNTs synthesis by laser ablation (Zhang et al., 1999)

Both arc discharge and laser ablation can synthesise CNTs with high quality. However, these two techniques suffer from the following four disadvantages which limit CNTs

production: (1) For some applications of CNTs such as composites, large scale of CNTs are required, arc discharge and laser ablation synthesis techniques have scale-up limitation, thus would make the cost of CNTs production increase; (2) Both techniques require solid carbon/graphite as target which can be evaporated for CNTs production. But for large scale industrial process, it is difficult to get such large graphite to be used as target; (3) Both methods grow CNTs with highly tangled form, mixed with other types of carbon. The by-products of these techniques include fullerenes, graphitic polyhedrons with enclosed metal particles and amorphous carbons. Therefore, the CNTs produced by these two methods require additional purification step to obtain purified and assembled CNTs. The addition step will largely increase the cost. (4) The growth temperature of both methods is higher than other CNT production technique, as a result more energy is needed for these processes.

1.3.3.3 Chemical vapour deposition

Chemical vapour deposition (CVD) is currently the most common widely accepted in the synthesis of CNTs, due to its simplicity and low cost. CVD is a method that nanotubes are formed by the deposition of carbon contained gases with the presence of catalyst. CNTs can be produced continuously by this technique since carbon sources can be replaced by flowing carbon-containing gases. There are mainly two processing systems for CVD method, horizontal (Figure 1.9) (Mubarak et al., 2014) and vertical (Figure 1.10) (Danafar et al., 2009). In the synthesis of CNTs by CVD method, catalyst is placed in furnaces. After furnaces are heated to the target reaction temperature (normally between

600 °C and 1200 °C), hydrocarbon gases (such as ethylene, methane, acetylene etc.) and a carrier gas (nitrogen, hydrogen, argon) is introduced to reactor for a given time period (usually 15–60 mins). CNTs keep growing on the catalytic particles while the decomposition of the carbon precursor takes place, then they can be collected after cooling the system to room temperature.

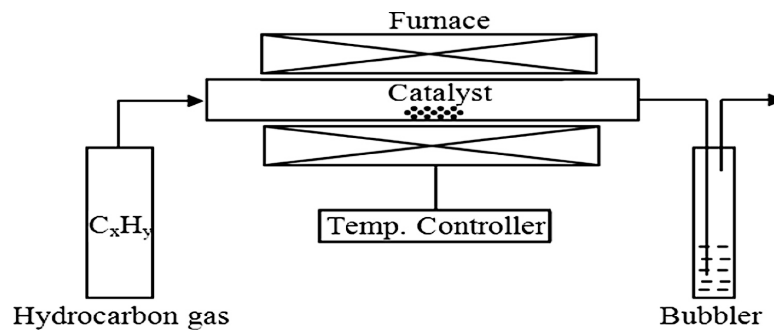


Figure 1.9 Schematic reactor of a horizontal CVD setup system (Mubarak et al., 2014)

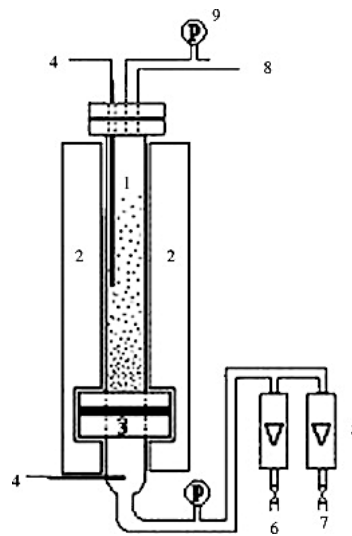


Figure 1.10 Schematic reactor of a CVD vertical setup system. (1) reactor, (2) furnace, (3) distributor, (4) thermocouple, (5) rotameter, (6) carbon source, (7) carrier gas, (8) outlet, (9) pressure sensor (Danafar et al., 2009)

The most common carbon sources are hydrocarbon gases such as methane, acetylene, ethylene, propylene, benzene, methanol, ethanol, camphor, xylene, cyclohexane, and carbon monoxide (Dasgupta et al., 2011). For example, Lee et al. (2001) produced vertically aligned CNTs on Fe/SiO₂ by CVD of acetylene gas at the temperature range 750-950 °C. CNTs were synthesised using CVD of ferrocene and acetylene over silicon substrate, kinetic model of CNTs grown was studied (Kim et al., 2005). The role of water vapour in CNTs formation via CVD method of methane was investigated by Lee et al. (2012). The usage of CVD method for CNTs synthesis is benefited from several advantages, including (1) CVD is a simple, economical, controllable and scalable technique compared to arc discharge and laser ablation. It can be used for industrial large scale CNTs production. (2) the carbon source can come from plenty of hydrocarbons including solid, liquid or gas for. (3) CNTs grown by CVD can be in different forms like aligned, straight, entangled or others, depending on the different parameters used in the system.

Plastic waste also attracts interest as a carbon source for CNTs production, due to its economic benefit. Catalytic pyrolysis of plastics produces hydrocarbon gases which could be used for CNTs synthesis. For example, Park et al. (2010) optimised operation conditions with Ru-based catalysts from waste plastic, in order to decrease the coke formation and increase the carbon conversion. Liu et al. (2011) used a two-stage reactor to convert PP into CNTs and hydrogen-rich gas with HZSM-5 as catalysts, and an optimum temperature (700 °C) was proposed. It was reported the production of CNTs and syngas study from different types of plastics with varies of catalysts (Wu et al., 2009b; Liu et al., 2011; Acomb et al., 2016). Thermochemical recycling of waste plastics can

produce other valuable materials, refers to an advanced technology process (Al-Salem et al., 2009). During this process, hydrogen-rich syngas is generated at high pyrolysis temperature ($>800\text{ }^{\circ}\text{C}$) or gasification of waste plastics. For example, Erkiaga et al. (2015) generated a syngas stream rich in H_2 from pyrolysis of plastic waste (high density polyethylene) with Ni catalysts. Syngas can be widely applied, including directly combusted for the production of heat and power, or conversion into liquid fuels through Fischer-Tropsch process (Gershman, 2013).

1.3.4 CNTs commercial value

CNTs are sold in tiny research quantity for hundreds or thousands dollars per gram decades ago, the higher purity costs more. In order to meet the growing demand, more companies have started entering the market for CNTs production. Thus the price fell to thousand dollars per kilogram. Table 1.4 summarises the increase of CNTs demand in different applications and regions (Dasgupta et al., 2011). From 2011 to 2016, the total production capacity of carbon nanotubes all over the world became twice, grew from about 10000 tonnes in 2011 to 20000 tonnes in 2016 (Wire, 2017). Carbon nanotubes market by area of applications changes from one region to another. At the beginning, North America and Europe were the two leading markets for CNTs. The rapidly growth of electronic and automobile sectors in Asia-Pacific region drives the carbon nanotube market to the top of CNTs region. In North America, Europe and other regions, carbon nanotube market is dominated by polymer and chemical industries. In 2016, the global CNTs market was USD 2.17 billion and is estimated to reach USD 5.63 billion by 2022

(Research and Market, 2017). The potential carbon nanotubes markets bound to grow exponentially. The demand for carbon nanotubes is estimated grow annually at an approximate rate of 20% in the coming years (Wire, 2017).

Table 1.4 The increase of CNTs demand with in different application and regions
(Dasgupta et al., 2011)

	<i>2004</i>	<i>2009</i>	<i>2014</i>
Total demand (\$ Millions)	6	215	1070
<i>By type</i>			
SWNT	0	95	600
MWNT	6	120	470
<i>By end-use</i>			
Electronics	0	90	395
Automotive	1	31	165
Aerospace/Defence	0	10	65
others	5	84	445
<i>By region</i>			
U.S.	2	57	290
Western Europe	1	32	180
Asia/Pacific	3	113	500
Other	0	13	100

1.4 Research aim and objectives

1.4.1 Research aim

Catalytic-pyrolysis of plastic waste provides an environmental friendly and economic method to produce valuable products such as H₂ rich syngas and CNTs. However, the quality and quantity of CNTs improvement is a challenge. The quality of CNTs can

significantly affect and limit their applications. The aim of this research is to improve the quantity and quantity of CNTs by developing different catalysts.

1.4.2 Research objectives

- (1) To investigate the influences of the types of metal (Fe and Ni) and the particle size of the metals on the catalyst in relation to the production of CNTs and hydrogen from thermo-chemical conversion of waste plastics.
- (2) Ni-based AAO catalysts were investigated to produce CNTs from pyrolysis/gasification of waste plastics aiming to generate high quality CNTs with uniform distributions of diameters. In addition, the influences of metal loading, conditioning catalysts, reaction temperature and steam injection were studied to optimise the process conditions.
- (3) Experimental conditions (both reaction temperature and Ni loading) were studied by using ceramic membrane as catalysts to determine the optimal conditions for the production of high quality CNTs, which is reflected by a narrow distribution of CNTs diameter.
- (4) Investigate the influences of the Ni content and reaction temperature in relation to the production of CNTs from thermo-chemical conversion of waste plastics over sphere supported catalysts.

Chapter 2. Literature review

2.1 Catalyst for CNTs growth

Catalyst plays a significant role in the CVD synthesis of CNTs. Therefore, improving the characteristic of catalysts will enhance both the quantity and quality of CNTs production. However, the coke carbon formed on the catalysts surface and catalysts sintering are the two main challenges for the catalysts development for CVD synthesis of CNTs. The catalysts used for CVD synthesis of CNTs formation normally consist of active sites and substrates. Either chemical or physical interaction between the active site and support of catalysts is significant for the catalytic properties of particles thus CNTs production. The chemical interaction can contribute to maintain the size distribution of catalysts particles during CNTs synthesis. An over strong chemical interaction causes a decreasing mobility of particles, leading to the catalysts growth limitation. The physical interaction between active sites and support (such as Van Der Waals or electrostatic forces) with obstruction of catalysts movement on the support surface due to its roughness, reduce the thermally driven diffusion and sintering of transition metals. This has effect on the stabilization of catalysts particle size distribution (Anna et al., 2003).

2.1.1 Active sites for CNTs growth

The peculiar ability of active sites is strongly related to following three factors: (1) catalytic activity for decomposition of carbon (2) diffusion of carbon through and over metal particles (3) ability of metastable carbides formation (Danafar et al 2011). The active nanoparticles are employed either in oxide or metallic forms. Nickel, iron, and cobalt are reported as the most effective catalytic sites due to their high solubility and

high diffusion rate of carbon. For example, Lee et al. (2003) compared the performance of Ni, Co and Fe based catalysts for CNTs growth from mixed gases. Fe was found to be the most active catalyst for CNTs growth under CO/NH₃ gas flow with a ratio of 18. Ago et al. (2006) also investigated the effect of these three active metals (Fe, Co and Ni) on CNTs formation from methane by CVD. Figure 2.1 shows the methane conversion and carbon deposition with reaction time for different metal based catalysts. The conversion was the highest at the beginning, and then decreased. For the whole process, the Fe/MgO shows the highest methane conversion and in the first minute, the highest value is 38%. However, the curve drops down within 2.5 mins, this indicates that Fe was active for methane conversion, but with short active life time. The carbon yield also was estimated in Figure 2.1 by TPO analysis. Carbon production over the Fe/MgO is more graphitic than the Co/MgO, as carbons formed on Co catalysts starts to oxidise at low temperature about 300°C. This suggests Fe was preferable for filamentous carbon and prevents the formation of amorphous carbon. The Fe/MgO catalyst also produced the highest yield of CNTs according to TPO results.

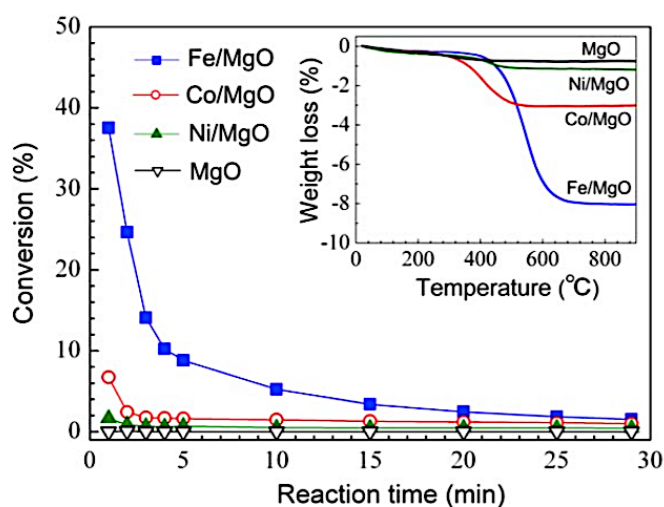


Figure 2.1 Methane conversion and carbon deposition for different metals based catalysts (Ago et al., 2006)

2.1.1.1 Fe-based catalysts

As the most effective active metal of CNTs synthesis catalysts, Fe-based catalysts were attracted interest by many researchers. For example, Seah (2012) studied single-walled CNTs which was produced from ethanol by Fe/SiO₂ catalysts. Hsieh et al. (2009) worked on the synthesis of multi-layered carbon nanotubes (CNTs) using the catalytic decomposition of acetylene at 700–850 °C over Ni/Al₂O₃ catalysts. The results showed that the CNTs grown in a fluidised bed reactor had higher production yield and better thermal stability, compared to those synthesised in fixed bed reactor. Table 2.1 shows different studies working on Fe-based catalysts. Carbon production with different carbon structure was presented (Li et al., 1996; Sohn et al., 2001; Deng et al., 2002; Kichambare et al., 2002).

Table 2.1 Carbon structure formed over Fe catalysts with different substrate (Li et al., 1996; Sohn et al., 2001; Deng et al., 2002; Kichambare et al., 2002)

<i>Active metal</i>	<i>Substrate</i>	<i>Formation of carbon structure</i>
Fe	Mesopous Si	MWCNTs
Fe	Porous Si	MWCNTs
Fe	Si	CNF
Fe	SiC on Si	CNTs
Fe	SiO ₂	CNTs
Fe	SiO ₂ on Si	CNTs

2.1.1.2 Ni-based catalysts

Nickel-based catalysts having good catalytic activity and a relatively low price are widely used for hydrogen production and CNTs from thermo-chemical conversion of plastics waste. Ni catalysts supported on different metal oxides including Al_2O_3 , ZrO_2 , TiO_2 , MgO and Ce_mO_2 and Cu/Mg/Al have been investigated with the aim to reduce the formation of coke on the surface of the reacted catalyst (Wu et al., 2009a, 2009d, 2010a). Alberton et al. (2008) synthesised filamentous CNTs from ethanol with Ni/ Al_2O_3 as catalysts. Zhao et al. (2011) produced CNTs with uniform diameter and high quality using Ni-loaded catalysts from the reforming of ethanol. Wei et al. (2008) reported that a catalyst with Ni addition had an increased catalytic stability due to the high activity and stable phase of Fe-Ni alloy formation.

2.1.1.3 Bi-metal and tri-metal based catalyst

Bi-metal and tri-metal based catalysts were also studied to increase CNTs production. Ni-Al (molar ratio 1:2) and Ni-Mg-Al (molar ratio 1:1:2) catalysts were found to show the most enhanced catalytic effectiveness in terms of H_2 and the prevention of coke formation (Wu et al., 2009c, Kumagai et al., 2015; Nahil et al., 2015). Yao et al. (2018) studied the Ni-Fe catalysts for catalytic pyrolysis of real-world waste plastics to produce CNTs and hydrogen. They found the Ni-Fe/ $\gamma\text{-Al}_2\text{O}_3$ had optimum interaction between metal and support, resulting in a higher yield of H_2 and better quality of CNTs produced compared with monometallic Ni and Fe catalysts. Fe-Co bimetallic catalysts supported on CaCO_3

were used as catalysts by Mhlanga et al. (2009) to improve the quality of CNTs with decreasing synthesis time from acetylene. CNTs with outer diameter of 20-30 nm and inner diameter about 10 nm have been successfully produced. Wu et al. (2011) produced high quality of CNTs from waste polypropylene with NiMnAl as catalysts. They reported that the increase of molar ratios of element Mn promoted carbon yield from 46.6% to 57.7%. Ni-Al catalysts doped with Ca and Zn have been investigated for both hydrogen and CNTs production from waste plastics (Shah et al., 2016). Compared to the Ni/Ca-Al catalyst, the Ni/Zn-Al catalyst have been reported to produce higher yield of H₂, but with less production of CNTs, due to the promotion of catalytic interactions between steam and carbon containing compounds (Kumagai et al., 2015; Shah et al., 2016).

2.1.1.4 Other metal based catalysts

Catalysts apart from these common catalysts, some other types of metals have been studied for CNTs formation, such as Cu, Ru, Mn and Cr. For example, Fonseca et al. produced well graphitised structure of CNTs with high activity from C₂H₂ over Cu/zeolite. Ru-based catalysts were used to study CNTs formation by catalytic CVD with acetylene as the carbon source (Popovska et al., 2011). However, these metals are less commonly used for CNTs production.

2.1.2 Catalytic support for CNT growth

The support of catalysts also significantly influences the CNTs growth. It is suggested that support with larger surface areas will promote the CNTs nucleation and growth (Danafar et al., 2011). The ability of substrates are also related to three factors: (1) ability

to improve the active phase; (2) to prevent catalytic sintering; and (3) ability to improve mechanical strength (Danafar et al., 2011). Various catalytic substrates have been widely used for CVD of CNTs synthesis, such as silicon dioxide, alumina, quartz, calcium carbonate, zeolite and etc. (Li et al., 2004; Mhlanga et al., 2009). The surface morphology and texture properties of substrates are reported to affect the yield and quality of CNTs formation (Shah et al., 2016). It is reported that at 700 °C growth temperature, the carbon production was increased in order of calcium < titania < silica < zeolite < ceria < alumina (Shah et al., 2016). Aluminium oxide substrate was found having a superior support and highly strong chemical interaction between aluminium oxide and metals than others (Anna et al., 2003). In addition, the physical properties (eg. thickness and structure) of support are also important. Varying the catalytic support influences the morphology of the catalytic metal cluster, and as a result, the chiral angle of the CNTs produced. This effect has been explained in terms of the energetics of the nanotube caps and the kinetics of their formation (Lolli et al., 2006).

2.1.2.1 Silicon oxide support

Lolli et al. (2006) used CO as a feed over Co-Mo/SiO₂ catalysts to form SWNT. Different parameters have been studied such as gaseous feed composition, the reaction temperature. The increasing temperature was found resulting in an increase in CNTs diameter without a change in the chiral angle. Similar SiO₂ supported catalysts were also studied by Kitiyanan et al. (2000). A group of Co–Mo/SiO₂ catalysts were reported to be able to produce SWNT with high selectivity, depending on the Co:Mo ratio, the reaction temperature, and the processing time. High quality of SWNTs was achieved over silica

supported catalysts from CVD of methane by Franklin et al. (2001). And the synthesis of 4 cm long SWNTs with a high growth rate of $11 \mu\text{m/s}^{-1}$ by catalytic chemical vapour deposition over SiO_2 supported catalysts (Zheng et al., 2004).

2.1.2.2 Aluminium oxide support

The interaction effects between reaction temperatures, catalytic properties, fluidization conditions, and deposition time during carbon nanotube (CNT) synthesis by chemical vapour deposition were investigated by See et al. (2008) over Fe-Co/ Al_2O_3 catalysts. The interaction parameters including temperature-time and temperature-catalyst were found having significantly effect on the resultant CNT yields. A 2.5% Fe/ Al_2O_3 was used to study catalytic growth of multi-walled CNTs from ethylene in a fluidised bed reactor. High purity MWCNTs have been obtained after catalyst dissolution and the kinetics of MWCNTs growth was found faster with the catalyst used (Morançais et al., 2007). Philippe et al. (2009) loaded Fe^{+3} metal particles inside the porosity of alumina support and a micrometric crystalline $\alpha\text{-Fe}_2\text{O}_3$ surface film. The CNTs grew aligned between the alumina support and the Fe_2O_3 catalytic surface film, resulted a uniform consumption and uprising of the film. When the catalytic film was consumed, the iron catalytic particles inside the Al_2O_3 support porosity were slowly reduced and activated resulting a secondary MWNTs formation, producing a generalised grain fragmentation and entangled MWCNT growth. Other studies on Al_2O_3 supported catalysts for CNTs synthesis are shown in Table 2.2 (Danafar et al., 2009).

Table 2.2 Studies on Al₂O₃ supported catalysts for CNTs synthesis (Danafar et al., 2009)

<i>Catalysts</i>	<i>Carbon source</i>	<i>Temperature^oC</i>	<i>CNTs type</i>
Fe/Al ₂ O ₃	C ₂ H ₄	500-700	MWNT
Fe/Al ₂ O ₃	C ₃ H ₆	550	MWNT
Co/Al ₂ O ₃	C ₂ H ₄	600-800	SWNT/MWNT
Fe-Co/Al ₂ O ₃	C ₂ H ₆ O	600	MWNT
Ni/Al ₂ O ₃	C ₂ H ₂	700-850	MWNT

2.1.2.3 Magnesium oxide

Magnesium oxide (MgO) is also widely used as a catalytic support for CNTs synthesis. It was reported having advantage that can be easily removed from SWCNTs by acid solution (Liu et al., 2006). Colomer et al (2000) produced a large scale of SWNTs over well-dispersed metal particles supported on MgO at 1000 °C by catalytic decomposition of methane. The produced SWNTs were separated easily from the support by a simple acidic treatment to obtain a product with high yields (70–80%) of SWNTs. CVD synthesis of CNTs on a Fe₂O₃/MgO precursor powder from isopentane (C₅H₁₂) and acetylene (C₂H₂) was studied with different Fe contents in the precursor (2.5–15%) at the synthesis temperature (450–850 °C) and the synthesis time (0.5–40 mins) by Mauron et al. (2003). Both MWNT and SWNT were obtained with acetylene as the carbon source. MgO was reported to have a high solubility in hydrochloric acid. Similarly, a Fe/MgO catalyst was also used by Liu et al. (2009). CNTs production with a specific surface area of 950 m²/g and a purity of 98% was obtained. Yen et al. (2008) synthesised high quality and high degree of graphitization CNTs from solid-stated polymers-polycarbosilane (PCS) and PE with reaction temperatures at 850–950 °C over a Fe/MgO catalyst.

2.1.2.4 Zeolite

Zeolites is used as a common catalytic support for CVD CNTs synthesis due to its stable mechanical property. Liu et al. (2011) converted PP into MWCNTs and hydrogen-rich gas over HZSM-5 zeolite catalysts. The yields of MWCNT and hydrogen concentration increased with the increase of decomposition temperature and reached the maximum at 700 °C. Fe-, Ru-, and Fe/Ru-nanoparticle catalysts on zeolite support were studied to produce CNTs by catalytic CVD with acetylene as the carbon source by Popovska et al. (2011). Vertically aligned SWNTs were successfully synthesized over both the Fe/Co based and Co/Mo based zeolite catalysts from alcohols (Maruyama, 2004). Willems et al. (2000) had studied MWCNs production by the catalytic decomposition of acetylene. Co–Mo, Co–V and Co–Fe mixtures supported on zeolite were used as catalysts. The Co–Mo/zeolite was found to produce high quality of CNTs.

2.1.2.5 Template support

In order to produce high quality CNTs in relation to the uniform distribution of CNTs diameter length and wall thickness (Stobinski et al., 2010), template controlled CNTs production starts to be studied as catalytic substrate. For example, Ni-coated glass was successfully used as a template by Ren et al. (1998) to synthesise ordered CNTs from acetylene at above 700 °C using plasma-enhanced hot filament CVD method. Che et al. (1998) prepared graphitic carbon nanotubes within a porous alumina template from ethylene and pyrene using a CVD method in the presence of a Ni-based catalyst. This template method provided a support with uniform structure for the growth of CNTs.

Among these membrane substrates, anodic aluminium oxide (AAO) particular presents several advantageous features compared to granular catalysts, such as achievable pore diameter, lengths and inner pore distances. These features could lead to the production of CNTs with a high morphological quality. In addition, AAO can be easily dissolved in alkaline or acidic during the separation of CNTs (Mijangos et al., 2016). Kyotani et al. (1996) produced CNTs at 800 °C on AAO membrane using pyrolytic propylene. CNTs presented with an outer diameter of 30 nm and a length of 60 nm corresponding to the channel diameter and the thickness of AAO membrane, respectively. Chen et al. (2006) synthesised CNTs by casting thin films of polyacrylonitrile and polystyrene-block-polyacrylonitrile within AAO membrane followed by pyrolysis. They found that the wall thickness of the produced CNTs was controlled by the concentration of the precursor solution. The effect of reaction gases (CO and C₂H₂) on the formation of CNTs has been studied by Jeong et al. (2004) with a Co-based AAO catalyst. CNTs synthesised in the presence of CO showed a lower growth rate as compared to C₂H₂. In addition, key parameters such as deposition time, temperature and precursor gas flow rate have been studied by Golshadi et al. (2014) to synthesise CNTs from a 30/70 (vol.%) ethylene/helium gas mixture using AAO-based catalysts. They found that longer deposition time and higher reaction temperature could enhance the yield and the thickness of CNTs.

Ceramic membrane also has been used as a catalytic substrate due to its commercial benefits and other good properties, such as high temperature stability, mechanical strength, chemical stability, and low cost (Labhsetwar et al., 2012; Thostenson et al., 2001). These properties make ceramic materials one of the best catalytic supports in the

fields of environmental and energy research (Labhsetwar et al., 2012). Quan et al. (2016) produced high quality syngas from biomass fuel gas over NiO/porous ceramic catalysts. Gao et al. (2015) studied steam reforming of biomass tar for hydrogen production using NiO/ceramic foam as catalysts.

2.1.3 Catalytic promoter

Generally, high dispersion of catalysis sites is preferred for reactions. Catalyst promoters were found to enhance catalytic activity in relation to H₂ and carbon yield. For example, Fe/Al₂O₃ is an active catalyst for CNTs growth, as Fe catalysts nanoparticles are easily sintered which resulting in the production of large diameter CNTs. If element Mo is added, catalysts with a stable structure at high temperature would be developed due to the segregation of Mo at the surface of Fe particles leading to excellent reaction activity and produce high yield of CNTs (Wei et al., 2008). Additional Mo was added to Fe/MgO catalysts to investigate the effect on CNTs from methane by CVD method. Figure 2.2 indicates that the addition of 6 wt.% of Mo increased both methane conversion and carbon yield (Wei et al., 2008). Methane conversion was increased from 38% for Fe/MgO to 48% for Fe-Mo/MgO, however, the further increase of Mo resulted in a lower conversion of methane. Additional Mo can stabilise the metal particle and increase the metal nanoparticles, consequently increase the CNTs production yield. In addition, the half-life of catalysts is extended from 2.5 mins for Fe/MgO to 7 mins with 6 wt.% Mo addition because the carbonization of Mo yields graphite through the formation of carbide compound Mo₂C. Therefore, the addition of Mo contributes to the increase in number of

metal particles formed on substrate and clean the metal surface, avoiding the formation of excess coke carbon on the surface of catalytic metal particles, thus preventing the rapid deactivation of catalysts.

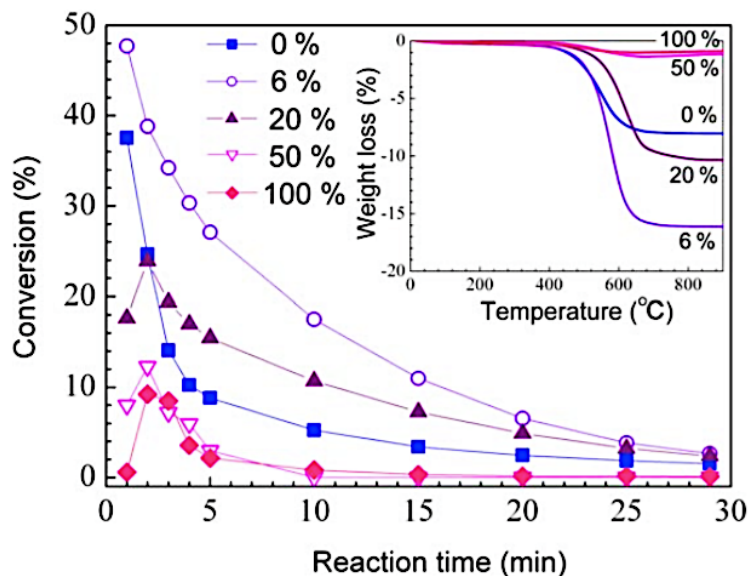


Figure 2.2 Methane conversion and carbon yield with different amount of Mo addition (Wei et al., 2008)

2.1.4 Catalytic particle sizes

Both catalytic particle size and metal crystal size have effect on CNTs growth by CVD. Particle size of catalysts has ability to influence the fluidization parameter, such as fluidization velocity and reaction efficiency (Ray et al., 2006), leading to both quantitative and qualitative changes on CNTs growth. The influence of particle size (10–20 μm , 20–53 μm , 53–75 μm , 75–100 μm , 100–200 μm , and 200–300 μm) on CNTs production was investigated by Danafar (2011). It was observed that a smaller catalytic particle diameter resulted in a greater CNT synthesis selectivity and a higher carbon deposition efficiency. The 10–20 μm catalytic particles exhibited 30% higher carbon

deposition than the 200–300 μm catalytic particles. As reported, small range particle size catalysts showed CNTs with uniform diameter and only small trace amorphous carbon (Figure 2.3a), but large range catalytic particle size presented relatively large spots of amorphous carbon (Figure 2.3b). This was due to the breakthrough capacities during diffusion would be bigger as a smaller diameter had a shorter diffusion path length within the particle.

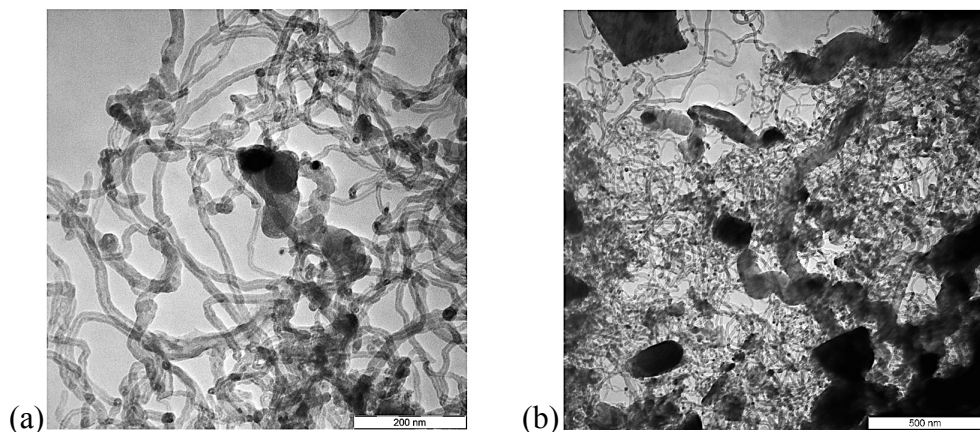


Figure 2.3 TEM results of CNTs growth in presence (a) 10–20 μm , and (b) 200–300 μm (Danafar et al., 2011)

Many studies also point out that CNTs growth and tube diameter are governed by the associated metal catalyst particle size, due to the mechanism of CNTs synthesis. The diameter of CNTs was reported to be roughly equal with metal particle sizes (Dasgupta et al., 2011). For example, Cheung et al. (2002) used iron (Fe) nanoparticles with average diameters of 3, 9 and 13 nm to form CNTs with relatively average diameters of 3, 7 and 12 nm, respectively. CNTs were grown at 800 $^{\circ}\text{C}$ from CVD of ethylene using the above Fe-based catalysts. Carbon nanotubes obtained from the 3, 9, and 13 nm average diameter Fe-catalysts had diameters of 2.6 ± 0.8 , 7.3 ± 2.2 , and 11.7 ± 3.2 nm, respectively. Results clearly showed that the larger metal sizes lead to larger diameter of CNTs. Schaffel et al. (2008) who studied CNTs from cyclohexane (C_6H_{12}) pyrolysis with a $\text{Fe}/\text{Al}_2\text{O}_3$ catalyst

obtained similar results. Therefore, there is a clear correlation between the catalyst metal size and the average diameter of CNTs.

Some researchers found that there is an optimally crystal size for CNTs growth. Chen et al. (2005) stated that a small crystal size would provide a large surface for surface reaction, a high diffusion area and a shorter diffusion length, thus leading a low growth rate and fast deactivation. Large crystals reduced the growth rate because of low surface area. Both low coking rate and fast deactivation resulted in a low yield of CNTs. An optimal crystal size could achieve an optimum growth rate and yield of CNTs. Ermakova et al. (2000) also noticed that the carbon production from methane decomposition was related to the average size of Ni catalysts; the maximum yield was produced with a particle size of 20-60 nm.

Based on the relationship between CNTs diameter and metal particle size, controlling the catalytic particle size distribution can manipulate the CNTs diameter distribution. A variety of methods have been investigated. Precipitation method is generally used to control particle size distribution of catalyst. Therefore, several attempts have been studied. For example, organic carrier 'apoferritin' has been successfully used to control the catalytic nanoparticles of various sizes by Li et al. (2001). Fe-based catalysts with diameter in the range of 1-2 nm and 3-5 nm were prepared by controlling the numbers of metal atoms in the cores of apoferritin, then used for CNTs growth by CVD from methane and hydrogen. The histogram plot results for two different sizes range of catalysts showed that the diameter of CNTs obtained were 3.0 ± 0.9 nm, which was close to the diameter of catalytic particles (3.7 ± 1.1 nm), and the catalyst with diameter of 1.9 ± 0.3 nm produced 1.5 ± 0.4 nm CNTs. The results showed that the diameter of nanotubes were closely

related to its catalytic nanoparticles (Li et al., 2001). Polyamidoamin dendrimers were also used as carriers to disperse Fe uniformly onto SiO₂ for the formation of catalysts with a diameter of 1-2 nm. Single-walled carbon nanotubes (SWNTs) with a diameter distribution in the range of 1-2 nm was synthesized (Li et al., 2001). Apart from these carriers, reaction temperature during the synthesis process also affects catalytic particle sizes, due to it accelerates the decomposition of carbon precursor on catalyst surface. When there is an increase of temperature, catalytic particles may collide to surface diffusion, subsequent sintering of particles resulted in the increase of the average particle size (Alvarez et al., 2001).

2.1.5 Catalytic metal content loaded

Active metal content has effect on both quality and quantity of CNTs formation, as well as the carbon source conversion, due to the content can change the metal particle size and catalytic activity. Different Fe contents was studied by Yao et al. (2017) for pyrolysis catalysis of plastic waste. CNTs was found with thinner diameter when low Fe content was used because of the smaller catalytic metal particles. In addition, more homogeneous and longer nanotubes were observed with higher Fe content. CNTs were grown at two Fe:C atomic ratios, 0.75 and 0.075 wt%; the results are shown in Table 2.3 (Sinnott et al., 1999). Larger diameter CNTs were produced with higher Fe:C. In addition, the lower Fe:C ratio was found producing CNTs with smaller average diameter. It is also shown that the larger CNTs at lower Fe ratio was directly in relative to the generation of larger Fe clusters. It was explained that a low Fe content in the vapour phase limited the ability

of Fe atoms to agglomerate into large clusters, resulting in the formation of smaller Fe clusters on the substrate.

The effect of Ru content (0.5 wt.% and 5.0 wt.%) were worked out on the carbon distribution of production by Park et al. (2010) , shown in Figure 2.4. The conversion of gas product for 0.5 wt.% Ru/Al₂O₃ was low, and the conversion of carbon to coke was over 20 mol.%. Therefore, they pointed out that 0.5 wt.% Ru-based catalysts couldn't provide a sufficient active sites area for PP pyrolysis, and the results showed that the activity of catalysts was increased with increasing metal contents until a certain point.

Table 2.3 Average diameter for CNTs and catalytic particles for different Fe content (Sinnott et al., 1999)

<i>Fe/C (at%)</i>	<i>Average nanotube inner diameter (nm)</i>	<i>Average nanotube outer diameter (nm)</i>	<i>Average Fe particle diameter (nm)</i>
0.75	5.8	33.6	35.3
0.075	4.3	28.3	28.2

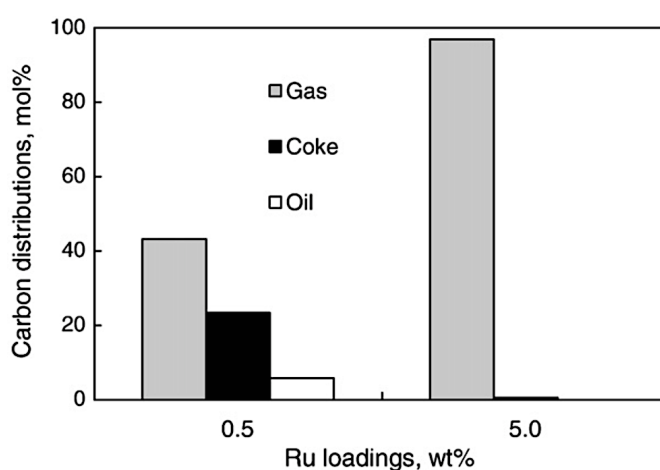


Figure 2.4 Production of PP pyrolysis over different Ru loaded catalysts (Park et al., 2010)

According to many research, there is an optimal content of catalytic active metal for each condition of experiment, in relative to different catalysts, different carbon source etc. Even for different supports with the same active metal, the optimal content of catalytic sites is different. For example, Figure 2.5 (Takenaka et al., 2004) shows the CNTs produced over $\text{Fe}_2\text{O}_3/\text{Al}_2\text{O}_3$ and $\text{Fe}_2\text{O}_3/\text{SiO}_2$ (7-77 wt.% as Fe_2O_3) from methane decomposition. The total carbon yield for the $\text{Fe}_2\text{O}_3/\text{Al}_2\text{O}_3$ was greater than that for the $\text{Fe}_2\text{O}_3/\text{SiO}_2$. The researchers found that the average particle size of catalytic species in the $\text{Fe}_2\text{O}_3/\text{Al}_2\text{O}_3$ was not affected by the metal loading, while the particle size in the $\text{Fe}_2\text{O}_3/\text{SiO}_2$ catalyst became larger with the increase of metal loading. In addition, the structure of CNTs was largely affected by the loading of Fe_2O_3 when the $\text{Fe}_2\text{O}_3/\text{SiO}_2$ was used (Figure 2.5). Venegoni et al. (2002) concluded that an increase of metal content increased the concentration of active metallic particles for CNTs formation, instead of increasing the mean particle size. Catalysts with too high metal content exhibit larger metallic particles leading to amorphous carbon formation. Figure 2.6 (Venegoni et al., 2002) shows the yield of carbons with increasing iron content from $\text{H}_2\text{-C}_2\text{H}_4$ pyrolysis. Below 1% Fe (w/w) the yield of carbon product is quite low; increasing the content of Fe from 0.5 to 1% (w/w), the yield carbon is doubled. Further increasing the content of Fe results in less changes of CNTs formation as large catalytic particles were formed. Combined with SEM and TEM analysis of the produced CNTs, the optimum value of iron content for CNTs growth is 1–2%. A higher content of iron led to the encapsulation of the metal particles.

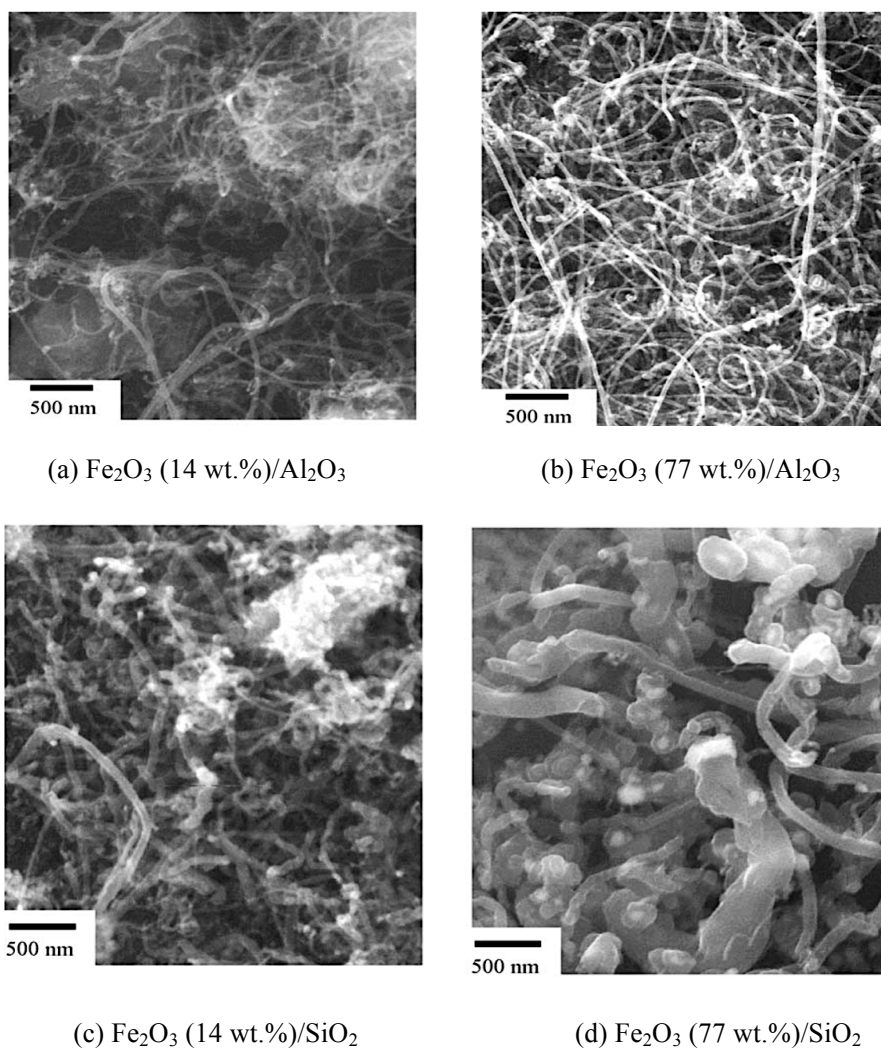


Figure 2.5 SEM results for CNTs produced over $\text{Fe}_2\text{O}_3/\text{Al}_2\text{O}_3$ and $\text{Fe}_2\text{O}_3/\text{SiO}_2$ (7-77 wt.% as Fe_2O_3) from methane decomposition (Takenaka et al., 2004)

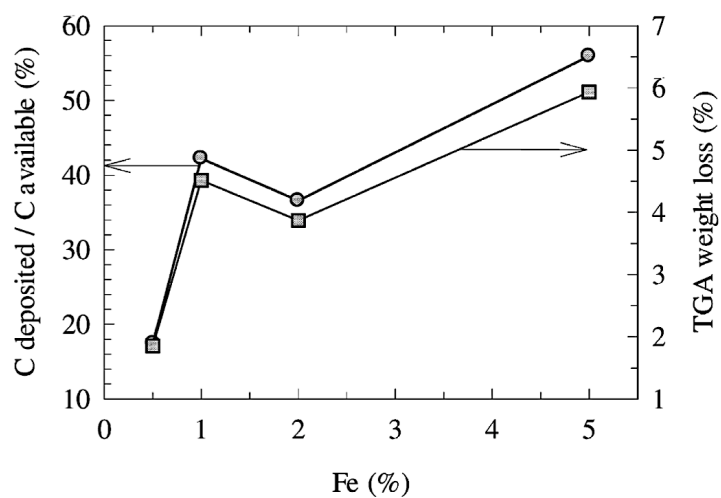


Figure 2.6 Carbon deposition yield with increasing Fe content of catalysts from $\text{H}_2\text{-C}_2\text{H}_4$ pyrolysis (Venegoni et al., 2002).

Furthermore, for some template substrate, the content of catalytic metal can significantly influence the structure of CNTs. For example, AAO membrane template (Figure 2.7a) (Jeong et al., 2004) was investigated in relation to the optimal catalytic content (Figure 2.7b). When the metal content is too small, CNTs bag is formed (Figure 2.7c), and the opening of membrane will be covered if the metal particle is too large.

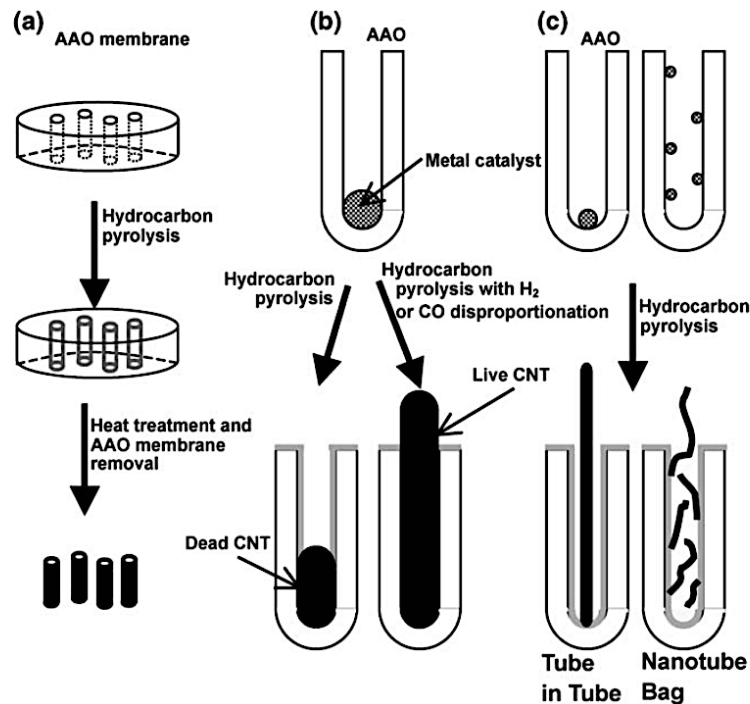


Figure 2.7 CNTs formation mechanism for AAO membrane support with different sizes metal particles (Jeong et al., 2004)

2.2 Growth mechanism of CNTs

Different CNTs growth mechanisms are proposed by different researchers according to varies of catalysts used. At present, the widely accepted CNTs growth mechanism can be outlined in Figure 2.8 (Yellampalli, 2011). Initially, the catalytic decomposition of hydrocarbon happens on the surface of active transition metal, then decomposed in to hydrogen and carbon atoms. The carbon atoms diffuse into metal particles. There are two different models according to the interaction between active sites and substrate including

tip-growth model (Figure 2.8a) and base-growth model (Figure 2.8b). When the catalyst-substrate interaction is weak, hydrocarbon decomposes on the top surface of the catalyst metal, carbon diffuses through catalytic particles. And CNTs are formed across the bottom of metal particles, pushing the catalyst particle off the substrate (Figure 2.8a-i). The CNTs growth process continues until the catalytic activity ceases (Figure 2.8a-iii). For the base-growth model, (Figure 2.8b) when the catalyst-substrate interaction is strong, initial hydrocarbon decomposition and carbon diffusion take place similar to that in the tip-growth model, but the catalyst particle remains at the bottom of the substrate (Figure 2.8b).

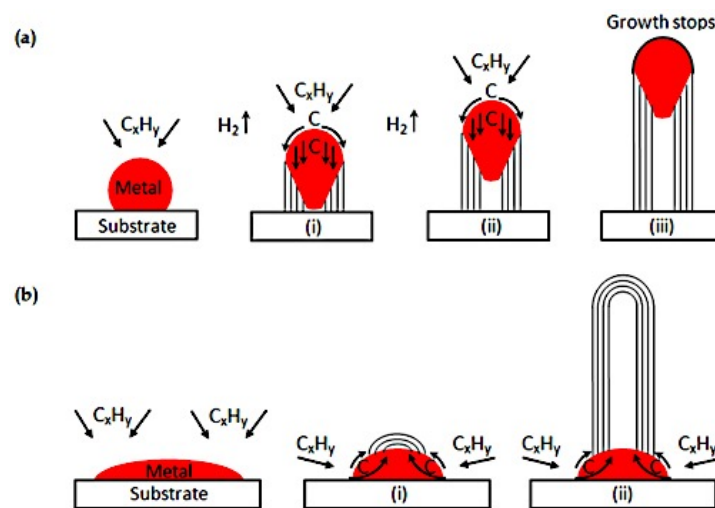


Figure 2.8 CNTs growth mechanisms via catalytic pyrolysis approaches (Yellampalli, 2011)

For CNTs growth on the powder catalyst, CNTs are not presented in individual form. Large amount of CNTs shows multi-agglomerate structure, and the SEM and TEM images in Figure 2.9 present such structure. A model related to this growth mechanism was discussed by Wei et al. (2008), and concluded in Figure 2.10. For a common powder catalyst, the growth of CNTs with a base growth mode initially crushes the catalytic particles and disrupts the structure to form separated catalyst sites. As in the process of

CNTs growth, the generated stress inside the catalysts will release, causing disorders in the graphite layer and defects of carbon deposition, followed by CNTs growth around the catalysts sites (Figure 2.10a-b). The growing CNTs push away and separate the catalytic sites, leading to the increase of agglomerate size and the decrease of CNTs density (Figure 2.10c-d).

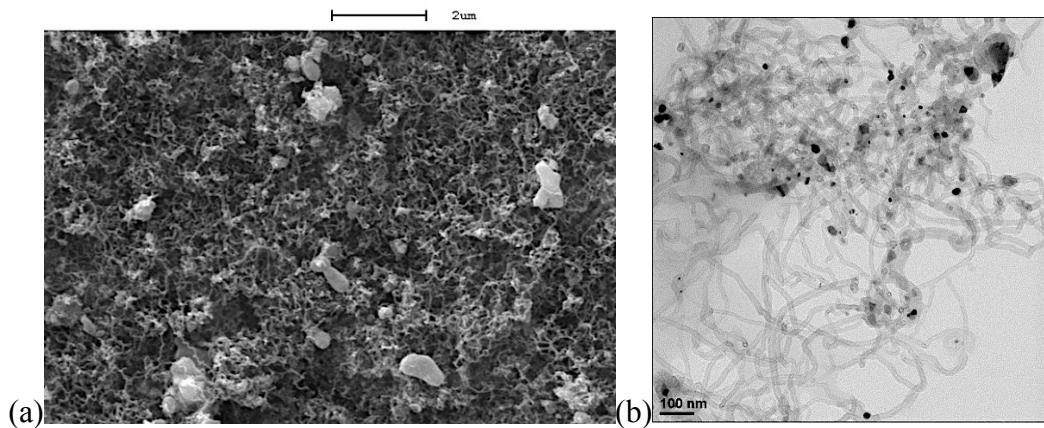


Figure 2.9 SEM (a) and TEM (b) result Ni/ceramic 740 °C from HDPE pyrolysis (Wei et al., 2008)

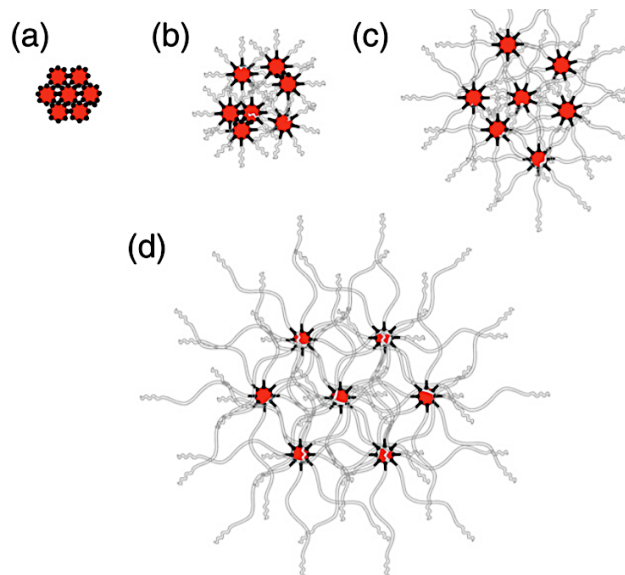


Figure 2.10 Growth mechanism of CNT agglomerate formation (Wei et al., 2008)

Furthermore, growth mechanism of CNTs is different for different catalysts. For example, CNTs produced using AAO membrane have two-side open (Figure 2.7). Ideally, the

diameter of CNTs is similar to that of AAO uniform channel, as metal catalysts fills into the entire space of the pore of AAO (Figure 2.7b). The CNTs grows based on one nickel particle loaded inside an AAO channel, while the hydrocarbon gases pass through the channel. For example, Lee et al. (2012) synthesised well-ordered bamboo-like CNTs with Au-AAO template at 700 °C (SEM results are shown in Figure 2.11).

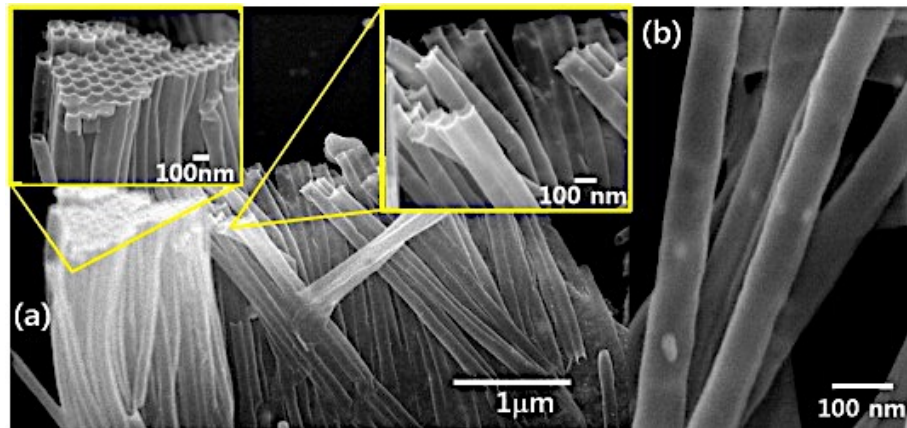


Figure 2.11 SEM images of Au-CNT-AAO prepared at 700 °C (Lee et al., 2012)

2.3 Effect of parameters on synthesis of CNTs

2.3.1 Carbon precursor

Carbon precursor plays an important role in the formation and properties of CNTs. CNTs formation is stated in relative to the chemical structure of hydrocarbons (Danafar et al., 2009). For example, Hernadi et al. (2000) tested different carbon precursors (acetylene, ethylene, propylene, acetone, *n*-pentane, methanol, toluene, and methane) and each resulted in carbon nanotube formation over Co, Fe-based catalysts. The quality of CNTs was investigated by TEM and diameter analysis. It was found that unsaturated hydrocarbons (e.g. acetylene) had much higher yield and deposition rate than saturated gases (e.g. ethylene and propylene). It was also reported that the chemical structure of

hydrocarbon source, like straight-chained ring or benzene-like structure, has more effect on CNTs formation rather than its thermodynamic structure, like enthalpy (Danafar et al., 2009). For bulk production of CNTs, the carbon precursor should be easy to pyrolysis and largely available (Dasgupta et al., 2011). Li et al. (2004) stated that the properties of carbon precursors played an important role in CNTs formation. For example, aromatic molecules are favoured for SWNTs growth, while aliphatic molecules tended to form MWNTs or non-tubular carbon structures. Hexane, tetradecane and toluene led to amorphous carbon formation, and paraffin was favoured to form mainly filamentous carbon (Barbarias et al., 2016).

Thermal catalytic pyrolysis has been studied in relation to various of plastic types. The type of plastics is one of the main crucial parameters influencing the quality and quantity of CNTs and syngas production. Table 2.4 summarises the conversion for different types of plastics through pyrolysis (Anuar et al., 2016). The feedstock includes polystyrene (PS), polyethylene terephthalate (PET), high density polyethylene (HDPE), low density polyethylene (LDPE), polypropylene (PP).

Polystyrene (PS) is made of styrene monomers, with high heat resistant, high durability, strength but light in weight. PS is normally applied in electronics, food packing, medical and etc. PS decomposed into about 58 vol.% original monomer styrene, 35 vol.% ethylbenzene, styrene dimer, styrene trimer, and small amount of 2-phenylpropene (Al et al., 2009). Scott et al. (1990) pyrolysed polystyrene at different temperatures (532 °C, 615 °C and 708 °C). The dominant product was styrene. PS pyrolysis oil contains high fraction of benzene, toluene and ethyl benzene.

Table 2.4 Production for different types of plastics pyrolysis (Anuar et al., 2016)

Type of plastics	Reactor	Process parameters				Yield		
		Temperature	Pressure	Heating rate	Duration	Oil	Gas	Solid
		°C		°C/min	min	wt.%	wt.%	wt.%
PET	Fixed Bed	500	-	10	-	23.1	76.9	0
PET	-	500	1 atm	6	-	38.89	52.13	8.98
HDPE	Horizontal	350	-	20	30	80.88	17.24	1.88
HDPE	Semi-batch	400	1 atm	7	-	82	16	2
HDPE	Batch	450	-	-	60	74.5	5.8	19.7
HDPE	Semi-batch	450	1 atm	25	-	91.2	4.1	4.7
HDPE	Fluidised	500	-	-	60	85	10	5
HDPE	Batch	550	-	5	-	84.7	16.3	0
HDPE	Fluidised	650	-	-	20-25	68.5	31.5	0
PVC	Fixed Bed	500	-	10	-	12.3	87.7	0
PVC	Vacuum	520	2 kPa	10	-	12.79	0.34	28.13
LDPE	Pressurised	425	0.8-4.3	10	60	89.5	10	0.5
			Mpa					
LDPE	Batch	430	-	3	-	75.6	8.2	7.5
LDPE	-	500	1 atm	6	-	80.41	19.43	0.16
LDPE	Fixed Bed	500	-	10	20	95	5	0
LDPE	Batch	550	-	5	-	93.1	14.6	0
LDPE	Fluidised	600	1 atm	-	-	51.0	24.2	0
PP	Horizontal	300	-	20	30	69.82	28.84	1.34
PP	Batch	380	1 atm	3	-	80.1	6.6	13.3
PP	Semi-batch	400	1 atm	7	-	85	13	2
PP	Semi-batch	450	1 atm	25	-	92.3	4.1	3.6
PP	-	500	1 atm	6	-	82.12	17.76	0.12
PP	Batch	740	-	-	-	48.8	49.6	1.6
PS	Semi-batch	400	1 atm	7	-	90	6	4
PS	Pressurised	425	0.31-1.6	10	60	97	2.50	0.5
			MPa					
PS	Batch	500	-	-	150	96.73	3.27	0
PS	Batch	581	-	-	-	89.5	9.9	0.6

The most common used for bottles container polyethylene terephthalate (PET) is also the most recycled plastics. Gaseous production (77 wt.%) is mainly obtained whilst the balance consisted of liquid production with high benzoic acid content (49 wt.%) by PET pyrolysis at 500 °C (Al et al., 2009). Gas from PET pyrolysis is typically the dominant fraction; this is contributed to the volatility of its original constituting monomers. During pyrolysis of PS, it also releases oxygen component which could react with carbon molecules to form CO and CO₂.

High-density polyethylene (HDPE) has high strength and durability. It has been widely used for milk bottles, detergent bottles and toys. About 74 wt.% of pyrolysis oil was obtained by HDPE pyrolysis at 440 °C (Sharma et al., 2014). The product was also reported with high fraction of propane (C₃) about 28 wt.% (Horvat et al., 1999). HDPE was used to investigate a range of process conditions (including the types of reactor, the reacting atmosphere, and the presence of catalysts) on syngas and carbon production by Saad et al. (2015).

High-density polyethylene (LDPE) also is used as a feedstock for plastics pyrolysis. High liquid yield (93.1 to 95 wt.%) with minimal gas product was produced from LDPE pyrolysis (Marcilla et al., 2009). A high of olefin gases yield obtained from LDPE pyrolysis at temperature between 800 °C and 900 °C (Sodero et al., 1996).

Temperature used for polypropylene (PP) pyrolysis is typically between 250 °C to 400 °C (Al et al., 2009). Park et al. (2010) used PP pellets as a carbon source to investigate the operation conditions on fuel gas production over Ru/Al₂O₃ catalysts. Mishra et al. (2012) also used PP as a precursor for synthesising CNTs by single stage CND over Ni

catalysts at different temperatures. A two-stage reaction process was used to convert PP into CNTs and hydrogen rich gas by Liu. et al. (2011); different pyrolysis and deposition temperature were studied.

Furthermore, many researchers used mixed plastics as feedstock. For example, pyrolysis of real world waste plastics was studied by Yao et al. (2018). They used crushed and grounded real-world waste plastics, including disposable drink cups, lunch boxes and plastics wrap (the mixed plastics waste was analysed comprising of 40 wt.% HDPE, 35 wt.% LDPE, 20 wt.% PP and 5 wt.% PP). About 62.88 vol.% H₂, 6.24 vol.% CO, 27.20 vol.% gas were produced, and about 40.7 wt.% carbon deposition (45% CNTs) was obtained over Ni-Fe based catalysts. Williams et al. (2014) analysed the gas production from a mix plastics waste (31.25 wt.% LDPE, 31.25 wt.% HDPE, 7.29 wt.% PP, 13.50 wt.% PS, 11.46 wt.% PVC, 5.21 wt.% PET) with different operation temperatures. Three different plastics (LDPE, PP, and PS) were studied by Acomb et al. (2014) to increase the quality of CNTs with water injection. The gas product and carbon production are shown in Table 2.5. It shows LDPE produced 19 wt.% of CNTs, much larger than 9 wt.% of PP and 10 wt.% PS. More CNTs with small amount amorphous carbon were formed from LDPE pyrolysis. Table 2.5 also shows that PP and PS produced a large amount of C₂-C₄ hydrocarbons. A larger amount of amorphous carbons were produced as a result of the presence of heavy hydrocarbons. However, when water vapor was introduced, the amount of filamentous carbon produced from LDPE is reduced to 8 wt.%, and for PP and PS it is increased to 10 wt.% and 32 wt.%, respectively. It was explained that olefinic feedstocks (such as pentane and hexane) resulted in the disappear of filamentous carbons

at high steam injection rates. Filamentous carbons production is benefited from aromatic sources (such as benzene, toluene and ethyl-benzene).

Table 2.5 Gas composition and carbon production of pyrolysis-gasification of LDPE, PP and PS (Yao et al., 2018)

<i>Sample</i>	<i>LDPE</i>				<i>PP</i>				<i>PS</i>			
	0	0.25	1.90	4.74	0	0.25	1.90	4.74	0	0.25	1.90	4.74
Steam injection (gh ⁻¹)	0	0.25	1.90	4.74	0	0.25	1.90	4.74	0	0.25	1.90	4.74
Gas	30.9	58.5	78.9	85.7	44.8	57.1	69.8	80.3	11.7	23.9	46.4	56.1
Oils	14.0	8.2	0.0	0.0	16.0	6.5	8.3	0.0	53.0	37.7	31.0	25.1
Solid	52.0	25.0	15.5	12.5	35.0	30.9	20.0	14.0	35.0	38.4	18.2	12.3
H ₂	58.3	50.3	53.8	53.1	51.1	50.0	51.6	49.5	77.2	68.5	64.4	60.0
CO	0.0	13.1	26.4	21.1	0.0	14.9	18.3	21.6	0.0	16.7	22.2	26.3
CO ₂	0.0	0.7	3.1	6.2	0.0	1.0	4.7	6.4	0.0	0.9	6.3	8.2
CH ₄	20.3	16.1	7.1	7.1	19.3	13.7	9.0	5.5	12.0	8.5	4.0	2.2
C ₂ -C ₄	21.4	19.7	9.7	12.5	29.7	20.4	16.3	17.0	10.7	5.3	3.2	3.2
H ₂ yield	3.3	4.7	9.0	9.2	3.3	4.4	6.2	6.9	2.7	3.8	6.9	7.4
Filamentous CNTs	18.8	7.6	7.6	0	8.8	10.4	3.3	3.4	9.6	32.4	6.3	7.0
CNTs:Amorphous carbons	2.30	0.67	0.67	0	0.44	0.89	0.33	0.57	0.46	4.47	0.49	0.92

The synthesis of CNTs from hydrocarbon gases generated from plastics virgin and waste plastics (polyethylene, polypropylene, polystyrene, polyamide, polyvinyl-chloride, municipal plastic waste) over Fe and Co catalysts was studied by Borsodi et al. (2016).

Table 2.6 summarises the composition of gas products. It is shown that pyrolysis of the 100% virgin HDPE, 99% HDPE + 1% PVC, 99% HDPE + 1% PA, 100% waste HDPE and MPW generated significant C₂, C₃ and C₄ compounds. A large amount of C₃ hydrocarbon (propene and propane) were produced from pyrolysis of PP. The amount of C₂ and C₄ hydrocarbon produced has the highest value by adding 20% PS to the commercial virgin HDPE. The branching structure of polypropylene resulted in high concentrations of branched hydrocarbons in gaseous products. Figure 2.12 also summarises CNTs production from plastic pyrolysis. The CNTs production conversion

was 35.6% for virgin HDPE pyrolysis, 54.0% for virgin PP pyrolysis, and 43.3% for 80% virgin HDPE + 20% virgin PS raw material pyrolysis, respectively. And the higher carbon conversion value was obtained with real waste plastics 48.1% (50% waste HDPE + 50% waste PP), 47.1% (waste HDPE) and 60.7% (MPW). for pyrolysis of virgin PP, 50% waste HDPE + 50% waste PP and MPW pyrolysis, the CNTs production yield was high (13%, 11% and 17%) due to high amount of gas production.

Table 2.6 The composition of production obtained by plastics pyrolysis (Borsodi et al., 2016)

<i>Compounds</i>		<i>Virgin</i>	<i>Virgin</i>	<i>80% virgin</i>	<i>99% virgin</i>	<i>99% virgin</i>	<i>50% waste</i>	<i>Waste</i>	<i>MPW</i>
		<i>HDPE</i>	<i>PP</i>	<i>HDPE+20% virgin PS</i>	<i>HDPE+1% virgin PVC</i>	<i>HDPE+1% virgin PA</i>	<i>HDPE+50% waste PP</i>	<i>HDPE</i>	
Hydrocarbons	Methane	5.8	4.8	10.3	5.0	7.9	5.7	4.2	6.4
	Ethene	17.3	8.0	12.3	13.8	14.6	11.6	15.6	16.6
	Ethane	8.6	4.2	7.4	9.5	9.6	9.7	10.6	9.7
	Propene	10.3	28.6	11.9	16.2	16.9	12.2	18.8	14.4
	Propane	12.7	24.8	10.2	11.9	11.5	10.7	13.5	9.6
	Butene	13.8	3.9	17.0	17.4	18.9	15.4	11.7	15.6
	Butane	9.4	3.1	12.2	12.7	11.3	13.2	11.0	13.8
	i-butane	3.8	11.5	3.5	3.1	2.9	8.0	4.5	4.5
	Pentene	7.5	2.5	5.6	4.9	1.7	3.6	2.4	2.4
	Pentane	6.6	2.0	6.4	2.7	2.1	3.0	2.5	3.2
	i-pentane	2.9	6.0	2.1	0.5	0.7	5.2	1.6	2.5
	Hexene	1.1	0.4	1.1	1.8	1.5	1.4	1.9	0.9
	Hexane	0.2	0.2	0.3	0.5	0.4	0.2	1.7	0.4
Contaminants	Chlorine	-	-	-	1131	-	1055	-	2410
	mgKg ⁻¹ Nitrogen	-	-	-	-	833	316	149	1937
	Sulphur	-	-	-	-	-	115	725	1073
	Phosphorous	-	-	-	-	-	158	-	934

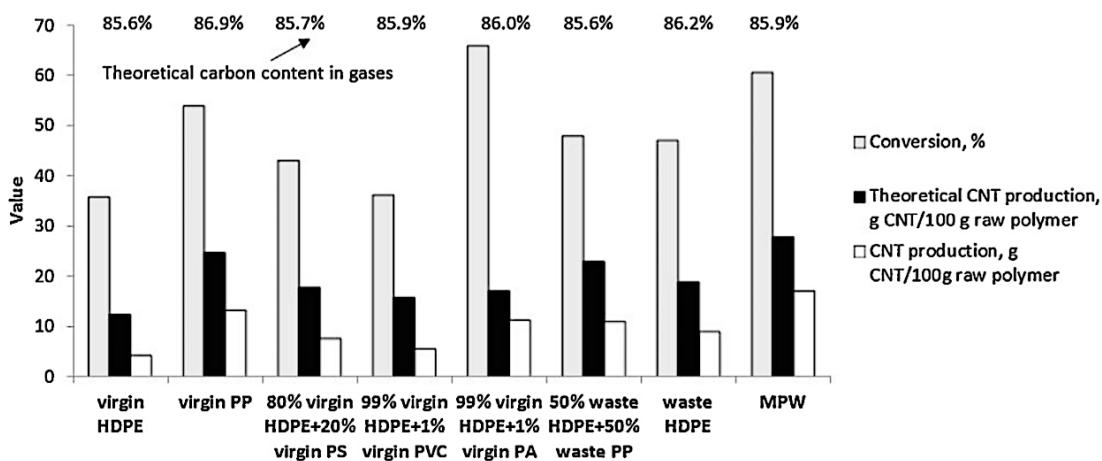


Figure 2.12 CNTs production from different plastic pyrolysis (Borsodi et al., 2016)

In addition, the amount of plastics used in system also has significant effect on gas and CNTs production. The optimum ratio of plastics and catalysts results in the increasing amount of CNTs and gas production. Wu et al. (2010b) investigated the influence of different catalyst : plastics waste ratio (0.5, 1.0, 1.5, and 2.0 g/g) on CNTs formation and hydrogen production using a two-stage catalytic steam pyrolysis-gasification process over Ni-Mg-Al catalysts. The product yield and gas concentration in relation to the different catalysts: plastics ratio are shown in Table 2.7 and Figure 2.13, respectively.

Table 2.7 Mass balance for different catalyst : plastics ratio (Wu et al., 2010b)

<i>Catalyst:plastics ratio</i>	<i>0.0</i>	<i>0.5</i>	<i>1.0</i>	<i>1.5</i>	<i>2.0</i>
Mass balance in relation to only plastics (wt.%)					
Gas yield	49.4	225.1	205.7	206.2	228.6
Oil yield	40.0	0.0	0.0	0.0	0.0
Solid yield	13.0	13.4	19.4	18.6	5.2
Mass balance	102.4	238.5	225.1	224.8	233.8

The gas yield shows the highest value when the ratio increased to the 2, but the lowest solid yield was observed. The analysis of gas concentration shows that hydrogen concentration has a significantly increase with the increase of the catalyst to plastic ratio, but the concentrations of C₂-C₄ hydrocarbons are decreased.

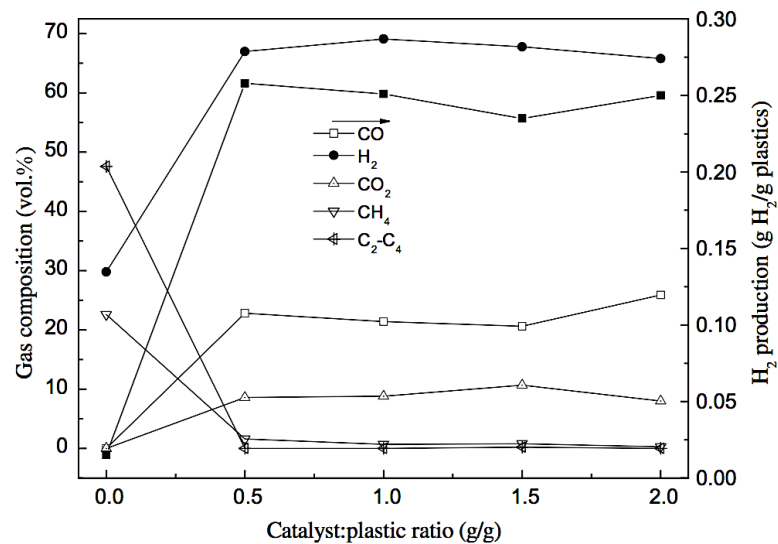


Figure 2.13 Gas production from pyrolysis of different catalysts:plastics ratio (Wu et al., 2010b)

2.3.2 Temperature

Temperature in each stage has a significant effect on CNTs growth. The temperature affects the morphology, growth rate, and reaction mechanism of CNTs in the CVD process.

2.3.2.1 Pyrolysis temperature

For a two-stage fixed catalytic pyrolysis system, carbon source is thermally decomposed at a pyrolyser (first stage), and then carbon containing gases flow into a reformer (catalysts stage). Since the composition of carbon sources and the flow rate of vapours are controlled by pyrolysis temperature, it is important to determine the optimum

operating temperature for pyrolysis. For example, in Park's research (2010), it was reported that increasing temperature led to a decrease of carbon conversion to coke; however, it can also lead to a decrease of carbon conversion to gaseous, as shown in Figure 2.14. It was explained that the polycyclic and condensation reactions of molten carbon sources were accelerated with the increase of reaction temperature. The growth of CNTs was reported to related to the carbon source feeding rate. A continuous growth of CNTs can only be obtained at an optimum feeding rate. The pyrolysis temperature affects the carbon sources decomposition rate and thereby the feed of carbon precursors to the stage of catalytic reactions. When the temperature is too high, it provides an excessive feeding of carbon atoms causing metal particles of catalyst poison (Yao et al., 2018). An optimum pyrolysis temperature could reduce the formation of amorphous carbons.

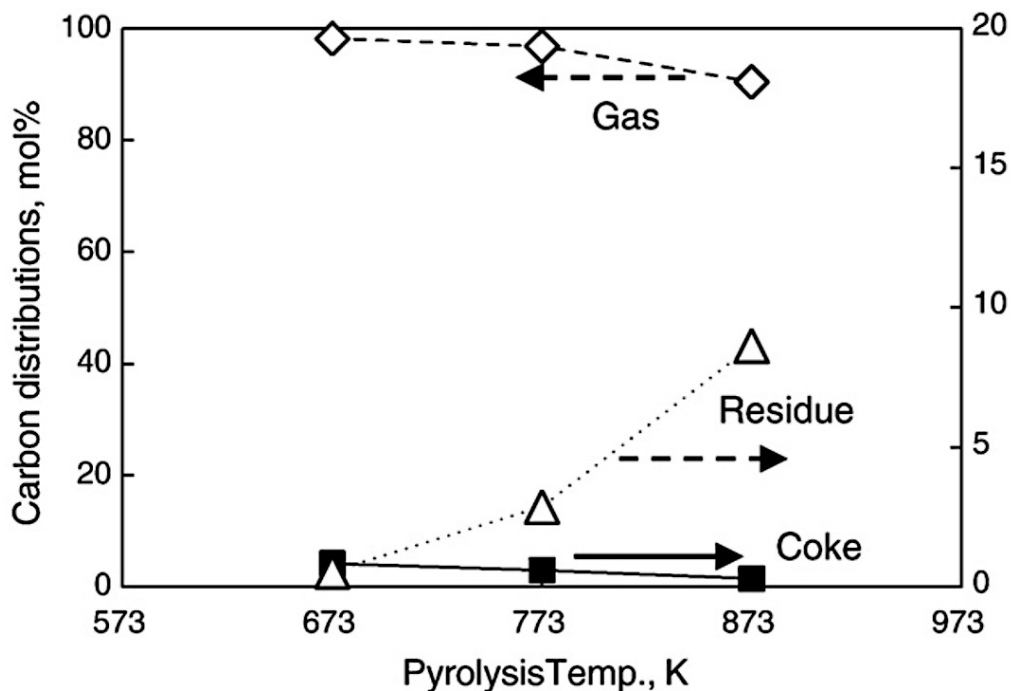


Figure 2.14 Effect of pyrolysis temperature on carbon distributions (Park et al., 2010)

The effect of pyrolysis temperature was also studied by Liu et al. (2011) who converted polypropylene into CNTs over a HZSM-5 zeolite. It was stated that different pyrolysis temperatures influenced the quantity and composition of pyrolysis gas product. Figure 2.15 shows the effect of pyrolysis temperature on the yields of different fractions at a fixed catalytic temperature (700 °C). There was a significant increase of pyrolysis gas from 8.6 to 56.1 L/100 g PP when the pyrolysis temperature increased from 550 °C to 750 °C, and the liquid yield decreased from 41.2 to 9.6 g/100 PP. The yield of hydrocarbon gases (propylene, propane, ethane and C₄-C₅) changed with different pyrolysis temperatures. CNTs yield increased with an increase of pyrolysis temperature and achieved a maximum value 37.6 g/100 g PP at 650 °C (Figure 2.16) (Liu et al., 2011). Methane was mainly produced at high temperature, suggesting that it produced less CNTs than propylene and butylene.

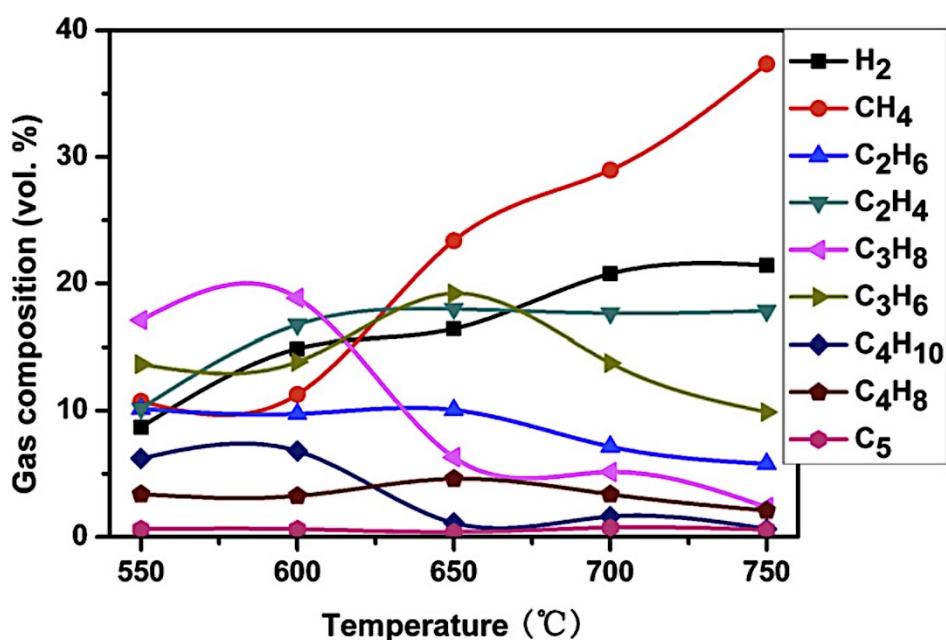


Figure 2.15 Gas composition at different pyrolysis temperatures (Liu et al., 2011)

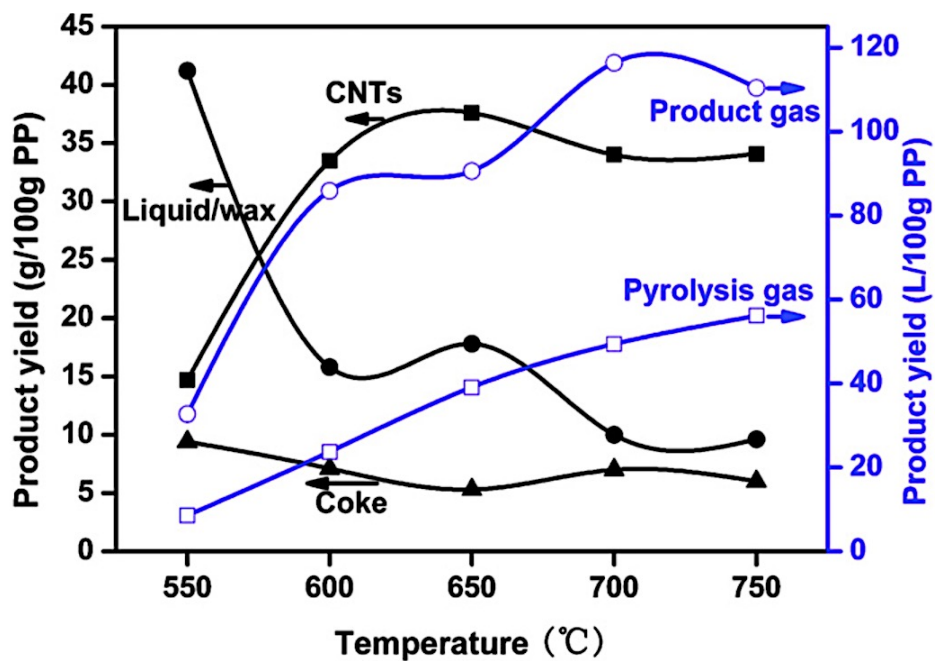


Figure 2.16 Product yield at different pyrolysis temperature (Liu et al., 2011)

2.3.2.2 Catalytic temperature

It is generally acknowledged that CNTs are generated by carbon atoms dissolving, diffusing and precipitating through catalysts in the CVD process. The rates of carbon atoms dissolving, diffusing and precipitating are affected by catalytic temperature. For example, Park et al. (2010) evaluated the effect of reaction temperature for Ru based catalysts from steam reforming of waste polypropylene pellet. The effect of temperature on carbon distribution is shown in Figure 2.17. Three different catalytic temperatures were studied, increasing temperature resulted a high carbon conversion to gas production, but also led to an increasing amount of coke deposition on the catalyst. They pointed out the increasing carbon conversion was caused by both pyrolysis reactions and steam reforming which were accelerated by an increase of reaction temperatures. At the same

time, the increasing amount of cake deposition formed because polycyclic and condensation reactions of PP were also accelerated by increasing reaction temperature.

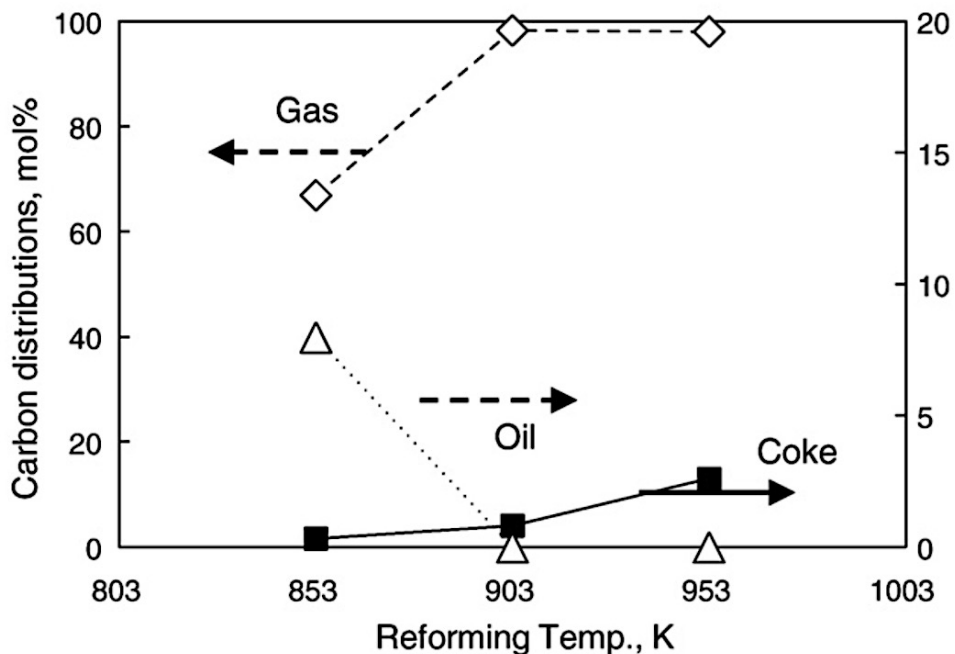


Figure 2.17 Effect of catalytic temperature on carbon deposition (Park et al., 2010)

The starting temperature of CVD synthesis of CNTs is mostly reported higher than 500 °C, but there is a conflicting result for the maximum temperature. Some optimum temperature operated at different conditions are summarised in Table 2.8 (Danafar et al., 2009). If the temperature is too high, chemical reaction between carbon atoms and catalysts may take place to form metal carbide losing its catalytic activity for CNTs formation. Too high catalytic temperature will cause the sintering of supported catalysts, the formation of alloy in catalysts and amorphous carbons (Danafar et al., 2009). It is likely the size and structure of catalysts will be more stable at lower temperature, leading to better control on the size and chirality of CNTs production (Danafar et al., 2009).

Table 2.8 Studies on optimum temperature operated with different conditions for CNTs growth (Danafar et al., 2009)

<i>Carbon Source</i>	<i>Catalyst</i>	<i>Temperature °C</i>	<i>CNT diameter (nm)</i>	<i>Wall</i>
Ethanol	Co/Al	550	10-20	MW
	Fe-Co	700-800	1	SW
	Fe/Al	800	0.78-1.05	SW
	Ferrocene	1100	20-40	MW
Acetylene	Fe-Co/Al	700	31-41	MW
	Ferrocene	600-800	10-20	MW
	Ferrocene	900-1000	-	SW
Methane	Fe/Al-Si	900	-	MW
	Fe-Mo/Al	900	0.9-2.7	SW
	Fe-Mo/MgO	860	-	MW
	Fe-Mo/Al	700, 750	2-45	SW
Toluene	Ferrocene	800,900	20-25	MW
	Ferrocene	1200	20-70	MW

Optimum catalytic temperature will change with different parameters. For example, Li et al. (2002) investigated the effect of temperature (600 °C – 1050 °C) on CNTs production using Fe-based catalysts under different gas pressure. At 0.6 Torr (Figure 2.18a), the yield of CNTs at both low and high temperature is low, about 10% at 650 °C and 48% at 1050 °C. In addition, at 1050 °C, only carbon particles were produced. Pure CNTs with a high yield was produced between 750 °C and 850 °C. However, at 760 Torr (Figure 2.18b), the largest yield of CNTs appeared between 900 °C to 950 °C. They also found the diameter of CNTs increased with an increase of temperature. This might be caused by (1) at high catalytic temperature, small catalytic particles join together to form a big one which CNTs with large diameter will grow; (2) the catalytic particles would become flat

due to the high status with an increase of temperature, the precipitation area on the catalysts are enlarged caused larger diameter CNTs formed; (3) an increasing temperature will promote the decomposition of carbon contained gases to increase the concentration of carbon atoms, which could increase the CNTs growth rate, consequently bigger CNTs formation (Li et al., 2002).

Similar results are also reported by Hanaei et al. (2010), in their study about CNTs production from acetone over Fe/Al₂O₃ catalysts at different catalytic temperatures. The results demonstrated that the ideal reaction temperature was about 750 °C. More amorphous carbons were produced when the temperature increased to 950 °C due to the deactivation of the catalysts. Different catalysts temperatures (700 °C, 800 °C, 900 °C) were explored with Ni-Fe catalysts of waste plastics by Yao et al. (2018). Bamboo-like, straight and crooked filamentous CNTs were formed at 700 °C (Figure 2.19a). In addition, encapsulating carbons with large metal particle sizes were found on the spent catalysts at 900 °C (Figure 2.19b) due to the aggregation of catalysts particles at high catalytic temperature.

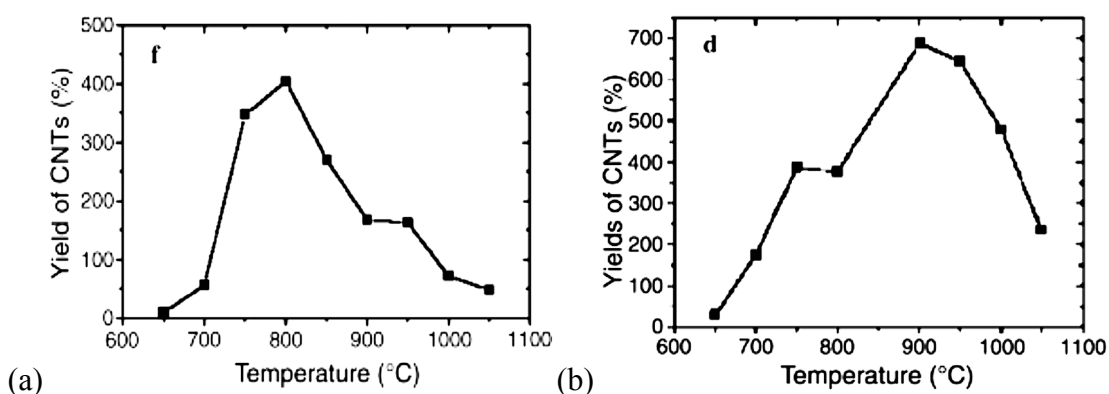


Figure 2.18 Yield of CNTs grown at (a) 0.6 Torr and (b) at 760 Torr (Li et al., 2002)

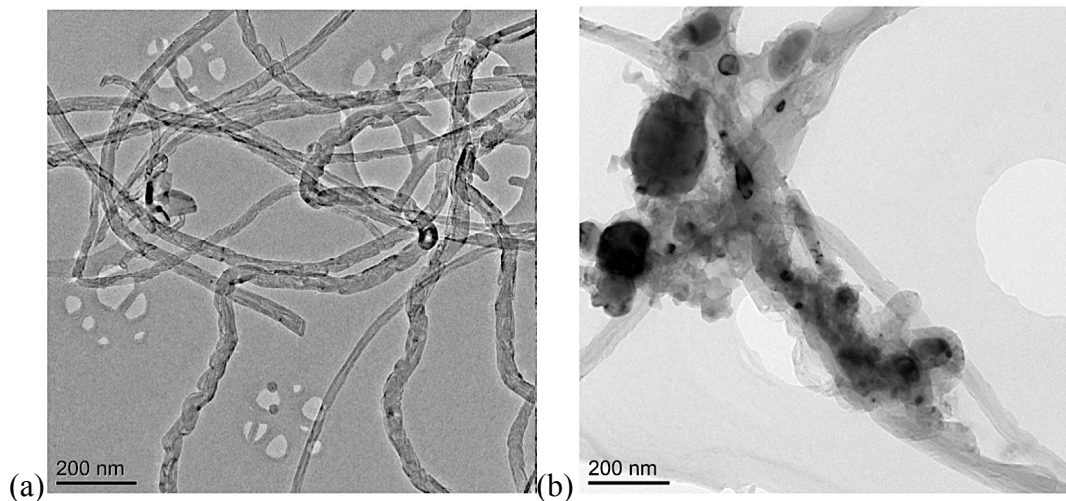


Figure 2.19 TEM results for CNTs formed (a) at 700 °C and (b) at 900 °C (Yao et al., 2018)

Some researchers focus on the influence of gas composition change at different catalytic temperatures on the formation of CNTs. Figure 2.20 shows the effect of catalytic temperature on the yield of production from PP pyrolysis with a HZSM-6 zeolite (Liu et al., 2011). The volume of product gas increased from 74.9 to 119.1 L/100 g PP as the catalytic temperature increases from 500 °C to 800 °C, and the carbon yield increases from 23.7 to 34.1 g/100 g PP from 500 °C to 700 °C, then decreases to 32.2 g/100 g PP with the further increase of temperature to 800 °C. The detailed composition of the product gas at different catalytic temperatures is displayed in Table 2.9. The major composition of gas includes hydrogen, and methane while ethane, ethylene, propane, propylene, butane, butylenes, pentane, pentene and carbon monoxide. It is indicated that during the catalytic decomposition of pyrolysis gas, thermal decomposition reactions can affect the composition of gas product. CNTs produced at different catalytic temperatures were also analysed according to TEM results as shown in Figure 2.21. CNTs have a smaller inner diameter with a broad diameter distribution produced at 500 °C, and a narrower diameter distribution with larger mean diameter obtained at 800 °C (Liu et al.,

2011). CNTs synthesised at high temperature have a higher graphitization compared to those grown at lower temperature.

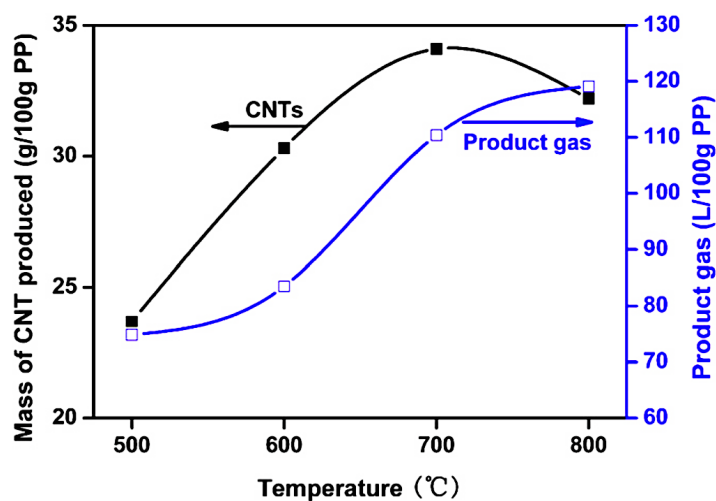


Figure 2.20 Mass of CNTs and gas produced at different catalytic temperatures (Liu et al., 2011)

Table 2.9 The composition of the product gas at different decomposition temperatures (Liu et al., 2011)

<i>Gas production (vol.%)</i>	<i>500°C</i>	<i>600°C</i>	<i>700°C</i>	<i>800°C</i>
H ₂	50.30	59.76	72.21	63.91
CH ₄	40.67	29.61	22.88	28.30
C ₂ H ₆	2.98	1.80	1.28	1.45
C ₂ H ₄	1.55	1.41	0.29	4.37
C ₃ H ₈	1.10	1.62	0.33	0.07
C ₃ H ₆	1.67	3.21	0.19	0.29
i-C ₄ H ₁₀	0.16	0.20	0.04	0.01
n- C ₄ H ₁₀	0.09	0.41	0.02	0.01
n-C ₄ H ₈	0.11	0.18	0.03	0.01
i- C ₄ H ₈	0.31	0.58	0.05	0.03
cis-C ₄ H ₈	0.03	0.06	0.00	0.00
i-C ₅ H ₁₂	0.01	0.17	0.01	0.01
n- C ₅ H ₁₂	0.00	0.00	0.01	0.00
C ₅ H ₁₀	0.21	0.04	0.01	0.02
CO	0.02	0.37	0.63	0.64

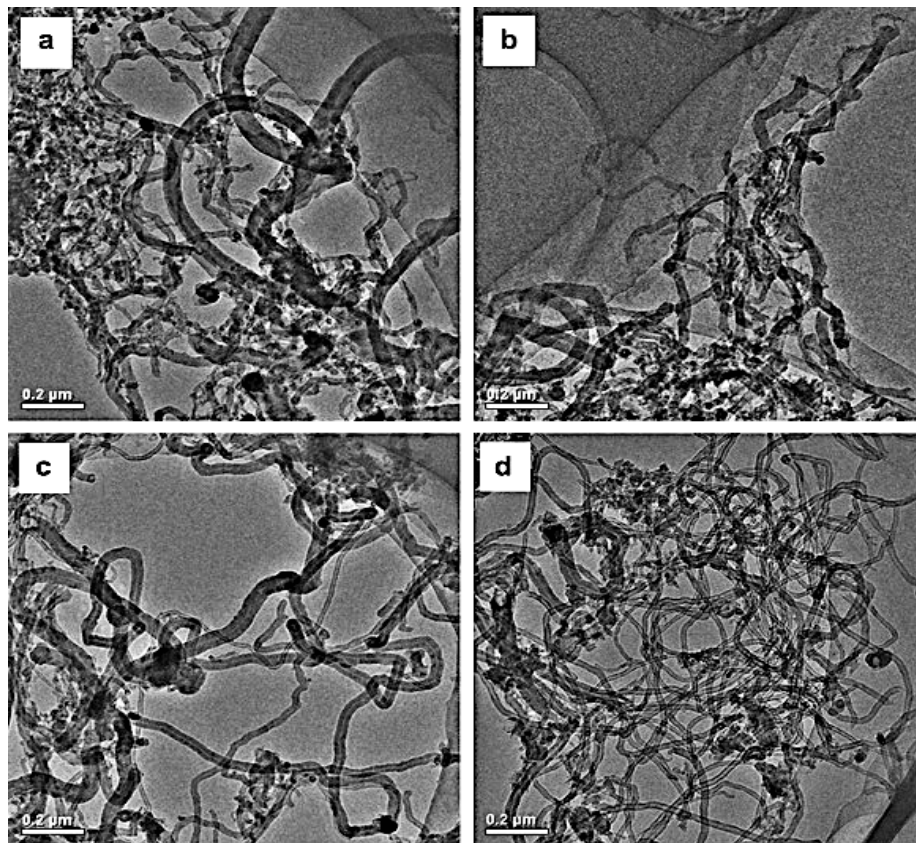


Figure 2.21 CNTs formed at (a) 500 °C, (b) 600 °C, (c) 700 °C, (d) 800 °C (Liu et al., 2011)

In addition, other researchers focused on CNTs morphology change at different catalytic temperatures. Muataz et al. (2006) synthesised CNTs from benzene and ferrocene with different temperatures. They found that CNTs produced at 500 °C have less impurity than that obtained at 850 °C. The higher catalytic temperature promoted the formation of non-tubular carbons like nanofibers. They also stated that there was a positive corrective between the average diameter, length of CNTs and reaction temperature, due to the main effect of increasing temperatures was to increase the metal particle size. Similar results have been reported by Mishra et al (2012), who used waste PP as a precursor for synthesizing CNTs with Ni-based catalysts under different temperatures (600 °C, 700 °C, and 800 °C). CNTs with smooth surface and less defects were synthesised at higher temperature, and higher impurities, defects and disorder CNTs were produced at lower

temperature. This could be explained based on CNTs formation mechanism. The mechanisms of CNTs formation can be examined by solubility, diffusion precipitation, involving the diffusion of carbons into the metal surface and the precipitation of carbons from metal surface. The decomposition rate of hydrocarbons to solid carbons could result the difference in morphology. The CNTs growth rate was also studied by Lee et al. (2001) who worked on CNTs synthesis from acetylene on a Fe/SiO₂ catalyst at a temperature range 750 °C-950 °C. The average rate of CNTs at 750 °C, 850 °C, and 950 °C was obtained as 0.5 ± 0.05 , 1.0 ± 0.1 and 2.0 ± 0.2 nm/min for 10 mins (Figure 2.22), and the diameter of CNTs is in the range of 20-40, 40-80, and 90-170 nm, respectively. The increase of growth rate with increasing catalytic temperature is due to the enhanced different diffusion and reaction rates of carbon. They found the average diameter of catalytic metal particles is 40 ± 10 , 90 ± 20 , and 150 ± 40 nm, respectively, at 750 °C, 850 °C, and 950 °C. The size of catalytic particles determines the diameter of CNTs. Therefore, larger diameter and lower density of CNTs were grown with increasing catalytic temperature. In addition, TGA results (Figure 2.23) provides a strong evidence that the degree of crystalline perfection of CNTs becomes better with an increase of catalytic temperature in the above study.

Kim et al. (2005) investigated the temperature-dependent (600 °C-800 °C) growth rate of CNTs of ferrocene and acetylene. The CNTs length and growth rate were affected by catalytic temperature (Table 2.10). The growth rate of CNTs is increased exponentially with increasing temperature. It was suggested that the diffusion of carbon atoms was promoted by increasing temperature. Golshadi et al. (2014) also proposed that the changes in catalytic temperature would change the reaction kinetics, consequently leading changes

on CNTs morphology, such as thickness of CNTs. The effect of temperature on CNTs synthesis and structure was studied at 675 °C, 700 °C, 750 °C, and 800 °C. TEM analysis of the produced CNTs at different temperatures is shown in Figure 2.24. CNT wall thickness is increased with an increase of temperature, due to the promotion of vapor deposition reaction kinetics.

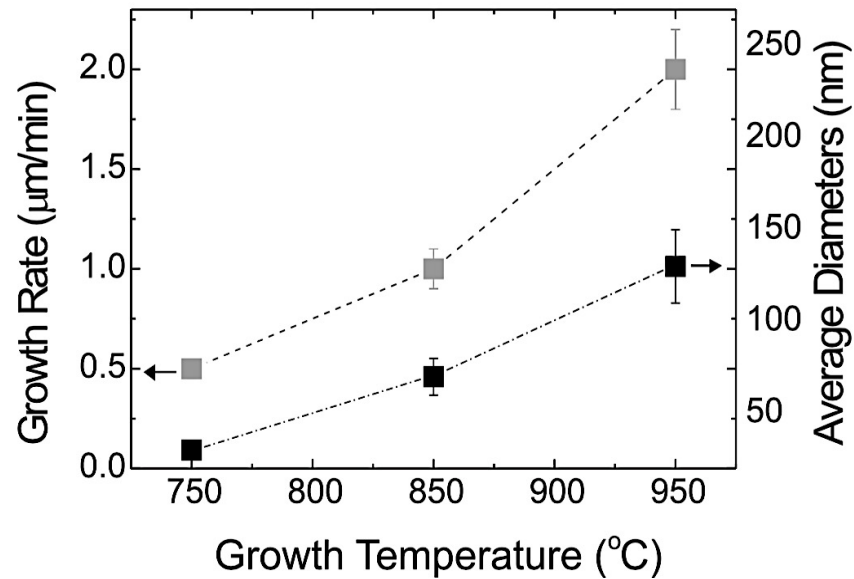


Figure 2.22 CNTs growth rate and diameter change with growth temperatures (Lee et al., 2001)

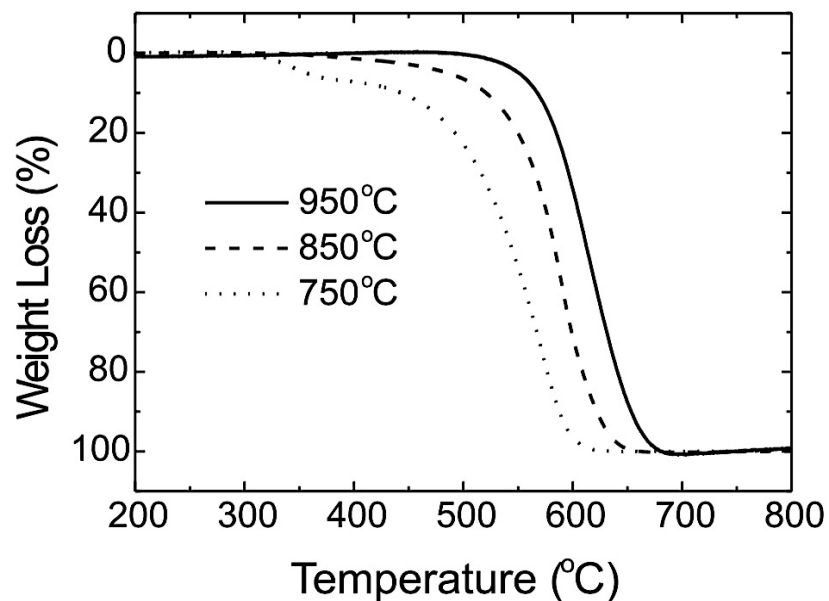


Figure 2.23 TGA results for CNTs growth at different temperatures (Lee et al., 2001)

Table 2.10 CNTs length and growth change with different catalytic temperatures (Kim et al., 2005)

<i>Temperature (°C)</i>	<i>Average length (μm)</i>	<i>Growth rate (μm)</i>
600	4±1	0.4±0.1
650	12±2	1.2±0.2
700	30±10	3±1
750	50±20	5±2
800	100±40	10±4

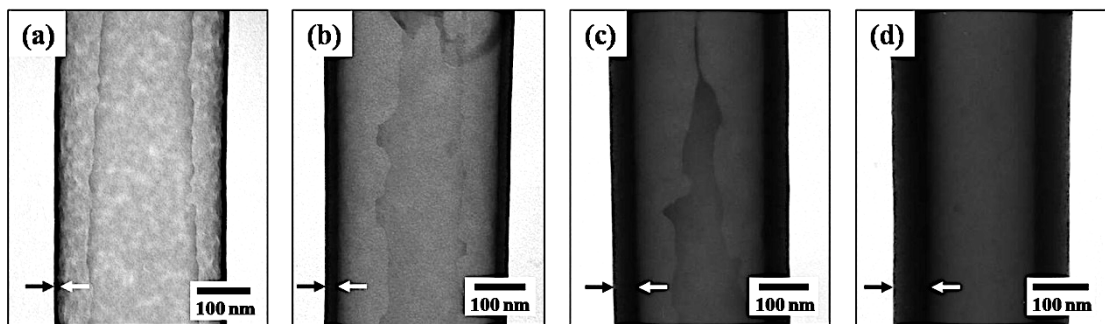


Figure 2.24 TEM results of grown CNTs for temperatures at (a) 675 °C, (b) 700 °C, (c) 750 °C, and (d) 800 °C (Golshadi et al., 2014)

Overall, different catalytic temperatures during pyrolysis process result in the changes of quality and quantity of CNTs, due to the derived changes of gas composition, kinetics, and diffusion rate of carbons on metal particles. Higher catalytic temperature is reported favouring for less defective, well crystallised, high yield and high purity CNTs. However, too high temperature could cause serious sintering of metal particles.

2.3.3 Additional steam to system

CNTs growth suffers from the generation of amorphous carbons on the surface of active catalysts. The formed amorphous carbons can deteriorate the activity and life time of catalysts and hinder the growth of CNTs. Catalyst deactivation by coking formation is a

common issue for CNTs formation in CVD process. A controlled amount of water vapour is reported to assist the growth of CNTs and extension of catalysts lifetime. It is explained that water vapour could etch amorphous carbons on the surface of metal nanoparticle catalysts. The amount of water selection is according to the surface area of catalyst support and metal particles. For example, the water concentration was considered higher for the higher surface area of catalyst (Ago et al., 2006). The introduction of water vapour in the growth ambient provides a new reaction pathway of cleaning the catalysts particles by etching away carbon coating through selective oxidation, as shown in Figure 2.25 (Hu et al., 2008). The dominant pathway shifts to synthesis and results in an improvement of CNTs production.

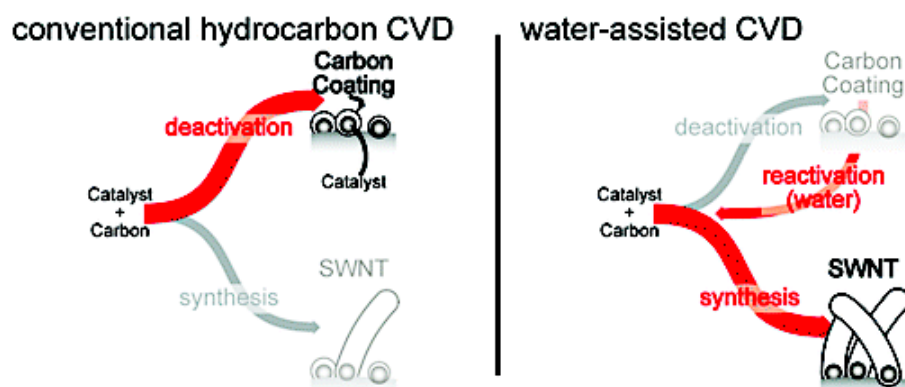


Figure 2.25 Mechanism of CNTs formation by CVD with water addition (Hu et al., 2008)

For example, the effect of water vapour on CNTs growth for methane over Fe/MgO catalysts was investigated by Ago et al. (2006). They found the lifetime of catalysts was extended by increasing water concentration in the system (Figure 2.26). At water concentration of 10300 ppm, the lifetime of catalyst was significantly increased from 7 min to 20 mins, and the carbon yield increased from 16.1% to 19.7%. The carbon yield increased with an increase of water addition until it reached about 11500 ppm and then decreased rapidly. It is suggested that not only amorphous carbons but also CNTs were

oxidised by excess water vapour. Lee et al. (2012) produced CNTs from methane catalytic pyrolysis. They also found the life time of catalysts and carbon yield changed with steam addition. 133.3 ppm seemed to be the optimum water vapour amount for CNTs production. The half-life time extended from 17 mins to 26 mins with 133.3 ppm introduction of water vapour, and the carbon yield reached the highest value. It was reported that CNTs exhibited inner cap structure with introduced water vapour, and the presence of these caps structure led to the formation of a closed internal compartment (Figure 2.27). A possible formation mechanism of these caps has been proposed in Figure 2.27. It was concluded within 4 step: (1) methane decomposition, (2) catalysts deactivation, (3) catalysts reactivation by water vapour addition, and methane decomposition again. The first 2 steps are the same as ordinary CNTs formation mechanism. After water vapour etched the amorphous carbons, the methane decomposition over the reactivated catalyst formed a new graphic layer between the catalyst and CNT interface and the subsequent growth of CNT resulted in the formation of inner cap structure.

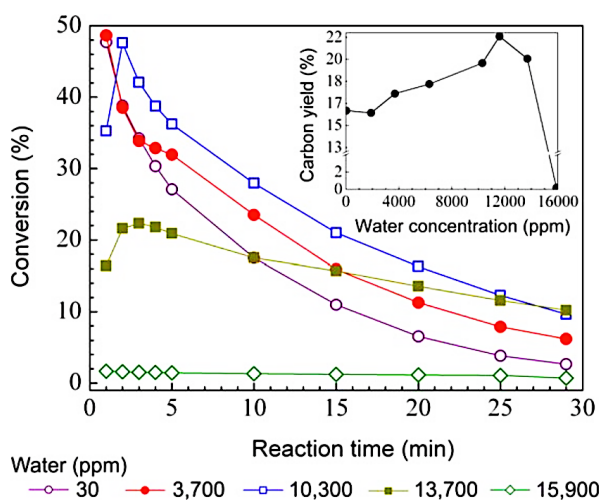


Figure 2.26 Methane conversion of the $\text{Fe}_{94}\text{-Mo}_6/\text{MgO}$ catalysts in the presence of different water concentrations (Ago et al., 2006)

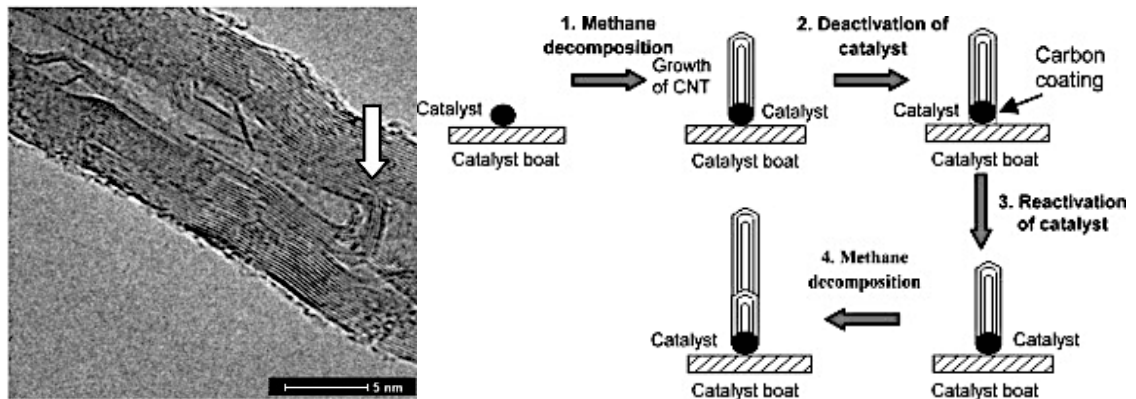


Figure 2.27 CNTs cap formation mechanism with water vapour (Lee et al., 2012)

It was found that there is an optimum value for water vapour for a particular system, depending on other process parameters. Hu et al. (2008) investigated the effect of water vapour on CNTs formation from ethylene over Mo/Fe catalysts. The best CNTs structure was synthesised with 200 sccm water vapour and then decayed with more water vapour addition at 150 sccm. The results showed that a controlled amount of water vapour addition can effectively remove amorphous carbons from active catalysts surface. However, too much water vapour also etched grown CNTs and damaged CNTs structure. Liu et al. (2010) produced CNTs with high purity and bulk yield on silicon substrate from aerosol, with different amounts of introduced water vapour (0, 150 and 700 sccm). Figure 2.28a shows some particles clinging to the CNTs surface without water addition. And the average diameter of CNTs is about 60 nm. Some defect about 2 nm amorphous carbons could be observed on the outside layers. When 150 sccm was used, CNTs diameter was reduced to about 40 nm, and most of the outer surface of tubes wall was free of amorphous carbons. As the amount of water vapor further increased to 700 sccm (Figure 2.28c), CNTs structure was destroyed and large numbers of defects were presented.

However, Acomb et al. (2014) investigated the effect of steam on CNTs from different types of plastics waste. As they reported, the increasing amount of water vapor had effect of not only reducing the amount of carbon deposits, but also reducing the amount of filamentous carbons. It was stated that CNTs are formed when the gasification of deposited carbons was less than the rate of formation. When the water vapour was introduced into the system, the rate of gasification was increased, resulting in the reduction of filamentous carbons. Overall, an optimal amount of water vapor in CVD system could remove the amorphous carbons, enhancing the catalysts activity, life time and the growth rate of CNTs.

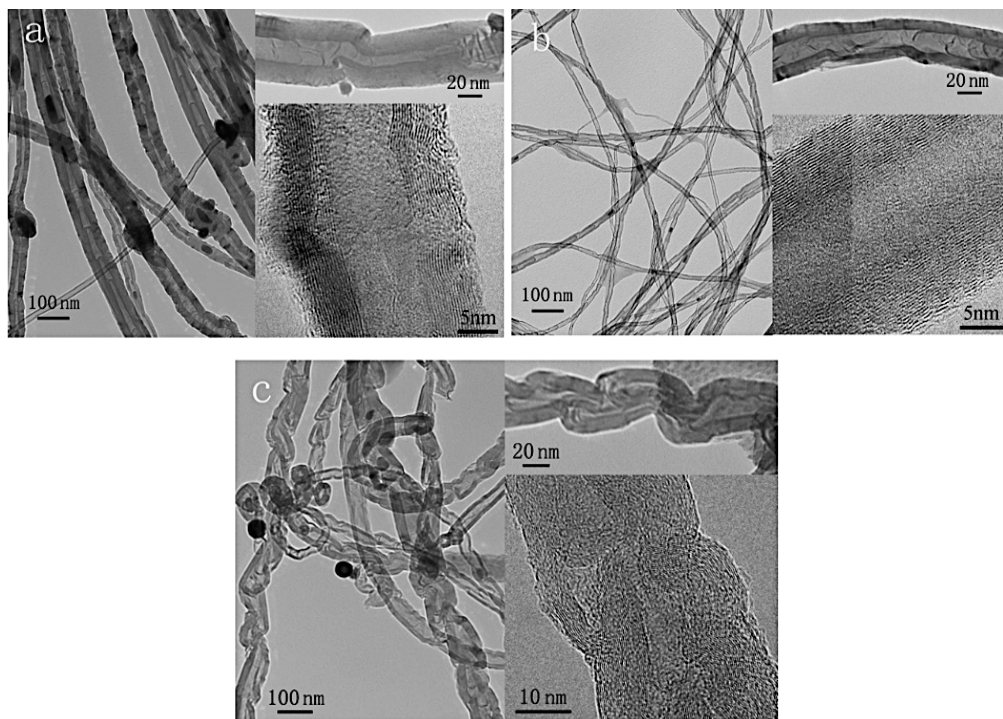


Figure 2.28 TEM images CNT using different amount of water vapor (a) 0, (b) 150 and (c) 700 sccm (Liu et al., 2010)

2.4 CNTs quality and quantity evaluation

The quality and quantity of CNTs can significantly affect and limit their applications. For example, An et al. (2003) synthesised CNT composite from the catalytic decomposition of acetylene over Fe/aluminum ceramic catalysts. It was reported that the CNT content increased with the increase of Fe content. The mechanical properties of the produced composite material were also enhanced with the increase of CNTs formation. Flahaut et al. (2000) prepared Fe-Al₂O₃ ceramics with and without CNTs to study composites properties, and they found those contained higher quantities of CNTs and much less nanofibers. A variety of different techniques can be used to characterise the surface chemistry or structure of CNTs. No single measurement tool provided a complete characterization to identify the quality and quantity of CNTs. Table 2.11 highlights the most important and common methods of analysis such as scanning electron microscopy (SEM), transmission electron microscopy (TEM), high resolution TEM (HRTEM), Raman spectroscopy, and thermogravimetric analysis (TGA) (Wepasnick et al., 2010). For example, the structure of CNTs such as diameter distribution, wall thickness, length could be analysed by SEM, TEM, and HRTEM. And the quantity of CNTs could be identified by TGA and Raman spectroscopy.

Table 2.11 Common techniques for CNTs analysis (Wepasnick et al., 2010)

<i>Analytical technique</i>	<i>Information provided</i>	<i>Limitations</i>
Infrared spectroscopy (IR)	Functional group identification	Not quantitative, some IR modes are too weak to be observed
X-ray photoelectron spectroscopy (XPS)	Surface composition and in principle, information about functional groups	Requires relatively large amounts of sample (about 5 mg) peak-fitting is often ambiguous and over interpreted
Chemical derivatization	Direct quantification of targeted functional groups	Not all functions groups can be derivatised
Boehm titrations	Quantification of protic functional group	Does not provide information on aprotic functionalities. Requires large amounts of sample (over 10 mg)
thermogravimetric analysis (TGA)	Concentration of organic species attached to CNTs	Requires large amount of sample (over 10 mg). Data interpretation is often subjective
Electron energy loss spectroscopy (EELS)	Surface composition and functional groups identification	Can be difficult to implement for routine analysis
scanning electron microscopy (SEM) and transmission electron microscopy (TEM)	Images of CNTs, observation of sidewalls, CNT diameter, length, and dispersion state can also be determined. Chemical analysis by EDX is also often available in TEMs	CNTs are susceptible to damage from the high-energy electron beam. Sample preparation and drying can result in ambiguous analysis
Raman spectroscopy	$I_D:I_G$ band ratios can provide a metric of sidewall damage or purity	The $I_D:I_G$ band ratios can be misinterpreted or misleading

2.4.1 Electron microscope analysis

Scanning electron microscope (SEM) and transmission electron microscope (TEM) are important techniques to study the ultrastructure of materials. SEM provide the images of CNTs by scanning the samples with an electrons beam which interact with atoms of CNTs. This method can be used to basically identify the morphology of CNTs, to evaluate the quality of CNTs production (Figure 2.29 a). For further high magnification measurement, transmission electron microscopy (TEM) is used. The high energy electrons (up to 300 keV) are applied to obtain higher resolution images of CNT (Latorre et al., 2015). The minor dimensions such as inner and outer diameter, length can be determined (Figure 2.29 b). In addition, high resolution TEM (HRTEM) could provide more details of CNTs, such as layers' number of one tube (Figure 2.29c)

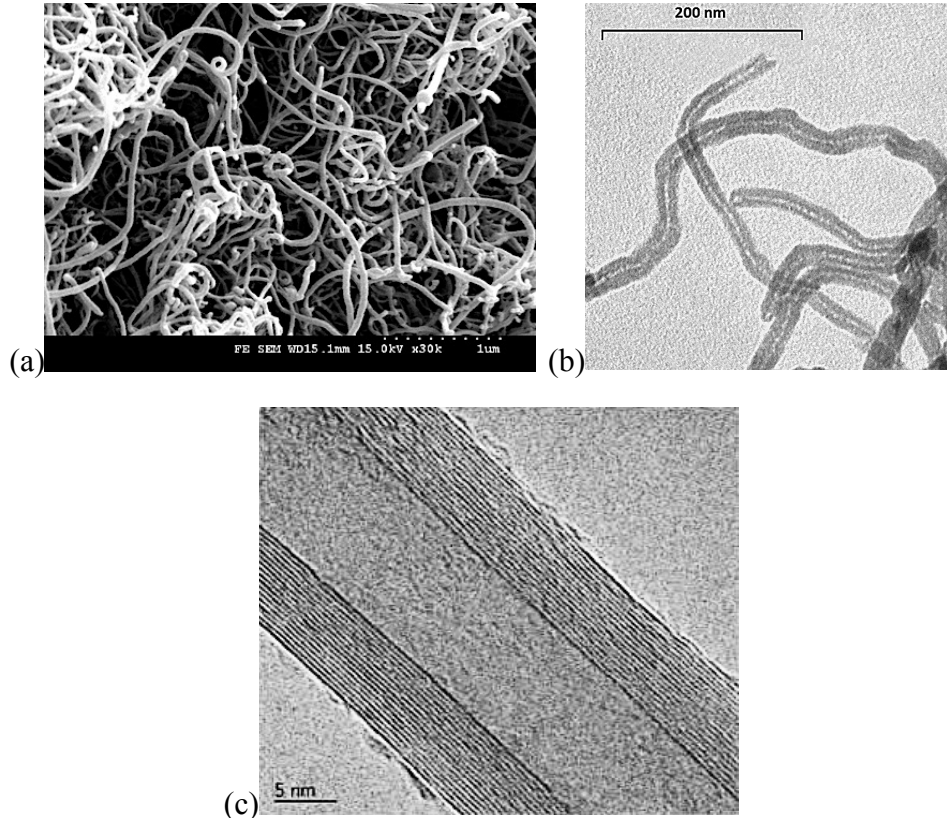


Figure 2.29 Electron microscope analysis of CNTs (a) SEM, (b) TEM, (c) HRTEM
(Latorre et al., 2015)

2.4.2 Raman spectroscopy analysis

Raman spectroscopy (RS) is one of the most useful evaluation techniques for carbon types identification. This technique is used for the characterization of purity of CNTs due to the simple sample preparation and the non-destructive and non-invasive nature (Dresselhaus et al., 2005). RS analysis of CNTs shows two main first order band: G band which is observed at around 1500–1600 cm^{-1} and D band which is observed at around 1300–1350 cm^{-1} (Figure 2.30) (Latorre et al., 2015). The measurement of the ratio between the areas of the two bands (D/G ratio) indicates an estimation of the level of defects in CNTs samples. A small D/G ratio presents a low level of defects in the CNT walls, however, if the CNTs sample contains a high level of impurities, high D/G ratios principally will indicate the presence of carbonaceous residues in the sample (Pillai, 2008).

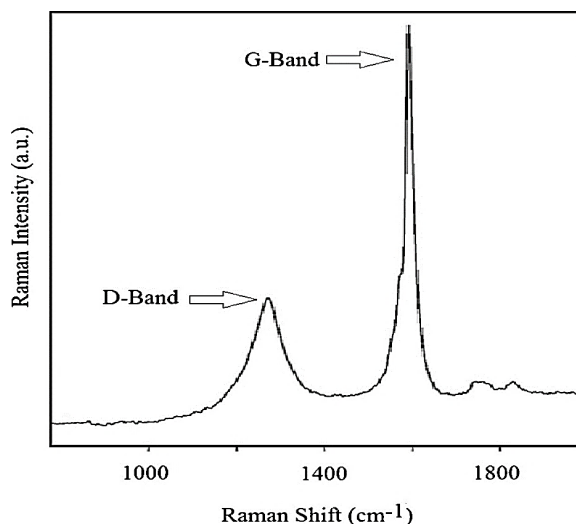


Figure 2.30 Raman spectroscopy analysis of CNTs (Pillai et al., 2008)

2.4.3 Thermogravimetric analysis

Thermogravimetric analysis (TGA) could identify the quality and quantity of carbon nanotubes on both the macro scale (carbon/metal ratio) and the nano scale

(SWCNT/MWCNT ratio). TGA analysis can provide a measurement on the thermal stability and a quantitative estimation of the sample purity on the basis of the distribution of the different burning temperature of carbon materials. In an oxidative atmosphere (TPO–temperature program oxidation), carbon materials are consumed by oxidation which causes their loss as CO and CO₂. And TPO analysis gives a weight-loss curve in three parameters (Figure 3.31). Firstly, the initiation temperature, the temperature at which the material begins to decompose. And then the oxidation temperature, which is the temperature where the weight loss is maximum and is related to the thermal stability of the sample. The oxidation temperature of carbonaceous materials is below 350 °C, for amorphous carbons, the oxidation temperature is below 550 °C. And the oxidation temperature is above 550 °C for filamentous carbons (CNTs) (Esteves et al., 2018). From the Y-axis, weight loss can be obtained at different oxidation temperatures. And finally (3) the residual mass, which is the mass that remains when the heating process is finished, is in relation to the fraction of catalyst employed in CNTs synthesis.

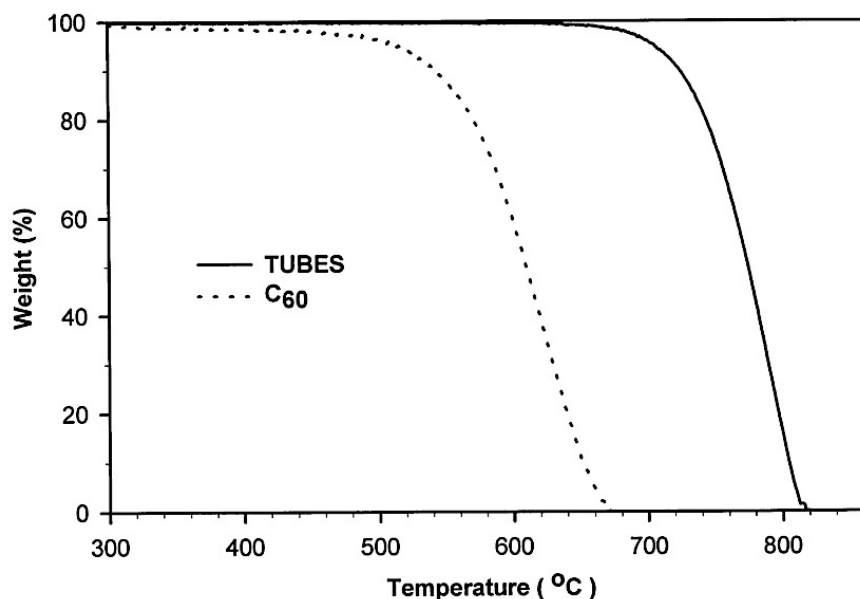


Figure 2.31 Thermogravimetric analysis of CNTs (Esteves et al., 2018)

Chapter 3. Experimental

3.1 Materials preparation

3.1.1 Raw materials

Plastics waste was used as raw materials in this research. The raw material plastic used for Ni-/Fe-based catalysts was polypropylene (PP) pellets with 2 mm diameter in grey (Figure A-A1), provided by BP Chemicals UK. For AAO membrane, ceramic and sphere supported catalysts based studies, waste high density polyethylene plastics (HDPE) with high purity ~ 90% was used (Figure A-A1). HDPE pellets have a diameter around 2 mm and were obtained from Poli Plastic Pellets Ltd., UK.

3.1.2 Catalysts preparation

3.1.2.1 Ni/Fe-based catalysts

Ni/SiO₂ and Fe/SiO₂ catalysts were synthesised by a sol-gel method. During the preparation of the catalysts, the required amount of Ni (NO₃)₂.6H₂O or Fe(NO₃)₃.9H₂O and tetrathoxysilane (TEOS) were dissolved in ethanol, detailed calculation indicated in Appendices A2. The mixture was stirred for one hour at a temperature of 60 °C, and dried at 100 °C overnight. The obtained catalyst precursors were calcined in N₂ and air, respectively, at 750 °C with 10 °Cmin⁻¹ heating rate for 3 hours. All the catalysts used in this study had been reduced under H₂ prior to the experimental tests. Finally, the prepared catalysts were ground and sieved to particle sizes below 50 µm. Catalysts calcined in N₂ were designated as ‘S’ as an indication of the catalyst with small metal particles, and calcined in air were designated as ‘L’ indicating large metal particles in Chapter 4.

3.1.2.2 AAO membrane support catalysts

AAO membrane used for AAO membrane study was from Whatman (Anodisc 13) with a 200 nm nominal pore diameter and a 60 μm thickness (Figure A-A2). Initially, the required amount of Ni $(\text{NO}_3)_2 \cdot 6\text{H}_2\text{O}$ (0.1, 0.5, 1 or 2 molL^{-1}) was dissolved in ethanol, calculation is displayed in Appendices A3. Nickel precursor was doped on AAO membrane by dropping the precursors on the surface of AAO membrane. Filter paper was used to absorb the extra solvent left on the AAO membrane avoiding metal accumulation on the surface of AAO membrane. The obtained Ni/AAO membrane precursor was dried in an oven at 100°C for 24 hrs, then calcined in air for 3 hrs at 700 °C with a 10 °Cmin⁻¹ heating rate (Figure A-A2). In addition, 10 wt.% Ni/Al₂O₃ catalyst (conditioning catalyst) was synthesised by a wet-impregnation method (calculation in Appendices A3). It is noted that the Ni/AAO catalysts prepared from using 0, 0.1, 0.5, 1.0 and 2.0 molL^{-1} of Ni $(\text{NO}_3)_2 \cdot 6\text{H}_2\text{O}$ were assigned as 0AAO, 0.1/AAO, 0.5/AAO, 1.0/AAO and 2.0/AAO catalysts, respectively in Chapter 5.

3.1.2.3 Ceramic membrane support catalysts

Ceramic membrane used was made of aluminium oxide, and with 1mm thickness and 30mm diameter provided by AIMR, Aston University. The original ceramic membrane preparation and formation method was described in Lee's paper (2015). It is noted that the BET surface area of the membrane is below 10 m^2/g . Impurities such as polyethersulfone was used as binder for membrane preparation. The required amounts (0.025 g for 0.1/ceramic, 0.125 g for 0.5/ceramic, 0.251 g for 1.0/ceramic, 0.508 g for 2.0

ceramic) of $\text{Ni}(\text{NO}_3)_2 \cdot 6\text{H}_2\text{O}$ were dissolved in 5ml ethanol, the mixture liquid was loaded on each membrane (≈ 1.32 g) by dropping the precursors into the membrane (calculation in Appendices A4). The obtained wet Ni/ceramic membrane was dried in the oven at 100°C for 24 hrs, then calcined in air at 800°C with 10°Cmin^{-1} heating rate for 3 hours. It is noted that the Ni/ceramic catalysts prepared from using 0.1, 0.5, 1.0 and 2.0 molL^{-1} $\text{Ni}(\text{NO}_3)_2 \cdot 6\text{H}_2\text{O}$ was assigned as 0.1/ceramic, 0.5/ceramic, 1.0/ceramic and 2.0/ceramic, respectively in Chapter 6.

3.1.2.4 Al_2O_3 sphere catalyst

Sphere catalytic support were prepared by co-precipitation method (Dasgupta et al., 2011). Catalyst substrate used was aluminium oxide sphere, which was purchased from Alladdin. The received sphere alumina catalyst was dried in oven at 100°C for 24 hours before Ni loaded. Then the required amounts (0.1 and 1.0 molL^{-1} of $\text{Ni}(\text{NO}_3)_2 \cdot 6\text{H}_2\text{O}$ were dissolved in water, the mixture liquid was loaded on spheres by dropping the precursors until it saturated (calculation in Appendices A5). The obtained wet Ni/sphere was dried in the oven at 100°C for 24 hrs, then calcined in air at 750°C with 2°Cmin^{-1} heating rate for 3 hrs. It is noted that the Ni/sphere catalysts prepared from using 0.1 and 1.0 molL^{-1} $\text{Ni}(\text{NO}_3)_2 \cdot 6\text{H}_2\text{O}$ was assigned as 0.1/sphere and 1.0/sphere, respectively in Chapter 7.

3.2 CNTs synthesis from waste plastics

3.2.1 Ni/Fe-based catalytic-chemical conversion of waste plastics

A two-stage catalytic-gasification reaction system consisting of a plastic pyrolysis stage and a catalytic gasification stage was used (Figure 3.1) (Acomb et al., 2015). In each

experiment, about 1 g waste PP was pyrolysed at 600 °C in the first stage, and the produced vapours representing a hydrocarbon source passed to the second gasification stage where 0.4 g Fe- or Ni based catalyst was located. The second stage temperature was 800 °C. N₂ was used as carrier gas with 80 ml min⁻¹ flow rate. The total reaction time was 50 mins. Two condensers were used to trap the condensable products; water and then dry ice cooled. The non-condensed gases were collected by a 25L TedlarTM gas sample bag for further analysis.

The collected gas samples were analysed off-line by two groups of gas chromatographs (GC). Hydrocarbons (C₁ to C₄) were analysed using a Varian 3380 gas chromatograph with a flame ionization detector, a 80–100 mesh HayeSep column and nitrogen as carrier gas. The permanent gases including hydrogen, oxygen, carbon monoxide and nitrogen, were analysed by a second Varian 3380 GC with two separate columns, using a 60–80 mesh molecular sieve column with argon carrier gas, whilst carbon dioxide was analysed with a HayeSep 80–100 mesh column.

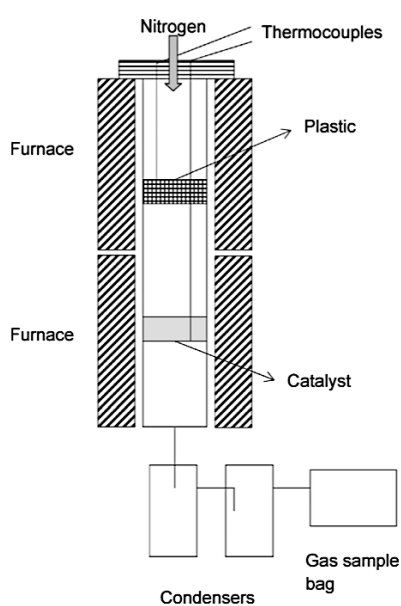


Figure 3.1 Reactor for Ni/Fe-based catalysts study (Acomb et al., 2015)

3.2.2 Ni/AAO catalytic-chemical conversion of waste plastic

A two-stage catalytic thermal-chemical conversion reaction system (Figure 3.2 and Figure A-A3) consisting of a plastic pyrolysis stage and a catalytic gasification stage was used in this study. In each experiment, about 1 g of HDPE was pyrolysed at temperature of 500 °C in the first stage, and the produced vapours representing a hydrocarbon source passed to the second reaction stage where the Ni/AAO catalyst was located. The layer of conditioning catalyst 10 wt.% Ni/Al₂O₃ was used to change the sources of hydrocarbons derived from the pyrolysis of waste plastics prior to the growth of CNTs on the Ni/AAO catalyst. N₂ was used as carrier gas with 100 mL min⁻¹ flow rate. It is to be noted that the catalytic reactor (2nd stage) was preheated to a desired catalytic temperature prior the heating of the 1st stage (pyrolysis). The total reaction time was 60 mins. The system was then slowly cooled down to the room temperature with continuous N₂ gas flow rate of 100 ml min⁻¹. The reacted Ni/AAO catalyst including the grown CNTs was collected for further characterizations. The effect of conditioning catalysts, gasification temperature, steam injection and the content of Ni on AAO membrane were studied in relation to their influences on growth of CNTs. It is to be noted that gas and liquid products that were produced as part of this work were not analysed as the main aim of the research work was to investigate the growth of CNTs.

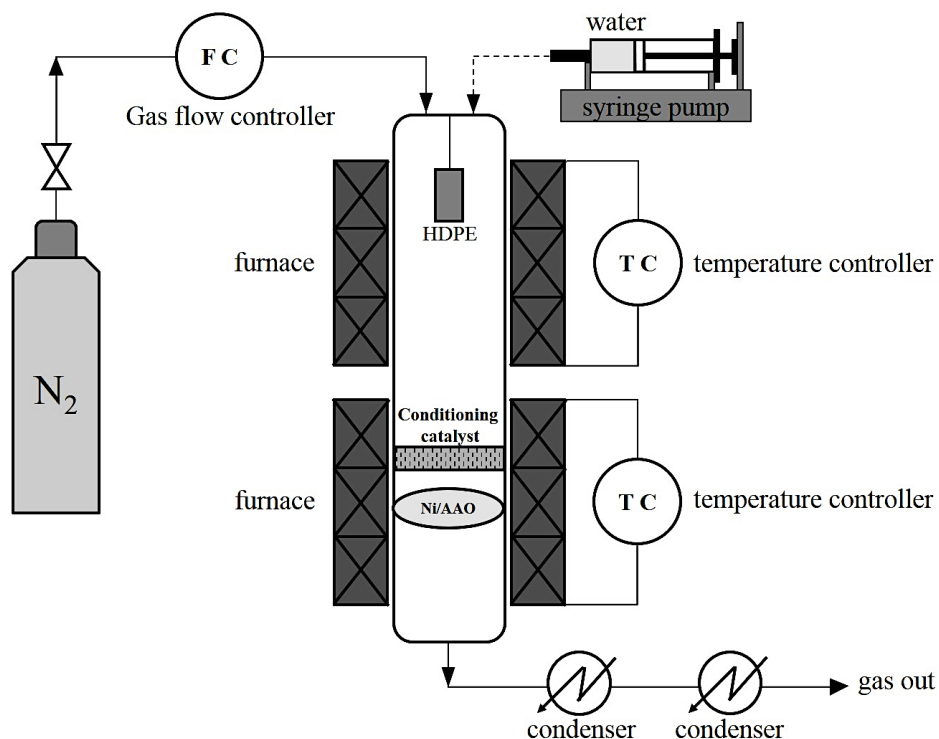


Figure 3.2 Reactor for AAO membrane supported catalysts study

3.2.3 Ceramic and sphere support catalytic-chemical conversion of waste plastics

A two-stage catalytic thermal-chemical conversion reaction system (Figure 3.3) consisting of a plastic pyrolysis stage and a catalytic gasification stage. In each experiment, about 1 g HDPE was pyrolysed at around 500 °C at the first stage, Different reaction temperatures were used in the second stage (600 °C, 700 °C, and 800 °C). N_2 was used as carrier gas with 100 ml min⁻¹ flow rate. The total reaction time was 60 mins. The system was then slowly cooled down to the room temperature with continuous 100 ml min⁻¹ N_2 gas. The reacted Ni/ceramic membrane catalyst including the grown CNTs were collected for further characterizations. The effect of pyrolysis temperature and the content of Ni on ceramic membrane were studied in relative to their influences on the growth of CNTs.

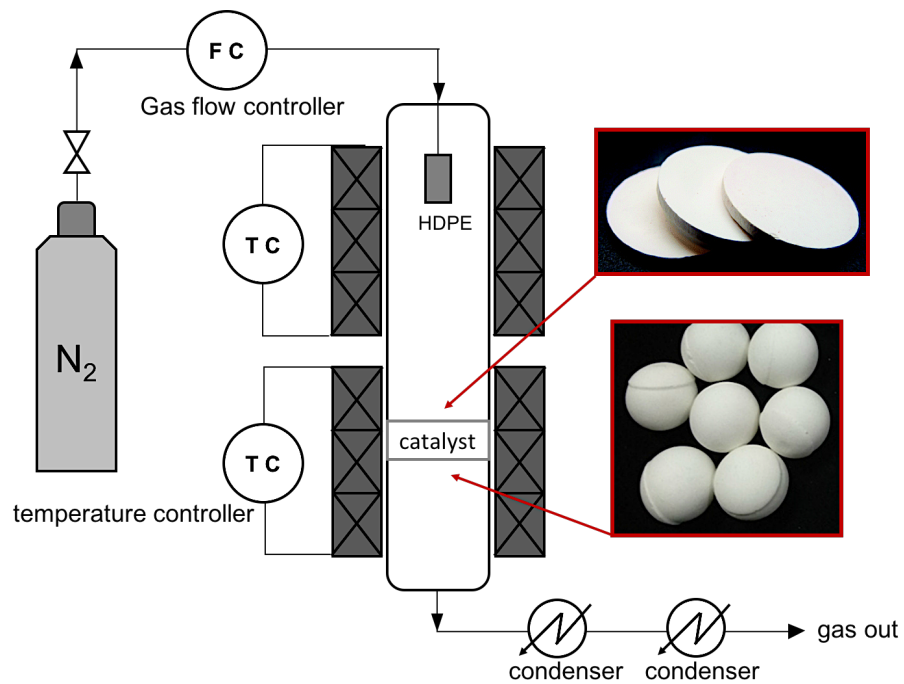


Figure 3.3 Reactor for ceramic and sphere supported catalysts study

3.3 Sample Characterisations

3.3.1 SEM analysis

As stated in Chapter 2.4.1, scanning electron microscope (SEM) is equipment that can produce the images of samples by scanning the surface with a beam of electrons. Various signals which are resulted by the interactions of the electron beam with atoms at various depths can produce the images of samples. Different types of signals include secondary electrons, back scattered electrons, X-rays, absorbed current and transmitted electrons. The SEM schematic is shown in Figure 3.4. The electron beam with an energy range from 0.2 – 40 keV is emitted from an electron gun which contain a filament cathode (Stokes, 2008). Two condenser lenses are used to focus the electron beam. Then, backscatter and secondary electrons detectors will give the images of images' surface. Gold coating are needed for all samples' preparation. In this research, a high resolution

scanning electron microscope (SEM) Stereoscan 360 (Figure A-A4) was used for both fresh and spent samples.

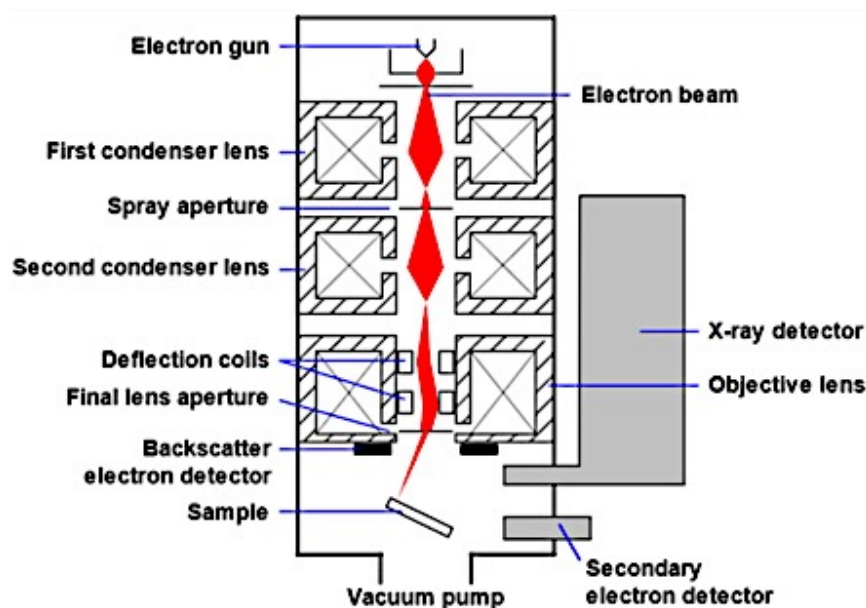


Figure 3.4 SEM schematic diagram (Stokes, 2008)

3.3.2 TEM analysis

Transmission electron microscope (TEM) is a similar technique to SEM, but provide images of samples with higher resolution. TEM transmits a beam of electrons through a specimen to form images of samples. The specimen is an ultrathin section with less than 100 nm thick on a grid. An image is formed from the different interaction of the electrons with the sample surface. JEOL 2010 (Figure A-A5) were used to study the surface morphology of both fresh and spent catalysts, and the distribution of CNTs diameters according to TEM results was carried out using Image-J software. In addition, TEM-EDX is also used for elements test of samples.

3.3.3 XRD analysis

X-ray diffraction XRD is a technique used for determining the atomic and molecular structure of a crystal. The different crystalline structures can result a beam of incident X-rays to diffract into different specific directions, and then identify the elements (Figure 3.5) (Ewald, 1962). Fresh and spent catalysts were characterised by XRD (Figure A-A6), with elemental analysis assessed by inductively coupled plasma mass spectrometry (ICP-MS), Thermo Scientific iCAP 7000 ICP spectrometer after complete sample digestion in conc. Nitric acid, shown in Figure A9, and the data was analysed with Stoe IPDS2 software. The particle size could be calculated from XRD results using Highscore software.

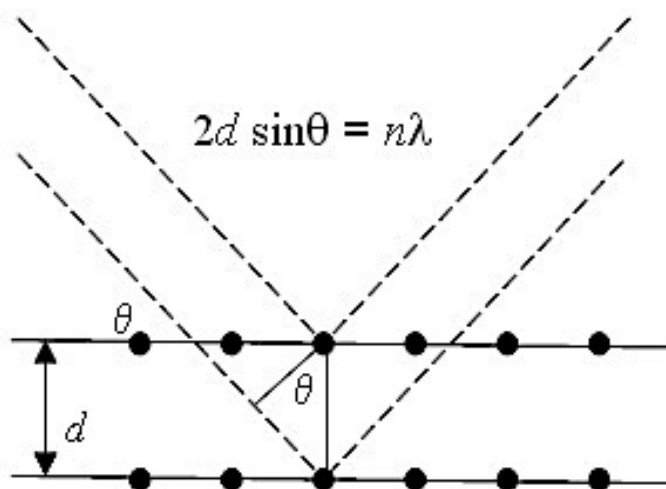


Figure 3.5 X-rays to diffract into specific direction (Ewald, 1962)

3.3.4 TGA analysis

Temperature programmed oxidation (TPO) of the reacted catalysts was analysed to obtain information of carbon coke formation on the surface of the spent catalysts; and the

reducibility of the fresh catalysts was determined using temperature programmed reduction (TPR) with a thermogravimetric analyser (TGA) STA-780 series (Figure A-A7) and TA Instruments, SDT-Q600 (Figure A-A8). During the TPO analysis, around 10 mg of the reacted catalyst was heated in an atmosphere of air at $10^{\circ}\text{C min}^{-1}$ to a final temperature of 800°C . For the TPR analysis, the fresh catalyst was heated at $40^{\circ}\text{C min}^{-1}$ to 150°C and held for 10 mins, then heated at $10^{\circ}\text{C min}^{-1}$ to 800°C in an atmosphere consisting of a gas mixture 5 vol.% H_2 and 95 vol.% N_2 with 50 ml min^{-1} flow rate.

Chapter 4. Carbon nanotubes growth with Ni/Fe- based catalysts

This chapter aims to investigate the influences of the types of metal (Fe and Ni) and the particle size of the metals on production of CNTs and hydrogen from thermo-chemical conversion of waste plastics (PP).

4.1 Characterisations of the fresh catalysts

XRD results of the Ni- and Fe-based catalysts are shown in Figure 4.1 and Figure 4.2, respectively. From Figure 4.1, the presence of NiO and Ni are shown in both Ni-based catalysts. The fresh Ni/SiO₂-L catalysts showed four main sharp NiO peaks at 37°, 43°, 64° and 71° (Kukovitskii, et al., 1997; Liu et al., 2011). Weak Ni diffraction peaks were observed in the Ni/SiO₂-S catalyst at 44° and 52° (Mishra et al., 2012). It is indicated that large Ni-based species are present in the Ni/SiO₂-L catalyst, while small Ni-based species were found in the Ni/SiO₂-S catalyst. In addition, a diffraction peak at 27° was observed indicating the presence of graphite carbon on the surface of the reacted Ni/SiO₂ catalyst. As shown in Figure 4.1, sharp diffraction peaks of Ni were observed for the Ni/SiO₂-L-reacted catalyst, compared with the Ni/SiO₂-S-reacted catalyst, indicating that larger Ni particles were produced in the reacted Ni/SiO₂-L catalyst as expected. Figure 4.2 shows the presence of Fe₃O₄ (Takenaka et al., 2004) on the fresh and reacted Fe-based catalysts, suggesting that Fe₂O₃ particles contained in the fresh Fe/SiO₂ catalyst were reduced during the thermo-chemical conversion process. Diffraction of graphite carbon was also observed for the reacted Fe/SiO₂ catalysts with small and large metal particles. Furthermore, compared to the Fe/SiO₂-S, sharp diffraction peaks were observed for the Fe/SiO₂-L catalyst, supporting that large metal particles were formed in the Fe/SiO₂-L catalyst.

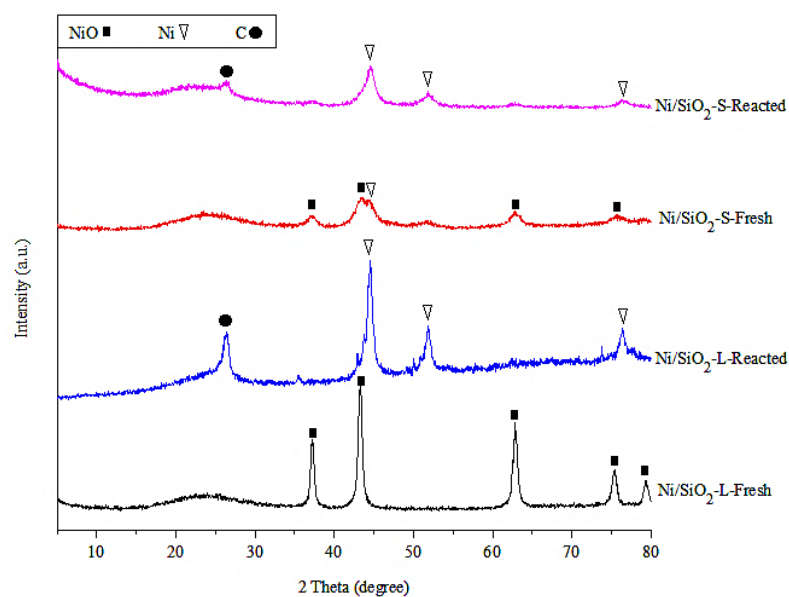


Figure 4.1 XRD results for Ni-based catalysts before and after reaction

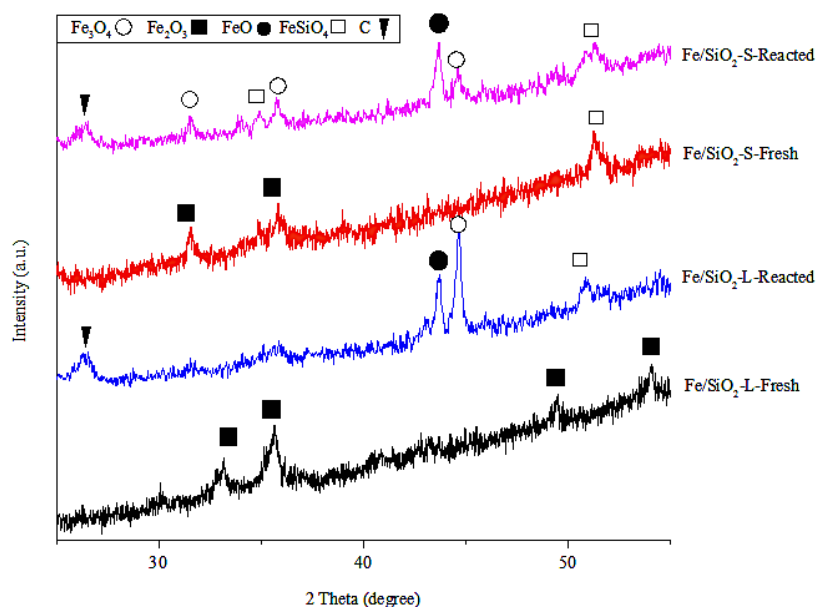


Figure 4.2 XRD results for Fe-based catalysts before and after reactions

Results of TPR analysis for the fresh Ni- and Fe-based catalysts were shown in Figure 4.3. The first reduction peak for the Fe-based catalysts appeared at temperature between 380 and 450 °C, ascribed to the reduction of Fe₂O₃ and FeO. The second reduction peak for the Fe-based catalysts was shown at temperature around 600 °C, which was attributed

to the further reductions of Fe^{2+} (Takenaka et al., 2004). High reduction temperature (around 590 °C) was observed for the Ni-based catalyst, which might be due to that Ni particles were much smaller compared with Fe-based particles. It was reported that higher temperature was required to reduce catalysts with small metal oxide particles (Acomb et al., 2014).

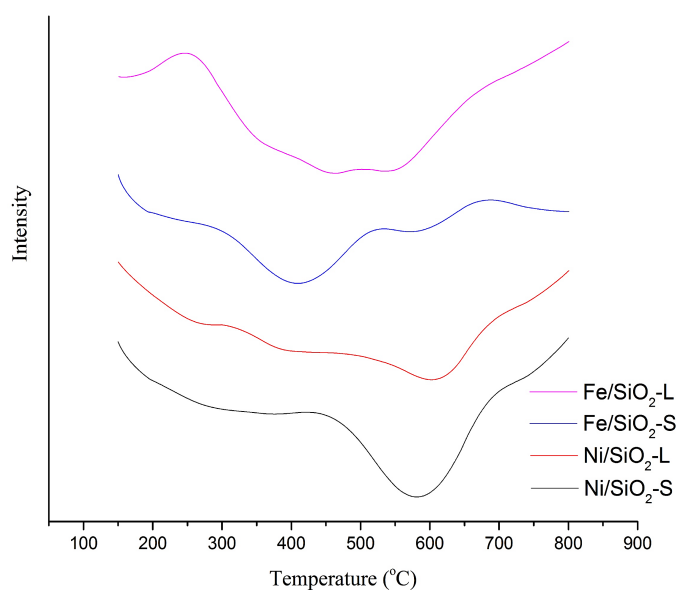


Figure 4.3 TPR results for fresh catalysts

As measured from TEM micrographs (Figure 4.4A-D), the diameter of metal particles of the fresh catalyst (Figure 4a-d) was around 85 nm for the Fe/SiO₂-L, 29 nm for the Fe/SiO₂-S, 13 nm for the Ni/SiO₂-L, and 8 nm for the Ni/SiO₂-S, respectively. Therefore, larger particle sizes were clearly observed on the Ni/SiO₂-L-fresh and the Fe/SiO₂-L-fresh catalysts, compared to the Ni/SiO₂-S-fresh and the Fe/SiO₂-S-fresh catalysts, respectively. The results are consistent with the XRD analysis and TPR analysis (Figure 4.1-4.3), where much higher temperature was required for the reduction of the Ni-based catalysts compared with the Fe-based catalysts. In addition, from the TEM analysis, the Fe-based catalysts show larger particle sizes than the Ni-catalysts.

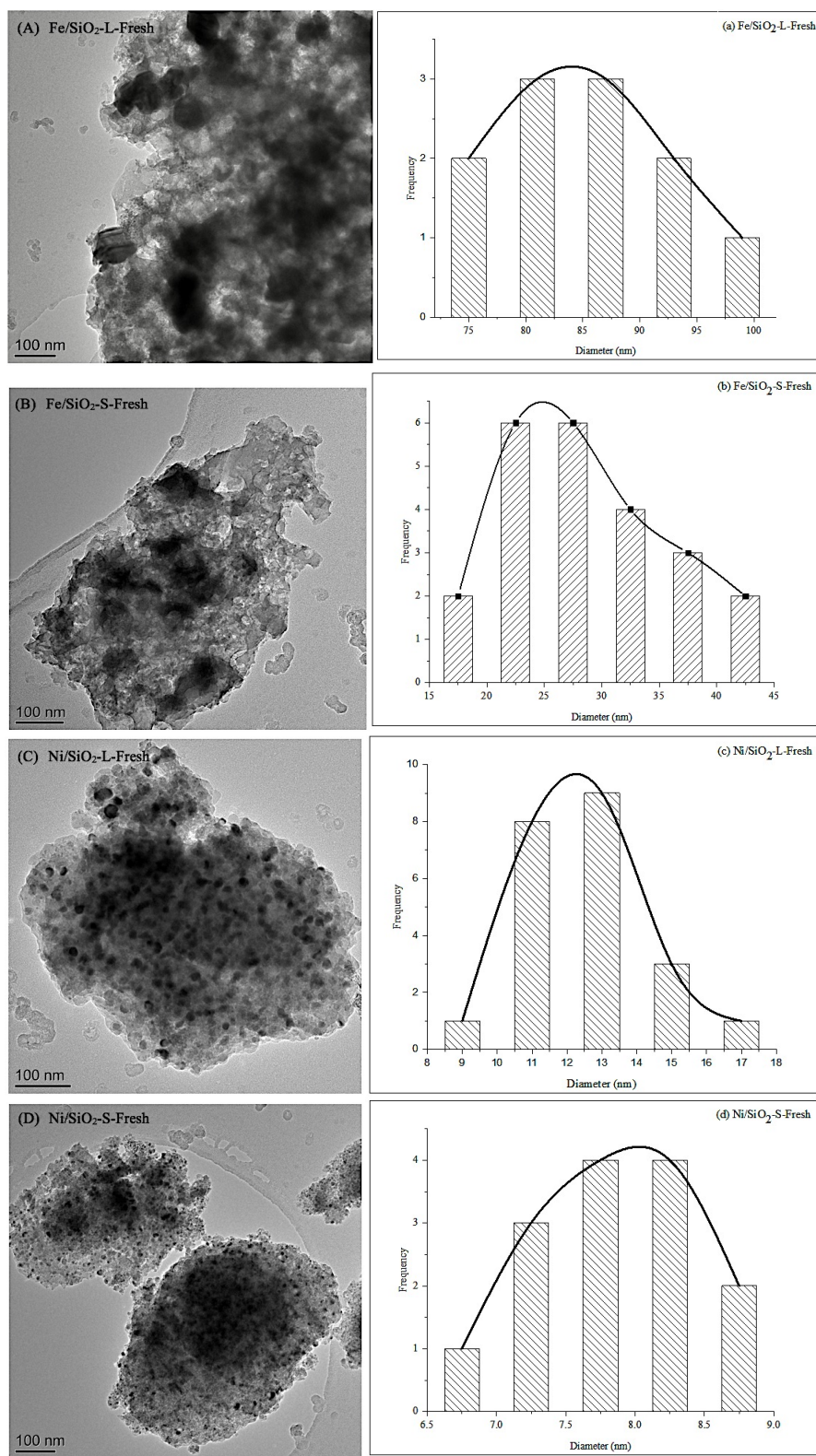


Figure 4.4 TEM results for fresh catalysts (A) Ni/SiO₂-L-fresh (B) Ni/SiO₂-S-fresh (C) Fe/SiO₂-L-fresh (D) Fe/SiO₂-S-fresh, and analysis for metal particles sizes (a) Ni/SiO₂-L-fresh (b) Ni/SiO₂-S-fresh (c) Fe/SiO₂-L-fresh (d) Fe/SiO₂-S-fresh

4.2 Gas yield and composition

Table 4.1 summarises the influence of different catalysts on the production of gas and hydrogen, as well as the yield of carbon from the catalytic thermo-chemical conversion of waste plastic. Regarding the yield of hydrogen production, the following trend was observed: Fe/SiO₂-L > Ni/SiO₂-L > Ni/SiO₂-S > Fe/SiO₂-S (Table 4.1). It seems that the catalyst with large particle size was more effective for H₂ production in this work, when the same metal based catalyst was used. For example, hydrogen production was increased from 15.40 to 25.60 (mmol g⁻¹ plastic), when the catalyst was changed from the Fe/SiO₂-S to the Fe/SiO₂-L catalyst. The hydrogen yield was also increased from 18.10 to 22.60 (mmol g⁻¹ plastic), when the catalyst was changed from the Ni/SiO₂-S to the Ni/SiO₂-L catalyst. In addition, hydrogen concentration was around 41 vol.% using catalysts with small metal particles, and was increased to around 50 vol.%, when the catalysts with large metal particles were used for polypropylene gasification. An increase of particle size of Pt from 2.97 to 3.56 nm resulted in an increase of gas yield during catalytic steam reforming of glycerol, when 5% Pt/C-black catalysts were used (Soares et al., 2016). However, catalyst with smaller Ni-particles was reported to produce higher yields of gas and hydrogen, when various Ni/MCM-41 catalysts were used for gasification of biomass; it was reported that small metal particles resulted in a better dispersion of active sites (Wu et al., 2013). When meso-porous SBA-15 support was used with 5 wt.% metal loading for dry reforming of methane, catalyst with smaller metal particles (≈5 nm) was reported to have higher metal dispersion and exhibited excellent catalytic activity for methane conversion and catalytic stability, compared with same metal loading catalysts with larger

Ni particles (~9 nm) (Karam et al., 2017). Herein, it is suggested that the influence of metal particle size on gas and hydrogen production might be related to the feedstock and the support of catalyst. Compared to the previous report using biomass and MCM-41 as catalyst support, in this work, waste plastic was used with disordered SiO₂ as catalyst support.

Table 4.1 Production of plastics waste by CVD over Ni/Fe-based catalysts

	<i>Fe/SiO₂-S</i>	<i>Fe/SiO₂-L</i>	<i>Ni/SiO₂-S</i>	<i>Ni/SiO₂-L</i>
Gas yield (wt.%)	49.20	63.90	51.20	52.50
Carbon production (wt.%)	26.00	29.00	16.00	16.00
H ₂ production (mmol g ⁻¹ plastics)	15.40	25.60	18.10	22.60
<i>Gas concentrations (Vol.%)</i>				
CO	5.32	7.80	3.30	6.32
H ₂	41.72	50.30	42.20	47.74
CH ₄	39.16	22.70	43.50	38.31
C ₂ -C ₄	13.80	19.20	11.00	7.62

In this work, the iron-based catalyst with large Ni particles produced the highest production of hydrogen. Nickel-based catalysts have been reported to promote hydrogen yield compared to iron based catalysts during hydrogen production from catalytic steam reforming of ethanol (Auprêtre et al., 2002). In addition, nickel catalysts are widely studied for hydrogen production compared to iron, however, in this study, the Fe/SiO₂-L has shown better performance in terms of hydrogen production compared with the nickel catalysts. Iron based catalyst has also been reported to have higher hydrogen production compared to nickel based catalyst, when different metal based catalysts were investigated for hydrogen production from pyrolysis of plastics feedstocks. (Acomb et al., 2016). Therefore, it is suggested that a large amount of carbon formation could result in a high yield of hydrogen due to hydrocarbon decomposition reactions, as shown in Equation 4.1.

As shown in Table 4.1, the Fe/SiO₂-L catalyst produced the highest yield of carbon (29 % in relation to the weight of plastic), while the Ni-based catalysts produced a relative low yield of carbon (16 wt.%).



4.3 The production of CNTs

4.3.1 The Influence of metal species on CNTs production

The reacted Fe- and Ni-based catalysts were analysed by TPO experiments (Figure 4.5). Three stages of carbon oxidation were identified: (1) amorphous carbons ($\approx 550^\circ\text{C}$); (2) filamentous carbons with small diameters ($\approx 660^\circ\text{C}$); and (3) filamentous carbons with large diameters ($\approx 730^\circ\text{C}$) (Ago et al., 2006). The reacted Ni/SiO₂-S catalyst showed significant weight loss at low temperature ($\approx 500^\circ\text{C}$) compared to the other catalysts, suggesting that high amounts of amorphous carbons were formed using the Ni/SiO₂-S catalyst. SEM analysis (Figure 4.6) of the reacted catalysts confirms that the morphology of the CNTs formed on the surface of the Ni/SiO₂-S catalyst was poor compared to the other reacted catalysts.

From Figure 4.5, the oxidation temperature of graphite type carbons (after 600°C) formed on the reacted Fe/SiO₂-L catalyst was higher compared to other catalysts. This is also consistent with the carbon yield as shown in Table 4.1, where the Fe/SiO₂-L catalyst resulted in the highest yield of carbon. Fe has been reported to be preferable for the precipitation of graphitic carbons instead of amorphous carbon during the thermochemical conversion of polypropylene (Mishra et al., 2012).

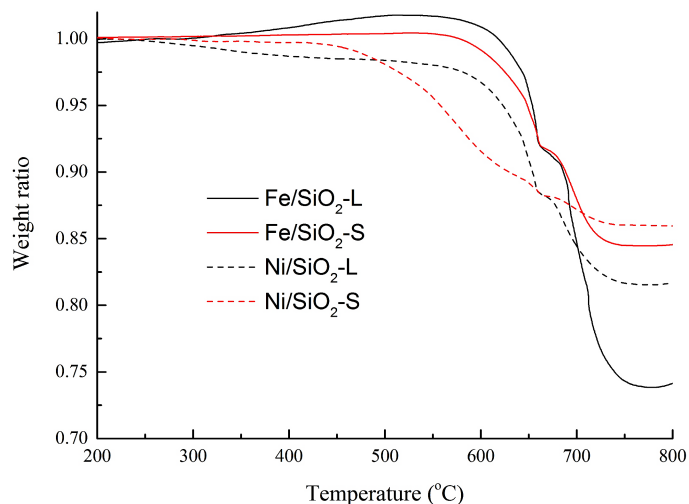


Figure 4.5 TPO results for Fe- and Ni-based catalysts after reaction

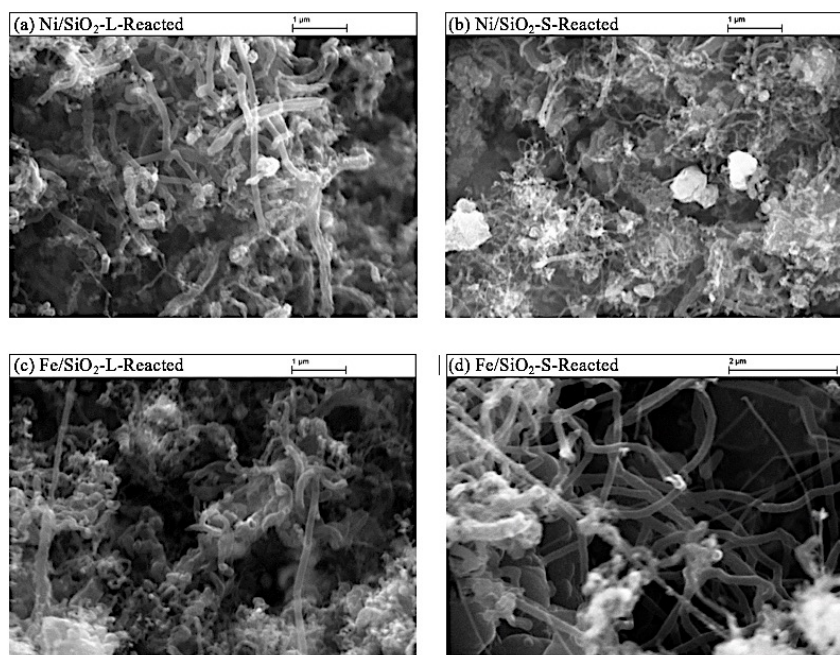


Figure 4.6 SEM results for catalysts after reaction

Similar results were found by Lee et al. (2002) who studied CNTs growth with Ni, Fe and Co catalysts on a silica support using C_2H_2 as feedstock; they reported that Fe-based catalyst produced the highest quality CNTs with homogeneous distributions. It is suggested that the interaction between catalytic metals and support played a key role in the growth of CNTs. A weak interaction between metal and catalyst support was suggested to promote the growth of CNTs, while a strong interaction restricted the

availability of metal particles and thus prohibited the production of CNTs (Danafar et al., 2009). According to the tip-growth mechanism, metal particles are involved in the growth of CNTs. The stronger metal-support interaction that occurs; the less metal particles are available to grow CNTs. In contrast, too weak a metal support interaction might cause the sintering of metal during high temperature reactions. The stronger interaction between Ni particle and SiO₂ support (higher reduction temperature was required for Ni-based catalyst as shown in Figure 4.4) might be ascribed to the poor production of CNTs in this work. Previously, Acomb et al. (2016) investigated the production of CNTs from gasification of plastic using Fe, Ni, Co and Cu-based catalyst and reported that Fe-based catalyst produced CNTs with better quality in terms of the yield and purity. Carbon solubility was suggested as an important factor governing CNTs production, the driving force for CNTs growth was enhanced with the increase of carbon solubility (Anna et al., 2003; Liu et al., 2013). The large carbon solubility of iron particles might be responsible for the better performance during the formation of CNTs (Liu et al., 2013).

4.3.2 The influence of metal particle size on CNTs production

TEM analysis (Figure 4.7) for the reacted catalysts shows that the diameter of CNT is about 98 nm for the Fe/SiO₂-L, 50 nm for the Fe/SiO₂-S, 23 nm for the Ni/SiO₂-L, and 18 nm for the Ni/SiO₂-S, respectively. Compared to the metal particle size of the fresh catalysts (Figure 4.4), the same order of metal particle size has been observed with Fe/SiO₂-L (85 nm) > Fe/SiO₂-S (29 nm) > Ni/SiO₂-L (13 nm) > Ni/SiO₂-S (8 nm). Therefore, it is demonstrated that the diameters of CNTs grown depends on the metal sizes of catalysts.

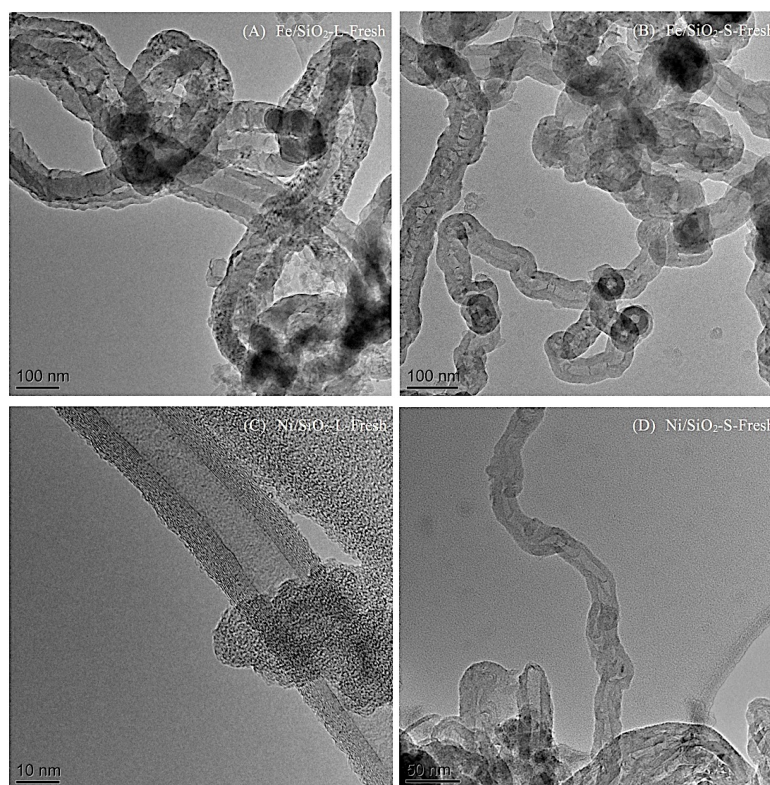


Figure 4.7 TEM results for reacted catalysts (a) Fe-L-Reacted (98 nm) (b) Fe-S-Reacted (50 nm) (c) Ni-L-Reacted (23 nm) (d) Ni-S-Reacted (18 nm)

As shown in Table 4.1, the yield of carbon was increased from 26.00 to 29.00 wt.%, when the Fe/SiO₂-L catalyst was used, compared to the Fe/SiO₂-S catalyst. In addition, the carbon production was also increased using the Ni-based catalyst, when the size of metal particles was increase from around 8 nm to 13 nm (Figure 4.4 and Table 4.1).

Large metal particle size was reported to generate increased yield of carbon deposition on reacted catalyst during catalytic steam reforming of ethanol (Silva et al., 2014). The authors proposed that carbon formation was related to a lower fraction of terrace atoms corresponding to a reducing number of unsaturated metal surface atoms, when catalyst with large metal particles was used during the ethanol steam reforming process. The formation of carbon during catalytic conversion of hydrocarbons was also suggested to require relative large domains of flat terraces of metal particles (Trimm, 1997) . Chen et

al (2005). investigated the influence of Ni particle size on the production of carbon fibers through methane decomposition. They concluded that an optimal metal size of Ni (around 34 nm) was found to be effective for the growth of carbon nanofibers, because smaller Ni particles resulted in a high saturation and a low diffusion of carbon atoms and thus leading to a low production of carbon nanofibers. Furthermore, they suggested that a slow decomposition of hydrocarbons on the surface of metal particles was observed when large crystal Ni particles were presented due to the low surface area of metal particles. This is consistent with the results showing in this work, where the particle size of NiO of around 23 nm was found to produce higher yield of carbon compared to the Ni/SiO₂-S catalyst having NiO particle sizes around 8 nm.

In addition, Cheung et al. (2002) carried out a diameter-controlled synthesis of carbon nanotubes using iron particles with different diameters (3, 9 and 13 nm); CNTs with average diameters of 3, 7 and 12 nm were reported to be produced, respectively. Ding et al. (2004) carried out a molecular dynamic study in relation to the influence of catalyst particle size on growth mechanism and structure of carbon nanotubes. They reported that large catalyst particles containing at least 20 atoms generated CNTs with much better tubular structure compared to CNTs nucleated from smaller clusters (Ding et al., 2004).

In conclusion, it was found consistency existing between metal parcel sizes of catalysts and diameter of CNTs produced. Fe-based catalysts with the larger metal particles resulted in the highest hydrogen production (25.60 mmol g⁻¹ plastic) and the highest yield of carbon (29 wt.%).

Chapter 5. Carbon nanotubes growth with AAO membrane

In this chapter, Ni-based AAO catalysts were investigated to produce CNTs from pyrolysis/gasification of waste plastics aiming to generating high quality CNTs with uniform distributions. The influence of conditioning catalysts, metal loading, reaction temperature and conditioning catalyst (used to modify hydrocarbon vapours derived from pyrolysis of plastic) were also studied to optimise the process conditions.

5.1 Role of AAO Membrane Substrate

AAO membrane was used as substrate of catalyst in this study. The original AAO without nickel loading was identified by XRD diffraction (Figure 5.1), the original AAO membrane showed the presence of three main diffraction peaks at around 43° , 50° and 74° , respectively. These three peaks were identified as Al_2O_3 (Mehrnia et al., 2015; Tapsuan et al., 2012) and marked as ‘AAO’ peaks for the following XRD analysis. According to SEM analysis, a large number of uniform pores (Figure 5.1) and highly ordered nanochannels (Figure A-B1) could be observed on the surface of the AAO membrane without nickel loading. The structure of the AAO membrane used and reported in this study was consistent with AAO templates used in other studies (Hou et al., 2012; Jeong et al., 2004; Sui et al., 2002).

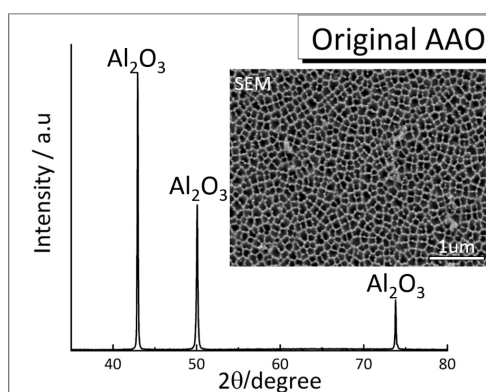


Figure 5.1 XRD results for original AAO membrane without Ni loading and surface SEM image

Ni/AAO catalysts with four different Ni loadings were characterised by XRD, EDX, SEM and TEM. The diffraction peaks of NiO were clearly observed at 37°, 62°, 75° and 78° (Wu et al., 2011) for the 0.5/AAO, 1.0/AAO, and 2.0/AAO (Figure A-B2B-D), respectively. Only one weak diffraction peak at 62° was observed in relation to NiO for the 0.1/AAO (Figure A-B2A). It is suggested the NiO particles in the 0.1/AAO were too small to be detected by XRD. However, the EDX analysis (Table A-B1) confirmed the presence of Ni on the surface of the 0.1/AAO. Semi-quantitative analysis using EDX showed that Ni content was increased from 2.4 to 28.2 wt.% with increasing Ni concentration in the precursor during catalyst preparation. Element of O was originated from NiO and AAO, and Al was from AAO. According to the TEM results (Figure 5.2i-v), the particle size of NiO for the 0.1/AAO (Figure 5.2i) was hardly observed, which was consistent with the XDR results. The NiO diameter was increased from around 20 nm to over 50 nm when the catalyst was changed from the 0.5/AAO to the 2.0/AAO. In addition, various sizes of NiO particles (5-60 nm) were observed on the 2.0/AAO. According to the SEM results (Figure 5.2A-D), the formation of large NiO particles would occur more on the AAO surface rather than the inner channel, resulting in covering and blocking the pores on the surfaces. The blockage of AAO pores with NiO particles is particularly observed on the surface of the 1.0/AAO and the 2.0/AAO in Figure 5.2. Ordered pores could still be clearly observed on surface of the 0.1/AAO and the 0.5/AAO (Figure 5.2A and 2B). The particle size of NiO calculated from the XRD analysis is shown in Table 5.1. The NiO particle sizes are consistent with the ones shown in the TEM results. The catalytic particle size was too small to be analysed through XRD, while around 32.6 nm

of NiO particles are obtained for the 0.5/AAO, and larger particle sizes of NiO were observed on the 1.0/AAO (36.9 nm) and the 2.0/AAO catalyst (47.7 nm).

It is suggested that the regular pores and ordered channels of AAO could control the diameters of NiO loaded inside the membrane when the Ni loading was low (e.g. the 0.1/AAO). However, when Ni content was further increased (e.g. the 1.0/AAO), the membrane could no longer control the size of NiO particles. Therefore, a larger range of diameters of NiO appeared. The CNTs diameter was reported highly depending on the sizes of active metals from our previous study (Liu et al. 2017). Therefore, the AAO used in this study aims to control the active metal sizes, in order to produce high quality of CNTs with uniform diameter distribution.

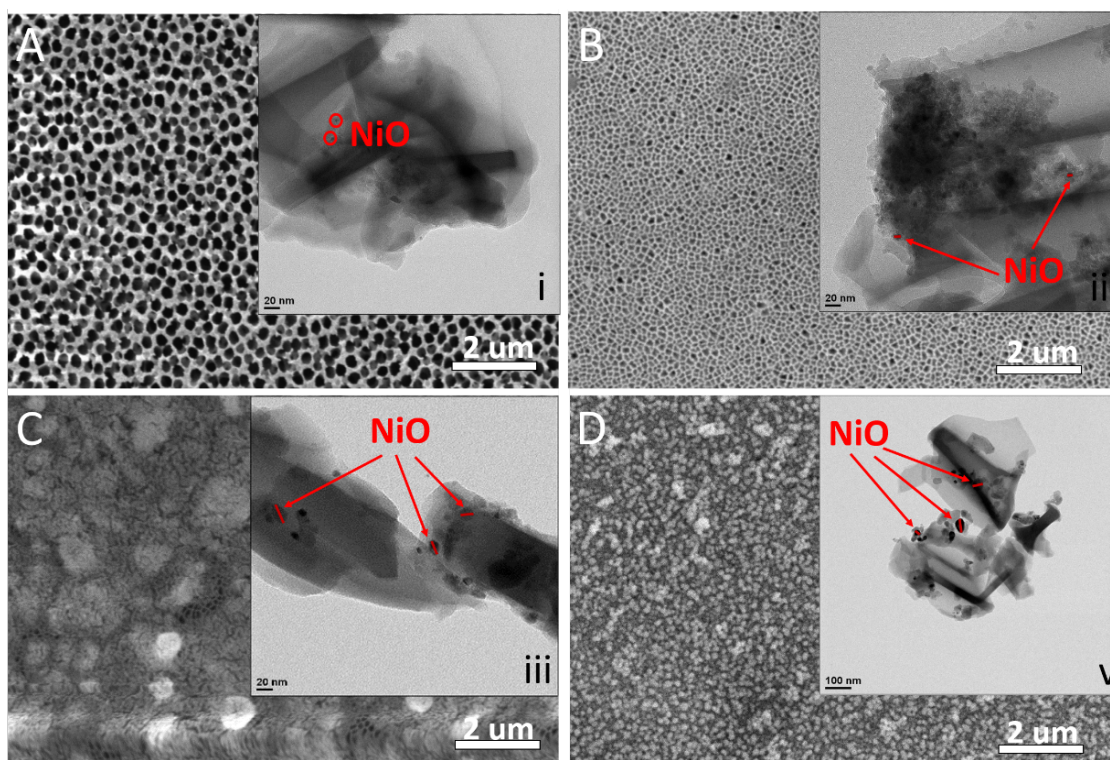


Figure 5.2 SEM (A-D) and TEM (i-v) results for fresh 0.1/AAO, 0.5/AAO, 1.0/AAO, and 2.0/AAO

Table 5.1 X-ray diffraction crystallite size measurements of NiO

	<i>0.1 / AAO</i>	<i>0.5 / AAO</i>	<i>1.0 / AAO</i>	<i>2.0 / AAO</i>
Crystallite size / nm	-	32.6	36.7	47.7

5.2 Production of CNTs over AAO membrane supported catalysts

Three reaction parameters using Ni/AAO membrane catalysts were investigated in relation to their effect on the formation of CNTs from waste plastics. Table 5.2 is a summary of different experimental reaction parameters (Ni content, reaction temperature, and steam addition) and the information of carbon formation (amount of amorphous carbon, filamentous carbon and CNTs average diameter). When the effect of Ni content was studied, thermo-chemical conversion of waste HDPE was carried out in the presence of Ni/AAO catalyst with four different Ni contents (0.1, 0.5, 1.0 and 2.0) at 700 °C. When the reaction temperature was studied, the 0.1/AAO catalyst was used to investigate the influence of reaction temperature (600 °C, 700 °C and 800 °C) on the formation of CNTs. The effect of water presence was studied with three different flow rates of 0, 2 and 5 ml h⁻¹ with the 0.1/AAO catalyst; thus the total amount of water injected into the reactor was 0, 2, and 5 ml, respectively.

In Table 5.2, the produced amorphous and filamentous carbons were calculated according to TGA analysis under air (TGA-TPO), as shown in Figure A-B3, A-B4, and A-B5. TGA-TPO analysis of the spent catalyst was carried out to obtain the quantification of the formed carbons on the reacted catalyst, and also to discuss the oxidation temperature of the formed CNTs. It is assumed that the oxidation temperature below 550 °C was assigned to amorphous carbons and the oxidation above 550 °C in TPO was assigned to

filamentous carbon (assumed as CNTs in this work) (Wu et al., 2014). The fractions of the two different types of carbon are summarised in Table 5.2. The carbon fraction/yield was obtained by the weight in relation to carbons divided by the weight of reacted catalyst. The quality of CNTs is discussed mainly according to the distribution of CNTs diameter. The average diameter of CNTs was calculated based on the SEM results and is summarised in Figure A-B6, A-B7 and A-B8. The standard deviation (SD) number is used as the factor which identifies the quality of CNTs in this study. A smaller SD indicates a better quality of the produced CNTs.

Table 5.2 Overall view of experiments parameters and carbon deposition

	<i>Ni</i> <i>Content</i> <i>(molL⁻¹)</i>	<i>Temperature</i> <i>°C</i>	<i>Steam</i> <i>addition</i> <i>(mL)</i>	<i>Amorphous</i> <i>carbon (%)</i>	<i>Filamentous</i> <i>carbon (%)</i>	<i>CNTs</i> <i>average</i> <i>diameter</i> <i>(nm)</i>
Effect of the Ni content	0.1	700	-	2.5	7.5	26.7±4.0
	0.5	700	-	1.2	5.3	38.3±14.2
	1.0	700	-	2.5	22.0	40.1±11.5
	2.0	700	-	2.5	20.5	54.1±7.5
Effect of temperature	0.1	600	-	1.2	1.8	26.2±6.6
	0.1	700	-	2.5	7.5	33.5±5.6
	0.1	800	-	3.8	4.0	27.2±7.2
Effect of steam addition	0.1	700	0	2.5	7.5	33.5±5.6
	0.1	700	2	1.7	3.3	29.2±5.7
	0.1	700	5	1.7	1.3	21.9±3.9

5.2.1 Effect of the conditioning catalyst on CNTs formation

A layer of conditioning Ni/Al₂O₃ (0 g, 0.2 g, 0.5 g, and 1 g) catalyst was placed on the top of the 0.1/AAO to form CNTs through catalytic thermal chemical conversion of waste plastics at 700 °C. The aim was to investigate the influence of the modification of carbon sources on the production of CNTs from waste plastics.

Tip-growth and base-growth are two models for the production of CNTs, according to the interaction between catalysts and substrate. When the catalyst-substrate interaction is weak, hydrocarbon sources decompose on the top surface of the catalyst metal, carbon diffuses through catalytic particles. And CNTs are formed across the bottom of metal particles, pushing the catalyst particle off the substrate. When the catalyst-substrate interaction is strong, initial hydrocarbon decomposition and carbon diffusion take place similar to that in the tip-growth model, but the catalyst particle remains at the bottom of the substrate.

Filamentous carbons were observed on the surface of the catalyst. Figure 5.3a shows the CNTs produced without the conditioning catalyst. The pores of 0.1/AAO could still be clearly observed, indicating that the surface was not covered with filamentous carbons.

When 0.2 g conditioning catalyst was placed on the top of the AAO catalyst, the SEM result (Figure 5.3b) showed that a small amount of filamentous was obtained. When more conditioning catalysts (0.5 g and 1 g Ni/Al₂O₃) were used, more filamentous carbons could be observed on the surface of the 0.1/AAO. TEM results (Figure 5.4) further confirm that the filamentous carbons were mainly carbon nanotubes. The quantity of CNTs was assessed by temperature programmed oxidation (TPO) analysis, and the TGA-

TPO (weight loss data) and DTG-TPO (derivate data) results are shown in Figure 5.5a and b, respectively. It is suggested that similar pattern of carbon oxidation was observed from the TPO results, as one main oxidation peak at around 620 °C was found for all the AAO-based catalysts using various amounts of conditioning catalysts. However, the amount of carbon yield seems to be increased with the increase of the amount of conditioning catalyst. For example, the weight loss was increased from 4 to 9 %, when the amount of conditioning catalyst was increased from 0 to 1 g.

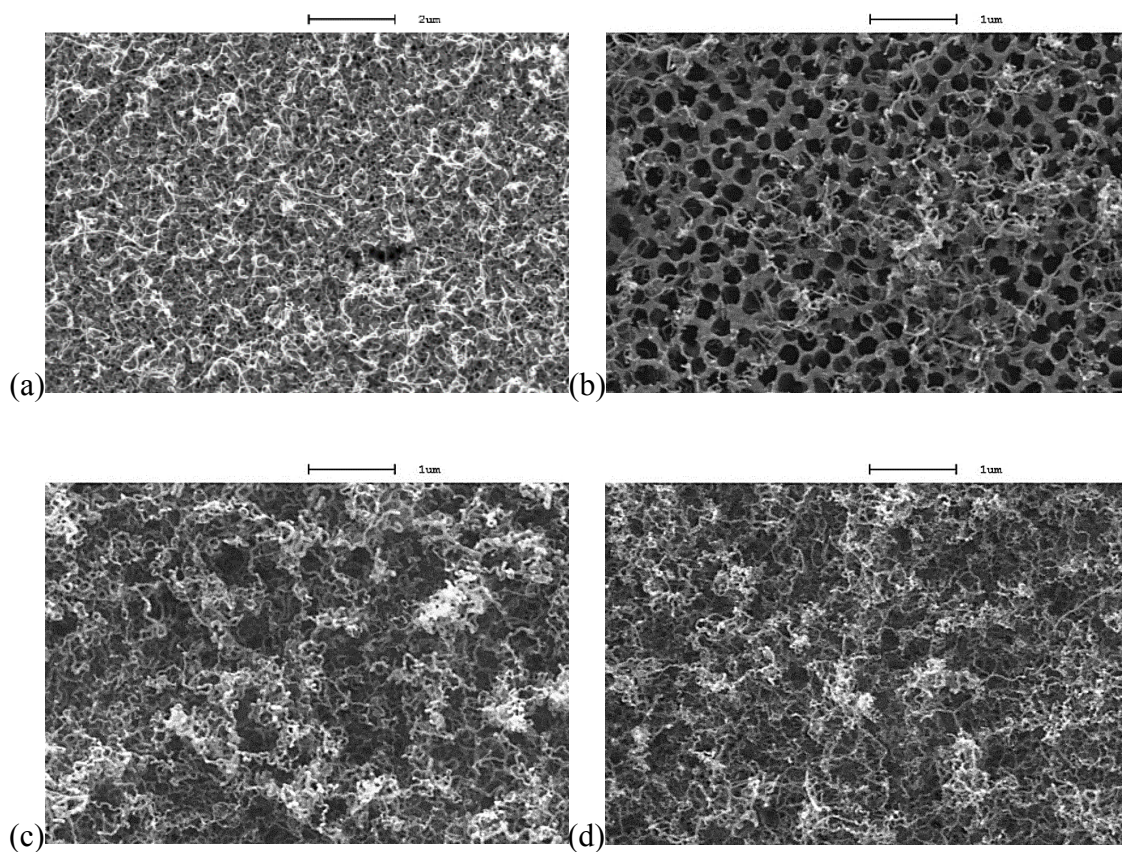


Figure 5.3 SEM results for CNTs formation on 0.1/AAO membrane with (a) 0 g; (b) 0.2 g; (c) 0.5 g; and (d) 1 g Ni/Al₂O₃ conditioning catalysts on the top

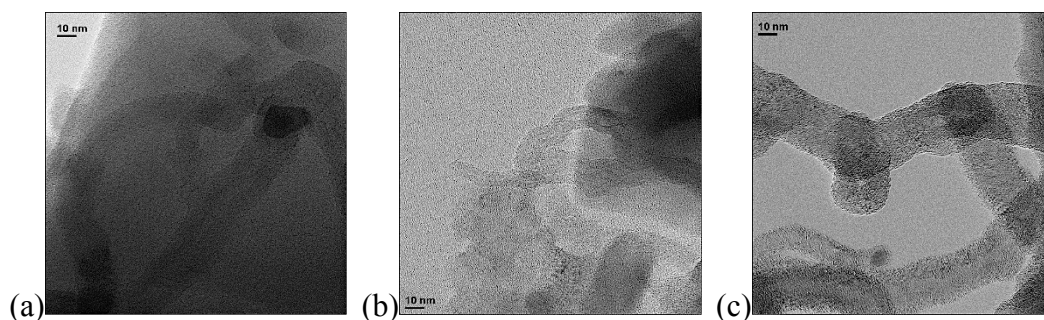


Figure 5.4 TEM results for CNTs formation on 0.1/AAO membrane with (a) 0.2 g; (b) 0.5 g; and (c) 1 g Ni/Al₂O₃ conditioning catalysts on the top

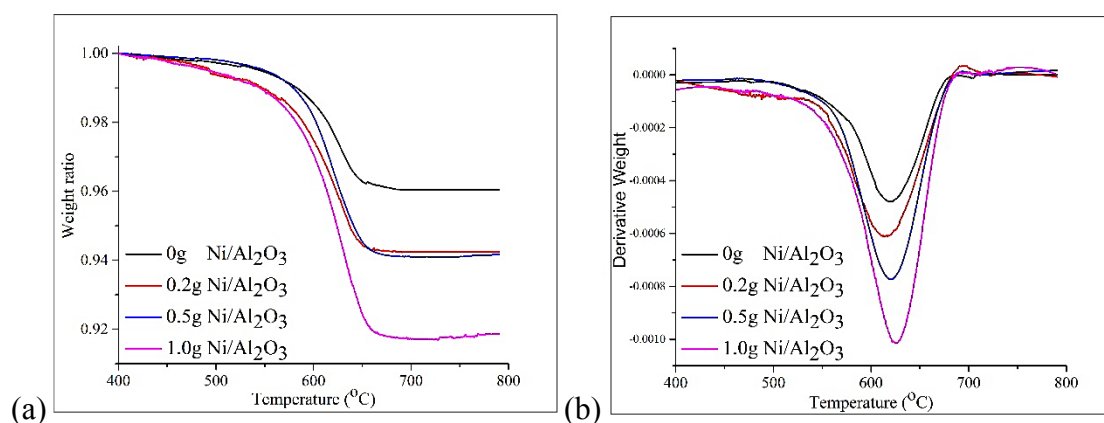


Figure 5.5 (a) TGA-TPO and (b) DTG-TPO results for the reacted catalysts obtained using different amounts of conditioning catalysts

The distribution of diameters of the CNTs produced using various amounts of conditioning catalysts was also investigated. Two or more peaks of diameter distribution were observed using 0 g (Figure 5.6b) and 0.2 g (Figure 5.6b) conditioning catalysts, indicating that non-uniform CNTs were produced under these conditions. When 0.5 g and 1.0 g of conditioning catalysts were used, the diameter distribution of the produced CNTs seems to be improved, as a small deviation (4 nm) of diameter was obtained.

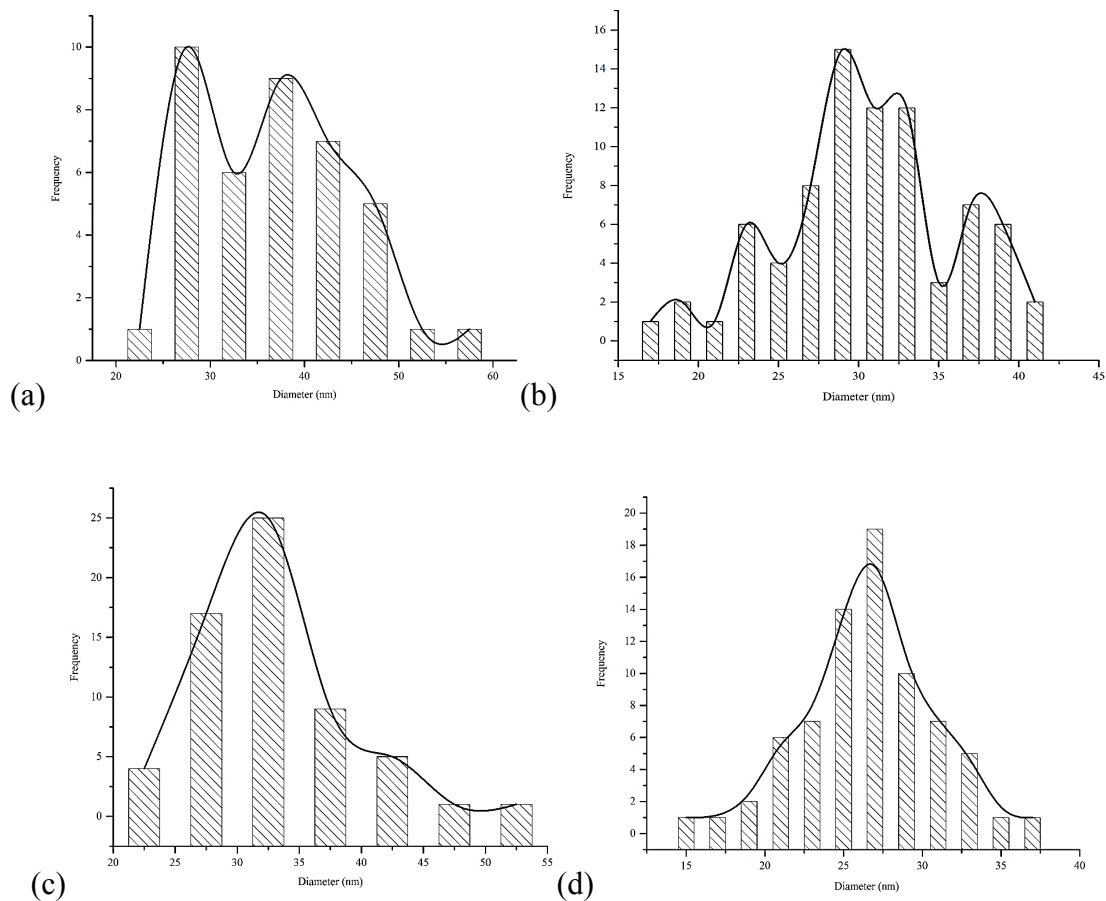


Figure 5.6 Diameter distribution for CNTs production with (a) 0 g; (b) 0.2 g; (c) 0.5 g; and (d) 1 g Ni/Al₂O₃ conditioning catalysts on the top

According to the above mentioned results, it is found that the presence of the conditioning catalyst could enhance the production of CNTs. This is because the carbon sources responsible for the production of CNTs were modified by the introduction of conditioning catalyst. It is known that the conditioning catalyst (Ni/Al₂O₃) was effective to crack heavy hydrocarbons into small molecules during gasification process (Barbarias et al., 2016). For example, Barbarias et al. (2016) used a Ni/Al₂O₃ catalyst to produce hydrogen from catalytic steam reforming of plastics (PS and HDPE).

The carbon source is one of the most important parameters for the synthesis of CNTs. A significant relationship between chemical structure of hydrocarbons and CNTs growth was reported by Lee et al. (2003). They studied the effect of different carbon sources on

the growth of CNTs using different catalysts (Ni, Co and Fe based). They reported that the growth rate of CNTs was much higher and the average diameter became smaller when the ratio of $\text{NH}_3/\text{C}_3\text{H}_4$ was increased. The influence of six types of hydrocarbons (methane, hexane, cyclohexane, benzene, naphthalene and anthracene) on the production of single walled CNTs was investigated with a Fe/MgO catalyst (Li et al., 2004). Methane was found to be responsible for producing high-purity CNTs, because the Gibbs free energies of hexane, cyclohexane and benzene were much lower than methane. In addition, the influence of virgin plastics and waste plastics on CNTs production were studied by Borsodi et al. (2016).

In this work, the presence of a layer of conditioning catalyst ($\text{Ni}/\text{Al}_2\text{O}_3$) on the top of the Ni/AAO catalyst was expected to modify the hydrocarbon sources derived from the pyrolysis of waste plastics. Hydrocarbon gaseous compounds produced from the pyrolysis of plastic waste were mainly large hydrocarbon molecules. These large compounds were cracked into smaller ones in the presence of the conditioning catalyst. It is suggested that smaller hydrocarbon molecules are beneficial for the growth of CNTs on the Ni/AAO catalyst. The effect of large hydrocarbon molecules on CNTs formation was also reported by Acomb et al (2014). They studied the formation CNTs from different types of plastic waste, and it was found that more CNTs could be produced from using low density polyethylene (LDPE) when compared with either polypropylene (PP) or polystyrene (PS). This is because larger hydrocarbon molecules produced from the pyrolysis of PP and PS could form more amorphous carbons.

Although the gases were not analysed in this work, when the conditioning catalyst was introduced, the production of H_2 , CH_4 , $\text{C}_2\text{-C}_4$, CO was suggested to be increased. For

example, when a 10 wt.% Ni/Al₂O₃ was used for the gasification of polypropylene, 56.3 vol.% H₂, 20 vol.% CO, 9.3 vol.% CO₂, 6.1 vol.% CH₄, and 8.3 vol.% C₂-C₄ were reported (Wu et al., 2009a). The presence of hydrogen could provide a reducing environment for catalytic metals and hence prevent the poisoning of catalyst (Danafar et al., 2009). The growth of CNTs has been reported to be enhanced in a hydrogen atmosphere (Teo, 2003). Cava et al. (1982) reported that H₂ had a ‘cleaning effect’ which could keep the active site of catalysts from encapsulating carbons. In addition, the increase of adding the amount of conditioning catalyst was suggested to increase hydrogen concentration in the carbon sources (Wu et al., 2010b), which might be beneficial for the production of CNTs. It is to be noted that the conditioning catalyst might be deposited with coke. In this work, the reacted conditioning catalysts (Ni/Al₂O₃) were not analysed, as the main objectives of this work was to study the Ni/AAO catalyst for the growth of CNTs.

5.2.2 Effect of Ni content on the production of CNTs

In this section, thermo-chemical conversion of waste HDPE was investigated in the presence of Ni/AAO catalyst with different Ni contents. Table 5.2 shows that the total carbon deposition was increased with the increase of Ni loading, indicating that the formation of carbons was enhanced. The fraction of amorphous carbons was also increased with the increase of Ni content, as the yield of carbon materials was enhanced when more Ni-based particles were available for the growth of carbons. Ni was a main active site for C-C and C-H bond cleavage to enhance the production of carbons (Jiang et al., 2016). Higher metal loading was reported to enhance the dehydrogenation of C₂

hydrocarbons to form CNTs (Richardson et al., 1979). Wu et al. (2009c) found that a comparatively lower amount of carbon deposition but a higher quality of CNTs was obtained when the Ni content in catalyst was reduced.

The quality of CNTs derived from the spent Ni/AAO catalysts with different Ni loadings were analysed by SEM. The images of surface and cross-section of the reacted Ni/AAO catalysts are shown in Figure 5.7 and Figure A-B9, respectively. Filamentous carbons were clearly produced in the presence of Ni-based catalyst (Figure 5.7A-D). For the 0.1/AAO, 0.5/AAO and 1.0/AAO catalysts, filamentous carbons are observed on the surface (Figure 5.7) and in the channels (Figure A-B9) of AAO. It seems that there is a large amount of amorphous carbons with short and un-uniform tube structure covered on the surface of the 2.0/AAO catalyst; this is consistent with that a large fraction of amorphous carbons is calculated from TPO analysis (Table 5.2). TEM results (Figure 5.8) further prove that most of the filamentous carbons are CNTs.

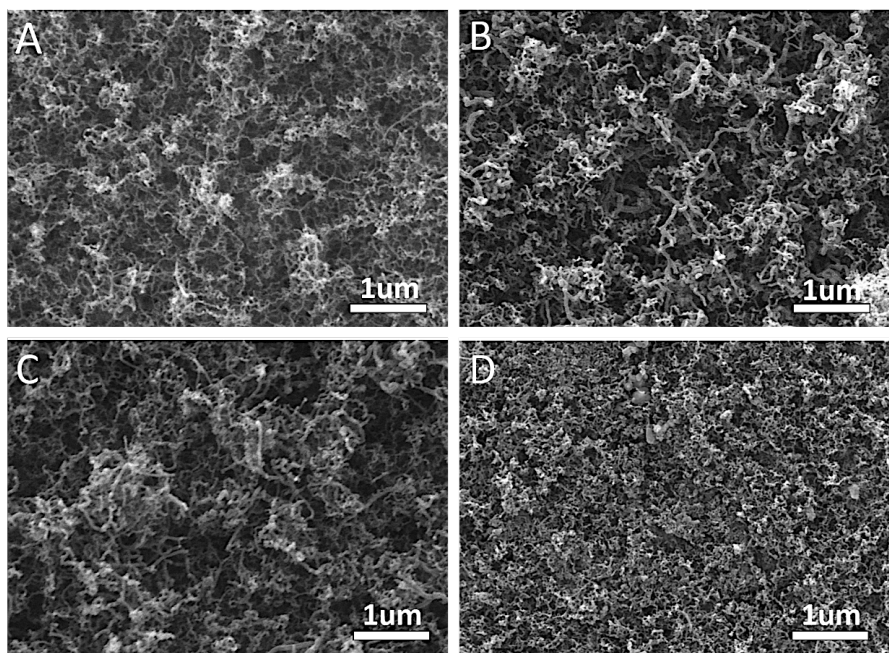


Figure 5.7 SEM results of the reacted Ni/AAO catalyst (A) 0.1/AAO; (B) 0.5/AAO; (C) 1.0/AAO and (D) 2.0/AAO

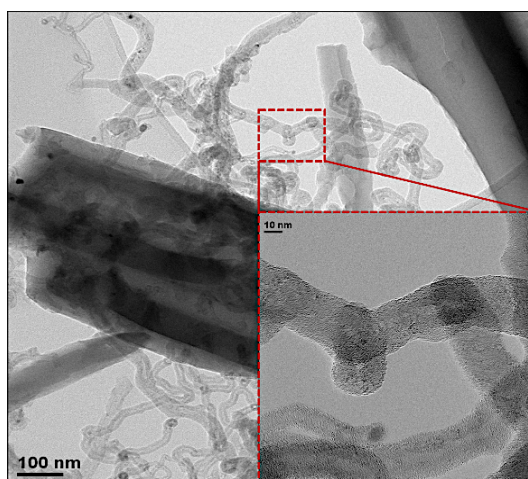


Figure 5.8 TEM results of CNTs for the reacted 0.1/AAO catalyst at different magnification

In this study, the mechanism of CNTs synthesis with AAO based catalyst was summarised in Figure 5.9, combining with SEM cross-section images of the reacted 0.1/AAO. AAO membrane with two-side open was used in this study. The diameter of NiO particles in the Ni-based catalysts in this study was around 20–50 nm, which was much smaller than the pore size of the AAO used (200 nm). It is indicated that many NiO particles could be located inside the pores, as shown in Figure 5.9A. In addition, the growth of CNTs was reported could be sustained and reached the outside of the pores (Jeong et al., 2004). Therefore, many CNTs could be produced inside and outside the pores of AAO (Figure 5.9B).

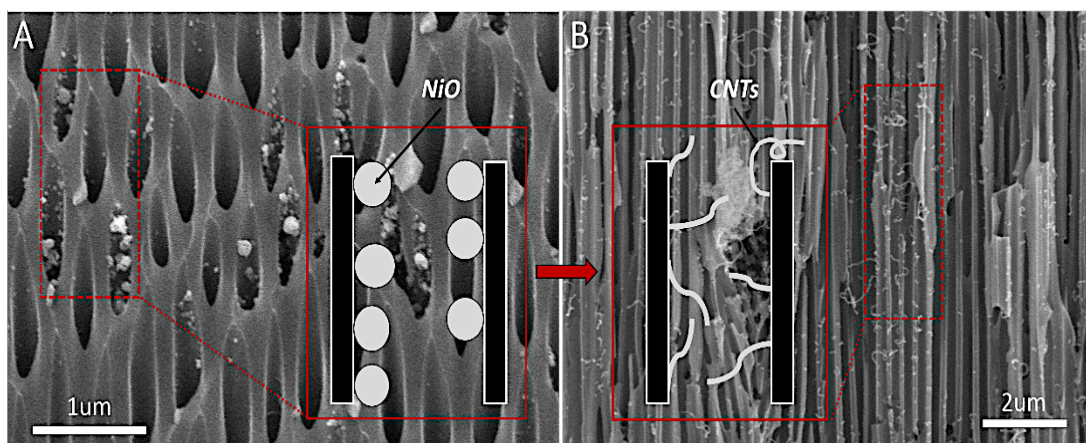


Figure 5.9 Mechanisms of CNTs growth using membrane-based catalyst

The distribution of CNTs diameters was analysed, and the results were summarised in Table 5.2 and Figure 5.10. It is demonstrated that the CNTs produced from the 0.1/AAO catalyst have the smallest average diameter of 26.7 nm and a deviation of 4 nm. The CNTs produced from the 0.5/AAO catalyst showed the largest deviation of average diameter (14.2 nm). The 2.0/AAO catalyst produced CNTs with the largest average diameter of 54.1 nm, which is corresponding to the size of metal particles as shown in the TEM results of Figure 3v. It can be noticed that the diameter of CNTs is increased with an increase of Ni content (Figure 5.10). It was reported that the growth of CNTs was governed by the diameter of metals (Chen et al., 2005; Cheung et al., 2002; Gorbunov et al., 2002; Wu et al., 2013). Sinnott et al. (1999) studied CNTs growth from methane with Fe/C based catalysts. They found that a lower metal content produced a smaller average diameter and a narrower diameter distribution of CNTs. Takenaka et al. (2004) reported that the diameter of Fe-based particles was increased with an increase of metal loading, resulting in a production of non-uniform CNTs. Other researchers have also reported that metal particles such as Ni, Fe, and Co had a proportionally relationship with the diameter of produced CNTs (Lee et al., 2002; Liu et al., 2011; Nahil et al., 2015; Namioka et al., 2011; Shah et al., 2016). Therefore, uniform distributed metal particles are important to produce high quality CNTs in relation to the distribution of CNTs diameters. It is suggested that an AAO substrate could contribute to the uniform production of CNTs.

Although the 1.0/AAO and 2.0/AAO catalysts generated a higher carbon yield compared to the 0.1/AAO and 0.5/AAO catalysts, the 0.1/AAO catalyst produced a higher quality of CNTs in relation to the purity (less amorphous carbons) and a uniform distribution of

the diameter of CNTs (Table 5.2). Therefore, the 0.1/AAO catalyst was used for further studies in this work.

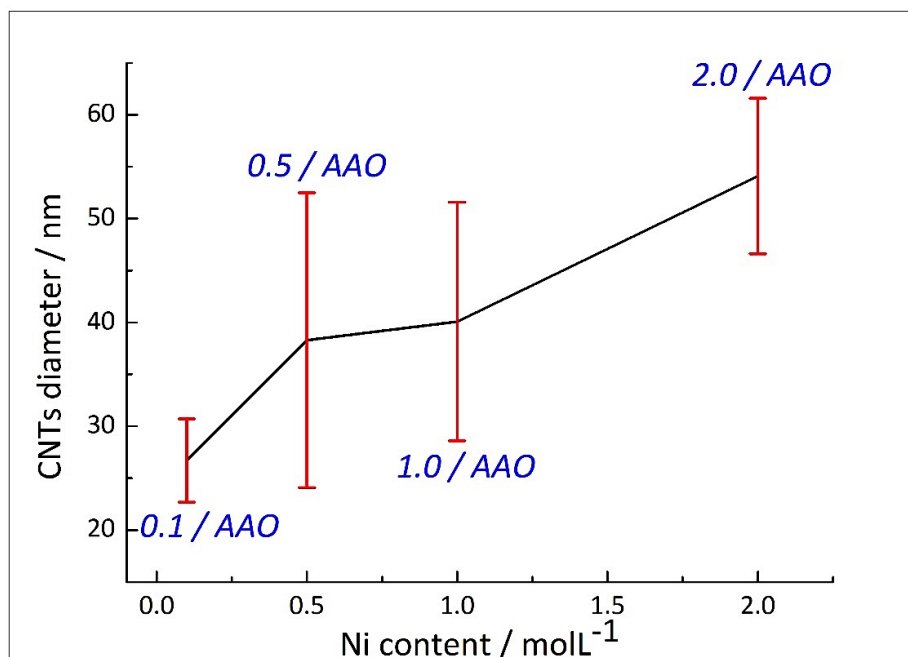


Figure 5.10 CNTs diameter distribution for different content of AAO membrane

5.2.3 Effect of reaction temperature on the production of CNTs

The 0.1/AAO catalyst was used to investigate the effect of reaction temperature (600 °C, 700 °C and 800 °C) on the formation of CNTs. SEM analysis (Figure 5.11) was carried out on the reacted catalysts. CNTs could be clearly observed on the reacted catalysts derived at reaction temperatures of 600 °C and 700 °C. However, less CNTs could be found when the reaction temperature was 800 °C (Figure 5.11C). In addition, at 800 °C, the AAO membrane was cracked, as shown on the surface (Figure 5.11C) and cross-section (Figure 5.11D).

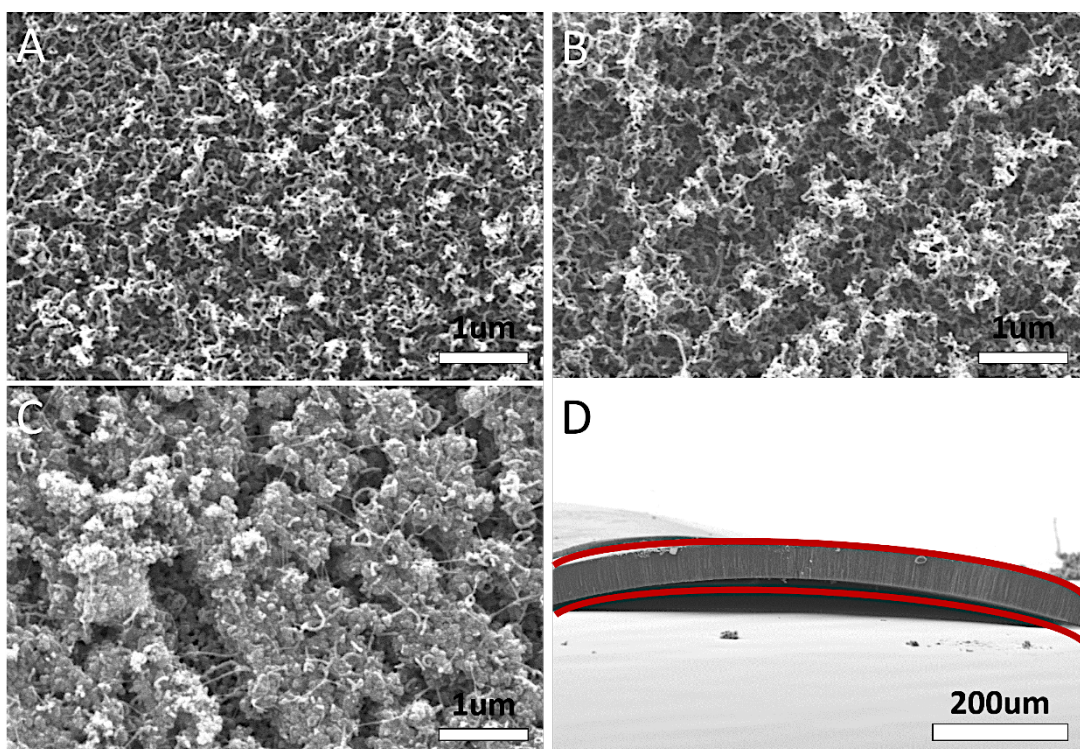


Figure 5.11 SEM results of 0.1/AAO catalyst for CNTs growth at different temperatures. (A) 600 °C; (B) 700 °C; (C) 800 °C; and (D) cross-section for cracking boundary at 800 °C

The distribution of the diameter of CNTs was analysed to further determine the quality of CNTs produced at different temperatures. The results are shown in Table 5.2. The diameter of CNTs was increased from 26.2 ± 6.6 nm to 33.5 ± 5.6 nm when the reaction temperature was increased from 600 °C to 700 °C. The average diameter of CNTs formed at 800 °C was around 27.2 nm with 7.2 nm deviation which is the largest among the three temperatures. This might be caused by the fracture of the AAO membrane at such high temperature. Reaction temperature was reported as a dominating factor influencing the morphology of CNTs by Kumar and Ando (2005), who found that the diameter range of CNTs was increased from 5-10 nm to 10-80 nm with the increase of reaction temperature from 550 °C to 1000 °C as the metal atoms of catalysts agglomerated to bigger clusters at high temperature. It was suggested that the reaction of vapour deposition was enhanced

with the increase of reaction temperature, causing faster carbon deposition and resulting in the production of thicker CNTs (Golshadi et al., 2014).

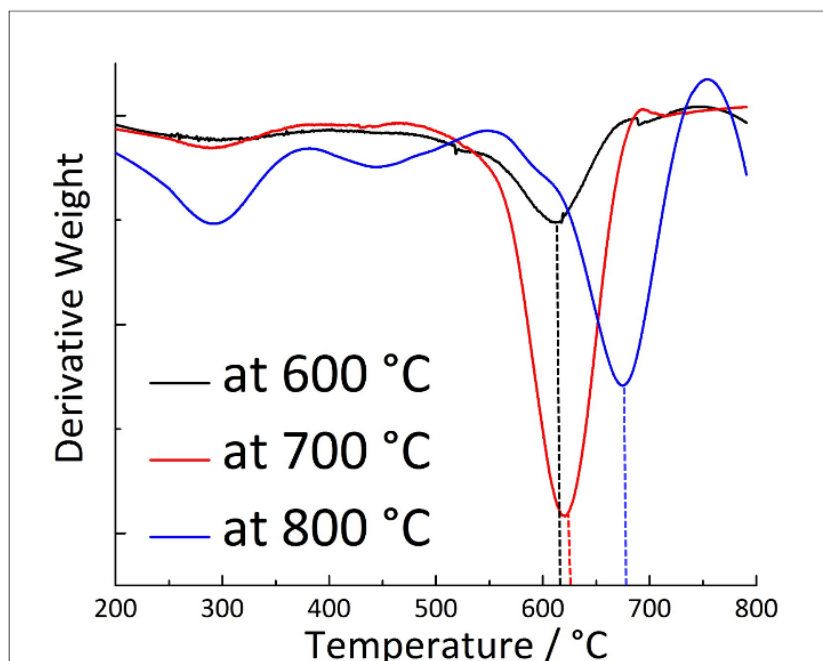


Figure 5.12 DTG-TPO results of the reacted 0.1/AAO catalyst tested at 600 °C, 700 °C and 800 °C

The yield and types of carbon deposition was further determined by TGA analysis (Figure 5.12 and Figure A-B4). As summarised in Table 5.2, the yield of carbon was increased with the increase of reaction temperature from 600 °C to 800 °C. A large amount of amorphous carbons was formed on the reacted catalyst at 800 °C, which was not preferred in this work. There are two decreasing peaks at around 300 °C and 450 °C, as assigned to the oxidation of heavy hydrocarbons deposited on the surface of the reacted catalysts. The carbon yield obtained at 700 °C was nearly three times higher than the carbon yield obtained at 600 °C, indicating that much more CNTs were produced at 700 °C. The influence of reaction temperature on the formation of CNTs has also been reported by other researchers. For example, Acomb et al. (2015) studied the effect of temperature (700, 800, and 900 °C) on the growth of CNTs growth using a low density polyethylene

and a Fe/Al₂O₃ catalyst. They found that the yield and the quality of CNTs were improved with the increase of reaction temperature. Wu and Williams (2010b) also reported that more reactive carbons were produced at higher temperature from the gasification of waste plastics. Mishra et al. (2012) used waste polypropylene as a precursor for synthesizing CNTs by CVD method with a nickel-based catalyst. They reported that a high degree of impurity and irregularities of CNTs was obtained at 600 °C and 700 °C. The quality of CNTs in relation to the purity and uniformity was enhanced when the reaction temperature was increased to 900 °C. In addition, a reaction temperature higher than 500 °C was suggested for the synthesis of CNTs (Aqel et al., 2012; Danafar et al., 2009; Stoner et al., 2014). However, the selection of reaction temperature for the growth of CNTs should also be related to other process conditions e.g. feedstock and catalyst. For instance, it was indicated that CNTs were produced at temperature higher than 1000 °C using ethanol and ferrocene as feedstock (Niu et al., 2007), while no CNTs were formed at high temperature of 1000 °C from acetylene as a feedstock (Kathyayini et al., 2006; Kukovec et al., 2000; Smajda et al., 2007).

Similar AAO catalysts were studied by Golshadi et al. (2014) to investigate the influence of reaction temperature of 650, 700, 750 and 800 °C, using ethylene/helium gas mixture. At 750–800 °C, a layer of amorphous carbon was formed, prohibiting the diffusion of hydrocarbon gases, resulting in a decrease of CNTs formation. The authors suggested that 650–700 °C was an optimal temperature for CNTs growth using AAO based catalyst. This is consistent with this work confirming that 700 °C is preferable for the growth of CNTs. Similar result was also reported by Li et al. (2002). They reported that the yield of CNTs was changed with increasing temperature from 500 to 800 °C and that the

maximum yield was obtained at 700 °C by using PP as feedstock and HZSM-5 zeolite as a catalyst. Furthermore, higher temperature was reported to cause the deformation or the sintering of catalyst, and the formation of amorphous carbons. Park et al. (2010) found that high temperature could lead to an increase of the deposition of amorphous carbons on the surface of catalyst particles to deactivate catalysts. Therefore, in this work, 700 °C is suggested to be an optimal temperature for the production of CNTs. 600 °C is too low in relation to the thermodynamics of carbon formation reactions, while 800 °C is too high to crack the AAO catalyst and also to form a large amount of un-desired amorphous carbons.

5.2.4 Effect of Steam Addition on the Production of CNTs

Water was reported as a catalytic enhancer to improve the quality of CNTs (Futaba et al., 2005). In this study, water with three different flow rates of 0, 2 and 5 ml h⁻¹ was injected into the system to investigate the effect of steam on CNTs synthesis. The results were analysed by SEM as shown in Figure 5.13 DTG-TPO results are presented in Figure 5.14.

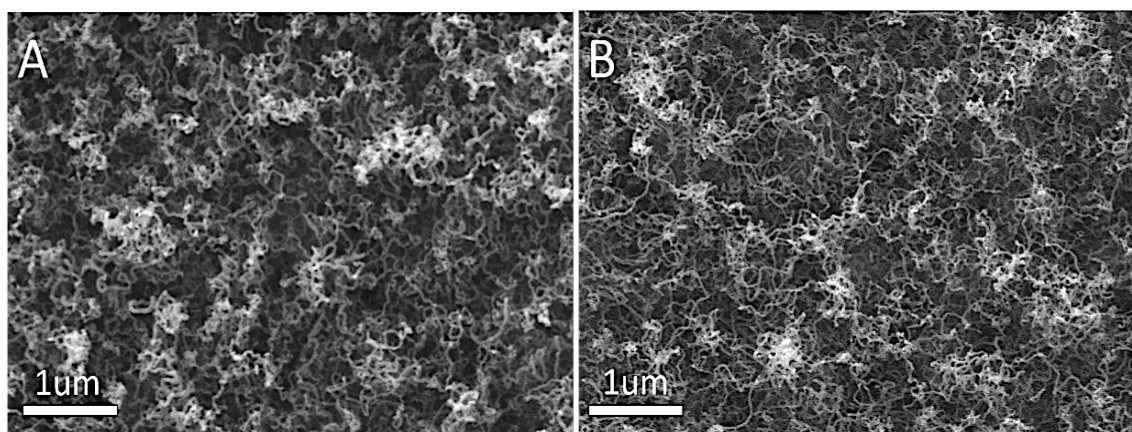


Figure 5.13 SEM results of the reacted 0.1/AAO catalyst at 700°C with different rate of steam injected. (A) 2 ml h⁻¹ and (B) 5 ml h⁻¹

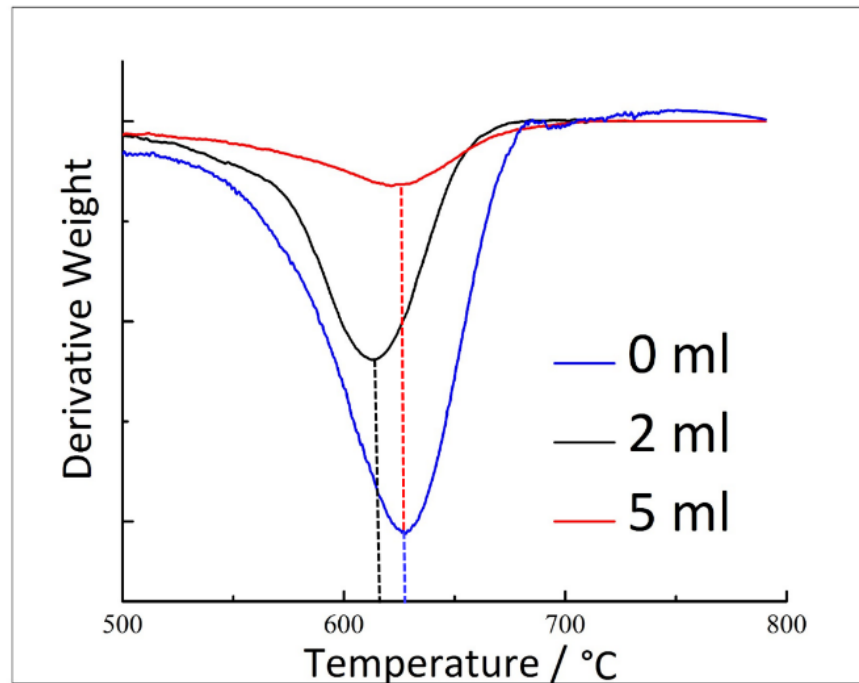
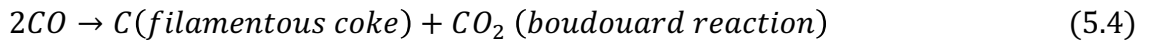
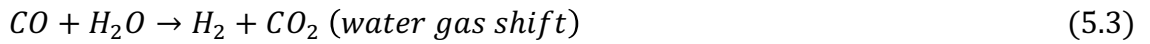
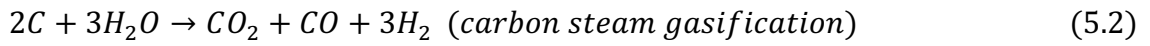


Figure 5.14 DTG-TPO results of the reacted 0.1/AAO catalyst tested with 0, 2 and 5 ml h⁻¹ steam injection

The key reactions of catalytic pyrolysis of plastics waste with steam injection are shown by Reactions 1–4. Initially, the hydrocarbons present in plastics are cracked into carbon and hydrogen (Reaction 5.1). In the presence of steam, water reacts with deposited carbons to produce CO₂, CO and H₂ (Reaction 5.2). Therefore, hydrogen and carbon dioxide in the gas could be increased with an increase of steam addition. The introduction of steam into plastic gasification has been widely reported to enhance the production of CO and H₂ (Acomb et al., 2015, 2016). According to the study from Barbarias et al. (2016), CO could further promote carbon growth, however, CO could also be transformed to CO₂ by water gas shift (Reaction 5.3) with the addition of water. Therefore, the decomposition of CO into carbon could be prohibited (Reaction 5.4).





SEM results (Figure 5.13) of the reacted Ni/AAO catalysts derived from using 2 and 5 ml h⁻¹ of water steam injection were studied. Long and thin uniform CNTs on the surface have been observed. According to the SEM results, it is difficult to find the differences of CNTs produced without steam (Figure 5.13), with 2 ml h⁻¹ steam and 5 ml h⁻¹ steam. However, the diameter distribution analysis shows that the average diameter of CNTs is decreased with an increase of the steam flow rate from 2ml h⁻¹ to 5 ml h⁻¹. The average diameter of CNTs is decreased to 29.7 ± 5.7 nm and 21.9 ± 3.9 nm, when 2, and 5 ml h⁻¹ of steam were used, respectively, compared to an average diameter of CNTs of 33.5 ± 5.6 nm with no steam injection. The deviation of CNTs diameter is similar for the CNTs produced with 0 and 2 ml h⁻¹ water injection. This deviation decreased to 3.9 nm as the steam injection was increased to 5 ml h⁻¹. It is suggested that the quality of CNTs could be improved with the increase of water injection in the process of catalytic steam conversion of waste plastics. The amorphous carbons were known to encapsulate the reactive catalytic sites and influence the quality of the formed CNTs (Wu et al., 2013). Amorphous carbons could be etched away through weak oxidation reactions with an appropriate amount of steam to enhance the continuous growth of CNTs. For example, water-assisted CNTs production was carried out on different catalysts (Fe, Al/Fe, Al₂O₃/Fe, and Al₂O₃/Co on Si wafers, quartz and metal foils) (Hata et al., 2004). Also Ago et al. (2006) generated CNTs from methane with Ni, Fe, and Co/MgO catalysts. Ago

and co-workers (2006) reported that the water injection prolonged the catalyst lifetime and enhanced the morphology of CNTs.

However, it is shown an obviously decrease of carbon deposition with increasing steam injection. 10% carbon formation without steam injection is obtained in relation to the weight of used catalyst. The yield of carbon was decreased to around 4.1% when the steam injection rate was 2 ml h^{-1} , and was further decreased to less than 2.5% with the increasing steam injection to 5 ml h^{-1} . It is suggested that the amount of steam injected into the reactor might be higher than the optimum value. It was reported that over injection of steam could increase carbon steam gasification (Reaction 2), resulting in a reduction of carbon yield (Donatelli et al., 2010). Lee et al. (2012) pointed out that the excess steam would limit the supply of carbon sources reaching the catalytic active sites, due to the reduced diffusion of carbon. Liu et al. (2010) studied the effect of wet argon flow rate of 0 to $700 \text{ cm}^3 \text{ min}^{-1}$ at standard temperature and pressure (sccm) on CNTs growth from m-xylene using SiO_2 based catalyst. They found that the flow rate of wet argon in the range of 100–150 sccm performed best for CNTs formation. With the introduction of excess steam, low quality of CNTs was produced because the diffusion and penetration of hydrocarbon through the nanotube bundles was reduced making it difficult for hydrocarbon molecules to reach catalytic sites for CNTs growth. Hu et al. (2008) prepared vertically-aligned CNTs by water assisted CVD using Mo/Fe/Al based catalyst from a C_2H_4 and H_2 gas mixture. They reported that the best CNTs were found at 100 sccm water vapour and that the formation of CNTs was reduced as the vapour was increased to over 150 sccm.

In addition, the excess steam would largely enhance the oxidation of catalytic metal, consequently, deactivating the catalyst for the formation of CNTs. In this work, the AAO membrane has about 100 mm diameter and 60 μm thickness. The amount of Ni loaded was small, just 0.1 molL^{-1} (2.4 wt.% according to EDX). Therefore, when more steam was injected, a small amount of active Ni catalysts might be oxidised in the process to lose the catalytic activity for CNTs growth. Yamada et al (2008) reported that water could oxidise metal catalyst, causing the deactivation of CNTs formation.

Chapter 6. Carbon nanotubes
growth with ceramic supported
catalysts

In this chapter, experimental conditions (both reaction temperature and Ni loading) were studied to determine the optimal conditions for the production of high quality CNTs, which is reflected by a narrow distribution of CNTs diameter.

6.1 Characterisation of fresh Ni/ceramic catalyst

Fresh catalysts before reaction with different Ni loadings have been analysed by SEM, TEM, ICP, XRD and TPR, respectively. SEM results of the surface and the cross section of the fresh Ni/ceramic catalyst are shown in Figure 6.1A and 1B, respectively. The surface and cross-section show a similar structure; porous structure can be clearly observed from both pictures. Therefore, SEM images on the surface of materials are used for following discussion.

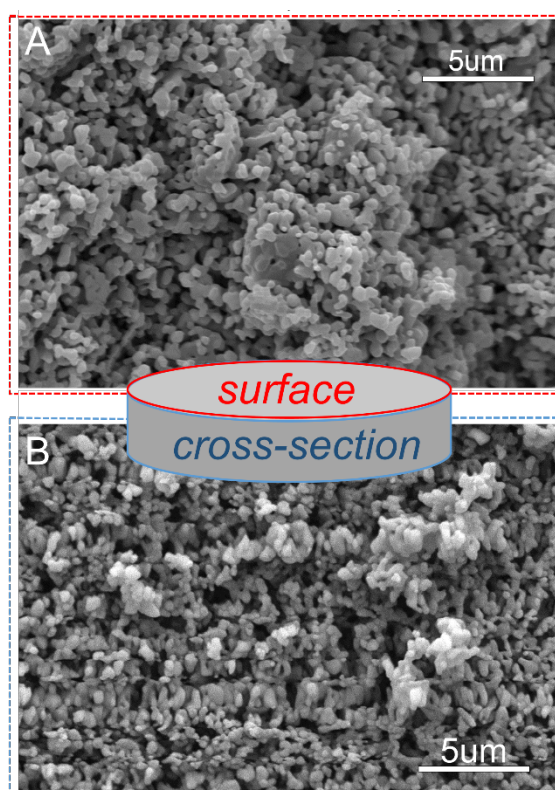


Figure 6.1 SEM results for original ceramic membrane (A) surface, (B) cross-section

Based on the XRD results (Figure 6.2), the original ceramic membrane without Ni loading shows diffraction peaks of Al₂O₃ (Muñoz et al., 2012), indicating the nature of the ceramic is Al₂O₃. NiO peaks appear at 63° and 76°, respectively, for the catalyst with different Ni contents loadings (Liu et al.). Two NiAl₂O₄ peaks appear at around 37° and 77° (Zygmuntowicz et al., 2016). ICP results as shown in Table 6.1 further indicate that the content of Ni element increased from 0.25 to 3.3 wt.% with the increase of Ni loading. Figure 6.3 shows the TEM results (A-D) for the Ni/ceramic samples. The distribution of NiO diameters was also calculated according to TEM results for the catalyst with different Ni loadings. Small amount of NiO particles was observed on the surface of the 0.1/ceramic, which has particles with 11.4 ± 2.4 nm diameter, with NiO diameter correlating with metal loading, in agreement with the literature (Wu et al., 2011), resulting in average particle size of 35.2 ± 3.5 nm for the 2.0/ceramic (Figure 6.2D).

TPR results of the fresh Ni/ceramic catalysts are shown in Figure 6.4. A major reduction temperature for all the catalysts occurred between 370 and 450 °C, assigned to the reduction of NiO particles (Wu et al., 2011). As shown in Figure 6.4, the catalysts were further reduced at 550°C (Wu et al., 2011), which is suggested to the reduction of Ni spinel as observed from the XRD analysis (Figure 6.2).

Table 6.1 ICP results of Ni/ceramic catalysts with different Ni contents

<i>Catalysts</i>	<i>0.1/ceramic</i>	<i>0.5/ceramic</i>	<i>1.0/ceramic</i>	<i>2.0/ceramic</i>
Ni content wt.%	0.25	1.1	2.1	3.3

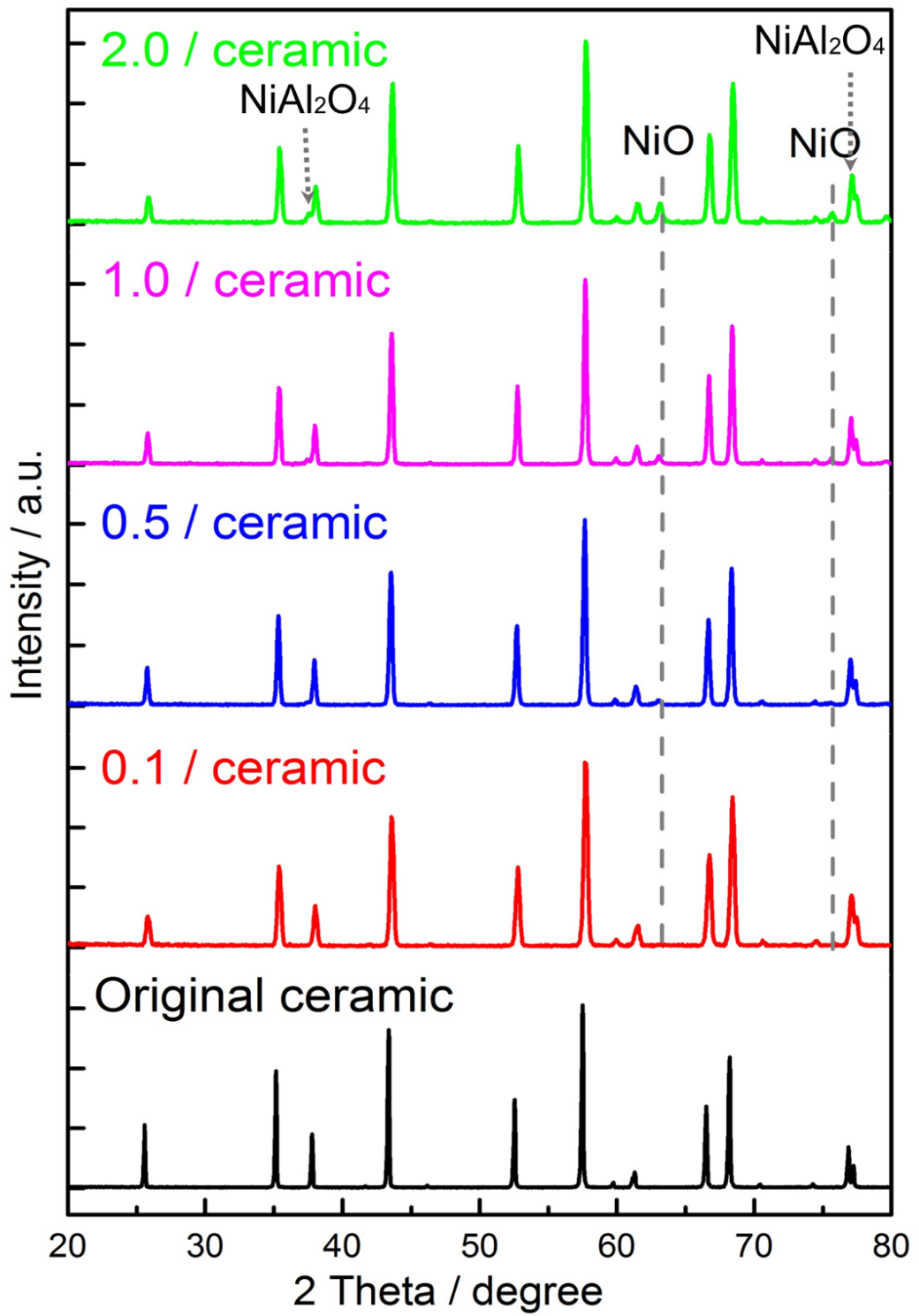


Figure 6.2 XRD analysis for original ceramic membrane and fresh Ni/ceramic catalysts

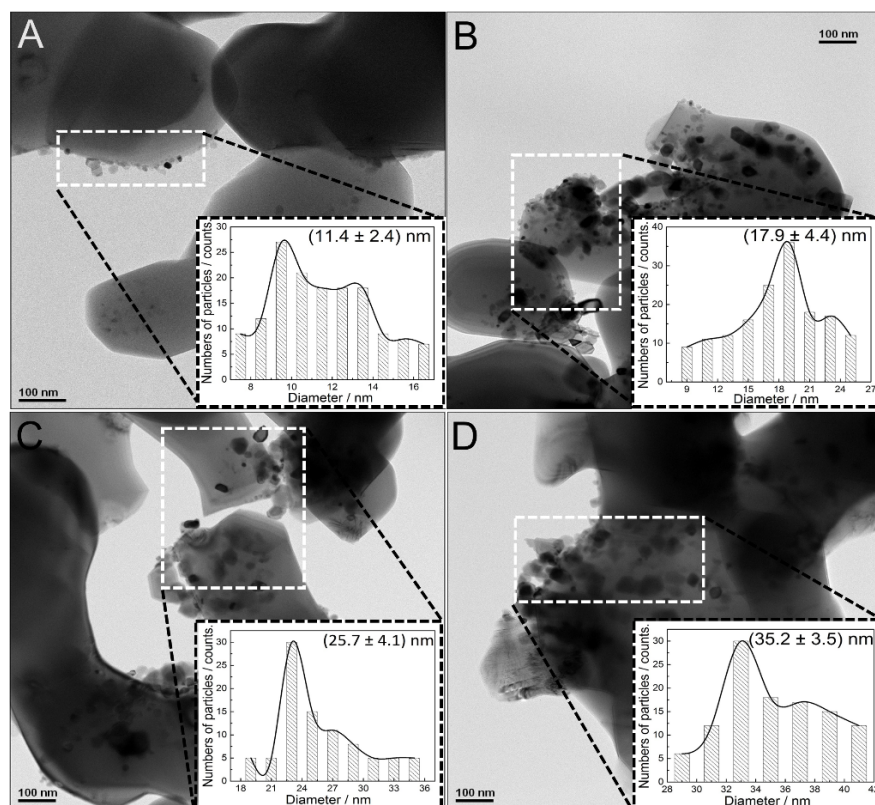


Figure 6.3 TEM results and diameter distribution of NiO for (A) 0.1, (B) 0.5, (C) 1.0 and (D) 2.0 fresh Ni/ceramic catalysts

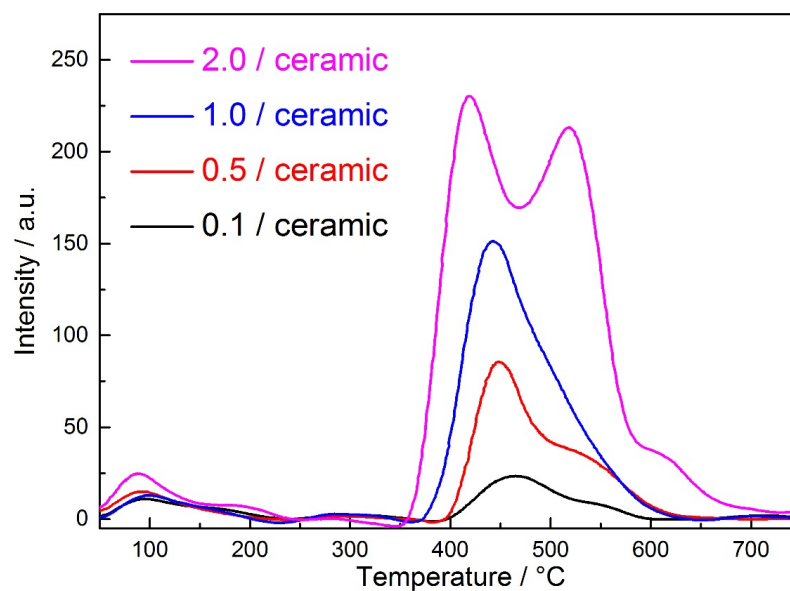


Figure 6.4 TPR analysis of the Ni/ceramic catalysts with different Ni content loadings (0.1, 0.5, 1.0, and 2.0 Ni mol/L)

6.2 Carbon nanotubes production

Two reaction parameters using ceramic membrane catalysts with different Ni contents loading were investigated in relation to the effect on the CNTs formation from plastics waste. Table 6.2 is a summary of different reaction parameters (Ni content and reaction temperature) and CNTs formation analysis (amount of amorphous carbon, filamentous carbon and CNT average diameter). When the effect of reaction temperature (600, 700, and 800 °C) was studied, the 0.5/ceramic catalyst was used. When the effect of Ni content (0.1, 0.5, 1.0 and 2.0) was studied, thermochemical conversion of waste HDPE was investigated at 700 °C.

Table 6.2 Overall view of experiments parameters and carbon deposition

	<i>Ni content</i> <i>/molL⁻¹</i>	<i>Temperature</i> <i>°C</i>	<i>Amorphous</i> <i>carbon/%</i>	<i>Filamentous</i> <i>carbon/%</i>	<i>CNTs</i> <i>average</i> <i>diameter/nm</i>
Effect of Ni content	0.1	700	1.1	3.1	15.7±3.6
	0.5	700	1.2	6.0	16.9±4.3
	1.0	700	2.0	9.4	20.8±1.9
	2.0	700	2.2	8.0	24.9±2.3
Effect of temperature	0.5	600	2.1	7.2	21.2±5.6
	0.5	700	1.2	6.2	16.9±4.3
	0.5	800	1.2	1.2	-

CNTs formation from thermochemical conversion of plastics waste in this study was investigated according to both quantitative analysis and qualitative analysis. The quantitative analysis of CNTs was further discussed based on the yields of amorphous carbons and filamentous carbons which was obtained by TGA-TPO analysis of the spent catalysts (Figure A-C1 and A-C2). It is assumed that the oxidation temperature below 550 °C was assigned to amorphous carbons and the oxidation above 550 °C in TPO was assigned to filamentous carbon (assumed as CNTs in this work) (Wu et al., 2015), two different types of carbon has been separated and analysed by vertical black imaginary line (Figure A-C1 and A-C2). The total carbon yield could be represented by X axis ‘the weight loss’ of catalyst in relation to the initial catalyst weight. The fractions of the two different types of carbons in relation to the weight of reacted catalysts are summarised in Table 6.2.

In addition, the quality of CNTs production is analysed and discussed mainly based on the distribution of CNTs diameters and their standard deviations. The average diameter of CNTs is calculated according to SEM and TEM results using Image J, and summarised in Table 6.2 (shown in Figure A-C3). The standard deviation (SD) number is used as a main factor to identify the quality of CNTs formation in this study. In addition, the ratio of filamentous and amorphous carbon was also discussed in following sections to obtain the optimum reaction parameter for CNTs formation. A better quality of CNTs is identified with a smaller SD number and higher ratio of filamentous and amorphous carbon in this paper.

6.2.1 Effect of Reaction Temperature on CNTs Growth

The effect of reaction temperature on the growth of CNTs through thermal conversion from HDPE using Ni/ceramic catalysts is discussed in this section. Three different reaction temperatures (600 °C, 700 °C and 800 °C) were investigated using the 0.5/ceramic catalyst. Scanning electron microscope (SEM), transmitted electron microscope (TEM), temperature programmed oxidation (TGA-TPO and DTG-TPO) analysis were carried out to the reacted CNTs/catalysts. For SEM results (Figure 6.5A-C), a small amount of uninform, short filamentous carbons were observed at 600 °C (Figure 6.5A). CNTs, which has a diameter ~10 nm and a length ~10 μm, is observed at catalytic reaction temperature of 600 °C. This result is corresponding with previous study, which used Ni/Al₂O₃ as catalysts to produce CNTs from waste plastics.

With the increase of reaction temperature to 700 °C (Figure 6.5B), a large amount of filamentous carbons with long length are found on the ceramic membrane. However, when the reaction temperature was further increased to 800 °C, only a few filamentous carbons could be observed on the surface of the catalyst (Figure 6.5C). The SEM results of the reacted catalyst were further supported by TEM analysis (Figure 6.5i-iii). CNTs with diameter 21.2 ± 5.6 and 16.9 ± 4.3 nm were clearly observed in Figure 6.5i and ii, respectively. It is difficult to find CNTs on the catalyst reacted at 800 °C (Figure 6.6iii). Therefore, it is suggested that 700 °C is an optimal reaction temperature for the formation of CNTs from waste plastics in this work. Similar results were reported by Li et al (2002), who studied various temperatures from 600 °C to 1050 °C for CNTs production from

C₂H₂ with Fe/SiO₂ catalysts. They reported minimal CNTs yield at either low (600 °C) or high (1050 °C) temperature.

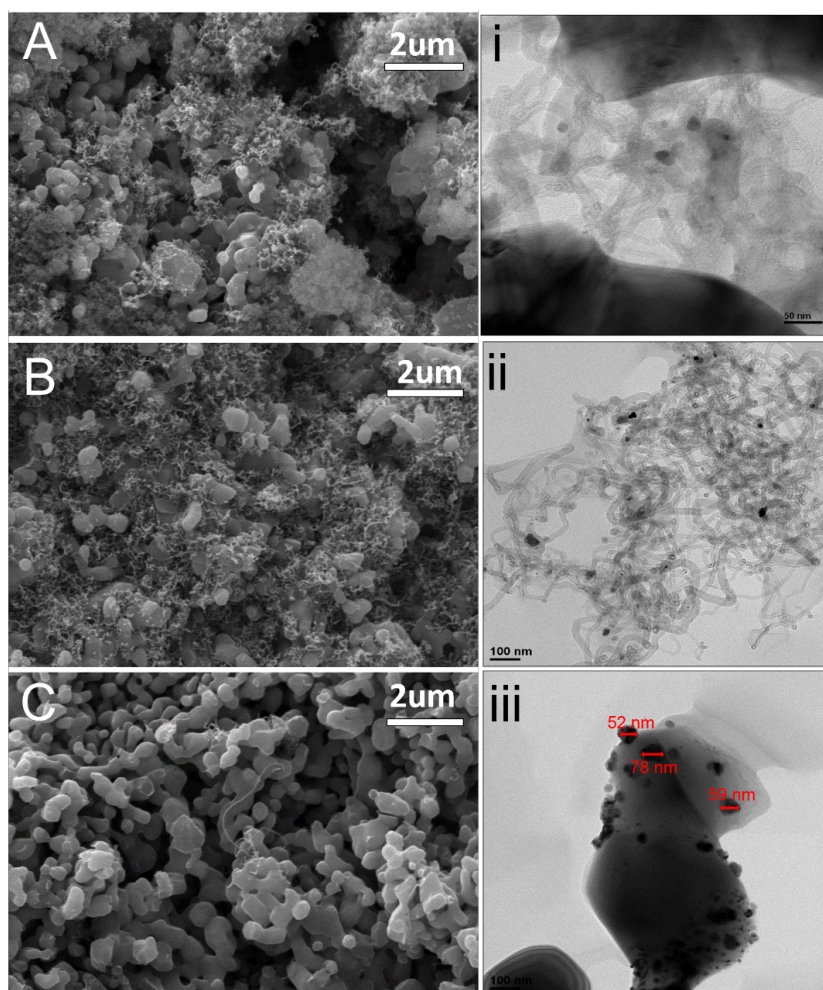


Figure 6.5 SEM (left) results for CNTs synthesis at (A) 600 °C, (B) 700 °C and (C) 800 °C; TEM (right) results (i) 600 °C, (ii) 700 °C, (iii) 800 °C

This result is further supported by carbon production analysis (Table 6.2). For amorphous carbons (oxidation temperature below 550 °C), the yield was decreased from 2.1 to 1.2 wt.%, when the temperature increased from 600 °C to 700 °C. This result is consistent with the SEM analysis (Figure 6.5), where amorphous carbons could be clearly observed on the reacted catalyst tested at 600 °C. Furthermore, the formation of CNTs was reduced from 7.2 wt.% and 1.2 wt.% when the reaction temperature was increased 600 °C and 800 °C. DTG-TPO results (Figure 6.6) with DCS (Differential Scanning Calorimetry) showed

that the oxidation peak moved to higher temperature with the increase of experimental temperature from 600 °C and 700 °C, indicating that the CNTs might be more crystallised at 700 °C reaction temperature. Similar results were also reported by Hornyak et al. (1999), who investigated the template synthesis of CNTs formation on porous alumina membrane (PAM) from propylene gas with Co-based catalysts. They reported that amorphous carbon was formed at around 550 °C, while CNTs was formed at temperature higher than 800°C. The starting temperature for CVD synthesis of CNTs was normally over 500 °C (Aqel et al., 2012; Danafar et al., 2009; Stoner et al., 2014).

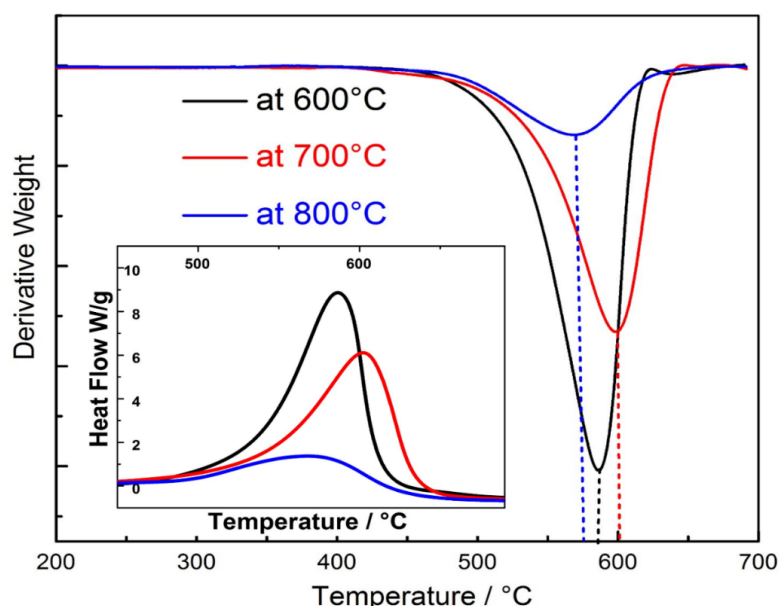


Figure 6.6 DTG-TPO and DSC results of the spent 0.5/ceramic at 600 °C, 700 °C, and 800 °C

It is suggested that the effect of reaction temperature on CNTs synthesis by CVD was mainly related to carbon source and catalytic sites. CNTs growth can be described as following steps, first carbon atoms from the dissociation of hydrocarbons dissolve into the catalytic metal sites. The diffused carbon atoms form graphitic sheets on the surface of metal particles (Kim et al., 2005). The diffusion of carbon atoms is a main factor to

determine the CNTs formation. The increasing temperature can promote the diffusion rate of carbon atoms, as a result, CNTs are synthesised with less defect. Lee et al. (2001) and Mishra et al. (2012) also reported that an increase of temperature promoted the diffusion and reaction rates of carbons, resulting in the enhanced formation of CNTs. In addition, Wu and Williams (2010b) reported that at high temperature, more reactive carbon sources were produced from pyrolysis of waste plastics. Therefore, in this study, less amorphous carbons were form at 700 °C compared to 600 °C, which supported by SEM and TPO analysis. Similar results were reported by Acomb et al. (2015) who carried out the effect of growth temperature (700 °C, 800 °C, and 900 °C) on the CNTs production using low density polyethylene (LDPE) with Fe/Al₂O₃ as catalyst. They found that a lower temperature produced less fraction of CNTs.

However, when the reaction temperature is too high, the sintering of catalytic sites could occur, which is responsible for the deactivation of catalysts (Danafar et al., 2009). Also, the excess of carbon atoms accumulated on the surface of catalyst could encapsulate catalytic sites causing catalyst deactivation. For example, Hanaei et al. (2010) investigated the influence of reaction temperatures (550 °C-950 °C) on CNTs from acetone with Fe-Mo/Al₂O₃ catalysts. 750 °C was reported as an ideal temperature as the deactivation of catalysts occurred at higher temperature. Toussi et al. (2011) reported the similar conclusion on CNTs synthesis form ethanol deposited on Fe-Mo-MgO catalyst; when temperature was lower than 750 °C, few CNTs could be produced. And the optimum growth of CNTs was reported at 850 °C. Kukoitsky et al. (2002) reported an optimal temperature of 700 °C for the growth of CNTs from polyethylene with Ni-based

catalyst at 700 °C; as narrow size distribution of CNTs was found at 700 °C than those grown at 800 °C, due to the loss of catalytic activity for CNTs forming at high temperature. In this study, it is noticed that there was little CNTs formed at 800 °C (Figure 6.5 and 6.6), which we attribute to loss of catalytic active sites at high temperature due to sintering. As shown in Figure 6.5iii, almost no CNTs production could be observed from TEM results. The diameter of NiO particles before reaction was 17.9 ± 4.4 nm (Figure 6.3B), however, large amount of large catalytic particles with diameter 52-78 nm could be observed after reaction (Figure 6.5iii). Overall, Figure 6.7 summarises the trends of SD of CNTs diameter and ratio of filamentous amorphous carbon as increasing reaction temperature. CNTs show the smallest SD and highest filamentous / amorphous carbon ratio at 700 °C reaction temperature. Therefore, 700 °C was assumed as the optimum temperature for this study.

6.2.2 Effect of Ni Content on the Production of CNTs

In this section, thermochemical conversion of waste HDPE was investigated in the presence of Ni/ceramic catalysts with different Ni contents at 700 °C. Figure 6.7 showed the SEM results and corresponding TEM results for the filamentous carbon production using the Ni/ceramic catalysts. With the increase of Ni loading, more filamentous carbons could be observed from SEM results. In particular, for the reacted 0.1/ceramic catalyst, the formation of filamentous carbons can be barely found. It is indicated that the 0.1/ceramic and 0.5/ceramic catalysts might have small amount of active metals loaded on the ceramic membrane. TEM results (Figure 6.7i-v) further proved that the filaments

carbons are mostly CNTs. The average diameter of CNTs (Table 6.2) was analysed according to the TEM results. It could be noticed that the diameter of CNTs increased with an increase of Ni content. The 0.1/ceramic had the smallest diameter 15.7 ± 3.6 nm, and the 2.0/ceramic had the largest diameter 24.9 ± 2.3 nm, in close agreement with the average sizes of the NiO nanoparticles. The changes of diameters of CNTs showed a similar trend with the metal particles size as shown in Figure 6.9, where the particle size of NiO was increased with the increase of metal loading. Similar results were also found by other researchers (Sinnott et al., 1999). Sinnott et al. (1999) studied the effect of Fe content on the diameter of CNTs produced from ferrocene-xylene mixture through chemical vapour deposition. They reported that the average Fe particle size was decreased from 35.3 to 28.2 nm with a decrease of Fe content from 0.75 to 0.075 wt.% and the lower Fe content resulted in the production of less CNTs. Li et al. (2001) synthesised CNTs from methane and hydrogen mixture using Fe_2O_3 -based catalysts with a range of 1-2nm and 3-5 nm respectively. CNTs with diameters of 1.5 ± 0.4 nm and 3.0 ± 0.9 nm were produced, respectively. The CNTs could be diffused by catalytic metal particles during growth process, therefore, the size of metal particles determine the diameter of filamentous carbons (Sinnott et al., 1999). For example, Cheung et al. (2002) used iron nanoparticles with average diameters of 3, 9, and 13nm to grow CNTs with average diameters of 3, 7, and 12 nm from ethylene, respectively.

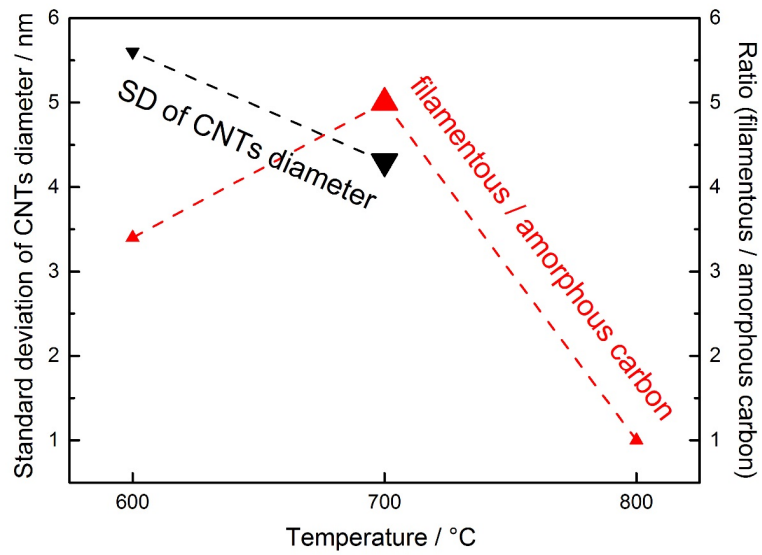


Figure 6.7 Trends of standard deviation (SD) of CNTs diameter and filamentous/amorphous carbon ratio at 600 °C, 700 °C, and 800 °C

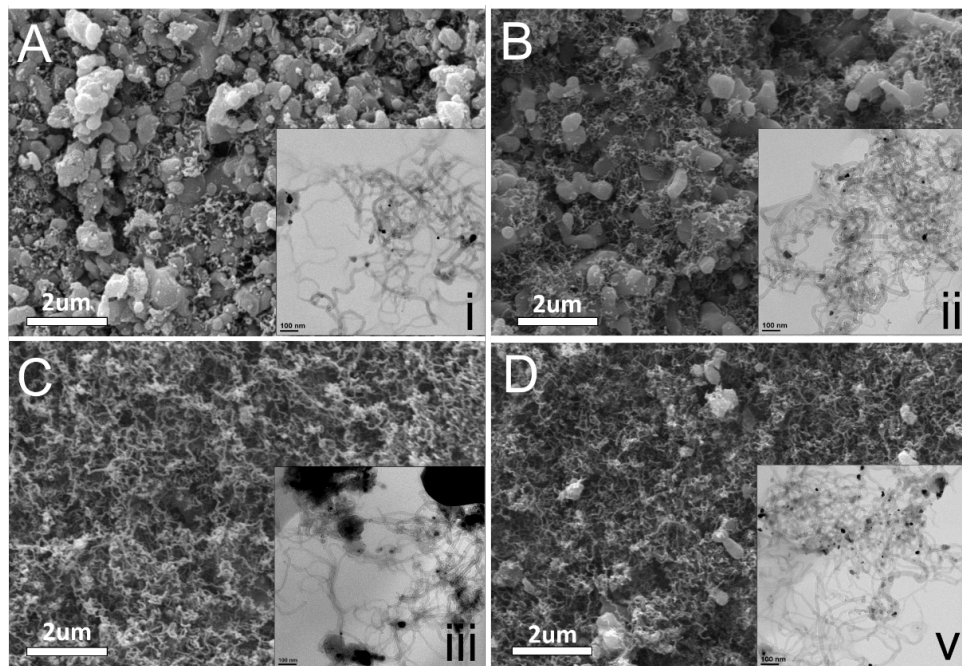


Figure 6.8 SEM results of CNTs formation for 0.1/ceramic (A), 0.5/ceramic (B), 1.0/ceramic (C), and 2.0/ceramic (D) and corresponding TEM (i-v)

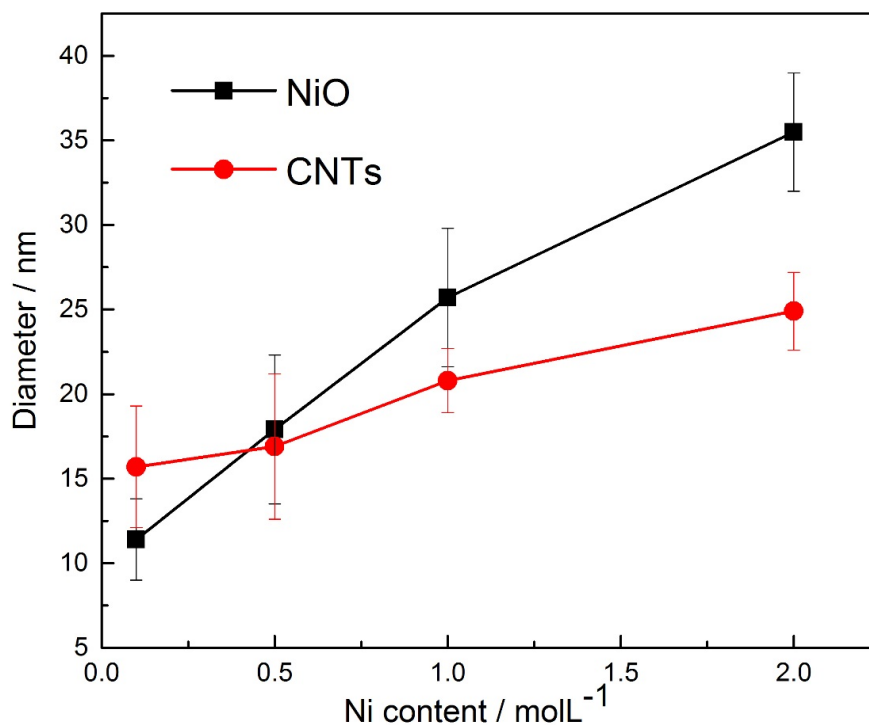


Figure 6.9 Diameter distribution comparison for fresh and spent 1.0/ceramic catalysts at 800 °C

The size of metal particles have also been reported to affect the activity of catalysts and the formation of CNTs (Cheung et al., 2002; Silva et al., 2014; Danafar et al., 2011; Gorbunov et al., 2002; Lastoskie et al., 1993; Baker, 1975). In addition, loading various amounts of metal on catalyst normally results in the formation of catalyst with various metal particle sizes, as obtain in this work, to control the production of CNTs. Baudouin et al. (2013) increased the Ni loading from 1.0 wt.% to 18.5 wt.% to increase the catalytic particle sizes from 1.6 to 7.3 nm. The diameter of metal particles was increased with the increase of metal loading. In addition, CNTs with larger diameters were produced with the increase of metal loading. However, a maximum diameter of CNTs should be expected, when the loading of metal in the catalyst is too high. For example, Chen et al.

(2005) referred to an optimally size of catalyst which could produce an optimum growth rate and a high yield of carbon nanofibers (CNFs). They reported that smaller (< 20 nm) Ni crystals caused a slow growth of CNFs and a fast deactivation of catalyst. However, when the metal particles were larger than 60nm, the rate of CNFs growth was prohibited due to the low surface area of active sites. Danafar et al. (2011) studied Fe-Co/Al catalysts with 6 ranges of metal particle sizes to study the influence on the synthesis of CNTs from ethanol. They found that the catalyst with 10-20 μ m metal particles produced about 30% higher carbon yield than the catalyst having the largest catalytic particles. It is reported that the catalysts with smaller diameters had larger breaking through capacities during frontal diffusion (shorter diffusion path length). In addition, the catalyst with large metal particle size produced more amorphous carbons and uninform CNTs, as the stability of metal agglomerates decreased with increasing particle sizes.

According to Table 6.2 and DTG-TPO (Figure 6.10) analysis of the reacted catalysts with different Ni loadings, a maximum production of CNTs was obtained in the presence of the 1.0/ceramic catalyst. CNTs production was increased from 3.1 to 9.4 wt.%, when the catalyst was changed from the 0.1/ceramic to the 1.0/ceramic. Similar results have been discussed by other researchers. For example, Venegoni et al. (2002) studied the effect of Fe content (0.5%, 1%, 2% and 5%) on CNTs growth in the presence of Fe/SiO₂ catalysts from a mixture of H₂ and C₂H₄. Catalyst with the most amount of Fe metal content (5% Fe-SiO₂) was least active in relation to the production of CNTs, due to the presence of large metal particles. In addition, it was reported that the active catalytic sites was increased to promote catalytic reactions with increasing catalytic metal content until an

optimal value was reached (Melo et al., 2005). In this study, the filamentous/amorphous carbon ratio was the highest about 5 with the 0.5/ceramic catalyst used (Figure 6.11), then slightly decreased to about 4.7 when the catalyst was changed to the 1.0/ceramic. However, the 0.5/ceramic catalyst showed the highest SD number (Figure 6.11). Overall, considering the filamentous/amorphous carbon ratio and SD of CNTs diameter, the 1.0/ceramic catalyst was suggested to be a better candidate for CNTs formation from thermochemical conversion from plastic waste.

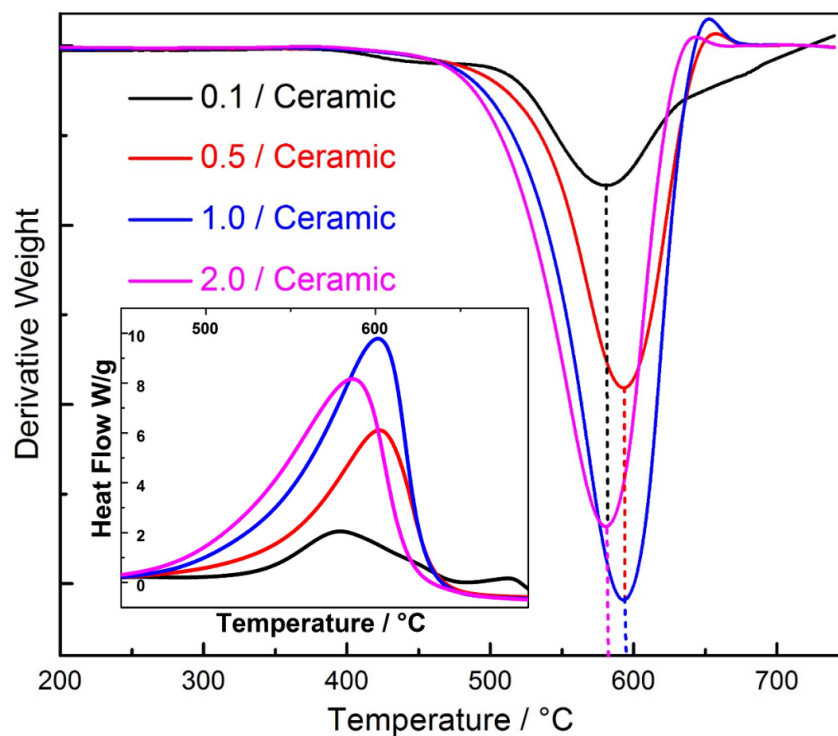


Figure 6.10 DTG-TPO and DSC results of the spent 0.1/ceramic, 0.5/ceramic, 1.0/ceramic and 2.0/ceramic catalysts at 700 °C

Chapter 7. Carbon nanotubes
growth with aluminium sphere
supported catalysts

In this chapter, Ni/sphere was used as catalysts to produce CNTs from plastics waste by CVD process. The novelty is to study the mechanism of CNTs formation using this special structure catalyst. Different process parameters (temperatures and catalysts content) have also been investigated.

7.1 Growth mechanism of CNTs on sphere supported catalysts

Original sphere substrate without Ni loading was studied by XRD, SEM and TEM analysis. Sphere substrate was identified made of Al_2O_3 by XRD analysis (Figure 7.1), and consist of 44.1 wt.% Al element and 55.9 wt.% O element, respectively (EDX analysis). Figure 7.2A shows a simulated sphere substrate with regular sphere shape and about 0.75 μm radius. SEM result (Figure 7.2B) further demonstrated the shape and diameters of sphere substrate. Inside of sphere (cross-section) is solid (Figure 7.2C) and Al_2O_3 with short fibre structure (Figure 7.2D) was clearly showed in TEM result.

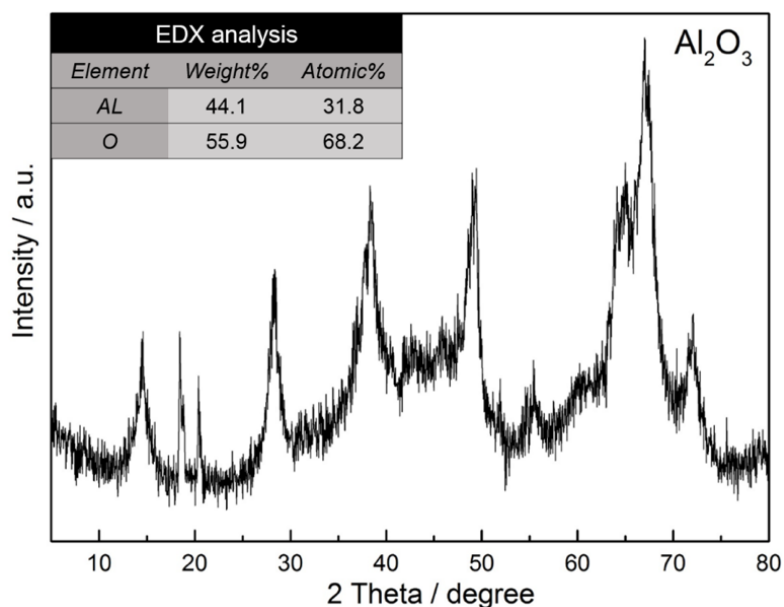


Figure 7.1 XRD and EDX-TEM analysis for original fresh Ni/sphere catalysts without Ni loading

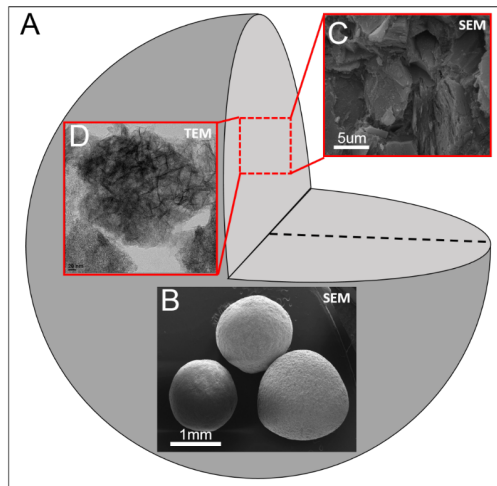


Figure 7.2 Original sphere structure (A) sphere support schematic shape; (B) surface SEM image; (C) cross-section SEM image; (D) cross-section TEM image

Based on this CNTs growth mechanism, CNTs growth and synthesis on Al_2O_3 sphere substrate from waste plastics was investigated with the help of TEM and SEM analysis. Figure 7.4 presents the TEM images of fresh 0.1/sphere and 1.0/sphere catalysts. Metal particles on the surface of the alumina sphere can be clearly observed. CNTs were synthesised under three different temperatures including 600 °C, 700 °C and 800 °C. The produced CNTs on the surface of the catalyst were studied using SEM on both cross-section and the surface of the spent sphere catalysts (Figure 7.3). It is noted that the produced filamentous carbons are assumed to be CNTs which will be confirmed by TEM analysis. At 600 °C, little amount of CNTs could be observed neither on the surface nor inside (cross-section) of the spent catalysts. As temperature increased to 700 °C, some short and disordered amorphous CNTs grown on the surface of sphere, but inside the catalysts (cross section SEM analysis), CNTs still could not be observed. With the further increase of catalytic reaction temperature to 800°C, many filamentous CNTs were observed on the surface of the spent catalysts, however, CNTs could still not be found from the cross-section of the spent catalysts.

According to the SEM analysis of the spent catalysts used at three different temperatures, CNTs grew could not be formed inside the spent alumina sphere based catalysts. Therefore, the CNTs growth mechanism is proposed in Figure 7.3A-B. Metal particles were just loaded on the surface of sphere, the Ni-liquid couldn't permeate inside the sphere by this co-precipitation method, therefore, there was no CNTs grown inside of spent catalysts.

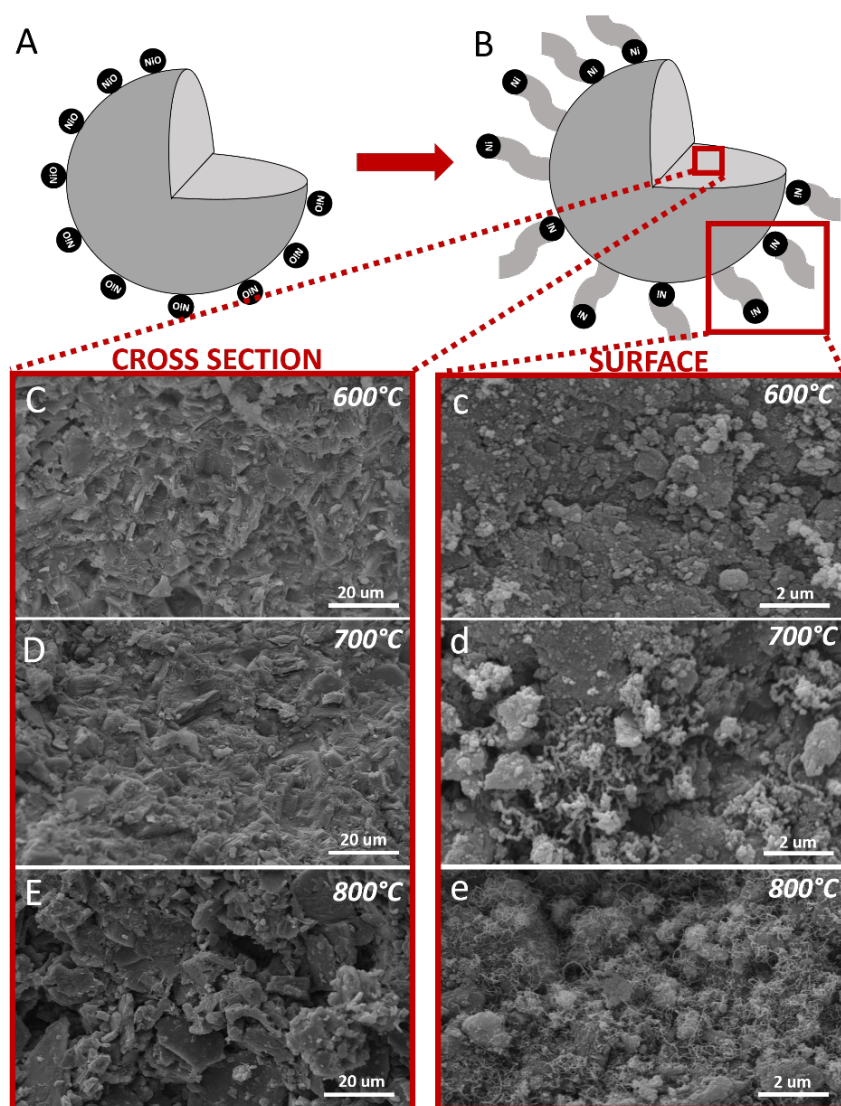


Figure 7.3 Growth mechanism of CNTs on 1.0/sphere catalyst (A) fresh catalyst schematic image; (B) spent catalysts schematic image; SEM results for cross-section of spent catalysts at (C) 600 °C, (D) 700 °C, (E) 800 °C; SEM results for surface of spent catalysts at (c) 600 °C, (d) 700 °C, (e) 800 °C

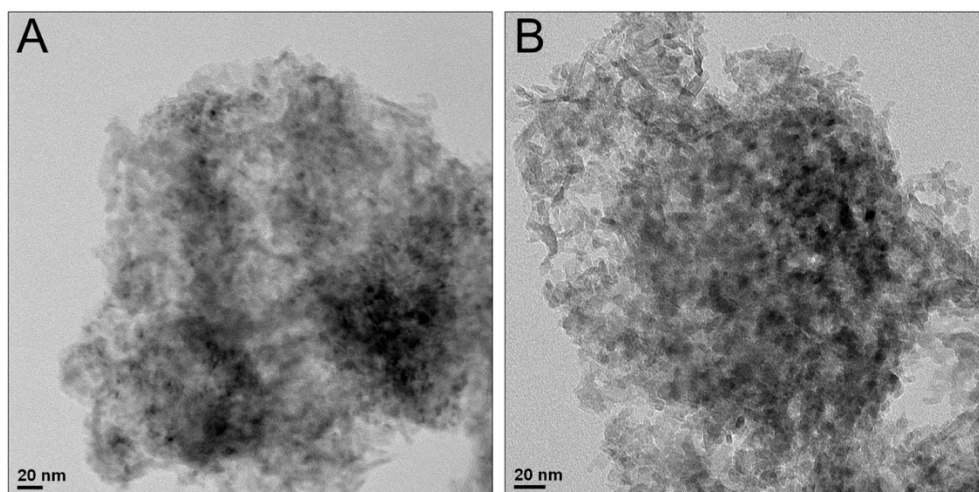


Figure 7.4 TEM results for (A) 0.1 and (B) 1.0 fresh Ni/sphere catalysts

7.2 Optimum reaction parameters investigation

The reaction parameters CNTs formation from catalytic pyrolysis of plastics play important roles. Different parameters could influence the morphology, length and diameter of CNTs, the growth rate of CNTs and also reaction mechanism in the process (Dasgupta et al., 2011). Therefore, optimum parameters for particular catalyst need to be studied for particular catalysts to produce the optimum quality and quantity of CNTs.

In this research, two reaction parameters using sphere catalysts were investigated in relation to the effect on the CNTs formation from plastics waste, temperature and metal loading content. When the effect of Ni content (0.1 and 1.0 molL⁻¹) was studied, thermochemical conversion of waste HDPE was investigated at 800 °C. When the effect of reaction temperature (600, 700, and 800 °C) was studied, the 1.0/sphere catalyst was used. CNTs formation from thermochemical conversion of plastics waste was investigated according to both quantitative analysis and qualitative analysis. The quantitative analysis of CNTs was further discussed based on amount of amorphous carbon and filamentous carbon production which was worked out by TGA-TPO analysis

of spent catalysts. And the quality of CNTs production is analysed and discussed mainly based on SEM and TEM results. Further details are shown as below.

7.2.1 Influence of nickel loading

Thermochemical conversion of waste HDPE was investigated in the presence of Ni/sphere catalysts with different Ni contents at 800 °C. Figure 7.5A-B show the SEM results and corresponding TEM results for the filamentous carbon production. Large amount of filaments carbons is covered on spent 0.1 and 1.0/sphere spent catalysts. TEM results further proved that the filaments carbons are mostly CNTs. Using SEM images, it is difficult to distinguish the quantity and quality between 0.1 and 1.0/sphere catalysts. For qualitative comparison, the average diameters of CNTs with standard deviation (Figure 7.5a-b) was analysed and discussed according to the SEM results using Image J, representative. The standard deviation (SD) number can be used as a main factor to identify the quality of CNTs formation, a better quality of CNTs is identified with a smaller SD number (Liu et al., 2017). It could be noticed that the diameter of CNTs slightly increased with an increase of Ni content. The 0.1/sphere had the diameter 40.2 ± 8.6 nm, and the 1.0/sphere had the largest diameter 55.2 ± 7.9 nm. And an increase of metal contents leads to an increase metal particle sizes (Chen et al., 2005; Jiang et al., 2016). For example, Daudouin et al. (2013) increased the Ni loading from 1.0 wt.% to 18.5 wt.% to increase the catalytic particle sizes from 1.6 to 7.3 nm. In addition, it is generally accepted that the diameter of formed CNTs by hydrocarbon deposition have almost the same diameter with catalytic metal particles, due to CNTs are diffused by catalytic metal particles during growth process. Therefore, the size of metal particles

determine the diameter of filamentous carbons (Sinnott et al., 1999). In this work, the average diameter of CNTs increased from 40.2nm to 55.2nm, as an increase of Ni loading from 0.1mL⁻¹ to 1.0mL⁻¹. Similar results were also found by other researchers (Sinnott et al., 1999; Li et al., 2001; Cheung et al., 2002; Silva et al., 2014; Danafar et al., 2011; Gorbunov et al., 2002; Lastoskie et al., 1993; Baker, 1975). Sinnott et al. (1999) studied the effect of Fe content on the diameter of CNTs produced from ferrocene-xylene mixture through CVD. They reported that the average Fe particle size was decreased from 35.3 to 28.2 nm with a decrease of Fe content from 0.75 to 0.075 wt.%. Cheung et al. (2002) used Fe-based catalysts with average diameters of 3, 9, and 13nm to synthesise CNTs from ethylene with average diameters of 3, 7, and 12 nm, respectively. The standard deviation decreased from 8.6nm to 7.9 nm with an increase Ni loading. That means the diameter distribution of CNTs by 1.0/sphere catalysts is slight more average than that of 0.1/sphere catalysts.

The quantitative analysis on amount of amorphous carbon and filamentous carbon production was worked out by TGA-TPO analysis (Figure 7.6). It is assumed that the oxidation temperature below 550 °C was assigned to amorphous carbons and the oxidation above 550 °C in TPO was assigned to filamentous carbon (assumed as CNTs in this work) (Wu et al., 2015). Two different types of carbon separated and analysed by vertical black imaginary line (Figure 7.6). The total carbon yield could be represented by X axis 'the weight loss' of catalyst in relation to the initial catalyst weight. According to TPO analysis of the spent catalysts with different Ni loadings, the amorphous carbon production is the same for 0.1 and 1.0/sphere catalysts, about 1.0%, and CNTs production

was increased from 6.2 to 7.5 wt.%, when the catalyst was changed from the 0.1/sphere to the 1.0/sphere. Two different Ni loading sphere have similar quality, but 1.0/sphere catalysts produced more filamentous carbon, therefore 1.0/sphere catalyst was assumed as the optimum Ni content for this study.

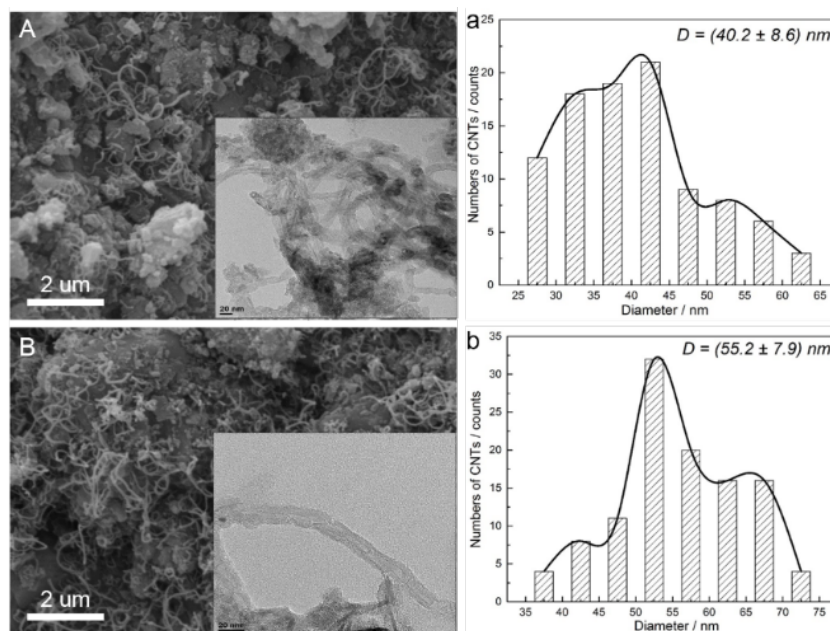


Figure 7.5 SEM, TEM results and diameter distribution CNTs for (A)(a) 0.1 and (B)(b) 1.0 spent Ni/sphere catalysts

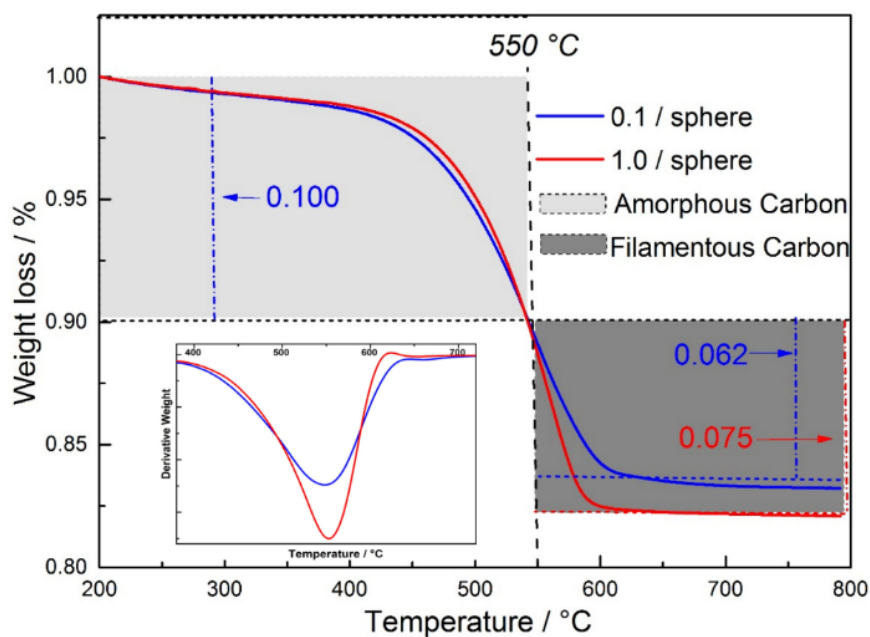


Figure 7.6 DTG-TPO and DSC results of the spent 0.1 and 1.0/sphere at 800 °C

7.2.2 Influence of reaction temperature

The effect of reaction temperature on the growth of CNTs through thermal conversion from HDPE is studied using Ni/sphere catalysts. Three different reaction temperatures (600 °C, 700 °C and 800 °C) were investigated using the 1.0/ sphere catalyst. Scanning electron microscope (SEM), and temperature program oxidation (TGA-TPO and DTG-TPO) analysis were carried out to the spent catalysts. SEM results (Figure 7.4) reveals that CNTs cannot grow at 600 °C for sphere substrate, it is formed between 700 °C and 800°C with different structure and yield. At 600 °C, no CNTs can be observed from SEM image, most of deposited materials were carbonaceous or amorphous carbon, which extensionally proved by TPO analysis. At 700 °C, small amount of CNTs mixed with amorphous carbon was observed. Increasing the temperature to 800 °C resulted in many carbon nanotubes with aligned and uniform diameter CNTs. This result is further supported by TPO analysis (Figure 7.7). At 600 °C, oxidation only exists below 550 °C, which meant there is no CNTs formed at this temperature. For amorphous carbons (oxidation temperature below 550 °C), the yield was decreased from 1.2 to 1.0 wt.%, when the temperature increased from 700 °C to 800 °C. This result is consistent with the SEM analysis (Figure 7.4), where amorphous carbons could be clearly observed on spent catalyst tested at 700 °C. Furthermore, the formation of CNTs was increased from 1.0 wt.% and 7.5 wt.% when the reaction temperature was increased 700 °C and 800 °C. DTG-TPO results with DCS (Differential Scanning Calorimetry) showed that the oxidation peak moved to higher temperature with the increase of experimental temperature from 600 °C

and 800 °C, indicating that the CNTs might be more crystallised at 800 °C reaction temperature.

The results suggest that the quantity and quality of CNTs are improved with increasing temperature for sphere substrate. This is also consistent with some research on the effect of temperature on CNTs formation. For example, Acomb et al. (2015) reported the effect of growth temperature (700 °C, 800 °C, and 900 °C) on the CNTs production using low density polyethylene (LDPE) with Fe/Al₂O₃ as catalyst. Their result showed that a higher temperature promoted higher fraction of CNTs formation. Also, Hornyak et al. (1999), who investigated the CNTs formation with Co-based catalysts from propylene gas, it was found that amorphous carbon was formed at around 550 °C, while CNTs was formed at temperature higher than 800 °C.

CNTs are formed by hydrocarbon atom dissolving, diffusion and precipitating through the catalyst in CVD process, and the rate of these three steps are affected by both temperature and atoms concentration (Mustaz et al., 2006). Higher temperature seems to prefer well crystallised, uniform, less defective nanotube with high yield and purity. The effect of reaction temperature on CNTs synthesis by CVD was mainly related to carbon source and catalytic activity. In this study, higher reaction temperature promoted the decomposition of HDPE to increase the concentration of carbon atoms, which would increase the growth rate of CNTs formation. And the dissolving and diffusing rates of carbon atoms would also be increased as an increase of temperature. The research from Wu and Williams (2010b) support this, they reported at high temperature, more reactive carbon sources were produced from pyrolysis of waste plastics. Lee et al. (2001) and also

reported higher temperature promoted the diffusion and reaction rates of carbons, resulting in the enhanced formation of CNTs. Therefore, in this study, less amorphous carbons and more CNTs were formed at 800 °C compared to 600 °C. In addition, the reaction temperatures can increase in catalytic activity, due to the alteration in the distribution of atoms. The metal particle size of catalyst will increase with an increase of temperature, consequently catalytic activity change. Many studies worked on the catalysts activity at different temperatures on effect of CNTs formation. For example, Mishra et al. (2012) synthesised MWCHT at three different temperatures (600 °C, 700 °C, and 800 °C) from pyrolytic degradation of PP with Ni catalyst, they found the increase in temperature led to the decrease of defects, disorder and amorphous carbon and improvement of CNTs purity. Therefore, 800 °C was assumed as the optimum temperature for this study.

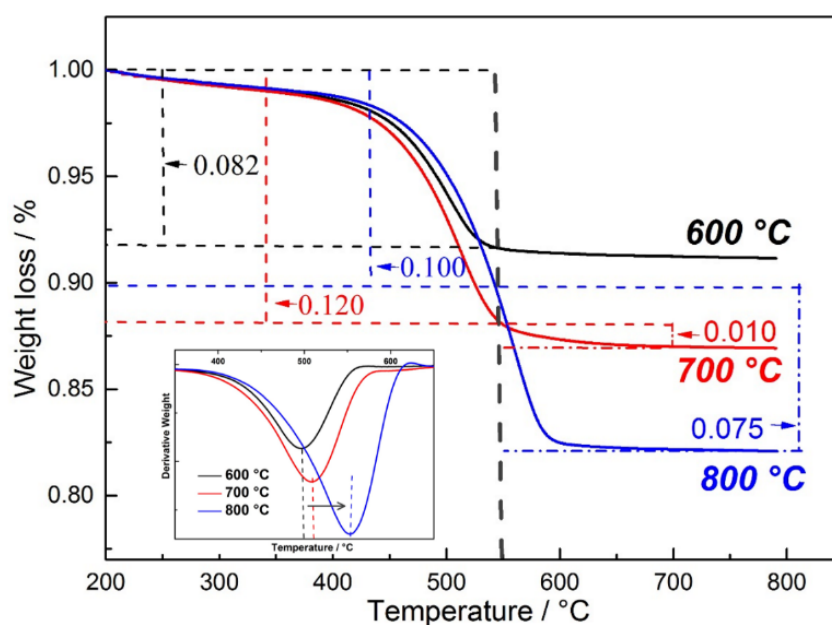


Figure 7.7 DTG-TPO and DSC results of the spent 1.0/sphere catalysts at 600 °C, 700 °C, and 800 °C

Chapter 8. Conclusion and future work

8.1 Summary of catalysts studied

Carbon nanotubes (CNTs) were successfully produced from waste plastics using all 4 groups of catalysts. The results and optimum reaction parameter for each catalyst has been summarised as below.

- (1) The Fe-based catalyst with the largest metal particles resulted in the highest hydrogen production ($25.60 \text{ mmol g}^{-1} \text{ plastic}$) and the highest yield of carbon (29 wt.%). It is suggested to be due to a high carbon solubility of iron metal particles compared to Ni-based catalysts. The consistency between metal particle size and the diameter of CNTs was observed in this work, as the catalysts with different metal particle sizes generated the CNTs with the corresponding diameters. In addition, a strong interaction between Ni and SiO_2 support is suggested to suppress the growth of CNTs, while many amorphous carbons were produced using the Ni/ SiO_2 -S catalyst.
- (2) The addition of a conditioning catalyst prior to the formation of CNTs on the Ni/AAO catalyst was found to be beneficial. The quality of the produced CNTs in relation to the uniformity was enhanced when more conditioning catalyst was introduced in the process. An increase of Ni content from 0.1 mol L^{-1} up to 2.0 mol L^{-1} on AAO resulted in the accumulation of metal particles on the surface of AAO membrane. As a result, more amorphous carbons were produced. 0.1 mol L^{-1} of Ni solution (catalyst precursor) assigned as 0.1/AAO is suggested to produce high quality CNTs in relation to the uniform distribution of diameter of CNTs. An optimal catalytic temperature of $700 \text{ }^\circ\text{C}$ is suggested in this work. $600 \text{ }^\circ\text{C}$ was too low to activate catalyst resulting in a low yield, while $800 \text{ }^\circ\text{C}$ might cause the sintering of Ni-based particles and resulting

in the production of a large fraction of amorphous carbons. An increase of steam injection is suggested to enhance the quality of CNTs formed on the Ni/AAO catalyst, but resulted a large decrease on CNTs production.

(3) An optimum temperature 700 °C was suggested for Ni-based ceramics membrane. An increase of Ni content on ceramic membrane resulted in increasing diameters of metal particle sizes which could affect the activity of catalysts and the formation of CNTs. The 1.0/ceramic was the optimum candidate for CNTs formation in this study giving the highest fraction of filamentous carbons with the narrowest distribution of CNTs diameter.

(4) 0.1/sphere and 1.0/sphere catalysts produced similar quality of CNTs, but 1.0/sphere catalysts produced more filamentous carbon, therefore 1.0/sphere catalyst was assumed as the optimum Ni content for this study. Increasing temperature improved both quality and quantity of CNTs produced. An optimum temperature 700 °C was suggested for nickel based sphere catalysts.

8.2 Challenges and future work

All these catalysts showed their advantages and disadvantages. For example, the Ni/Fe-based catalyst produced high quality of CNTs production, but also suffered the production of amorphous carbons and disordered diameter of CNTs. The AAO membrane catalyst produced the highest purity of CNTs due to its uniform structure, however, these membranes have weak toughness. They are too easy to break during the preparation, reaction and transformation process (Figure A-A9). As sphere support is solid, CNTs

could only be produced on its surface; thus it largely limits the quantity of CNTs. Through studying these catalysts, it was found that it is difficult to obtain high purity of CNTs and at same time with a high yield. Each AAO membrane has light weight (about 0.5 g), 10% CNTs would be produced with 1g plastics waste as feedstock (about 0.05 g). If this small amount of CNTs needs to be separated from catalysts for real applications, it will be some loss during the separation process. And at the end there will be a small amount of CNTs remain. This phenomenon also exists for CNTs production from arc discharge and laser ablation methods. Jourdain et al. (2013) stated that there is a qualitatively good description of many phenomena acting for CNTs growth, but often the quantity of CNTs is low.

For future research of CNTs production from waste plastics, new catalysts could be developed to produce a large amount of CNTs with high purity. Catalytic support with different structure such as porous is worth to study for increasing the quantity of CNTs production. Using stainless steel mesh as a catalyst support for CNTs production from catalytic pyrolysis of waste plastics could be interesting, as the produced CNTs can be easily separated by physical vibration. Obtained CNTs could be further separated from catalysts and continue detailed characterization on CNTs properties. For example, tube chirality which determined the electrical property of CNTs can be further analysed, it would determine the applications of CNTs we produced. However, separation progress leads to loss of CNTs. In another way, these spent catalysts contained CNTs could be applied directly without separation. For example, the spent catalysts with produced CNTs could be further developed as new catalysts or composites directly without separation process. Furthermore, using other plastic wastes which are more difficult recycled (e.g.

hard plastics and printed circulated board) these days for CNTs production could further enhance environmental benefit and economic feasibility. As these wastes have higher disposal gate fees and environmental impacts.

References

- Acomb, J. C., Wu, C., & Williams, P. T. (2014). Control of steam input to the pyrolysis-gasification of waste plastics for improved production of hydrogen or carbon nanotubes. *Applied Catalysis B: Environmental*, 147, 571-584.
- Acomb, J. C., Wu, C., & Williams, P. T. (2015). Effect of growth temperature and feedstock:catalyst ratio on the production of carbon nanotubes and hydrogen from the pyrolysis of waste plastics. *Journal of Analytical and Applied Pyrolysis*, 113, 231-238.
- Acomb, J. C., Wu, C., & Williams, P. T. (2016). The use of different metal catalysts for the simultaneous production of carbon nanotubes and hydrogen from pyrolysis of plastic feedstocks. *Applied Catalysis B: Environmental*, 180, 497-510.
- Ago, H., Uehara, N., Yoshihara, N., Tsuji, M., Yumura, M., Tomonaga, N., & Setoguchi, T. (2006). Gas analysis of the CVD process for high yield growth of carbon nanotubes over metal-supported catalysts. *Carbon*, 44(14), 2912-2918.
- Al-Salem, S. M., Lettieri, P., & Baeyens, J. (2009). Recycling and recovery routes of plastic solid waste (PSW): a review. *Waste Management*, 29(10), 2625-2643.
- Alvarez, W. E., Kitiyanan, B., Borgna, A., & Resasco, D. E. (2001). Synergism of Co and Mo in the catalytic production of single-wall carbon nanotubes by decomposition of CO. *Carbon*, 39(4), 547-558.
- An, J. W., You, D. H., & Lim, D. S. (2003). Tribological properties of hot-pressed alumina–CNT composites. *Wear*, 255(1), 677-681.

- Anna, M., Albert, G. N., & Esko, I. K. (2003). The role of metal nanoparticles in the catalytic production of single-walled carbon nanotubes—a review. *Journal of Physics: Condensed Matter*, 15(42), S3011-S3030.
- Anuar Sharuddin, S. D., Abnisa, F., Wan Daud, W. M. A., & Aroua, M. K. (2016). A review on pyrolysis of plastic wastes. *Energy Conversion and Management*, 115, 308-326.
- Aqel, A., El-Nour, K. M. M. A., Ammar, R. A. A., & Al-Warthan, A. (2012). Carbon nanotubes, science and technology part (I) structure, synthesis and characterisation. *Arabian Journal of Chemistry*, 5(1), 1-23.
- Astrup, T., Fruergaard, T., & Christensen, T. H. (2009). Recycling of plastic: accounting of greenhouse gases and global warming contributions. *Waste Management & Research*, 27(8), 763-772.
- Auprêtre, F., Descorme, C., & Duprez, D. (2002). Bio-ethanol catalytic steam reforming over supported metal catalysts. *Catalysis Communications*, 3(6), 263-267.
- Ban, C., Wu, Z., Gillaspie, D. T., Chen, L., Yan, Y., Blackburn, J. L., & Dillon, A. C. (2010). Nanostructured Fe₃O₄/SWNT Electrode: Binder-Free and High-Rate Li-Ion Anode. *Advanced Materials*, 22(20), E145-E149.
- Barbarias, I., Lopez, G., Amutio, M., Artetxe, M., Alvarez, J., Arregi, A., Bibao, J. & Olazar, M. (2016a). Steam reforming of plastic pyrolysis model hydrocarbons and catalyst deactivation. *Applied Catalysis A: General*, 527, 152-160.

- Barbarias, I., Lopez, G., Artetxe, M., Arregi, A., Santamaria, L., Bilbao, J., & Olazar, M. (2016b). Pyrolysis and in-line catalytic steam reforming of polystyrene through a two-step reaction system. *Journal of Analytical and Applied Pyrolysis*, 122, 502-510.
- Barnes, D. K. A., Galgani, F., Thompson, R. C., & Barlaz, M. (2009). Accumulation and fragmentation of plastic debris in global environments. *Philosophical Transactions of the Royal Society B: Biological Sciences*, 364(1526), 1985-1998.
- Baudouin, D., Rodemerck, U., Krumeich, F., Mallmann, A. d., Szeto, K. C., Ménard, H., Veyre, L., Candy, J., Webb, P. B., Thieuleux, C. & Copéret, C. (2013). Particle size effect in the low temperature reforming of methane by carbon dioxide on silica-supported Ni nanoparticles. *Journal of Catalysis*, 297, 27-34.
- Bethune, D. S., Kiang, C. H., de Vries, M. S., Gorman, G., Savoy, R., Vazquez, J., & Beyers, R. (1993). Cobalt-catalysed growth of carbon nanotubes with single-atomic-layer walls. *Nature*, 363, 605-607.
- Borsodi, N., Szentes, A., Miskolczi, N., Wu, C., & Liu, X. (2016). Carbon nanotubes synthesized from gaseous products of waste polymer pyrolysis and their application. *Journal of Analytical and Applied Pyrolysis*, 120, 304-313.
- Che, G., Lakshmi, B. B., Martin, C. R., Fisher, E. R., & Ruoff, R. S. (1998). Chemical Vapor deposition based synthesis of carbon nanotubes and nanofibers using a template method. *Chemistry of Materials*, 10(1), 260-267.
- Chen, D., Christensen, K. O., Ochoa-Fernández, E., Yu, Z., Tøtdal, B., Latorre, N., Holmen, A. (2005). Synthesis of carbon nanofibers: effects of Ni crystal size during methane decomposition. *Journal of Catalysis*, 229(1), 82-96.

- Chen, J. T., Shin, K., Leiston, J. M., Zhang, M., & Russell, T. P. (2006). Amorphous carbon nanotubes with tunable properties via template wetting. *Advanced Functional Materials*, 16(11), 1476-1480.
- Cheung, C. L., Kurtz, A., Park, H., & Lieber, C. M. (2002). Diameter-controlled synthesis of carbon nanotubes. *The Journal of Physical Chemistry B*, 106(10), 2429-2433.
- Colomer, J. F., Stephan, C., Lefrant, S., Van Tendeloo, G., Willems, I., Kónya, Z., Nagy, J. B. (2000). Large-scale synthesis of single-wall carbon nanotubes by catalytic chemical vapor deposition (CCVD) method. *Chemical Physics Letters*, 317(1). *Science for Environment Policy*. (2011). Plastic waste: ecological and human health impacts. DG environment news alert service, Available online: http://ec.europa.eu/environment/integration/research/newsalert/pdf/IR1_en.pdf [Accessed November 2011]
- Da Silva, A. L. M., den Breejen, J. P., Mattos, L. V., Bitter, J. H., de Jong, K. P., & Noronha, F. B. (2014). Cobalt particle size effects on catalytic performance for ethanol steam reforming – smaller is better. *Journal of Catalysis*, 318, 67-74.
- Danafar, F., Fakhru'l-Razi, A., Mohd Salleh, M. A., & Awang Biak, D. R. (2011). Influence of catalytic particle size on the performance of fluidized-bed chemical vapor deposition synthesis of carbon nanotubes. *Chemical Engineering Research and Design*, 89(2), 214-223.
- Danafar, F., Fakhru'l-Razi, A., Salleh, M. A. M., & Biak, D. R. A. (2009). Fluidized bed catalytic chemical vapor deposition synthesis of carbon nanotubes—a review. *Chemical Engineering Journal*, 155(1–2), 37-48.

- Dasgupta, K., Joshi, J. B., & Banerjee, S. (2011). Fluidized bed synthesis of carbon nanotubes – a review. *Chemical Engineering Journal*, 171(3), 841-869.
- Deng, S. Z., Wu, Z. S., Zhou, J., Xu, N. S., Chen, J., & Chen, J. (2002). Synthesis of silicon carbide nanowires in a catalyst-assisted process. *Chemical Physics Letters*, 356(5), 511-514.
- Ding, F., Rosen, A., & Bolton, K. (2004). Molecular dynamics study of the catalyst particle size dependence on carbon nanotube growth. *J Chem Phys*, 121(6), 2775-2779.
- Donatelli, A., Iovane, P., & Molino, A. (2010). High energy syngas production by waste tyres steam gasification in a rotary kiln pilot plant. Experimental and numerical investigations. *Fuel*, 89(10), 2721-2728.
- Dresselhaus, M. S., Dresselhaus, G., Saito, R., & Jorio, A. (2005). Raman spectroscopy of carbon nanotubes. *Physics Reports*, 409(2), 47-99.
- Endo, M., Kim, Y. A., Hayashi, T., Nishimura, K., Matusita, T., Miyashita, K., & Dresselhaus, M. S. (2001). Vapor-grown carbon fibers (VGCFs): basic properties and their battery applications. *Carbon*, 39(9), 1287-1297.
- Erkiaga, A., Lopez, G., Barbarias, I., Artetxe, M., Amutio, M., Bilbao, J., & Olazar, M. (2015). HDPE pyrolysis-steam reforming in a tandem spouted bed-fixed bed reactor for H₂ production. *Journal of Analytical and Applied Pyrolysis*, 116, 34-41.
- Ermakova, M. A., Ermakov, D. Y., & Kuvshinov, G. G. (2000). Effective catalysts for direct cracking of methane to produce hydrogen and filamentous carbon: part I. Nickel catalysts. *Applied Catalysis A: General*, 201(1), 61-70.

- Esteves, L. M., Oliveira, H. A., & Passos, F. B. (2018). Carbon nanotubes as catalyst support in chemical vapor deposition reaction: a review. *Journal of Industrial and Engineering Chemistry*, 65, 1-12.
- Ewald, P. P. (1962). *Fifty Years of X-Ray Diffraction*. Springer.
- Fan, S., Chapline, M. G., Franklin, N. R., Tomblor, T. W., Cassell, A. M., & Dai, H. (1999). Self-oriented regular arrays of carbon nanotubes and their field emission properties. *Science*, 283(5401), 512-514.
- Flahaut, E., Peigney, A., Laurent, C., Marlière, C., Chastel, F., & Rousset, A. (2000). Carbon nanotube–metal–oxide nanocomposites: microstructure, electrical conductivity and mechanical properties. *Acta Materialia*, 48(14), 3803-3812.
- Frackowiak, E., Metenier, K., Bertagna, V., & Beguin, F. (2000). Supercapacitor electrodes from multiwalled carbon nanotubes. *Applied Physics Letters*, 77(15), 2421-2423.
- Franklin, N. R., Li, Y., Chen, R. J., Javey, A., & Dai, H. (2001). Patterned growth of single-walled carbon nanotubes on full 4-inch wafers. *Applied Physics Letters*, 79(27), 4571-4573.
- Futaba, D. N., Hata, K., Yamada, T., Mizuno, K., Yumura, M., & Iijima, S. (2005). Kinetics of water-assisted single-walled carbon nanotube synthesis revealed by a time-evolution analysis. *Physical Review Letters*, 95(5), 056104(1-4).
- Gao, N., Liu, S., Han, Y., Xing, C., & Li, A. (2015). Steam reforming of biomass tar for hydrogen production over NiO/ceramic foam catalyst. *International Journal of Hydrogen Energy*, 40(25), 7983-7990.

- Gershman, B. B., Inc. (2013). Gasification of non-recycled plastics from municipal solid waste in the United States. Solid Waste Management Consultants, GBB/12038(1), 1-45.
- Golshadi, M., Maita, J., Lanza, D., Zeiger, M., Presser, V., & Schrlau, M. G. (2014). Effects of synthesis parameters on carbon nanotubes manufactured by template-based chemical vapor deposition. *Carbon*, 80, 28-39.
- Gorbunov, A., Jost, O., Pompe, W., & Graff, A. (2002). Role of the catalyst particle size in the synthesis of single-wall carbon nanotubes. *Applied Surface Science*, 197–198, 563-567.
- Gu, L., & Ozbakkaloglu, T. (2016). Use of recycled plastics in concrete: a critical review. *Waste Management*, 51, 19-42.
- Hata, K., Futaba, D. N., Mizuno, K., Namai, T., Yumura, M., & Iijima, S. (2004). Water-assisted highly efficient synthesis of impurity-free single-walled carbon nanotubes. *Science*, 306(5700), 1362-1364.
- He, C., Zhao, N., Shi, C., Du, X., Li, J., Li, H., & Cui, Q. (2007). An approach to obtaining homogeneously dispersed carbon nanotubes in Al powders for preparing reinforced Al-matrix composites. *Advanced Materials*, 19(8), 1128-1132.
- Hanaei, H., Biak, D., Ahamad, I. & Danafar, F. (2010). Effects of synthesis reaction temperature, deposition time and catalyst on yield of carbon nanotubes. *Asian Journal of Chemistry*, 24(6), 2407-2414.
- Hernadi, K., Fonseca, A., Nagy, J. B., Siska, A., & Kiricsi, I. (2000). Production of nanotubes by the catalytic decomposition of different carbon-containing compounds. *Applied Catalysis A: General*, 199(2), 245-255.

- Herrero-Latorre, C., Álvarez-Méndez, J., Barciela-García, J., García-Martín, S., & Peña-Crecente, R. M. (2015). Characterization of carbon nanotubes and analytical methods for their determination in environmental and biological samples: A review. *Analytica Chimica Acta*, 853, 77-94.
- Hornyak, G. L., Dillon, A. C., Parilla, P. A., Schneider, J. J., Czap, N., Jones, K. M., Fagoon, F. S., Mason, A. & Heben, M. J. (1999). Template synthesis of carbon nanotubes. *Nanostructured Materials*, 12(1), 83-88.
- Horvat, N., & Ng, F. T. (1999). Tertiary polymer recycling: study of polyethylene thermolysis as a first step to synthetic diesel fuel. *Fuel*, 78(4), 459-470.
- Hou, P., Liu, C., Shi, C., & Cheng, H. (2012). Carbon nanotubes prepared by anodic aluminum oxide template method. *Chinese Science Bulletin*, 57(2), 187-204.
- Hsieh, C. T., Lin, Y. T., Chen, W. Y., & Wei, J. L. (2009). Parameter setting on growth of carbon nanotubes over transition metal/alumina catalysts in a fluidized bed reactor. *Powder Technology*, 192(1), 16-22.
- Hu, J. L., Yang, C. C., & Huang, J. H. (2008). Vertically-aligned carbon nanotubes prepared by water-assisted chemical vapor deposition. *Diam Relat Mater*, 17(12), 2084-2088.
- Iijima, S., & Ichihashi, T. (1993). Single-shell carbon nanotubes of 1-nm diameter. *Nature*, 363, 603-605.
- Najafabadi, A., Yasuda, S., Kobashi, K., Yamada, T., Futaba, D. N., Hatori, H. & Hata, K. (2010). Extracting the full potential of single-walled carbon nanotubes as durable supercapacitor electrodes operable at 4 V with high power and energy density. *Advanced Materials*, 22(35), E235-E241.

- Janajreh, I., Alshrah, M., & Zamzam, S. (2015). Mechanical recycling of PVC plastic waste streams from cable industry: A case study. *Sustainable Cities and Society*, 18, 13-20.
- Jeong, S. H., Hwang, H. Y., Hwang, S. K., & Lee, K. H. (2004). Carbon nanotubes based on anodic aluminum oxide nano-template. *Carbon*, 42(10), 2073-2080.
- Ji, L., Lin, Z., Alcoutlabi, M., & Zhang, X. (2011). Recent developments in nanostructured anode materials for rechargeable lithium-ion batteries. *Energy & Environmental Science*, 4(8), 2682-2699.
- Jia, X., Zhang, Q., Zhao, M.-Q., Xu, G.-H., Huang, J.-Q., Qian, Qian, W., Lu, Y. & Wei, F. (2012). Dramatic enhancements in toughness of polyimide nanocomposite via long-CNT-induced long-range creep. *Journal of Materials Chemistry*, 22(14), 7050-7056.
- Jiang, B., Zhang, C., Wang, K., Dou, B., Song, Y., Chen, H., & Xu, Y. (2016). Highly dispersed Ni/montmorillonite catalyst for glycerol steam reforming: Effect of Ni loading and calcination temperature. *Applied Thermal Engineering*, 109, Part A, 99-108.
- Jourdain, V., & Bichara, C. (2013). Current understanding of the growth of carbon nanotubes in catalytic chemical vapour deposition. *Carbon*, 58, 2-39.
- Teo, K. B. K., Singh, C., Chhowalla, M. & Milne, W. I. (2003). Catalytic synthesis of carbon nanotubes and nanofibers, *Encyclopedia of Nanoscience and Nanotechnology*. American Scientific Publisher, X1-22.

- Karam, L., Casale, S., El Zakhem, H., & El Hassan, N. (2017). Tuning the properties of nickel nanoparticles inside SBA-15 mesopores for enhanced stability in methane reforming. *Journal of CO2 Utilization*, 17, 119-124.
- Kaskhedikar, N. A., & Maier, J. (2009). Lithium storage in carbon nanostructures. *Advanced Materials*, 21(25-26), 2664-2680.
- Kathyayini, H., Willems, I., Fonseca, A., Nagy, J. B., & Nagaraju, N. (2006). Catalytic materials based on aluminium hydroxide, for the large scale production of bundles of multi-walled (MWNT) carbon nanotubes. *Catalysis Communications*, 7(3), 140-147.
- Kichambare, P. D., Qian, D., Dickey, E. C., & Grimes, C. A. (2002). Thin film metallic catalyst coatings for the growth of multiwalled carbon nanotubes by pyrolysis of xylene. *Carbon*, 40(11), 1903-1909.
- Kim, K. E., Kim, K. J., Jung, W. S., Bae, S. Y., Park, J., Choi, J., & Choo, J. (2005). Investigation on the temperature-dependent growth rate of carbon nanotubes using chemical vapor deposition of ferrocene and acetylene. *Chemical Physics Letters*, 401(4-6), 459-464.
- Kitiyanan, B., Alvarez, W. E., Harwell, J. H., & Resasco, D. E. (2000). Controlled production of single-wall carbon nanotubes by catalytic decomposition of CO on bimetallic Co-Mo catalysts. *Chemical Physics Letters*, 317(3), 497-503.
- Kukovecz, A., Konya, Z., Nagaraju, N., Willems, I., Tamasi, A., Fonseca, A., Nagy, J. B. & Kiricsi, I. (2000). Catalytic synthesis of carbon nanotubes over Co, Fe and Ni containing conventional and sol-gel silica-aluminas. *Physical Chemistry Chemical Physics*, 2(13), 3071-3076.

- Kukovitskii, E. F., Chernozatonskii, L. A., L'Vov, S. G., & Mel'nik, N. N. (1997). Carbon nanotubes of polyethylene. *Chemical Physics Letters*, 266(3), 323-328.
- Kukovitsky, E. F., L'Vov, S. G., Sainov, N. A., Shustov, V. A., & Chernozatonskii, L. A. (2002). Correlation between metal catalyst particle size and carbon nanotube growth. *Chemical Physics Letters*, 355(5-6), 497-503.
- Kumagai, S., Alvarez, J., Blanco, P. H., Wu, C., Yoshioka, T., Olazar, M., & Williams, P. T. (2015). Novel Ni-Mg-Al-Ca catalyst for enhanced hydrogen production for the pyrolysis-gasification of a biomass/plastic mixture. *Journal of Analytical and Applied Pyrolysis*, 113, 15-21.
- Kumar, M., & Ando, Y. (2005). Controlling the diameter distribution of carbon nanotubes grown from camphor on a zeolite support. *Carbon*, 43(3), 533-540.
- Kumar, S., Panda, A. K., & Singh, R. K. (2011). A review on tertiary recycling of high-density polyethylene to fuel. *Resources, Conservation and Recycling*, 55(11), 893-910.
- Kyotani, T., Tsai, L.-f., & Tomita, A. (1996). Preparation of ultrafine carbon tubes in nanochannels of an anodic aluminum oxide film. *Chemistry of Materials*, 8(8), 2109-2113.
- Cava, A. I., Bernardo, C. A., & Trimm, D. L. (1982). Studies of deactivation of metals by carbon deposition. *Carbon*, 20(3), 219-223.
- Labhsetwar, N., Doggali, P., Rayalu, S., Yadav, R., Mistuhashi, T., & Haneda, H. (2012). Ceramics in environmental catalysis: applications and possibilities. *Chinese Journal of Catalysis*, 33(9-10), 1611-1621.

- Lastoskie, C., Gubbins, K. E., & Quirke, N. (1993). Pore size distribution analysis of microporous carbons: a density functional theory approach. *The Journal of Physical Chemistry*, 97(18), 4786-4796.
- Lee, C. J., Park, J., Huh, Y., & Yong Lee, J. (2001). Temperature effect on the growth of carbon nanotubes using thermal chemical vapor deposition. *Chemical Physics Letters*, 343(1–2), 33-38.
- Lee, C. J., Park, J., & Yu, J. A. (2002). Catalyst effect on carbon nanotubes synthesized by thermal chemical vapor deposition. *Chemical Physics Letters*, 360(3–4), 250-255.
- Lee, K.-Y., Yeoh, W.-M., Chai, S.-P., Ichikawa, S., & Mohamed, A. R. (2012). The role of water vapor in carbon nanotube formation via water-assisted chemical vapor deposition of methane. *Journal of Industrial and Engineering Chemistry*, 18(4), 1504-1511.
- Lee, M., Hong, S. C., & Kim, D. (2012). Formation of bamboo-like conducting carbon nanotubes decorated with Au nanoparticles by the thermal decomposition of sucrose in an AAO template. *Carbon*, 50(7), 2465-2471.
- Lee, M., Wang, B., Wu, Z., & Li, K. (2015). Formation of micro-channels in ceramic membranes – Spatial structure, simulation, and potential use in water treatment. *Journal of Membrane Science*, 483, 1-14.
- Lee, T. Y., Han, J.-H., Choi, S. H., Yoo, J.-B., Park, C.-Y., Jung, T., Yu, S., Yi, W. K., Han, I. T. & Kim, J. M. (2003). Effects of source gases on the growth of carbon nanotubes. *Diam Relat Mater*, 12(3–7), 851-855.

- Lee, T. Y., Han, J.-H., Choi, S. H., Yoo, J.-B., Park, C.-Y., Jung, T., Yu, S., Lee, J., Yi, W. & Kim, J. M. (2003). Comparison of source gases and catalyst metals for growth of carbon nanotube. *Surface and Coatings Technology*, 169–170, 348-352.
- Li, Q., Yan, H., Zhang, J., & Liu, Z. (2004). Effect of hydrocarbons precursors on the formation of carbon nanotubes in chemical vapor deposition. *Carbon*, 42(4), 829-835.
- Li, W. Z., Wen, J. G., & Ren, Z. F. (2002). Effect of temperature on growth and structure of carbon nanotubes by chemical vapor deposition. *Applied Physics A*, 74(3), 397-402.
- Li, W. Z., Xie, S. S., Qian, L. X., Chang, B. H., Zou, B. S., Zhou, W. Y., Wang, G., Li, W. Z. Xie, S. S., Chang, B. H., Zhou, W. Y., Zhao, R. A. & Wang, G. (1996). Large-scale synthesis of aligned carbon nanotubes. *Science*, 274(5293), 1701-1703.
- Li, Y., Kim, W., Zhang, Y., Rolandi, M., Wang, D., & Dai, H. (2001). Growth of single-walled carbon nanotubes from discrete catalytic nanoparticles of various sizes. *The Journal of Physical Chemistry B*, 105(46), 11424-11431.
- Liu, H., Zhang, Y., Li, R., Sun, X., Wang, F., Ding, Z., Merel, P. & Desilets, S. (2010). Aligned synthesis of multi-walled carbon nanotubes with high purity by aerosol assisted chemical vapor deposition: Effect of water vapor. *Applied Surface Science*, 256(14), 4692-4696.
- Liu, J., Jiang, Z. W., Yu, H. O., & Tang, T. (2011). Catalytic pyrolysis of polypropylene to synthesize carbon nanotubes and hydrogen through a two-stage process. *Polymer Degradation and Stability*, 96(10), 1711-1719.

- Liu, Q., & Fang, Y. (2006). New technique of synthesizing single-walled carbon nanotubes from ethanol using fluidized-bed over Fe–Mo/MgO catalyst. *Spectrochimica Acta Part A: Molecular and Biomolecular Spectroscopy*, 64(2), 296-300.
- Liu, W. W., Aziz, A., Chai, S. P., Mohamed, A. R., & Hashim, U. (2013a). Synthesis of single-walled carbon nanotubes: effects of active metals, catalyst supports, and metal loading percentage. *Journal of Nanomaterials*, 8, 1-8
- Liu, W. X., Chin, T. J., Carneiro, G., & Suter, D. (2013b). Point correspondence validation under unknown radial distortion. *Digital Image Computing: Techniques and Applications*, 10(5), 1-8.
- Liu, W. Y., & Jiang, J. L. (2013c). A new Chinese character recognition approach based on the fuzzy clustering analysis. *Neural Computing and Applications*, 25(2), 421-428.
- Liu, X., Sun, H., Wu, C., Patel, D., & Huang, J. (2017). Thermal chemical conversion of high-density polyethylene for the production of valuable carbon nanotubes using Ni/AAO membrane catalyst. *Energy Fuel*. 32, 4511-4520
- Liu, X., Zhang, Y., Nahil, M. A., Williams, P. T., & Wu, C. (2017). Development of Ni- and Fe- based catalysts with different metal particle sizes for the production of carbon nanotubes and hydrogen from thermo-chemical conversion of waste plastics. *Journal of Analytical and Applied Pyrolysis*. 125, 32-39.
- Liu, Y., Qian, W. Z., Zhang, Q., Ning, G. Q., Luo, G. H., Wang, Wei, F. (2009). Synthesis of high-quality, double-walled carbon nanotubes in a fluidized bed reactor. *Chemical Engineering & Technology*, 32(1), 73-79.

- Lolli, G., Zhang, L., Balzano, L., Sakulchaicharoen, N., Tan, Y., & Resasco, D. E. (2006). Tailoring (n,m) Structure of single-walled carbon nanotubes by modifying reaction conditions and the nature of the support of CoMo catalysts. *The Journal of Physical Chemistry B*, 110(5), 2108-2115.
- Marcilla, A., Beltrán, M. I., & Navarro, R. (2009). Thermal and catalytic pyrolysis of polyethylene over HZSM5 and HUSY zeolites in a batch reactor under dynamic conditions. *Applied Catalysis B: Environmental*, 86(1), 78-86.
- Research and Market (2017). Global carbon nanotubes market & patent insight 2023. Research and Market, Available online:
<https://www.researchandmarkets.com/reports/4380017/global-carbon-nanotubes-market-and-patent-insight> [Accessed August 2017]
- Maruyama, S. (2004). CVD Generation of Single-Walled Carbon Nanotubes from Alcohol. *Hyomen Kagaku*, 25(6), 318-325.
- Mauron, P., Emmenegger, C., Sudan, P., Wenger, P., Rentsch, S., & Züttel, A. (2003). Fluidised-bed CVD synthesis of carbon nanotubes on Fe₂O₃/MgO. *Diam Relat Mater*, 12(3), 780-785.
- Mehrnia, M. R., Mojtahedi, Y. M., & Homayoonfal, M. (2015). What is the concentration threshold of nanoparticles within the membrane structure? A case study of Al₂O₃/PSf nanocomposite membrane. *Desalination*, 372(Supplement C), 75-88.
- Melo, F., & Morlanés, N. (2005). Naphtha steam reforming for hydrogen production. *Catalysis Today*, 107–108, 458-466.

- Menon, M., Andriotis, A. N., & Froudakis, G. E. (2000). Curvature dependence of the metal catalyst atom interaction with carbon nanotubes walls. *Chemical Physics Letters*, 320(5), 425-434.
- Mhlanga, S. D., Mondal, K. C., Carter, R., Witcomb, M. J., & Coville, N. J. (2009). The effect of synthesis parameters on the catalytic synthesis of multiwalled carbon nanotubes using Fe-Co/CaCO₃ catalysts. *South African Journal of Chemistry*, 62, 67-76.
- Mijangos, C., Hernández, R., & Martín, J. (2016). A review on the progress of polymer nanostructures with modulated morphologies and properties, using nanoporous AAO templates. *Progress in Polymer Science*, 54–55, 148-182.
- Mishra, N., Das, G., Ansaldo, A., Genovese, A., Malerba, M., Povia & Sharon, M. (2012). Pyrolysis of waste polypropylene for the synthesis of carbon nanotubes. *Journal of Analytical and Applied Pyrolysis*, 94, 91-98.
- Mittal, G., Dhand, V., Rhee, K. Y., Park, S.-J., & Lee, W. R. (2015). A review on carbon nanotubes and graphene as fillers in reinforced polymer nanocomposites. *Journal of Industrial and Engineering Chemistry*, 21, 11-25.
- Morançais, A., Caussat, B., Kihn, Y., Kalck, P., Plee, D., Gaillard & Serp, P. (2007). A parametric study of the large scale production of multi-walled carbon nanotubes by fluidized bed catalytic chemical vapor deposition. *Carbon*, 45(3), 624-635.
- Muataz, A.A., Ahmadun, F., Guan, C., Mahdi, E., & Rinaldi, A. (2006). Effect of reaction temperature on the production of carbon nanotubes. *Nano*, 01(03), 251-257.

- Mubarak, N. M., Abdullah, E. C., Jayakumar, N. S., & Sahu, J. N. (2014). An overview on methods for the production of carbon nanotubes. *Journal of Industrial and Engineering Chemistry*, 20(4), 1186-1197.
- Muñoz, V., & Martinez, A. G. T. (2012). Thermal evolution of Al₂O₃-MgO-C refractories. *Procedia Materials Science*, 1, 410-417.
- Mwanza, B. G., & Mbohwa, C. (2017). Drivers to sustainable plastic solid waste recycling: a review. *Procedia Manufacturing*, 8, 649-656.
- Nahil, M. A., Wu, C., & Williams, P. T. (2015). Influence of metal addition to Ni-based catalysts for the co-production of carbon nanotubes and hydrogen from the thermal processing of waste polypropylene. *Fuel Processing Technology*, 130, 46-53.
- Namioka, T., Saito, A., Inoue, Y., Park, Y., Min, T. J., Roh, S. A., & Yoshikawa, K. (2011). Hydrogen-rich gas production from waste plastics by pyrolysis and low-temperature steam reforming over a ruthenium catalyst. *Applied Energy*, 88(6), 2019-2026.
- Niu, J. J., Wang, J. N., Jiang, Y., Su, L. F., & Ma, J. (2007). An approach to carbon nanotubes with high surface area and large pore volume. *Microporous and Mesoporous Materials*, 100(1-3), 1-5.
- Park, Y., Namioka, T., Sakamoto, S., Min, T.-J., Roh, S.-a., & Yoshikawa, K. (2010). Optimum operating conditions for a two-stage gasification process fueled by polypropylene by means of continuous reactor over ruthenium catalyst. *Fuel Processing Technology*, 91(8), 951-957.

- Pérez-Mayoral, E., Calvino-Casilda, V., & Soriano, E. (2016). Metal-supported carbon-based materials: opportunities and challenges in the synthesis of valuable products. *Catalysis Science & Technology*, 6(5), 1265-1291.
- Huu, C., Keller, N., Roddatis, V. V., Mestl, G., Schlögl, R., & Ledoux, M. J. (2002). Large scale synthesis of carbon nanofibers by catalytic decomposition of ethane on nickel nanoclusters decorating carbon nanotubes. *Physical Chemistry Chemical Physics*, 4(3), 514-521.
- Plastic Europe (2016). *Plastics - the Fact 2016 An analysis of European plastics production*, Plastic Europe.
- Plastic Europe (2017). *Plastics - the Fact 2017 An analysis of European plastics production*, Plastic Europe.
- Philippe, R., Caussat, B., Falqui, A., Kihn, Y., Kalck, P., Bordère, S., Plee, D., Gaillard, P., Bernard, D. & Serp, P. (2009). An original growth mode of MWCNTs on alumina supported iron catalysts. *Journal of Catalysis*, 263(2), 345-358.
- Pillai, S. K., Ray, S. S., & Moodley, M. (2008). Purification of multi-walled carbon nanotubes. *J Nanosci Nanotechnol*, 8(12), 6187-6207.
- Popovska, N., Danova, K., Jipa, I., & Zenneck, U. (2011). Catalytic growth of carbon nanotubes on zeolite supported iron, ruthenium and iron/ruthenium nanoparticles by chemical vapor deposition in a fluidized bed reactor. *Powder Technology*, 207(1), 17-25.
- Quan, C., Gao, N., & Wu, C. Utilization of NiO/porous ceramic monolithic catalyst for upgrading biomass fuel gas. *Journal of the Energy Institute*. 91(3), 331-338.

- Baker, R. J. W. (1975). Formation of carbonaceous deposits from the platinum-iron catalyzed decomposition of acetylene. *Journal of Catalysis*, 37(1), 101-105.
- Ragaert, K., Delva, L., & Van Geem, K. (2017). Mechanical and chemical recycling of solid plastic waste. *Waste Management*, 69, 24-58.
- Ray, Y.-C., Jiang, T.-S., & Wen, C. Y. (1987). Particle attrition phenomena in a fluidized bed. *Powder Technology*, 49(3), 193-206.
- Ren, Z. F., Huang, Z. P., Xu, J. W., Wang, J. H., Bush, P., Siegal, M. P., & Provencio, P. N. (1998). Synthesis of large arrays of well-aligned carbon nanotubes on glass. *Science*, 282(5391), 1105-1107.
- Richardson, J. T., & Crump, J. G. (1979). Crystallite size distributions of sintered nickel catalysts. *Journal of Catalysis*, 57(3), 417-425.
- Rul, S., Lefèvre-schlick, F., Capria, E., Laurent, C., & Peigney, A. (2004). Percolation of single-walled carbon nanotubes in ceramic matrix nanocomposites. *Acta Materialia*, 52(4), 1061-1067.
- Saad, J. M., Nahil, M. A., & Williams, P. T. (2015). Influence of process conditions on syngas production from the thermal processing of waste high density polyethylene. *Journal of Analytical and Applied Pyrolysis*, 113, 35-40.
- Sadat, M., & Bakhshandeh, G.-R. (2011). Recycling of PVC wastes. *Polymer Degradation and Stability*, 96(4), 404-415.
- Saito, Y., Nishikubo, K., Kawabata, K., & Matsumoto, T. (1996). Carbon nanocapsules and single-layered nanotubes produced with platinum-group metals (Ru, Rh, Pd, Os, Ir, Pt) by arc discharge. *Journal of Applied Physics*, 80(5), 3062-3067.

- Savva, P. G., Polychronopoulou, K., Ryzkov, V. A., & Efstathiou, A. M. (2010). Low-temperature catalytic decomposition of ethylene into H₂ and secondary carbon nanotubes over Ni/CNTs. *Applied Catalysis B: Environmental*, 93(3), 314-324.
- Schäffel, F., Rummeli, M. H., Kramberger, C., Queitsch, U., Mohn, E., Kaltofen, R., Pichler, T., Buchner, B., Rellinghaus, B. & Schultz, L. (2008). Tailoring the diameter, density and number of walls of carbon nanotubes through predefined catalyst particles. *Physica Status Solidi (a)*, 205(6), 1382-1385.
- Schnorr, J. M., & Swager, T. M. (2011). Emerging applications of carbon nanotubes. *Chemistry of Materials*, 23(3), 646-657.
- Scott, D. S., Czernik, S. R., Piskorz, J., & Radlein, D. S. A. G. (1990). Fast pyrolysis of plastic wastes. *Energy & Fuels*, 4(4), 407-411.
- Seah, M.P. (2012). Topography effects and monatomic ion sputtering of undulating surfaces, particles and large nanoparticles: sputtering yields, effective sputter rates and topography evolution. *Surface and Interface Analysis*, 44, 208-218
- See, C. H., Dunens, O. M., MacKenzie, K. J., & Harris, A. T. (2008). Process parameter interaction effects during carbon nanotube synthesis in fluidized beds. *Industrial & Engineering Chemistry Research*, 47(20), 3769-3776
- Serp, P., Corrias, M., & Kalck, P. (2003). Carbon nanotubes and nanofibers in catalysis. *Applied Catalysis A: General*, 253(2), 337-358.
- Setareh Monshi, T., Fakhru'l-Razi, A., Luqman Chuah, A., & Suraya, A. R. (2011). Optimization of synthesis condition for carbon nanotubes by catalytic chemical vapor deposition (CCVD). *IOP Conference Series: Materials Science and Engineering*, 17(1), 012003-012007.

- Shah, K. A., & Tali, B. A. (2016). Synthesis of carbon nanotubes by catalytic chemical vapour deposition: A review on carbon sources, catalysts and substrates. *Materials Science in Semiconductor Processing*, 41, 67-82.
- Sharma, B. K., Moser, B. R., Vermillion, K. E., Doll, K. M., & Rajagopalan, N. (2014). Production, characterization and fuel properties of alternative diesel fuel from pyrolysis of waste plastic grocery bags. *Fuel Processing Technology*, 122, 79-90.
- Shi, Z., Lian, Y., Liao, F. H., Zhou, X., Gu, Z., Zhang, Y., Lijima, S., Li, H., Yue, K. T. & Zhang, S.-L. (2000). Large scale synthesis of single-wall carbon nanotubes by arc-discharge method. *Journal of Physics and Chemistry of Solids*, 61(7), 1031-1036.
- Singh, N., Hui, D., Singh, R., Ahuja, I. P. S., Feo, L., & Fraternali, F. (2017). Recycling of plastic solid waste: a state of art review and future applications. *Composites Part B: Engineering*, 115, 409-422.
- Sinnott, S. B., Andrews, R., Qian, D., Rao, A. M., Mao, Z., Dickey, E. C., & Derbyshire, F. (1999). Model of carbon nanotube growth through chemical vapor deposition. *Chemical Physics Letters*, 315(1-2), 25-30.
- Sodero, S. F., Berruti, F. & Behie, L. A. (1996), Ultrapyrolytic cracking of polyethylene - a high yield recycling method, 51(11), 2805-2810.
- Sohn, J. I., Lee, S., Song, Y., Choi, S., Cho, K. & Nam, K. (2001) Patterned selective growth of carbon nanotubes and large field emission from vertically well-aligned carbon nanotube field emitter arrays. *Applied Physics Letters*, 78(7), 901-903.

- Stobinski, L., Lesiak, B., Kövér, L., Tóth, J., Biniak, S., Trykowski, G., & Judek, J. (2010). Multiwall carbon nanotubes purification and oxidation by nitric acid studied by the FTIR and electron spectroscopy methods. *Journal of Alloys and Compounds*, 501(1), 77-84.
- Stokes, D. (2008) Principles and practice of variable pressure/environmental scanning electron microscopy. John Wiley & Sons Ltd.
- Stoner, B. R., Brown, B., & Glass, J. T. (2014). Selected topics on the synthesis, properties and applications of multiwalled carbon nanotubes. *Diam Relat Mater*, 42, 49-57.
- Sui, Y. C., Cui, B. Z., Guardián, R., Acosta, D. R., Martínez, L., & Perez, R. (2002). Growth of carbon nanotubes and nanofibres in porous anodic alumina film. *Carbon*, 40(7), 1011-1016.
- Takenaka, S., Serizawa, M., & Otsuka, K. (2004). Formation of filamentous carbons over supported Fe catalysts through methane decomposition. *Journal of Catalysis*, 222(2), 520-531.
- Tapsuan, K. & Niyomwas, S. (2012). Effect of preform conditions on synthesis of Fe₃Al-TiB₂-Al₂O₃ composite by self-propagating high-temperature synthesis. *Procedia Engineering*, 32(Supplement C), 635-641.
- Thess, A., Lee, R., Nikolaev, P., Dai, H., Petit, P., Robert, J., Xu, C., Lee, Y. H., Kim, S. G., Rinzler, A. G., Colbert, D. T., Scuseria, G. E., Tomanek, D., Fischer, J. E. & Smalley, R. E. (1996). Crystalline Ropes of Metallic Carbon Nanotubes. *Science*, 273(5274), 483-487.

- Thostenson, E. T., Ren, Z., & Chou, T.-W. (2001). Advances in the science and technology of carbon nanotubes and their composites: a review. *Composites Science and Technology*, 61(13), 1899-1912.
- Trimm, D. L. (1997). Coke formation and minimisation during steam reforming reactions. *Catalysis Today*, 37(3), 233-238.
- Vahlas, C., Caussat, B., Serp, P., & Angelopoulos, G. N. (2006). Principles and applications of CVD powder technology. *Materials Science and Engineering: R: Reports*, 53(1), 1-72.
- Venegoni, D., Serp, P., Feurer, R., Kihn, Y., Vahlas, C., & Kalck, P. (2002). Parametric study for the growth of carbon nanotubes by catalytic chemical vapor deposition in a fluidized bed reactor. *Carbon*, 40(10), 1799-1807.
- Watch (2003). *Plastics in the UK economy - a guide to polymer use and the opportunities for recycling*. Wisconsin.
- Wei, H., Wang, E. (2008) FeO₃O₄ magnetic nanoparticles as peroxidase mimetics and their applications in H₂O₂ and glucose detection. *Analytical Chemistry*, 80(6), 2250-2254.
- Wepasnick, K. A., Smith, B. A., Bitter, J. L., & Howard Fairbrother, D. (2010). Chemical and structural characterization of carbon nanotube surfaces. *Analytical and Bioanalytical Chemistry*, 396(3), 1003-1014.

Willems, I., Kónya, Z., Colomer, J. F., Van Tendeloo, G., Nagaraju, N., Fonseca, A., & Nagy, J. B. (2000). Control of the outer diameter of thin carbon nanotubes synthesized by catalytic decomposition of hydrocarbons. *Chemical Physics Letters*, 317(1), 71-76.

Global carbon nanotubes market report 2017 - by type, application, method, end-use & region - research and markets (2017). Available online:

<https://www.businesswire.com/news/home/20171005005553/en/Global-Carbon-Nanotubes-Market-Report-2017--> [Accessed date 05/10/2017]

Wu, C., Dong, L., Onwudili, J., Williams, P. T., & Huang, J. (2013). Effect of Ni Particle Location within the Mesoporous MCM-41 Support for Hydrogen Production from the Catalytic Gasification of Biomass. *ACS Sustainable Chemistry & Engineering*, 1(9), 1083-1091.

Wu, C., Nahil, M. A., Norbert, M., Huang, J., & Williams, P. T. Production and application of carbon nanotubes, as a co-product of hydrogen from the pyrolysis-catalytic reforming of waste plastic. *Process Safety and Environmental Protection*. 103(A), 107-114

Wu, C., Wang, L., Williams, P. T., Shi, J., & Huang, J. (2011). Hydrogen production from biomass gasification with Ni/MCM-41 catalysts: Influence of Ni content. *Applied Catalysis B: Environmental*, 108–109, 6-13.

Wu, C., & Williams, P. T. (2009a). Hydrogen production by steam gasification of polypropylene with various nickel catalysts. *Applied Catalysis B: Environmental*, 87(3–4), 152-161.

- Wu, C., & Williams, P. T. (2009b). Hydrogen production from the pyrolysis–gasification of polypropylene: influence of steam flow rate, carrier gas flow rate and gasification temperature. *Energy & Fuels*, 23(10), 5055-5061.
- Wu, C., & Williams, P. T. (2009c). Investigation of Ni-Al, Ni-Mg-Al and Ni-Cu-Al catalyst for hydrogen production from pyrolysis–gasification of polypropylene. *Applied Catalysis B: Environmental*, 90(1–2), 147-156.
- Wu, C., & Williams, P. T. (2009d). Ni/CeO₂/ZSM-5 catalysts for the production of hydrogen from the pyrolysis–gasification of polypropylene. *International Journal of Hydrogen Energy*, 34(15), 6242-6252.
- Wu, C., & Williams, P. T. (2010a). Investigation of coke formation on Ni-Mg-Al catalyst for hydrogen production from the catalytic steam pyrolysis-gasification of polypropylene. *Applied Catalysis B: Environmental*, 96(1–2), 198-207.
- Wu, C., & Williams, P. T. (2010b). Pyrolysis–gasification of post-consumer municipal solid plastic waste for hydrogen production. *International Journal of Hydrogen Energy*, 35(3), 949-957.
- Xiao, L., Cao, Y., Xiao, J., Schwenzer, B., Engelhard, M. H., Saraf, L. V., Nie, Z., Exarhos, G. & Liu, J. (2012). A soft approach to encapsulate sulfur: polyaniline nanotubes for lithium-sulfur batteries with long cycle life. *Advanced Materials*, 24(9), 1176-1181.
- Yamada, T., Maigne, A., Yudasaka, M., Mizuno, K., Futaba, D. N., Yumura, M., Lijima, S. & Hata, K. (2008). Revealing the secret of water-assisted carbon nanotube synthesis by microscopic observation of the interaction of water on the catalysts. *Nano Letters*, 8(12), 4288-4292.

- Yao, D., Wu, C., Yang, H., Zhang, Y., Nahil, M. A., Chen, Y., Williams, P. T. & Chen, H. (2017). Co-production of hydrogen and carbon nanotubes from catalytic pyrolysis of waste plastics on Ni-Fe bimetallic catalyst. *Energy Conversion and Management*, 148(Supplement C), 692-700.
- Yao, D., Zhang, Y., Williams, P. T., Yang, H., & Chen, H. (2018). Co-production of hydrogen and carbon nanotubes from real-world waste plastics: Influence of catalyst composition and operational parameters. *Applied Catalysis B: Environmental*, 221, 584-597.
- Yellampalli, S. (2011) *Carbon nanotubes: synthesis, characterization, application*, Intech Open.
- Yen, Y.-W., Huang, M.-D., & Lin, F.-J. (2008). Synthesize carbon nanotubes by a novel method using chemical vapor deposition-fluidized bed reactor from solid-stated polymers. *Diam Relat Mater*, 17(4), 567-570.
- Zhang, J., Sun, B., McDonagh, A. M., Zhao, Y., Kretschmer, K., Guo, X., & Wang, G. (2017). A multi-functional gel co-polymer bridging liquid electrolyte and solid cathode nanoparticles: An efficient route to Li-O₂ batteries with improved performance. *Energy Storage Materials*, 7, 1-7.
- Zhang, Q., Huang, J.-Q., Qian, W.-Z., Zhang, Y.-Y., & Wei, F. (2013). The road for nanomaterials industry: a review of carbon nanotube production, post-treatment, and bulk applications for composites and energy storage. *Small*, 9(8), 1237-1265.

- Zhang, Y., & Iijima, S. (1999). Formation of single-wall carbon nanotubes by laser ablation of fullerenes at low temperature. *Applied Physics Letters*, 75(20), 3087-3089.
- Zhao, Q., Jiang, T., Li, C., & Yin, H. (2011). Synthesis of multi-wall carbon nanotubes by Ni-substituted (loading) MCM-41 mesoporous molecular sieve catalyzed pyrolysis of ethanol. *Journal of Industrial and Engineering Chemistry*, 17(2), 218-222.
- Zheng, L. X., O'Connell, M. J., Doorn, S. K., Liao, X. Z., Zhao, Y. H., Akhadov, E. A., Hoffbauer, M. A., Roop, B. J., Jia, Q. X., Dye, R. C., Peterson, D. E., Huang, S. M., Liu, J. & Zhu, Y. T. (2004). Ultralong single-wall carbon nanotubes. *Nature Materials*, 3, 673-676.
- Zhuo, C., & Levendis, Y. A. (2014). Upcycling waste plastics into carbon nanomaterials: a review. *Journal of Applied Polymer Science*, 131(4), 39931(1-14).
- Zuo, L. (2018). Carbon Nanotubes: the future of the planet's freshwater. *Materials Science. YS Journal*. Available online: <https://ysjournal.com/carbon-nanotubes-the-future-of-the-planets-freshwater/> [Accessed 11/01/2018]
- Zygmuntowicz, J., Wiecińska, P., Miazga, A., & Konopka, K. (2016). Characterization of composites containing NiAl₂O₄ spinel phase from Al₂O₃/NiO and Al₂O₃/Ni systems. *Journal of Thermal Analysis and Calorimetry*, 125(3), 1079-1086.

Appendices

Appendices A - Materials and equipment in the research

A1.Raw materials

Plastics waste PP pellet which was used for Ni/Fe-based catalysts and HDPE pellet which was used for AAO membrane, ceramic membrane and sphere support study were shown in Figure A-A1.

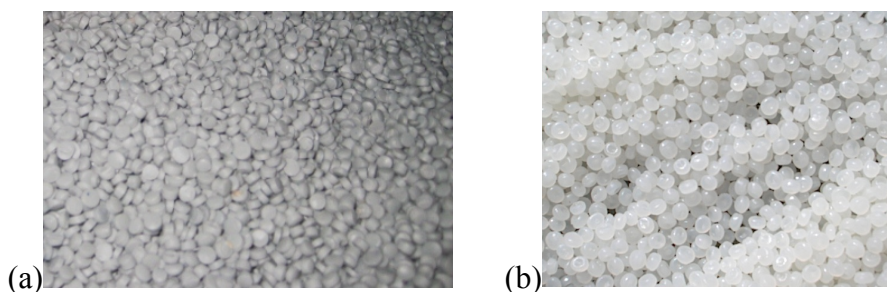


Figure A-A1 Waste plastics pellets (a) PP pellets (b)HDPE pellets

A2.Ni/Fe-based catalysts

The catalysts preparation calculation is shown in Table A-A1, and the molar mass references is in Table A-A2.

Table A-A1 Ni/Fe-based catalysts calculations

<i>Catalysts</i>	<i>Support SiO₂/g</i>	<i>Total catalyst/g</i>	<i>Ni(NO₃)₂·6H₂O/g</i>	<i>Fe(NO₃)₃·9H₂O</i>
10 wt.% Ni/SiO ₂	10	11.46	5.68	-
10 wt.% Fe/SiO ₂	10	14.005	-	0.194

Table A-A2 Molar mass reference

	<i>Ni(NO₃)₂·6H₂O</i>	<i>Fe(NO₃)₃·9H₂O</i>	<i>Ni</i>	<i>NiO</i>	<i>Fe</i>	<i>Fe₂O₃</i>
Molar mass g/molar	290.79	404	58.69	74.692	55.85	159.7

A3.AAO membrane supported catalysts

Blank AAO membrane and 1.0/AAO catalyst were shown in Figure A-A2. And catalysts calculation is in Table A-A3.

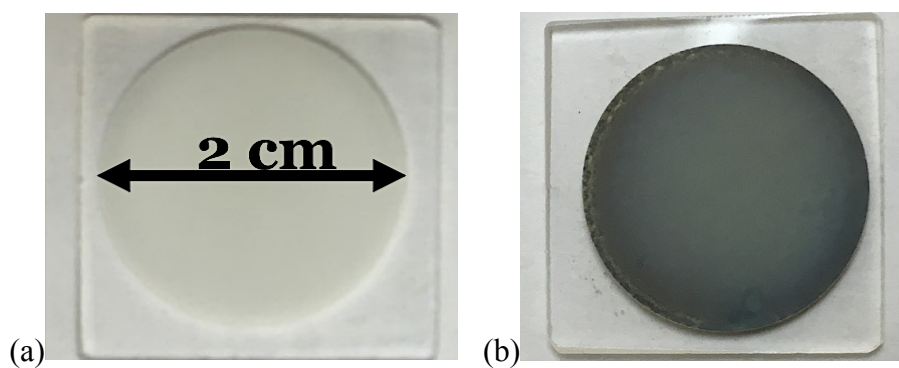


Figure A-A2 AAO membrane (a) blank membrane, (b) 1.0/AAO

Table A-A3 AAO membrane catalysts calculations

<i>Catalysts</i>	<i>AAO Support /g</i>	<i>Total catalyst/g</i>	<i>Ni(NO₃)₂·6H₂O/g</i>
0.1/AAO	1	1.001	0.005
0.5/AAO	1	1.006	0.025
1.0/AAO	1	1.013	0.050
2.0/AAO	1	1.026	0.102
10 wt.% Ni/Al ₂ O ₃	10	11.46	5.68

A4.Ceramic supported catalysts calculation

Table A-A4 Ni/ceramic catalysts calculations

<i>Catalysts</i>	<i>Ceramic Support /g</i>	<i>Total catalyst/g</i>	<i>Ni(NO₃)₂·6H₂O/g</i>
0.1/ceramic	5	5.006	0.025
0.5/ceramic	5	5.032	0.125
1.0/ceramic	5	5.064	0.251
2.0/ceramic	5	5.131	0.508

A5. Sphere supported catalysts calculation

Table A-A5 Ni/sphere catalysts calculations

<i>Catalysts</i>	<i>Sphere Support</i> <i>/g</i>	<i>Total catalyst/g</i>	<i>Ni(NO₃)₂·6H₂O/g</i>
0.1/sphere	10	10.013	0.050
1.0/sphere	10	10.129	0.502

A6. Equipment

The reactor and analysis equipment are displayed in this section.



Figure A-A3 Two-stage catalytic-pyrolysis reaction system



Figure A-A4 Scanning electron microscope (SEM) stereoscan 360



Figure A-A5 Transition electron microscope (TEM) JEOL 2010

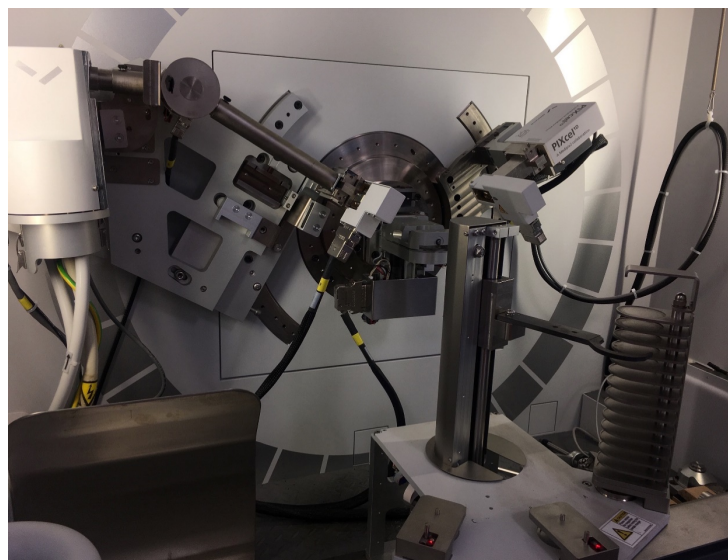


Figure A-A6 X-ray diffraction



Figure A-A7 Thermogravimetric analyser (TGA) STA-780 Series

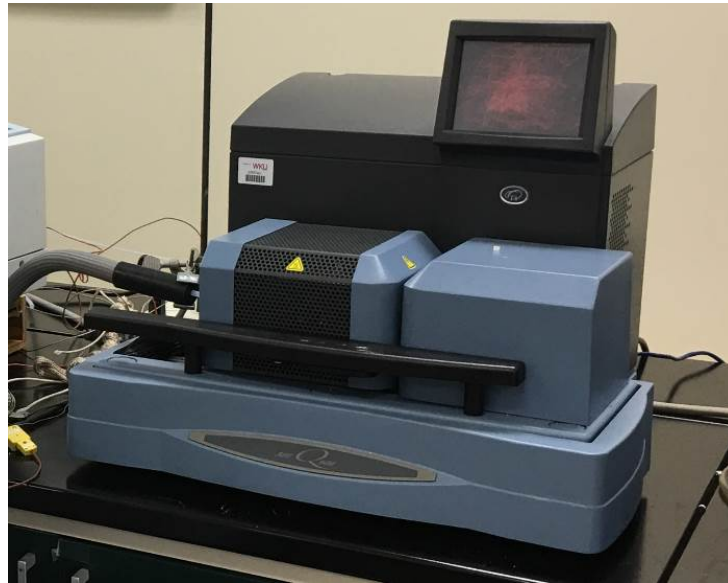


Figure A-A8 TA instruments, SDT-Q600



Figure A-A9 Broken AAO membrane during calcine process

Appendices B - Support materials for Ni/AAO catalysts study

Table A-B1 is the EDX results for Ni/AAO catalysts, Ni content wt.% shows increased trend as an increase of Ni loading from 0.1/AAO to 2.0/AAO.

Table A-B1 EDX results of Ni/AAO catalysts with different Ni contents

<i>Element content</i> <i>wt. %</i>	<i>0.1/AAO</i>	<i>0.5/AAO</i>	<i>1.0/AAO</i>	<i>2.0/AAO</i>
O	59.6	53.8	50.7	45.2
Al	37.0	42.6	33.1	26.6
Ni	2.4	3.6	26.6	28.2

Figure A-B1 shows the cross-section SEM image for the original AAO membrane without any nickel loading, highly ordered channels are displayed.

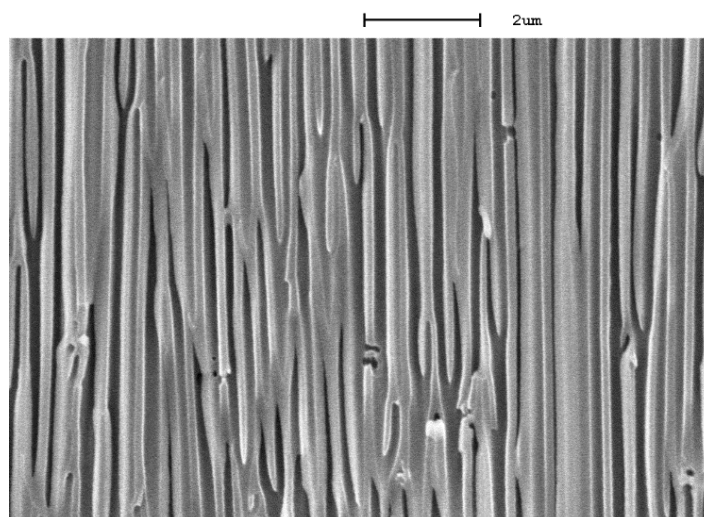


Figure A-B1 Cross-section SEM result for original AAO membrane without Ni loading

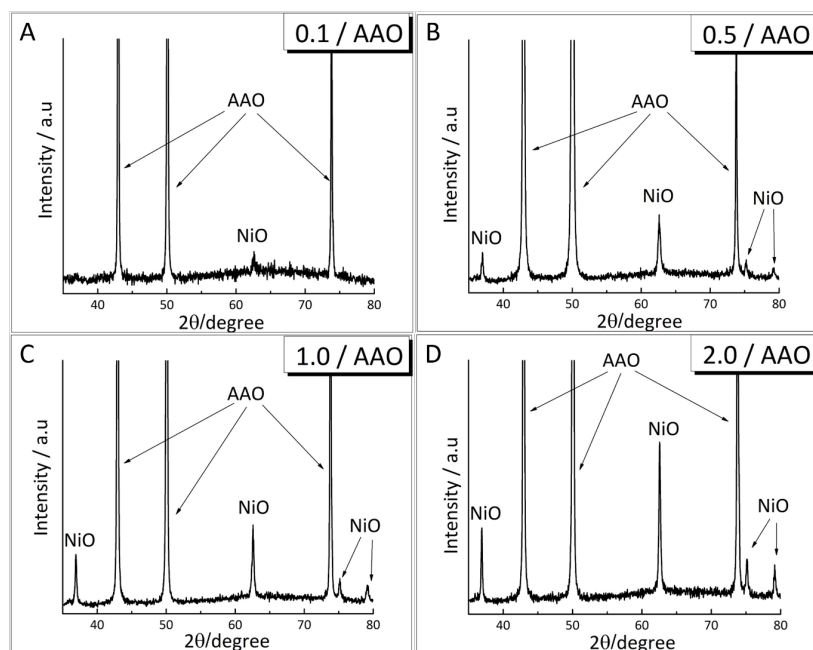


Figure A-B2 XRD results for Ni/AAO catalysts with different Ni content

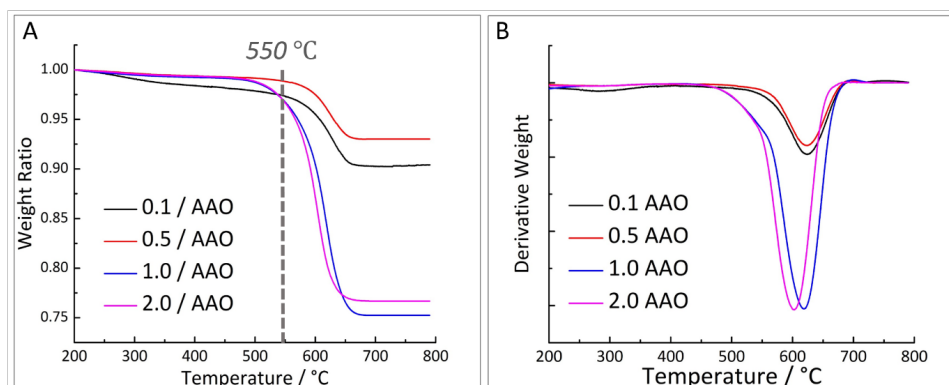


Figure A-B3 (A) TGA-TPO and (B) DTG-TPO results of the reacted Ni/AAO catalysts with different Ni content

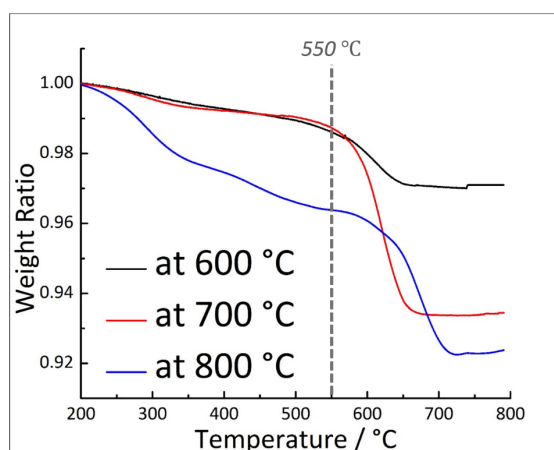


Figure A-B4 TGA-TPO results of the reacted 0.1/AAO catalyst tested at 600 °C, 700 °C and 800 °C

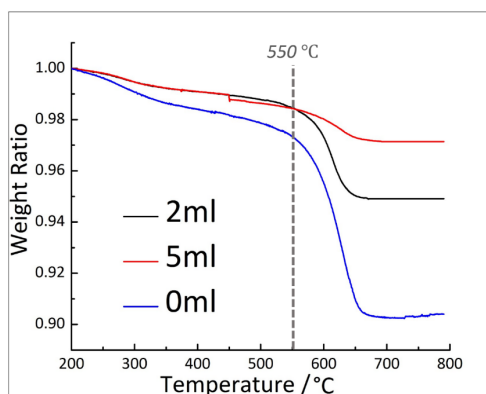


Figure A-B5 TGA-TPO results of the reacted 0.1/AAO catalyst tested with 0, 2 and 5 mL h⁻¹ steam injection

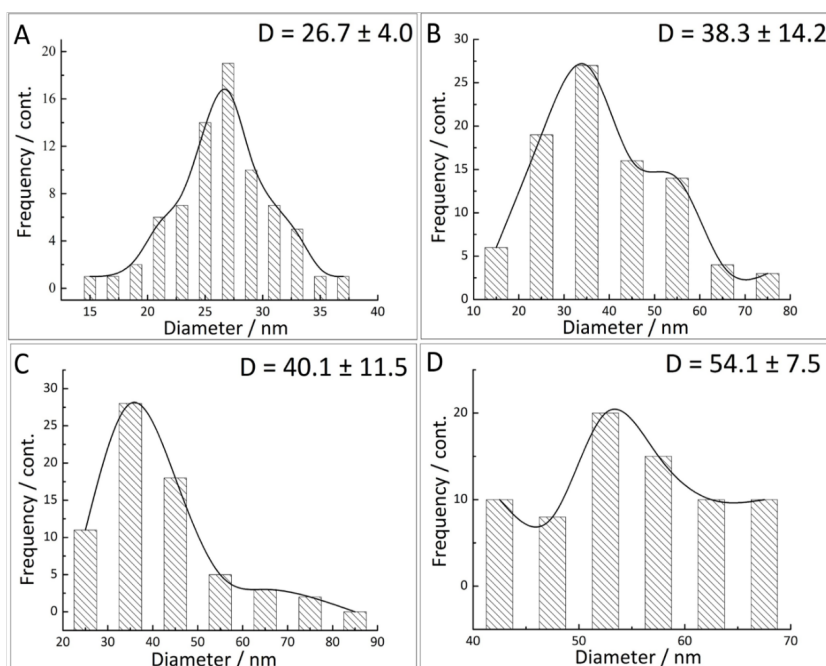


Figure A-B6 CNTs diameter distribution results of the reacted Ni/AAO catalysts with different Ni content (A) 0.1/AAO, (B) 0.5/AAO, (C) 1.0/AAO (D) 2.0/AAO

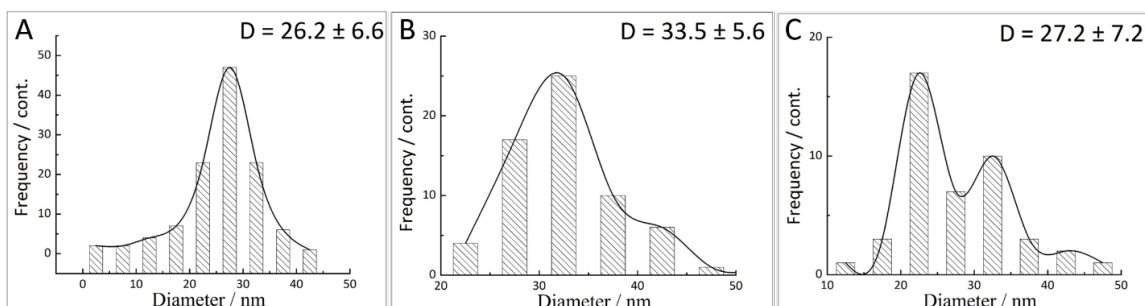


Figure A-B7 CNTs diameter distribution results of the reacted 0.1/AAO catalysts at different temperature (A) 600 °C, (B) 700 °C, (C) 800 °C

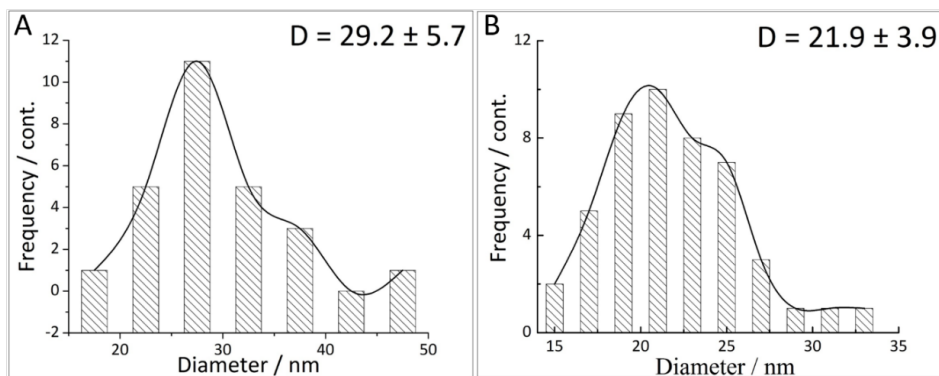


Figure A-B8 CNTs diameter distribution results of the reacted 0.1/AAO catalysts with different steam injection (A) 2mlh^{-1} (B) 5mlh^{-1}

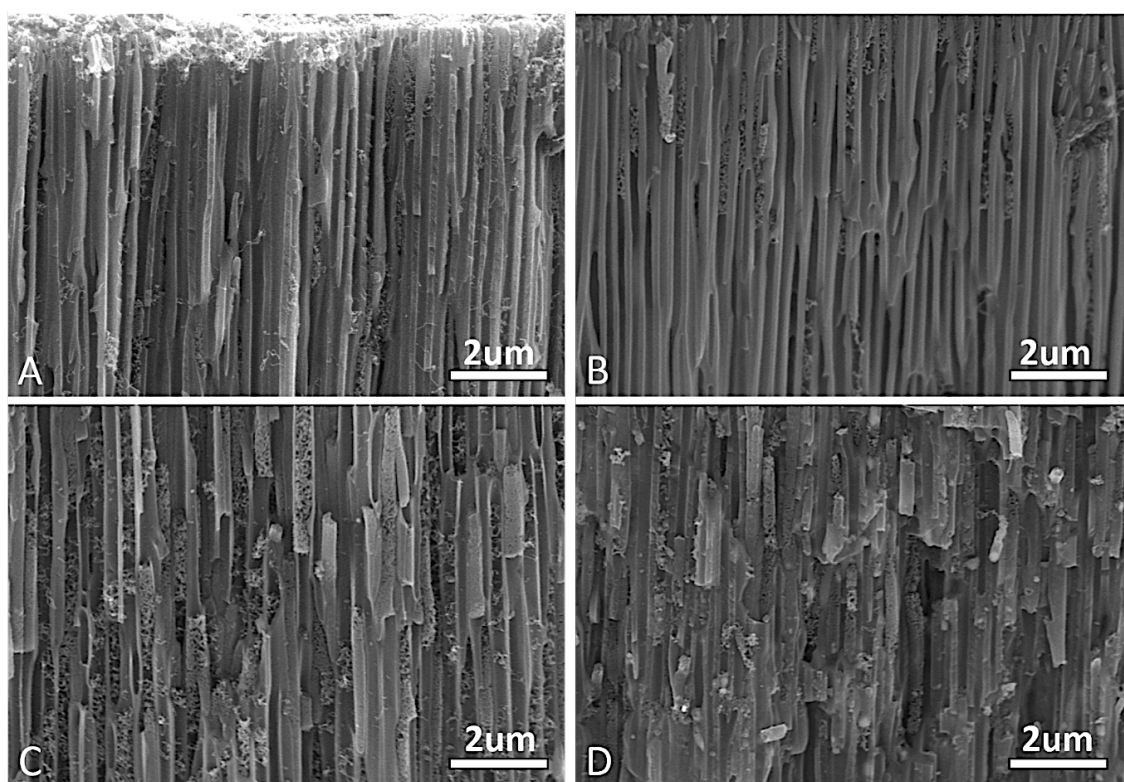


Figure A-B9 cross sectional SEM results of the reacted AAO catalyst with different Ni content. (A) 0.1/AAO; (B) 0.5/AAO; (C) 1.0/AAO and (D) 2.0/AAO catalyst

Appendices C - Support materials for Ni/ceramics catalysts study

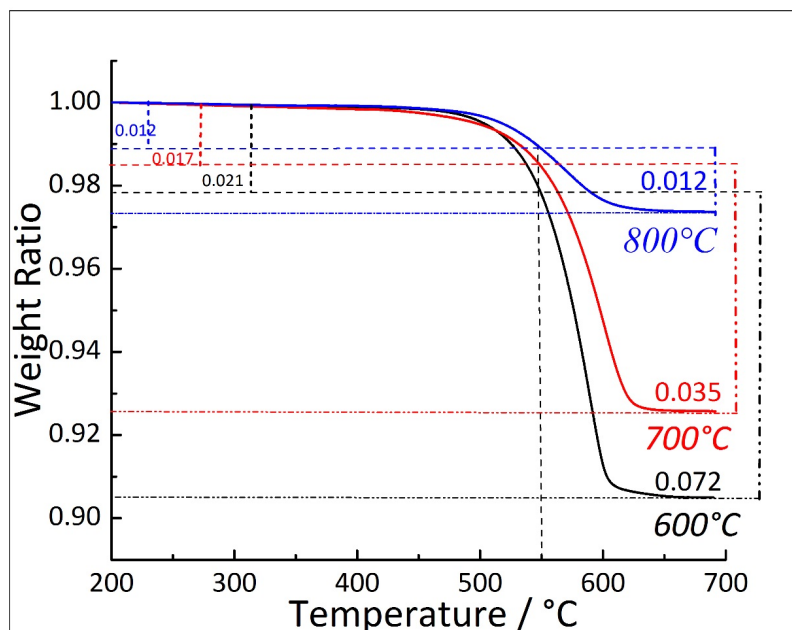


Figure A-C1 TGA-TPO results of the spent 0.5/ceramic at 600 °C, 700 °C, and 800 °C

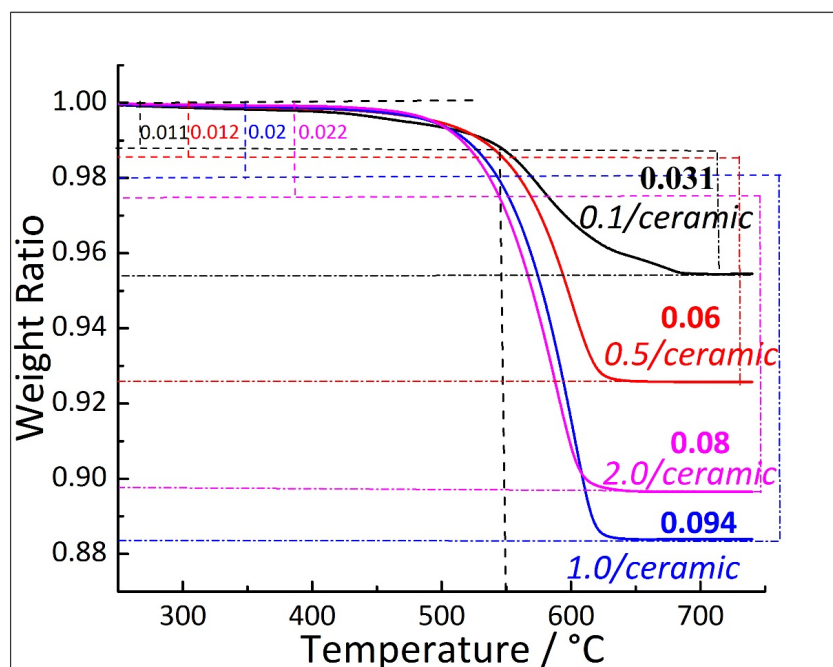


Figure A-C2 TGA-TPO results of the spent 0.1/ceramic, 0.5/ceramic, 1.0/ceramic and 2.0/ceramic catalysts at 700 °C

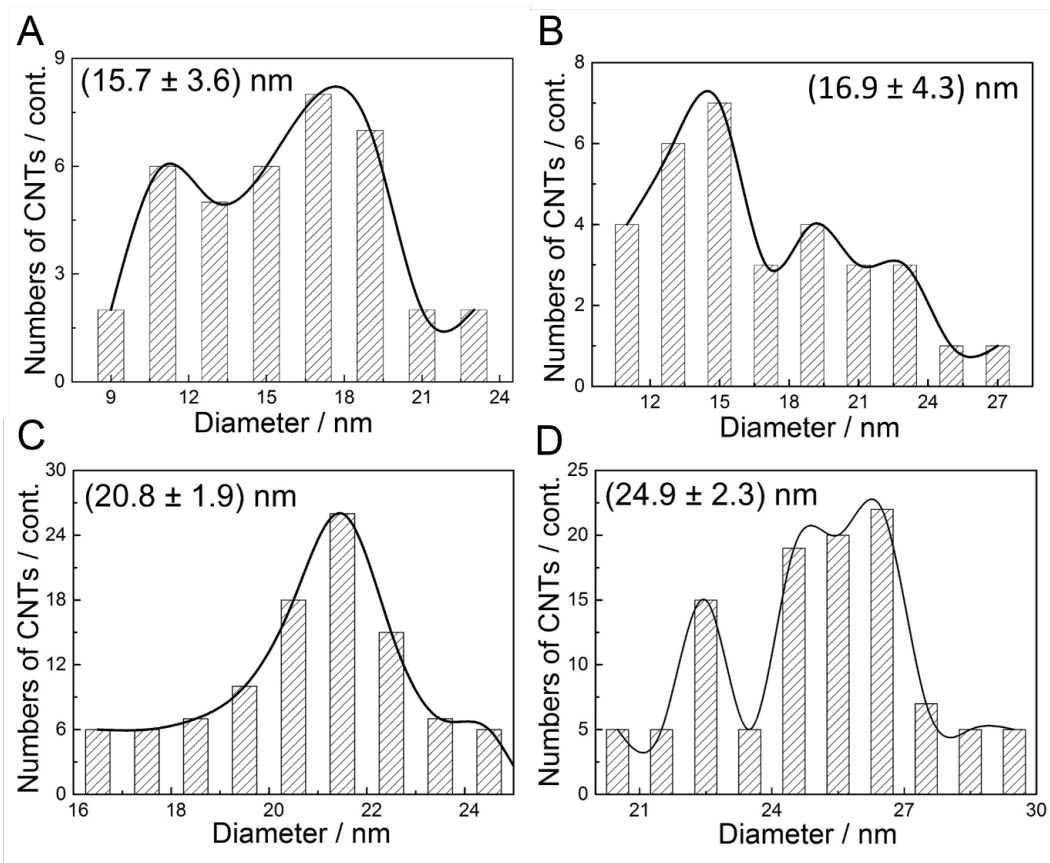


Figure A-C3 CNTs average diameter distribution for the spent 0.1/ceramic, 0.5/ceramic, 1.0/ceramic and 2.0/ceramic catalysts at 700 °C

Appendices D - Publications

Liu, X., Shen, B., Wu, Z., Parlett, C., Han, Z., George, A., Yuan, P., Patel, D. & Wu, C. (2018). Producing carbon nanotubes from thermochemical conversion of waste plastics using Ni/ceramic based catalyst, *Chemical Engineering Science*, 192, 882-891.

Liu, X., Shen, B., Yuan, P., Patel, D., & Wu, C. (2017). Production of carbon nanotubes (CNTs) from thermochemical conversion of waste plastics using Ni/anodic aluminium oxide (AAO) template catalyst, *Energy Procedia*, 142, 525-530.

Liu, X., Sun, H., Wu, C., Patel, D., and Huang, J. (2017). Thermal chemical conversion of high-density polyethylene for the production of valuable carbon nanotubes using Ni/AAO membrane catalyst, *Energy and Fuels*, 32 (4), 4511-4520.

Liu, X., Zhang, Y., Nahil, M. A., Williams, P. T., & Wu, C. (2017). Development of Ni- and Fe- based catalysts with different metal particle sizes for the production of carbon nanotubes and hydrogen from thermos-chemical conversion of waste plastics, *Journal of Analytical and Applied Pyrolysis*, 125, 32-39.

Borsodi, N., Szentes, A., Miskolczi, N., Wu, C., & **Liu, X.** (2016). Carbon nanotubes synthesized from gaseous productions of waste polymer pyrolysis and their application, *Journal of Analytical and Applied Pyrolysis*, 120, 304-313.

Parlett, C., Aydin, A., Durndell, L., Frattini, L., Isaacs, M., Lee, L., **Liu, X.**, Olivi, L., Trofimovaite, R., Wilson, K., & Wu, C. (2017). Tailored mesoporous silica supports for Ni catalyzed hydrogen production from ethanol steam reforming, *Catalysis Communications*, 91, 76-79.

Sun, H., Parlett, C., Isaacs, M., **Liu, X.**, Adwek, G., Wang, J., Shen, B., Huang, J. & Wu, C. (2018). Development of Ca/KIT-6 adsorbents for high temperature CO₂ capture, Fuel, 235, 1070-1076.

Appendices E - Conferences and training attendance

E1. Conference

Table A-E1 Conferences attended during PhD

<i>Conference</i>	<i>Date</i>	<i>Location</i>	<i>Work present</i>	<i>Award</i>
H2FC Supergen	14 th -16 th Dec 2015	University of Bath	Poster (<u>Figure A-E1</u>)	-
All Energy	4 th – 6 th May 2016	Glasgow	-	-
Pyro 2016	9 th – 12 th May 2016	Nancy, France	Poster (<u>Figure A-E1</u>)	-
The 24 th Annual SC- CSCST Conference	23 rd -24 th June 2017	Newcastle	Oral presentation (<u>Figure A-E2</u>)	Joint 3 rd prize oral presentation
ICAE 9 th International Conference on Applied Energy	21 st -24 th August 2017	Cardiff	(1) Oral presentation (2) Paper publication (<u>Chapter 5</u>)	-
Pyro 2018	4 th -10 th June 2018	Kyoto, Japan	Poster (<u>Figure A-E3 and E4</u>)	Young scientist award

Production of Hydrogen and Carbon Nanomaterials from Plastics Waste Using Ni- and Fe-based Catalysts

INTRODUCTION

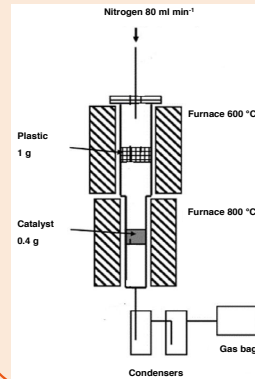
Around 38 wt.% of waste plastics ended up as landfill in 2012 in the EU, causing big environmental problems and wasting large amounts of energy stored inside the waste plastics. In this work, we focus on converting plastic waste into high value carbon nanomaterials (CNMs). Ni/SiO₂ and Fe/SiO₂ catalysts with controlled metal particle sizes will be reported about their performances related to the productions of CNMs and H₂-rich syngas from catalytic gasification of waste polypropylene, using a two-stage fixed-bed reaction system.



AIM

To study the influences of the types of metals and the crystal size of metal particles on the yield of hydrogen and the quality of CNMs

EXPERIMENT



Catalysts – Fe/SiO₂ ; Ni/SiO₂

L- large particles

S- small particles

Reaction time – 50 mins

Analysis – GC

XRD

SEM

TPO

BET

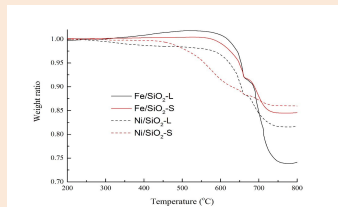
RESULTS

Product Yield

	Fe/SiO ₂ -S	Fe/SiO ₂ -L	Ni/SiO ₂ -S	Ni/SiO ₂ -L
Gas yield (wt.%)	49.23	63.90	51.20	52.50
Carbon production	26.00	29.00	16.00	16.00
H ₂ production (mmol g ⁻¹)	15.40	25.60	18.10	22.60
Gas concentrations (Vol.%)				
CO	5.32	7.80	3.30	6.32
H ₂	41.72	50.30	42.20	47.74
CH ₄	39.16	22.70	43.50	39.31
C ₂ -C ₄	13.80	19.20	11.00	7.62

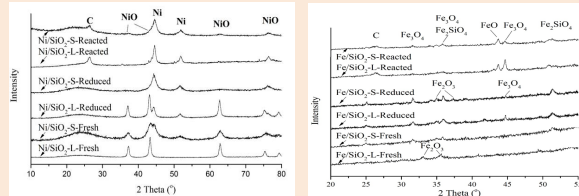
Fe-based catalysts produced larger amount of carbon production. Fe-based with large metal particles produced highest yield of hydrogen gas.

TPO Results of Reacted Catalysts



Three stages oxidation of carbons: amorphous (~500 °C); filamentous with small diameters (~600 °C) and with large diameters (~700 °C)

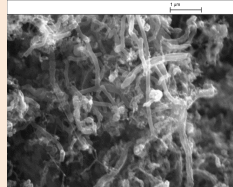
XRD Analysis



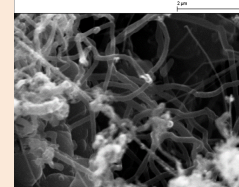
Particle size was confirmed by the XRD analysis. NiO, Fe₂O₃ peaks: Fresh > Reduced > Reacted. Carbon peak was shown in both reacted catalysts.

SEM Analysis

Ni-based Catalysts



Fe-based Catalysts



Catalysts showed a covering of filamentous carbons. Lots of metal particles are also seen inside the carbon nanomaterials in Ni-based catalysts.

CONCLUSIONS

Both carbon nanomaterials and hydrogen gas were successfully produced on Ni/SiO₂ and Fe/SiO₂ catalysts using plastic feedstock. CNMs yields were followed Fe > Ni. Larger metal crystal size showed better ability to produce CNMs. This work also shows that the Fe-based catalyst produced the largest yield of hydrogen.

REFERENCES

Jonathan C. et al. The use of different metal catalysts for the simultaneous production of carbon nanotubes and hydrogen from pyrolysis of plastic feedstocks. Applied Catalysis B: Environmental 180 (2016) 497–510

CONTACTS

Xiaotong Liu*, Yeshui Zhang^a, Mohamed A. Nahil^b, Paul T. Williams^a, Chunfei Wu*
 Email: Xiaotong.liu@2014.hull.ac.uk
^aSchool of Engineering, University of Hull, Hull, HU6 7RX
^bEnergy Research Institute, University of Leeds, Leeds, LS2 9JT, UK

Figure A-E1 Poster for H2FC supergen and Pyro 2016 conferences



This is to certify that
Xiaotong Liu
was awarded the
Joint Third Prize
Oral Presentation
for
Excellence in Chemical Research
at the 2017 24th Joint Annual Conference
of the SCI Chinese UK Group and
the Chinese Society of Chemical Science & Technology in the UK



Weiping Wu
Weiping Wu
Chairman, SCI Chinese UK Group

Sharon Todd
Sharon Todd
SCI Executive Director

Society of Chemical Industry
14/15 Belgrave Square, London, SW1X 8PS UK
T: +44 (0)20 7598 1500 www.soci.org

SCI founded in London 1881 and in New York 1894
Incorporated by Royal Charter 1907. Reg-tered as UK Charity 206883
Recognised as a not-for-profit organisation across the world

Figure A-E2 Oral presentation prize for the 24th annual SC-CSCST conference

CARBON NANOTUBES PRODUCED FROM THERMO-CHEMICAL CONVERSION OF WASTE PLASTICS USING NI-BASED SPHERIC CATALYSTS

X. Liu^a, B. Shen^{b*}, P. Yuan^b, C. Wu^{a,b*}

* Corresponding author: c.wu@hull.ac.uk

^a School of Engineering and Computer Science, Faculty of Science and Engineering, University of Hull, Hull, HU6 7RX, UK

^b School of Energy and Environmental Engineering, Hebei University of Technology, Tianjin, China

1. Introduction

Converting plastics waste into valuable products (such as CNTs) is an important and profitable option for environmental protection [1, 2]. This work focuses on converting plastic waste into high value carbon nanotubes (CNTs) using Ni-based spherical catalysts.



- **Aim:** parameters study to produce high quality and quantity of CNTs from plastics waste.
- **Objectives:** (1) Ni content effect on CNTs growth (2) reaction temperature effect on CNTs growth

3. CNTs Growth Mechanism

➤ General CNTs Growth Mechanism

Two general methods according to the interaction between catalysts and substrate[3], tip-growth model (Figure.3B) and base-growth model (Figure.3C). Figure 4 is an example of CNTs TEM morphology.

- (1) **Tip-growth:** when the catalyst-substrate interaction is weak, CNTs are formed across the bottom of metal particles, push the catalyst particle off the substrate.
- (2) **Base-growth:** when the catalyst-substrate interaction is strong, the catalyst particle remains at the bottom of the substrate.

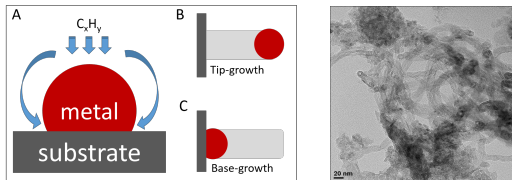


Figure 3. General CNTs growth mechanism

Figure 4. CNTs TEM analysis

➤ CNTs Growth Mechanism for Al₂O₃ Sphere Catalysts

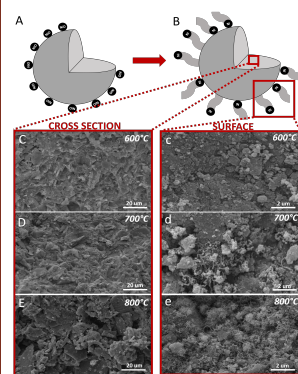


Figure 5. General CNTs growth mechanism

According to the CNTs SEM analysis from three different temperatures, no CNTs grew inside the spent catalysts. The CNTs growth mechanism in this study was assumed as Figure 5 A and B shown. Metal particles were just loaded on the surface of sphere, the Ni catalytic particle couldn't permeate inside the sphere by this precipitation preparation method. So, no CNTs grown inside the catalysts.

2. Experimental

➤ Experimental details

- Reactor: two-stage catalytic thermal-chemical conversion reaction system (Figure 1)
- Feedstock: High density polyethylene plastics (HDPE) pellets with 2mm diameter
- Catalysts: Ni/Al₂O₃ sphere catalysts (Figure 2) with 0.1 and 1.0 molL⁻¹ Ni (NO₃)₂·6H₂O was assigned as **0.1/sphere** and **1.0/sphere**, respectively in this paper
- 500 °C at the first stage, Different reaction temperatures were used in the second stage (600, 700, and 800 °C)

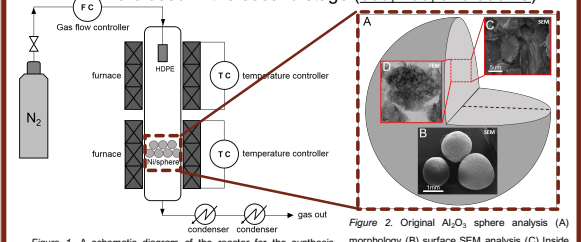


Figure 1. A schematic diagram of the reactor for the synthesis of CNTs from waste plastics by Ni/sphere catalysts

Figure 2. Original Al₂O₃ sphere analysis (A) morphology (B) surface SEM analysis (C) Inside SEM Analysis (D) TEM analysis

4. CNTs Qualitative and Quantitative Analysis

In this study, temperature program oxidation (TPO) analysis (Figure 6 and 7) was used for CNTs quantitative analysis. Quality analysis was analysed based on CNTs diameter distribution with standard deviation SD number (Figure 8).

➤ Temperature Effect

The total carbon yield could be represented by X axis 'the weight loss' of catalyst in relation to the initial catalyst weight. At 800 °C, CNTs has the largest yield, about 7.5 wt%.

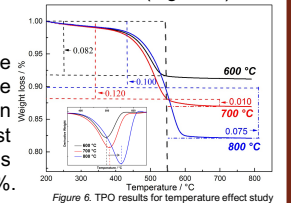


Figure 6. TPO results for temperature effect study

➤ Ni Content Effect

1.0/sphere produced more CNTs, 7.5 wt %. 1.0/sphere had the larger diameter 55.2 nm, and better quality with small SD, 7.9 nm.

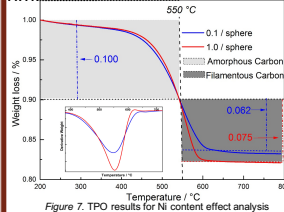


Figure 7. TPO results for Ni content effect analysis

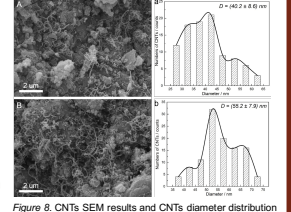


Figure 8. CNTs SEM results and CNTs diameter distribution

5. Conclusion

CNTs are successfully produced by Ni/sphere catalysts from plastic waste. The optimum parameters are 1/sphere at 800 °C.

References:

- [1]X. Liu, H. Sun, C. Wu, D. Patel and J. Huang, *Thermal Chemical Conversion of High-Density Polyethylene for the Production of Valuable Carbon Nanotubes Using Ni/AAO Membrane Catalyst*, 2017, p.
- [2]B. Jiang, C. Zhang, K. Wang, B. Dou, Y. Song, H. Chen and Y. Xu, *Applied Thermal Engineering*, 109, Part A, (2016) 89.
- [3]D. Chen, K.O. Christensen, E. Ochoa-Fernández, Z. Yu, B. Tødtal, N. Latorre, A. Monzon and A. Holmen, *Journal of Catalysis*, 229, (2005) 82.

Acknowledgements:

Supervisor: Chunfei Wu, Queen's University Belfast University of Hull, UK

Conference Pyro 2018 organizers

Xiaotong Liu

University of Hull, UK

Email: xiaotong.liu@hull.ac.uk



Figure A-E4 Poster prize for Pyro 2018 conference

E2. Training

Training attended during PhD study has been summarized

Table A-E2 Training attended during PhD

<i>Training</i>	<i>Date</i>	<i>Organizer</i>	<i>Chapter</i>
Fundamentals of bioenergy	13 rd -15 th Apr. 2015	Aston University	E2.1
Online GC-MS for catalytic pyrolysis of plastics	3 rd Feb. – 16 th Mar. 2016	EU ‘RISE’ Project	E2.2
Electron microscope training	27 th -31 rd Mar. 2017	Royal Microscope Society	E2.3
Catalytic pyrolysis of biomass	17 th -21 st Sep. 2018	BRIKS	E2.4

E2.1 Fundamentals of bioenergy

Module aim: to learn various technologies available to convert biomass into energy and develop concepts to understand the challenges and limitation that these technologies might face.

Learning outcomes:

- (1) Understanding of biomass feedstock, including the properties and classifications.
- (2) Understanding of bioenergy technologies, process, reactions, and energy conversion.
- (3) Evaluation of challenges and limitation of technologies.
- (4) Evaluation of technology efficiencies and comparison of technologies.

E2.2 EU 'RISE' Project

Title: Pyrolysis-gasification of Plastics and Biomass Mixture with/without Catalysts

Aim: Investigation of the enhancing of catalysis and plastic addition to the production of bio-oil from biomass pyrolysis using Pyro-GC (Gas chromatography)-MS (mass spectrometry).

Experimental Design

Setting temperature – 600°C; materials: polypropylene (PP), wood sawdust powder (Lignin) and Ni/ZSM-5 catalyst

1. Wood sawdust powder + plastic powder (weight ratio 4:1)
2. Wood sawdust powder + plastic powder (weight ratio 2:1)
3. Wood sawdust powder + plastic powder (weight ratio 1:1)
4. Wood sawdust powder + plastic powder (weight ratio 1:2)
5. Wood sawdust powder + plastic powder (weight ratio 1:4)
6. Wood sawdust powder + Ni/ZSM-5 catalyst (weight ratio 1:1)
7. Plastic + Ni/ZSM-5 catalyst (weight ratio 1:1)

Experimental Details

- (1) Grind the mixture (as different weight ratios)
- (2) Weight about 4 mg sample, and put into the sample quartz tube
- (3) Put the sample tube into mass spectrometry with 600°C reaction temperature, N₂ was used as carrier gas.
- (4) Quality analysis has been done and shown in tables below

GC Results for Plastic + Ni/ZSM-5 catalyst (weight ratio 1:1)

Table A-E3 Compounds produced with the time from GC-MS analysis (mass:4.04 mg)

<i>Time/min</i>	<i>Substance</i>	<i>molecular formula</i>
1.443	1-pentene, 2-methyl	C ₆ H ₁₂
1.67	2-Butene, 2-methyl	C ₅ H ₁₀
2.074	2-pentene, 3-methyl	C ₆ H ₁₂
2.504	Cyclohexene	C ₆ H ₁₀
3.06	Cyclopentene	C ₇ H ₁₂
4.042	Cyclohexene, 1-methyl	C ₇ H ₁₂
4.268	Toluene	C ₇ H ₈
4.36	Toluene	C ₇ H ₈
5.39	Cyclobutene,1,2,3,4-tetramethyl-	C ₈ H ₁₄
7.332	o-Xylene	C ₈ H ₁₀
8.049	p-Xylene	C ₈ H ₁₀
10.626	Benzene, 1-ethyl-2-methyl-	C ₉ H ₁₂
11.822	benzene, 1,2,3-trimethyl-	C ₉ H ₁₂
12.825	benzene, 1,3,5-trimethyl-	C ₉ H ₁₂
13.968	benzene, 1-methyl-3-propyl-	C ₁₀ H ₁₄
14.121	benzene, 1-methyl-3-propyl-	C ₁₀ H ₁₄
14.242	benzene, 1-methyl-3-propyl-	C ₁₀ H ₁₄
15.003	benzene, 1-methyl-2-	C ₁₀ H ₁₄
15.225	benzene, 2-ethyl-1, 3-dimethyl-	C ₁₀ H ₁₄
16.363	benzene, 1,2,3,5-tetramethyl-	C ₁₀ H ₁₄
16.533	benzene, 1,2,3,5-tetramethyl-	C ₁₀ H ₁₄
17.176	Benzene, 1-methyl-4-	C ₁₀ H ₁₂
18.545	benzene, 1-methylpropyl	C ₁₁ H ₁₆
18.793	azulene	C ₁₀ H ₈
18.975	1H-indene, 2,3-dihydro-4, 7-dimethyl	C ₁₁ H ₁₄
22.673	Naphthalene, 2-methyl-	C ₁₁ H ₁₀
26.733	naphthalene, 1,4-dimethyl-	C ₁₂ H ₁₂

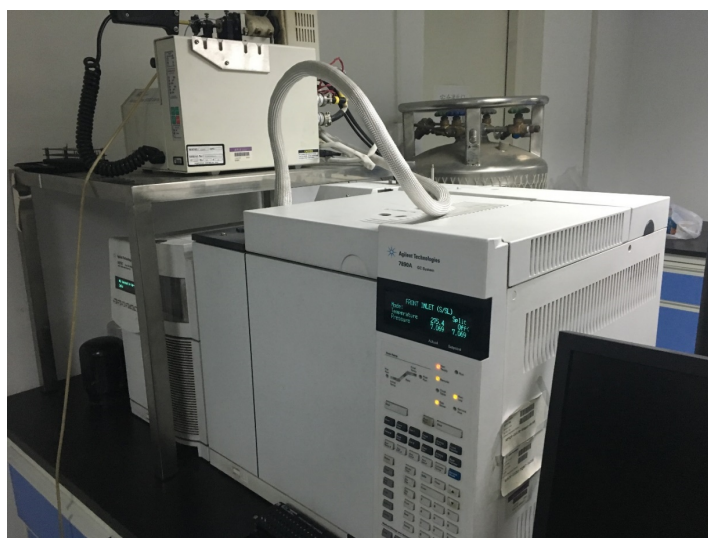


Figure A-E5 online GC-MS

Conclusion

From the quality analysis of 7 groups' samples with different ratios, compounds produced from lignin and plastics mixture didn't change with different ratios. It may need further quantity analysis. The result also shows the amounts of compounds produced decrease when lignin and plastics mixed with catalyst separately.

E2.3 Electron microscope training

As microscope analysis is the main analysis technique for my research, I attended this training for further understanding this technique.



Certificate of attendance

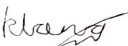
This certifies that

Xiaotong Liu

has attended the
Electron Microscopy Spring School

27 - 31 March 2017 at
University of Leeds

Organised by:


Karina Lang
Event Assistant
Royal Microscopical Society


Rik Brydson
Course Organiser
University of Leeds


Rebecca Thompson
Course Organiser
University of Leeds


Nicole Handow
Course Organiser
University of Leeds



www.rms.org.uk

Figure A-E6 Certification for electron microscopy training

E2.4 BRISK

Title: Gas and liquid oil production analysis from catalytic pyrolysis of biomass

Objectives

- (1) To study gas production from lignin pyrolysis with three different membrane catalysts.
- (2) To study liquid oil production lignin pyrolysis with three different membrane catalysts.
- (3) compare the production of lignin pyrolysis with and without catalysts.

Achievements

- (1) Lignin moisture had been worked out.

(2) Gas study for lignin pyrolysis with and without catalysts has been done by on-line GC.

(3) Liquid oil analysis of plastics pyrolysis with and without catalysts has been done by GC-MS.



Figure A-E7 Catalytic pyrolysis of plastics with online GC

